# FINAL REPORT

# PRELIMINARY DESIGN STUDY FOR THE ACCENT SYSTEM

(3 April 1967 - 2 December 1967)

CONTRACT NO. NAS5-10366






Prepared by

THE DANE COMPANY

Ft. Collins, Colorado


for

GODDARD SPACE FLIGHT CENTER

GREENBELT, MARYLAND

THE DANE COMPANY TECHNICAL REPORT

TR-002-1

Final Report

for

# Preliminary Design Study for the ACCENT System

(2 March 1967 - 2 December 1967)

Contract No. NAS5-10366

Goddard Space Flight Center

Contracting Officer: A.L. Essex

Technical Monitor: William C. Isley

Prepared by
The DANE Company
Fort Collins, Colorado

Project Manager: William R. Mickelsen

for

Goddard Space Flight Center
Greenbelt, Maryland

The DANE Company Technical Report
TR-002-1

## ABSTRACT

A preliminary design study of the ACCENT system is reported in detail. This study includes considerations of the basic physical processes, parametric analyses of system performance, recommended fabrication methods, and final electro-mechanical design of the complete system.

Two electrogenerator designs are proposed for the ACCENT system, one with promethium-147-oxide fuel and the other with strontium-90-titanate fuel. Either of these electrogenerators could be integrated with either a cesium-contact ion thruster or with a charged-particle thruster. When aerospace safety design factors are included, it appears that the strontium-90 fueled system with a charged-particle thruster will be superior for applications where the spacecraft is not sensitive to low levels of radiation.

The final recommendation of the study is that a prototype ACCENT system be assembled and tested as a proof of principle. In the interests of economy, it is recommended that this prototype system be fueled with promethium-147-oxide, and be sized for a 10-micropound charged-particle thruster. Concurrently with the development of the promethium-147 prototype system, it is recommended that fabrication methods and flight-prototype designs be developed for electrogenerators of designs suitable for ACCENT systems with 20- to 350-micropound charged-particle thrusters.

CONTENTS

# LIST OF ILLUSTRATIONS

# LIST OF TABLES

## ACCENT DESIGN SUMMARY

Both the cesium contact ion and the charged particle (Colloid) microthrust systems have received considerable study and hardware development over the past four years for spacecraft application. Unique mission requirements for east-west station keeping of 24 hour geosynchronous, gravity gradient stabilized spacecraft have given rise to the 10- to 20-micropound thrust electric rocket. North-south station keeping on similar spacecraft has also introduced the requirement for 300- to 500-micropound thrust level systems.

The cesium contact ion microthruster is well suited to mission applications where the optimum specific impulse is above 4000 seconds. Presently developed colloid microthruster systems are best suited to applications where the optimum specific impulse is in the range below 1000 seconds. For the above mentioned mission applications, the ion microthruster appears better suited for large $\Delta V$ requirements such as north-south station keeping but suffers in power efficiency for the relatively low $\Delta V$ east-west correction. The colloid system appears best suited to the east-west correction, but has some propellant weight penalty for large $\Delta V$ applications. Such comparisons are necessarily based upon existing state-of-the-art systems.

A typical cesium contact ion system can be broken down into ten functional sub-assemblies as shown in Sketch A. The corresponding colloid system also can be broken down into ten sub-assemblies as shown in Sketch B. In such conventional systems, it is notable that electrical power is required for (a) ionizer heater, (b) vaporizer heater, (c) neutralizer heater, (d) high voltage supply, and (e) control electronics.

The ACCENT System concept embodies an adaptation of the electrostatic microthruster to provide a completely self-contained and self-powered propulsion system. This is

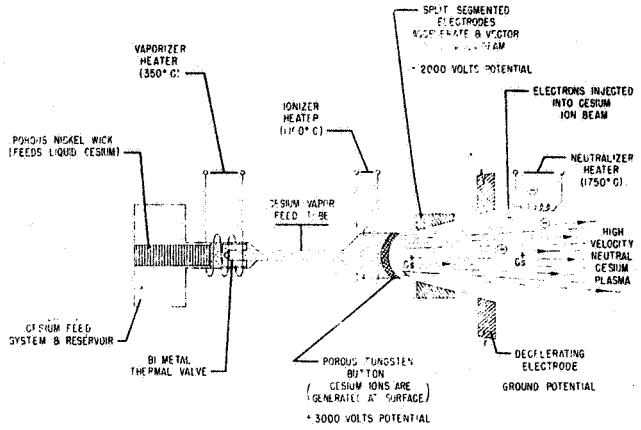


SCHEMATIC OF CESIUM ION THRUSTER

Sketch A

Cesium Ion Microthruster Functional Subassemblies

* 1. Vaporizer Thermal Control

* 2. Ionizer Thermal Control

* 3. Positive Hi-voltage Source

* 4. Negative Hi-voltage Source

* 5. Neutralizer Power Supply

6. Feed System and Reservoir

7. Ionizer

8. Hi-voltage Optics

9. Neutralizer

10. Beam-vectoring and Thrust Level Adjust Electronics

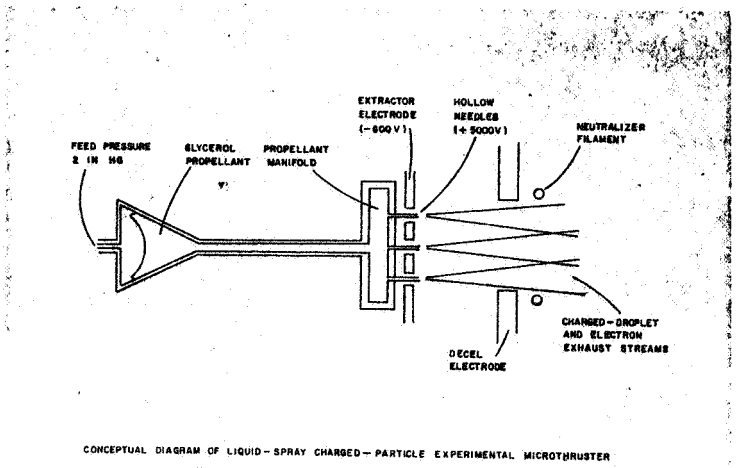


CONCEPTUAL DIAGRAM OF LIQUID−SPRAY CHARGED−PARTICLE EXPERIMENTAL MICROTHRUSTER

Sketch B

Charged-Particle (Colloid) Microthruster Functional Subassemblies

* 1. Propellant-feed Thermal Control

* 2. Needle Thermal Control

* 3. Positive Hi-voltage Source

* 4. Negative Hi-voltage Source

* 5. Neutralizer Power Source( not required for Bipolar Thruster)

6. Feed System and Reservoir

7. Needle Assembly

8. Hi-voltage Optics

9. Neutralizer (not required for Bipolar Thruster)

10. Beam Vectoring Electronics

accomplished by the following: (1) use of radioisotope thermal source for ionizer or needle thermal control, (2) use of a radioisotope electro-generator for high voltage supplies, and (3) provision for incorporation of a thermo-electric isotope generator (RTG) for neutralizer heaters, vaporizer vernier heater, and control electronics. It can be seen (asterick terms) in Sketch A or Sketch B that such modifications would, in fact, permit a self-contained system concept with only the need for command inputs. Also, the ACCENT System permits full utilization of conventional system capabilities such as thrust level adjustment and two-axis thrust vector deflection. Thus, the origin of ACCENT, of: Autogenetically-Controlled-Cesium (or Colloid)-Electro-Nuclear-Thrust System.

The ACCENT System design study has revealed a number of important advantages of this concept over conventional (non-nuclear) approaches. These may be summarized as follows:
(1) ACCENT is completely self-powered. It is completely divorced from onboard power sources, thus affording a great simplification in the spacecraft interface and in the associated power saving which can now be used for prime experiments. For the 20-micropound ion system the anticipated power saving would be in the range of 30 electrical watts per thruster.
(2) ACCENT is self-contained. The only required interfaces are command inputs and telemetry outputs to the spacecraft. The system enclosure can provide for its own thermal control, radiated from the surface of the envelope to space. Spacecraft interface control requirements are substantially reduced.
(3) ACCENT will have fewer total component parts count than comparable conventional systems. The high voltage generator should provide a higher reliability than electronics involving solid state devices. It would eliminate failure due to current surge or arcing. It reduces the series length of critical parts in high voltage circuits. It should drastically

reduce or eliminate the need for current-limiting and arc-control circuitry.

(4) The isolation of power supplies should reduce or eliminate the RFI transmitted through circuitry. This one factor may prove to be highly important in the ultimate application of electric propulsion to long term communications spacecraft.

(5) ACCENT can generate very high voltages (direct current) for onboard spacecraft use other than propulsion.

The total system design is somewhat more complicated for the cesium ion thruster application than for the colloid thruster system due to the extremely high temperatures required for ionizer thermal control in the former case. Experimental data has shown, however, that close thermal control will more than likely be required for needle temperatures in the case of the colloid system. For purposes of describing the total design approach, the cesium ion application will be used. Sketch C presents a functional layout of such a system. In this case direct heating of the ionizer button is employed to raise its temperature to approximately 1100°C. The ratio of conductive to radiative heat losses is held to a very low value by use of concentric heat shields with wire separators. This reduces the contact area to a small portion of the heat transfer area. At operating temperature radiative losses from the front face of the ionizer will be about 3 watts. Assuming that the feed tube is one-eighth inch in diameter capillary tubing, heat losses are estimated to be 15 watts. The surface radiation and conduction losses will be a function of the radioisotope employed. If $Pm_2O_3$ were used in the heat source with nichrome V as radiation shields and wire separators, it appears feasible that 1100°C surface temperature could be reached at a power output of 65-80 thermal watts. Calculations show, however, that the slope of the temperature-power curve is quite sensitive to conductive losses in this regime. This means that exacting heat insulation must be employed to reach such operating conditions.

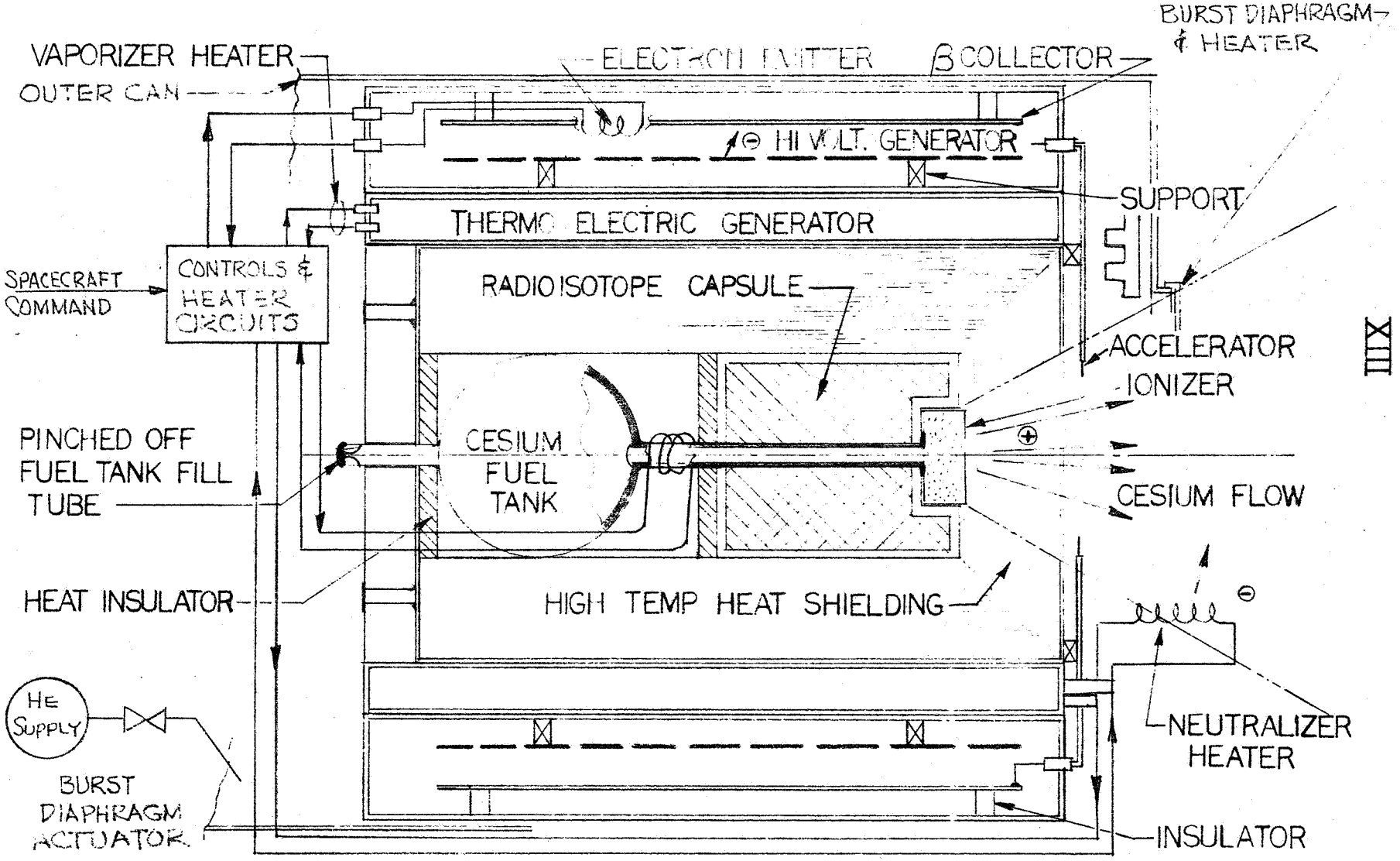


CONCEPTUAL ELECTRO-NUCLEAR GENERATOR SKETCH C

XIII

If curium-244 radioisotope sources were employed, the surface to volume would be substantially improved. In this case the increase in power density of the radioisotope indicates that 30 thermal watts should be adequate. Direct heating of the ionizer may not be the preferred approach if thermal gradients within the capsule are severe, because of the reduced temperatures obtained at the ionizer surface. Another possibility is the heat pipe. This has a potential advantage in that the heat source can be physically removed from the required button position and thereby permit optimization of overall system geometry.

In the configuration shown in Sketch C, a concentric cylinder RTG is employed at the outer periphery of the ionizer heat shield, which provides a hot junction for the thermoelectric generator. The heat shield is designed to permit an operating temperature in the vicinity of 700°F at the hot junction. Thermal insulation for the RTG will permit a cold junction temperature in the range of 150°F. Overall RTG efficiency would be approximately 7%. The high-voltage electro-generator forms the outer sub-assembly in the configuration shown. It consists of multiple concentric cylinders electrically insulated from adjacent layers. On alternate layers a thin surface deposit of $Pm_2O_3$ or other isotope would be applied. All layers, so coated, are electrically inter-connected. The total surface area requirement is based upon optimization of voltage-current at a given thrust level. The beta current produced by this radioisotope would be collected and would furnish the required high voltage supplies. Regulation would be maintained over a given operating potential through use of conventional electronic circuitry which would provide a bias to ground. The outer enclosure would serve as the thermal control sub-assembly and would include a method of sealing the inner containment when necessary. One technique would be the use of an inert gas pressurizing vial, together with a burst diaphragm and associated heater. Once in a space environment, power can be applied to the heater and the pressurizing vial actuated. This should be

sufficient to eject the diaphragm cover plate and expose the high temperature ionizer to free space. During ground tests it would be necessary to keep the unit sealed and under internal inert gas pressure in order to keep from poisoning the ionizer at such temperatures. It is anticipated that the development of such containment assembly will be the most pressing development under the ACCENT approach. If the heat pipe is employed, it may be possible to operate the heating cycle in two modes. In mode 1 the heat would be rejected by a thermal control unit. In mode 2 the heat pipe provides thermal input to the ionizer. The neutralizer filaments and the vernier vaporizer heater would be powered directly from the RTG at low voltage.

The ultimate configuration of an ACCENT system will be highly dependent upon the specific design conditions. It may be necessary to place the high voltage electrogenerator behind the thruster assembly as shown in Sketch D in order to minimize diameter of envelope while providing adequate surface area.

The use of radioisotope sources for thermal heaters in the temperature range up to 1100°C has been and is now under investigation* as one adaptation to existing ion engines. The next major step in this regard will have to be experimental in nature due to the exacting thermal insulation requirements. $Pm_2O_3$ may be inadequate from a power density standpoint, so tests will be required. NASA tests** on the Radioisojet have shown that $Pm_2O_3$ can provide estimated surface temperatures up to 900°C. It is expected that higher temperatures could be obtained by more careful design of the heat shields and thermal support members.

---

* James, et al; Microthruster Development with Simulated Radioisotope Heating. AIAA Paper No. 67-734. September, 1967.

**Radioisojet Program Summary Report. NASA X-734-67-475. September, 1967.

The use of radioisotope sources for RTG devices is also quite well developed at this stage. It is anticipated that conventional units* could be directly incorporated into the ACCENT configuration.

The major development area at this point is the high voltage electronuclear generator (HV-EG). With this thought in mind, the predominant emphasis of the design study described in the following sections deals with this sub-assembly. It should be noted that any one or all of the three design features (i.e. ionizer heater, RTG, HV-EG) could be incorporated into conventional systems. For example, all power for bi-polar liquid-spray microthrusters could be provided by two HV-EG of opposed polarity located in the same containment vessel. A modest amount of heat would be required for needle temperature, and this could be provided from the HV-EG heat rejection. In bi-polar liquid-spray thrusters, a neutralizer is not required, so that in this application of the ACCENT System, the HV-EG would provide all power needs. For other applications of the ACCENT System, information presently being developed on radioisotope-heating and RTG technology could be adapted to the particular system design. The major objective of this design study is to develop an understanding of the HV-EG to the point where it can be considered ready for detailed laboratory hardware testing along with the former sub-assemblies.

---

* Advanced Large Milliwatt Radioisotope Generator Study Program. Summary Brochure, Contract No. AT(30-1)-3627. May 31, 1966.

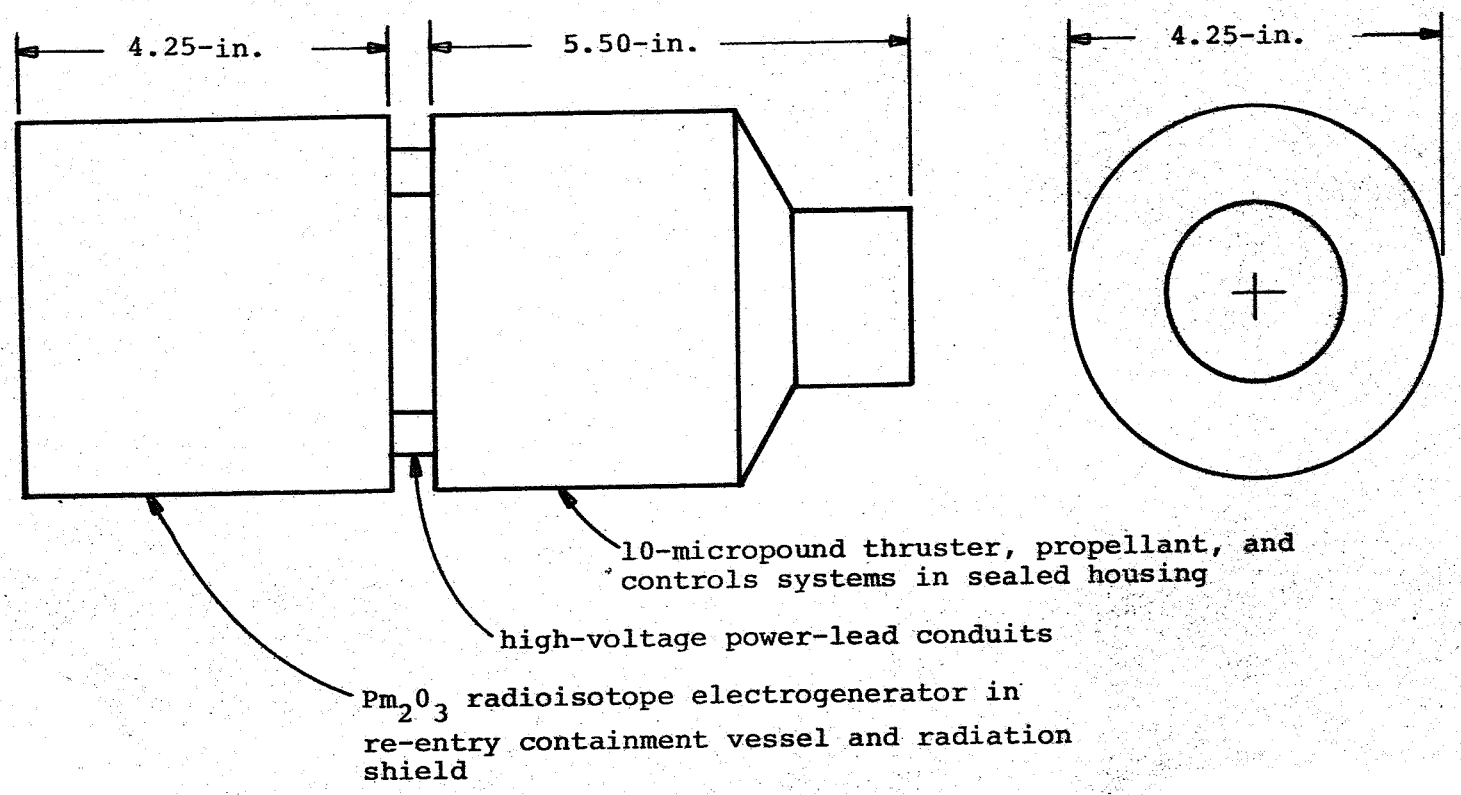






Sketch D - Conceptual design of ACCENT System with 10-micropound cesium contact-ion thruster.

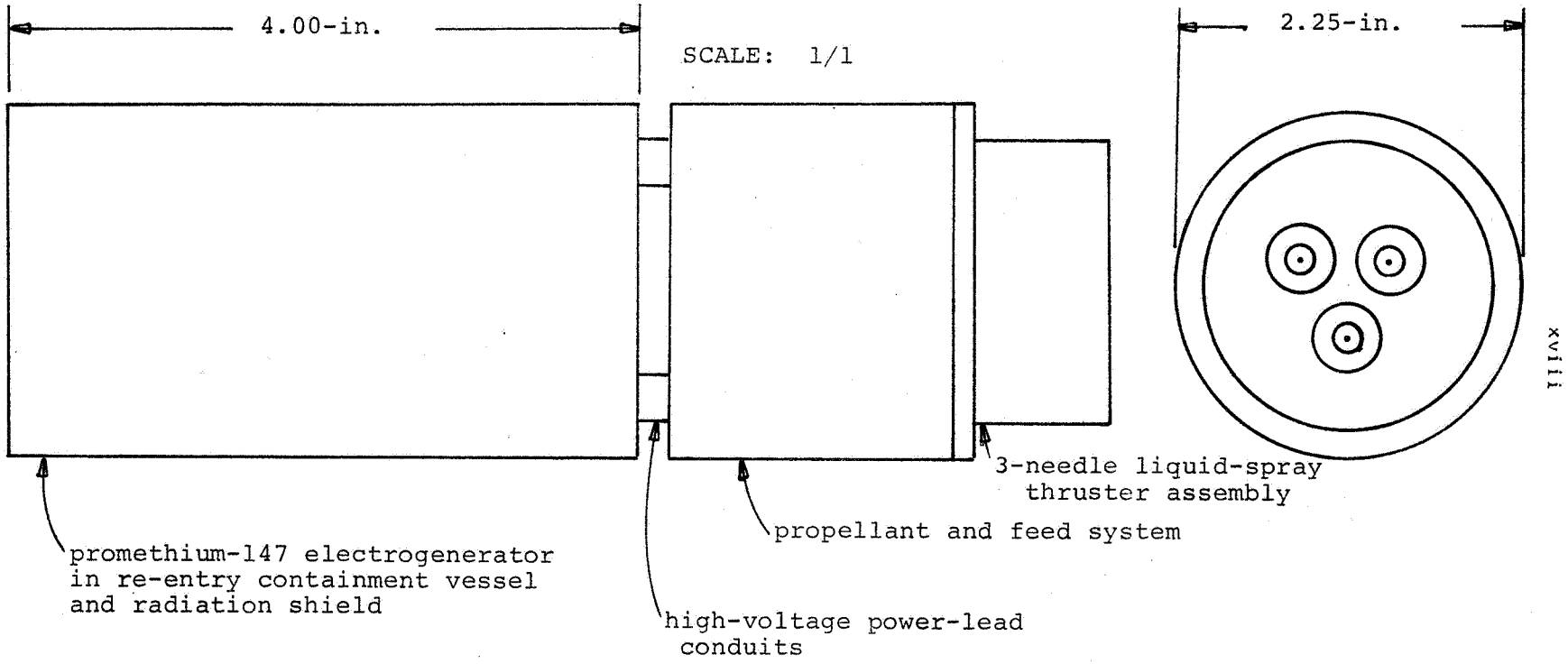


THE DANE COMPANY



Sketch D(b). Conceptual design of ACCENT System with 10-micropound liquid-spray thruster.

# ACCENT PARAMETRIC DESIGN STUDY

The ACCENT system* is a type of auxiliary electric propulsion system[1] in which a radioisotope electrogenerator is coupled with an electrostatic thruster through autogeneous controls to produce thrust in the micro-pound to milli-pound range. An ACCENT system with a cesium-contact ion thruster is shown diagrammatically in Figure 1, and an ACCENT system with a liquid-spray charged-particle thruster is illustrated in Figure 2.

Electric power for the thruster is generated in the radioisotope electrogenerator by the direct conversion of decay-particle kinetic energy into electric potential energy. This action is analogous to the conversion of electron kinetic energy to electric potential energy in thermionic diodes. Auxiliary power requirements could be provided by radioisotope heating as in Figure 1, or by thermoelectric power for the system shown in Figure 2.

Attainment of high electric potential with radium was suggested by Strutt[2] in 1903, and actually demonstrated by Moseley[3] in 1912. In the Moseley experiment, about 20 millicuries of radium was located in a thin-wall 1-cm diameter bulb supported by a 0.8 mm fused-silica rod in a silver-coated vacuum chamber. Although the beta current was only $10^{-11}$ amperes, potentials of 150,000 volts were reached.

In 1924, Kramer[4] reported some experiments done with radioisotope materials such as monazite† sand or radioactive ilmenite± coated directly on a flat plate electrode and

---

*autogenically-controlled-cesium-electro-nuclear-thrust system, or autogenically-controlled-colloid-electro-nuclear-thrust system.

†$(Ce,Nd,Pr,La)PO_4(+Th_3[PO_4]_4)$

±$FeO \cdot TiO_2$

separated by an air gap from a flat-plate collector electrode. Batteries of this kind built by Kramer produced 25 to 100 volts. Successful operation also was attained with no air gap, that is, with the radioisotope fuel layer in direct contact with the collector electrode.

Pool[5] pointed out in 1944 the possibility of using radioisotope electrogenerators in vacuum tubes and electron microscopes, and remarked on the similarity to the Edison effect. Lobanev and Beliakov[6] reported in 1945 on a radioisotope electrogenerator which delivered $10^{-10}$ to $10^{-9}$ ampere. Miller[7] proposed a polonium-210 alpha-particle radioisotope electrogenerator in 1946.

Linder[8] reported in 1946 on plans to construct a beta-ray radioisotope electrogenerator. Notable reasons for this development were the longer range of beta particles, and the lower cost of beta-emitting radioisotopes. With the greatly increased availability of radioisotopes from the Manhattan Project, it appeared that Moseley's results could be exceeded several fold. In 1951, Linder and Christian[9] reported that a voltage of 365,000 volts had been attained with a 0.25-curie strontium-90 vacuum electrogenerator. Short-circuit current in this electrogenerator[10] was $1.05 \times 10^{-9}$ amperes, and pre-breakdown leakage current was of the same order of magnitude in the kilovolt range of operation. Further work in this program* was done with solid-dielectric radioisotope electrogenerators as reported by Linder and Rappaport[11,12] in 1953. Although the strontium-90 sources were only 25 to 250 millicuries, current and voltage were generated, thereby demonstrating the basic feasibility of radioisotope electrogenerators.

Vacuum electrogenerators fueled with up to 6 curies of polonium-210 have been developed by Anno, et al[13-16] to

---

*supported in large part by the Components and Systems Laboratory, Wright Air Development Center, Air Research and Development Command, United States Air Force.

generate about $10^{-8}$ ampere at 100,000 volts. Because of delta rays (electrons) generated by the alpha particles leaving the radioisotope fuel layer, an electron-suppression grid is required in this type of electrogenerator.

Radioisotope electrogenerators for primary electric propulsion have been proposed by Mickelsen and Low[17-21]. These proposed designs were for 10 kilowatt (electric) power levels and larger and recommended either polonium-210 or cerium-praseodymium-144 for the radioisotope fuel. Because of the necessity for a delta-ray suppression grid with alpha-emitting fuels as shown by Anno, the polonium-210 design concept appeared to be too heavy for primary propulsion[19]. For this reason, the cerium-144 design concept is presently being investigated experimentally at the NASA Lewis Research Center. The NASA Lewis electrogenerator consists of two coaxial cylinders with cerium-144 deposited on the inner cylinder. There is a large vacuum gap between the cylinders to support the desired voltage of about 600,000 volts.

The ACCENT system differs basically from the NASA Lewis concept in that the ACCENT system is intended for auxiliary propulsion, while the NASA Lewis concept is intended for primary propulsion. Thrust levels for these two applications are vastly different, so exceedingly low specific mass is not essential for the ACCENT system. Because of the higher thrust level for primary propulsion, electrogenerator size is a crucial factor in the NASA Lewis concept. Primary-propulsion mission durations are usually less than one year, while auxiliary propulsion for satellites may require durations of more than two years. Such differences in application requirements result in basically different design philosophies, so that there is little in common between the NASA Lewis concepts and the ACCENT system.

## Fundamental Design Concepts

Two design features must be determined before detailed parametric analyses can be done to find the optimum final

design:

1. radioisotope type for electrogenerator fuel
2. electrogenerator geometrical configuration

These design features have been discussed in the Interim Design Report[22], and in Appendixes of this report. This discussion is summarized here in support of the recommended design features.

Electrogenerator Radioisotope Fuel. The ACCENT system electrogenerator design study has been limited to consideration of beta-emitting radioisotopes only. In principle, alpha-emitters could be used in the electro-generator, but then a grid is required to suppress the copious emission of delta electrons that accompanies alpha emission from a surface as discussed previously. Study of the ACCENT electrogenerator has shown that close-spaced electrodes are essential for satisfactorily small generator size and weight. Under these circumstances, a suppression grid does not seem feasible.

There are a number of beta-emitting radioisotopes that have properties conducive to high performance electrogenerators. The preliminary design study has shown that four characteristics of radioisotopes are of major interest for use in the ACCENT system electrogenerator: half life, volume activity, end-point energy, and nuclear radiation.

Activity decays of some typical radioisotopes are shown in Figure 3. For auxiliary propulsion missions of several years duration, long half-life radioisotopes such as strontium-90 are attractive from the viewpoint of activity uniformity. For two- or three-year missions, promethium-147 would be satisfactory with some means for power flattening. For auxiliary propulsion missions of only a few months duration, thulium-170 would be satisfactory. If uniform activity were not an important factor, then much more flexibility in choice would be possible. For example, if most of the propulsion requirement (e.g., $\Delta V$) were required in the first portion of the mission, then shorter half-life radioisotopes would be permissible or even preferable.

It is evident that the mission requirements will have much bearing on radioisotope half-life specification. For the present purposes of finalizing the design concept, it seems advisable to require a half-life commensurate with a three-year mission in order to provide adequate demonstration of the utility of the ACCENT system.

Shielding weight can be a major fraction of the overall weight of the ACCENT system, and so the shielding requirements are a very important factor in radioisotope selection. Before considering the shielding requirements it should be noted that a containment vessel will be needed, and that the shielding might serve the dual purpose of nuclear-radiation shielding and of containment. These aspects of aerospace safety design features are discussed in a later section. It will suffice to point out here that a radioisotope such as strontium-90 could prove to be most attractive if electrogenerator size is minimized. In other words, the containment vessel required for re-entry may be sufficiently thick to attenuate the strontium-90 bremsstrahlung to an allowable level, in which case, small electrogenerator size would become a dominant factor.

Beta-emitting radioisotopes have been surveyed in the preliminary design study. From an extensive list, a reduced list has been formulated within the following constraints:

end-point energy: .2 to 2 Mev
minimum half life: 115 days
compound form: solid at room temperature

The lower limit on end-point energy is to provide enough beta energy to escape a reasonably thick fuel layer, and the upper limit on end-point energy is to prevent excessive bremsstrahlung. Other constraints include the requirement for negligible gamma emission, and practical availability. For example, cerium-144 is admirable in all respects except for the 2-Mev gamma emission which would require very heavy radiation shielding.

All of the factors considered have led to the recommendation of the following radioisotope fuel forms for the ACCENT system:

promethium-147-oxide
strontium-yttrium-90-titanate
thulium-170-oxide

Of these, thulium-170 could be used only for short-duration missions, and promethium-147-oxide is the easiest to handle in fabrication and system development.

Electrogenerator Geometrical Configuration. Analyses of electrogenerators such as in Appendixes A to D of this report have shown that there is a maximum value of beta-current density leaving the fuel-element surface, and that this maximum value is reached when the fuel-layer thickness is equal to the end-point-energy range for the particular radioisotope fuel form. For this reason, radioisotope electrogenerators are current-limited devices, that is, the total electrogenerator current is proportional to the fuel-layer surface area. In ACCENT electrogenerators conceived so far, the dominant mass will probably be the aerospace safety containment shield, and this mass will be determined by the fuel-element surface area and electrode spacing in the electrogenerator. Fuel-element surface area will be determined by the beta-current density arriving at the collector and by the total current requirement.

Total current required from the electrogenerator depends on the type of electric thruster, the thrust level, and the net accelerating voltage. This dependence is illustrated in Figures 4 and 5 for a thrust of 10-micropounds; exhaust-beam current $J$ is proportional to thrust $F$ for a given net accelerating voltage $\phi_{net}$ :

$$F = J(m/q)\, g_c I = J(m/q)\left[2(q/m)\,\phi_{net}\right]^{\frac{1}{2}}$$
$$= (2m/q)^{\frac{1}{2}}\, J\phi_{net}^{\frac{1}{2}} \qquad (1)$$

where $g_c$=9.806 m/sec$^2$, I is specific impulse in seconds, and q/m is charge/mass ratio in coulombs/kilogram.

From Figure 4, it is evident that there is not much relative reduction in contact-ion thruster current for net accelerating voltages above 20,000 volts. The end-point energy of promethium-147 is 223,000 ev , so the range of interest for electrogenerator voltage is .1 of the end-point energy or less. As shown by Figure 5, this observation is valid also for charged-particle thrusters operating at 200,000 volts net accelerating potential, because strontium-90 electrogenerators would be used with such thrusters and the end-point energy for strontium-90 is 2.2 Mev.

Some possible electrogenerator geometries are illustrated in Figure 6. In each of these geometries, the intent is to provide a maximum emitter area in a given volume.

Geometrical configuration does not have a major effect on collector current in cerium-144 electrogenerators for operating voltages less than .1 of the end-point energy, as shown in Figure 7. The information in Figure 7 has been normalized from theoretical calculations for cerium-144 electrogenerators[21], and should be valid for any beta-emitter electrogenerator that has a typical beta energy spectrum. By inspection of Figure 7, it is evident that very small radius ratios will provide nearly as much current as large radius ratios, for both concentric spherical and coaxial cylindrical configurations. This immediately implies that flat-plate configurations are roughly as effective as spherical or cylindrical configurations when the operating voltage is less than about .1 of the end-point-energy.

This last observation has very important consequences. In effect, the conclusion is that spherical, cylindrical, or flat electrodes are roughly equally effective in generating electric current in the ACCENT system. The important consequence is that fabrication and mechanical design advantages probably will dictate which configuration is the most

desirable. There is little doubt that the flat-plate configuration is superior with respect to fuel-layer deposition or bonding. Cermets could be rolled easily into a cylindrical form, but spherical shapes would present special problems. Cylindrical geometries with a vacuum or gas dielectric would be plagued with positioning problems, particularly when many fuel-element/collector pairs are required; however, the coaxial cylindrical geometry has greater strength and a better shape for reentry. If the positioning problems could be solved, then the coaxial-cylinder configuration would provide minimal total system weight because the aerospace safety containment vessel is the most massive component of the system. There would be no positioning problems with a solid dielectric, for the fuel-element/solid-dielectric/collector assembly could be rolled up like a cylindrical capacitor. However, calculations in Appendix E indicate that solid dielectrics may fail due to radiation damage. An alternative to the continuous solid dielectric is the use of dielectric spacers that cover only a small fraction of the total electrode surface area, as discussed in a later section. The dielectric-spacer design concept is equally applicable to coaxial-cylinder, circular-disc, or flat-plate geometries, and is therefore treated here simply as a means for providing mechanical integrity of electrogenerators with close-spaced electrodes.

From this discussion, it is concluded that the flat-plate geometrical configuration is the best choice for the initial stages of ACCENT system prototype development. A typical flat-plate configuration is shown in Figure 6(a). Analysis of this configuration is described in detail in Appendixes A to D of this report. This configuration is used as a standard and as the source of information for most aspects of this preliminary design study. The modular design feature of the flat-plate and circular-disc geometries illustrated in Figure 6 is of special advantage in providing the various voltages and currents required by electrostatic thrusters over a range of thrust levels. The ultimate flight configuration

may well be the cylindrical geometry, so the parametric analyses described in the next section include this geometry also.

## Parametric Performance Analysis

Performance of the ACCENT system is primarily dependent on the performance of the electrogenerator, and on the matching between electrogenerator and thruster characteristics. Thruster characteristics are fixed by the state-of-the-art in electrostatic thrusters, or by confident extrapolation of experimental thrusters into a flight-prototype status. Therefore, the primary variables in the ACCENT system performance analysis are those of the electrogenerator; for example, it is assumed that the electric thruster can be designed to meet the current-voltage characteristic shown in Figures 4 and 5. In the interest of completeness, only minimal constraints are placed on the parametric study with regard to fabrication feasibility, for such constraints are discussed in a later section.

Electrogenerator Current. Beta-current density leaving the fuel-layer surface is treated theoretically in Appendixes A to D. Losses due to pre-breakdown, secondary-electron, reflected-primary, and ohmic-leakage currents are discussed in Appendix E. These results are used throughout the present analysis.

Beta-current densities leaving the fuel-layer surface in $Pm_2O_3$ , 90% dense, electrogenerators are shown in Figure 8. In preparing this figure it was assumed that the support foil, or substrate, would be much thicker than the $Pm_2O_3$ fuel layer, so that all betas emitted toward the support foil would be lost. As shown in Appendix C, not much gain in primary-beta current can be realized from $Pm_2O_3$ fuel-layers thicker than 0.005 cm (2-mil). For these reasons, the current density for $\tau_f$ = .005 cm shown in Figure 8 is used as a standard throughout the parametric study of promethium-147-oxide electrogenerators.

Strontium-90 betas have a much greater range than those from promethium-147, so thin support foils are certainly feasible in $SrTiO_3$ electrogenerators. For example, a 10-mil aluminum support foil will allow many beta particles to pass through, and in this way the beta-current density can be augmented if the fuel layer is placed on both sides of the support foil. The method developed in Appendix E to account for beta losses in solid dielectrics can be used for calculating the current augmentation by rearward-emitted betas. Results of such calculations for strontium-90-titanate, 90% dense, electrogenerators are shown in Figure 9. This figure can be compared directly with Figure C15, and from this comparison, it is clear that rearward-emitted betas make a very significant contribution. These results are cross-plotted in Figure 10, and it is evident from this figure that a 0.10-cm fuel-layer thickness will provide nearly as much current as a 0.20-cm fuel-layer thickness. In other words, the inventory of Sr-Y-90 can be reduced to 1/2 and the current is reduced by only 5%.

If very thin substrates, say, 0.5-mil aluminum foil, could be used in promethium-147-oxide electrogenerators, then the radioisotope inventory could be reduced with essentially the same primary-beta current density. Whether such thin foils are feasible remains to be seen. Also, cermet fuel elements could provide the same kind of advantages as thin support foils do, if the cermet can be made thin enough. Because of the matrix material in cermets, primary-beta current is reduced somewhat as described in Appendix G, but this reduction can be less than the gain provided by rearward-emitted betas if the cermet is thin enough. These deviations from the 0.005-cm $Pm_2O_3$ and 0.10-cm $SrTiO_3$ , both 90% dense, fuel layers are minor, so the primary-beta-current-densities shown in Figures 8 and 10 are used throughout this analysis.

Electrogenerator current-density can be estimated quite simply with the information contained in Appendix E. Secondary-electron current is estimated to be about 3% of primary-beta current, and primary-electron reflection is estimated to

be about 20% of primary-beta current. These two mechanisms comprise a total of 23% leakage current in a vacuum-dielectric. In other words, electrogenerator current density would be 77% of the values shown in Figures 8 and 10, for vacuum-dielectric electrogenerators. Gas-dielectric or solid-dielectric electrogenerators probably would not have the 3% secondary-electron leakage current, but most of the reflected primary electrons would be returned to the emitter. Since the 3% difference between vacuum-dielectric and gas- or solid-dielectric electrogenerator current density is small, the 23% leakage current is assumed throughout this analysis.

Electric Field Strength. As noted previously, it is of crucial importance to minimize the volume of the ACCENT electrogenerator in order to minimize the mass of the aerospace-safety containment vessel. This requirement immediately implies that the inter-electrode gap between the fuel element and the collector must be as small as possible for the given operating voltage. Small spacing for a given voltage results in a high electric field strength. In fact, the maximum allowable electric field strength will dictate electrogenerator size.

As discussed in Appendix E, data for vacuum-dielectric electrode systems show that electric field strengths of $10^5$ to $10^6$ volts/cm can be held without appreciable pre-breakdown current or actual electric breakdown. In principle, even higher field strengths can be attained with $SF_6$ gas dielectric, but then very high gas pressures are required, as illustrated in Figure 11. Dielectric strengths of pyrolytic boron nitride, polyester, poly-para-xylylene, and polyimide solid dielectrics are listed in Table E2, and these correspond to effective field strengths of $1.6 \times 10^6$ to $2.8 \times 10^6$ volts/cm. Allowable field strength with solid dielectrics is important also when the solid is used as a separator between fuel elements and collectors in vacuum- or gas-dielectric electrogenerators.

It is not possible to predict with certainty an exact value of allowable electric field strength for the ACCENT electrogenerator. Only direct experience in the development of the electrogenerator can provide reliable values for electric field strength. For this reason, the recommended electrogenerator design will have provision for varying the emitter/collector spacing over a reasonably wide range. In the light of the experimental evidence for vacuum-, gas-, and solid-dielectrics, the range of interest for electric field strength is taken to be $10^5$ to $10^6$ volts/cm, and the parametric study is done over this range.

Rectangular Flat-Plate Electrogenerators. The feasibility of fabricating electrogenerator fuel elements by various methods is discussed in Appendix G. Of the many possible configurations, it is concluded in that Appendix that 1x6-inch rectangular flat-plate fuel-elements could be fabricated with confidence within the existing state-of-the-art. It is of interest, therefore, to include this particular configuration in the parametric performance analysis.

It is assumed that the fuel elements consist of 1x6-inch fuel layers of promethium-147-oxide or strontium-90-titanate on two sides of 10-mil aluminum support foils. Since the fuel-layer area on each fuel element (total of both sides) is known, and since the exhaust-beam current requirements for cesium-contact and charged-particle thrusters are known (Figures 4 and 5), then the electrogenerator current density (77% of values in Figures 8 and 10) can be used to calculate the number of fuel elements required for a 10-micropound thruster. Mission duration must be included as another parameter in this calculation because of the activity decay of the radioisotope fuel. Results of such calculations are shown in Figures 12 to 15. The comparatively large number of fuel elements required for the cesium-contact ion thruster is due to the large ion-beam current requirement for this type of thruster as illustrated in Figure 4. The relatively small number of fuel elements required by charged-particle

thrusters is indicative of the better match between thruster and electrogenerator characteristics afforded by the charged-particle thruster. This improved matching of thruster to electrogenerator is due to the much smaller values of q/m which greatly reduce the exhaust beam current as shown by equation (1). In fact, it can be said categorically at this point that the charged-particle thruster is much superior to the contact-ion thruster for integration in the ACCENT system; however, the contact-ion thruster can still be used effectively in the ACCENT system.

Size of the electrogenerator with a rectangular flat-plate configuration can be expressed in terms of the total height $H$ of a stack of 1x6-inch fuel-elements and collectors. Typical designs for promethium-147-oxide and strontium-90-titanate electrogenerators are shown in Figures 16 and 17. In each of these designs, the total height $H$ is:

$$H=nh \tag{2}$$

where $n$ is the number of fuel elements, and $h$ is the height occupied by one fuel element, the two inter-electrode gaps, and half of each of the two collectors:

$$h=\tfrac{1}{2}\tau_c + g + \tau_f + \tau_s + \tau_f + g + \tfrac{1}{2}\tau_c$$

$$=(\tau_c + 2\tau_f + \tau_s) + 2g \tag{3}$$

Fuel-layer thickness $\tau_f$ has been assigned in the previous text as 0.005-cm for the promethium-147-oxide electrogenerators and as 0.10-cm for the strontium-90-titanate electrogenerators. A support-foil thickness of 0.010-inch has been mentioned as being feasible from the fabrication standpoint (see Appendix G), and aluminum is a good material from the standpoint of low bremsstrahlung production as discussed in connection with aerospace safety in a later section. For the same reason, aluminum is indicated as the collector material in both Figures 16 and 17.

The 10-mil aluminum collector in Figure 16 is more than sufficient to stop all betas from promethium-147; that is, the range of betas with the end-point energy of 0.223 Mev is about 0.008-inch in aluminum. However, the end-point energy of betas from strontium-90 is 2.28 Mev, and these have a range of about 0.18-inch in aluminum. Since most of the betas leave the fuel-layer surface at angles much less than the surface-normal, it is reasonable to expect that nearly all the betas can be stopped in a collector with a thickness less than that required to stop end-point betas at a normal incidence. For this reason, a collector thickness of 0.125-inch is assumed adequate for the present design analysis. In a final flight-prototype strontium-90-titanate electrogenerator, the optimum design will minimize electrogenerator volume and minimize beta current passing completely through the collector. It is possible in principle to make theoretical calculations of energy and angle-of-incidence of betas arriving at the collector, such as reported[21] for cerium-144 electrogenerators with the assumption of straight-line paths of betas within the fuel-layer. Exact calculations require results from Monte Carlo methods[23], and such calculations are beyond the scope of the present work.

Total heights of 1x6-inch flat-plate promethium-147-oxide and strontium-90-titanate electrogenerators are shown in Figures 18 and 19 respectively. All of these arrays have an inter-electrode electric field strength of $\phi/g=10^5$ volts/cm. For example, from Figure 18 a promethium-147-oxide electrogenerator with a contact-ion thruster, for a mission duration of two years, and an operating voltage of $\phi=2000$ volts, could consist of five stacks of 1x6-inch emitter/collector arrays each stack being 5.3-inch in height (ie, each stack would be 1x6x5.3-inch, not including support structure). If a charged-particle electrostatic thruster could be used with the promethium-147-oxide electrogenerator, dramatic reductions in the total height $H$ could be effected as shown in Figure 18.

By comparing Figures 18 and 19, it is evident that strontium-90-titanate ACCENT electrogenerators would be considerably smaller than the promethium-147-oxide electrogenerators for long mission durations. It is notable that very thick aluminum collectors and thick fuel layers have been specified for the strontium-90-titanate electrogenerators. Aluminum was chosen as the collector material because of the relatively low primary-electron backscattering coefficient as shown in Figures E4 and E5. If tantalum were used as the collector material, the backscattered current would be about three times greater than with aluminum collectors, so that:

$$j_{Ta}/j_{Al}=(1-.03-3x.20)/(1-.03-.20)=.37/.77=.48 \qquad (4)$$

where the term .03 represents the leakage current due to secondary electron emission. A measure of electrogenerator volume is the ratio h/j where h is the module dimension given by equation (3), and j is the electrogenerator current density. The ratio of h/j for aluminum and tantalum collector designs is:

$$(h/j)_{Al}/(h/j)_{Ta}=$$

$$(j_{Ta}/j_{Al})(\tau_c+2\tau_f+\tau_s+2g)_{Al}/(\tau_c+2\tau_f+\tau_s+2g)_{Ta} \qquad (5)$$

The end-point-energy range of betas in aluminum is 0.458-cm (see Appendix B1), but the collector thickness is assumed to be only 70% of the end-point-energy range, ie, $\tau_c$=0.318-cm. In tantalum, the end-point-energy range is 0.0622-cm, so the collector thickness can be assumed to be $\tau_c$=0.046-cm (18-mil). For a fuel-layer thickness of $\tau_f$=0.10-cm, and a support-foil thickness of $\tau_s$=10-mil, equation (5) becomes:

$$(h/j)_{Al}/(h/j)_{Ta}=.48(.215+2g)/(.108+2g) \qquad (6)$$

The ratio expressed by equation (6) is less than unity for all inter-electrode spacings, e.g., for g=0.1-inch, the ratio

is 0.73. If the fuel-layer thickness were substantially reduced, there would be some gain with tantalum collectors, but this would be more than offset by the reduced current density (see Figure 9). For example, if the fuel-layer thickness were reduced to 0.05-cm, then $h$=175-mil with the 125-mil aluminum collector and with a negligible gap $g$, so that a reduction in $h$ of .175/.215=0.81 would be effected. However, by inspection of Figure 10, it can be seen that current density would be reduced by a factor of 305/377=0.81 at $\phi$=0 volts, and by a factor of 181/254=0.71 at $\phi$=100,000 From these calculations it is concluded that aluminum is a superior material to tantalum for the collector electrode, but that other materials such as beryllium might prove of interest. Further studies of other materials will depend on the available data on electron backscattering coefficients.

Electrogenerator size can be reduced significantly with higher electric field strengths, ie, with closer spacing between emitter and collectors for a given operating voltage. The effect of electric field strength is illustrated in Figure 20 for promethium-147-oxide electrogenerators with cesium-contact ion thrusters. Although higher field strength greatly reduces the size of promethium-147-oxide electrogenerators, the closer spacing between emitter and collector may bring about mechanical design problems. For example, an electrogenerator operating at $\phi$=20,000 volts, and $\phi/g=10^6$ volts/cm would have a total height of $H$=12-inches, but the electrode spacing would be $g$=0.02-cm, which is only 0.008-inch. Whether such close spacings will be feasible must be answered in development phases of the ACCENT system.

Cylindrical Electrogenerators. Cylindrical electrogenerators with circular-disc electrodes as shown in Figure 6(d) have a size dependent on the emitter surface area $S$ that is required to provide the current $J$ :

$$S=J/j \qquad (7)$$

where $j$ is the electrogenerator current density. Emitter

area for circular discs is:

$$S=2(\pi D^2/4)n \tag{8}$$

where the factor 2 accounts for fuel layers on both sides of the disc, D is the fuel-layer diameter, and n is the number of fuel elements. Length L of the stack of circular discs is:

$$L=nh \tag{9}$$

where the module height h is given by equation (3). Combining equations (8) and (9):

$$S=\tfrac{1}{2}\pi D^2 L/h \tag{10}$$

Emitter surface area S in the coaxial cylinder configuration shown in Figure 6(b) is:

$$S=\sum_{k=0}^{n} S_k \tag{11}$$

whre $S_k$ is the surface area of a particular cylindrical fuel element:

$$S_k=2(2\pi r_k L)=4\pi L(r_o+\tfrac{1}{2}h+kh) \tag{12}$$

where $r_o$ is the radius of the innermost collector, and h is the module dimension given by equation (3). The sum of the arithmetic progression formed by combining equations (11) and (12) is:

$$\begin{aligned} S&=4\pi L\sum_{k=0}^{n}(r_o+\tfrac{1}{2}h+kh)\\ &=4\pi Ln\left[r_o+\tfrac{1}{2}h+\tfrac{1}{2}(n-1)h\right]\\ &=4\pi Ln(r_o+\tfrac{1}{2}nh) \end{aligned} \tag{13}$$

Outer diameter D of the array is the diameter of the outermost collector, so:

$$D=2(r_n+\tfrac{1}{2}h)=2\left[r_o+(n+1)h\right] \tag{14}$$

From equation (14), the number n of fuel elements is:

$$n=\left[(\tfrac{1}{2}D-r_o)/h\right]-1 \qquad (15)$$

When the electrogenerator contains a large number of fuel elements, $\frac{1}{2}D \gg r_o$, and $D/2h \gg 1$, so that equation (15) can be simplified to:

$$n \doteq D/2h \qquad (n \gg 1,\ D/2 \gg r_o) \qquad (16)$$

With this expression for n, equation (13) becomes:

$$S=4\pi L(D/2h)\left[r_o+\tfrac{1}{2}h(D/2h)\right]$$
$$\doteq \tfrac{1}{2}\pi D^2 L/h \qquad (n \gg 1,\ D/2 \gg r_o) \qquad (17)$$

which is identical to equation (10). From this analysis, it is evident that circular-disc and coaxial-cylinder geometries will have approximately the same emitter surface area if the module dimension h is the same, as well as the cylinder outer dimensions. The same observation should hold true for the spiral-wound cylindrical geometry shown in Figure 6(c), therefore all three cylindrical configurations should have equal size for a given electric current requirement.

Fuel-layer diameters for promethium-147-oxide electrogenerators are shown in Figures 21 and 22 for L/D ratios of 1.0 and 3.0 respectively. It is notable that the inner diameter of the containment vessel will be somewhat larger than the fuel-layer diameter because of support structure around the periphery of the electrode discs. This will be true to a lesser degree for the coaxial-cylinder and spiral-wound cylindrical configurations.

The information shown in Figures 21 and 22 can be used to scale the ACCENT system to other thrust levels by noting that electric current J is directly proportional to thrust at a given voltage and q/m, as shown by equation (1). For example, a charged-particle thruster with q/m=4000 coul/kg might be operated at 10,000 volts with $\phi/g=10^6$ volts/cm, and the fuel-layer diameter for 350-micropounds thrust would be $2.8(35)^{1/3}=2.8\text{x}3.27=9.2\text{-cm}(3.6\text{-inch})$. By inspection of

equation (1), a q/m=1000 coul/kg would provide a reduction in fuel-layer diameter by a factor of $0.5^{1/3}$=.794, so the 350-micropound thrust system could have an electrogenerator diameter of somewhat over 7.3-cm (2.9-inch).

Electrogenerator Component Mass. The mass of the collector, the support foil, and the radioisotope fuel can be expressed in terms of mass/area as shown in Table I for the design concepts described in previous sections. These values of specific mass only account for the active areas of the electrogenerator; support structure mass will depend on the particular geometry used.

Values of fuel-layer specific mass in Table I for the strontium-90-titanate electrogenerator designs are much higher than for the promethium-147-oxide design, so the variation of fuel-layer specific mass with fuel-layer thickness $\tau_f$ is of interest. The ratio of mass/current can be formed:

$$(kg/m^2)/(microamp/m^2)=\tau_f\sigma/j \qquad (18)$$

where $\sigma$ is density of the radioisotope fuel form (Table B1). This specific mass (kg/microamp) is shown in Figure 23 for a range of fuel-layer thickness $\tau_f$, and electrogenerator voltage $\phi$. From this figure, it is evident that thinner fuel layers will provide a lower specific mass, but it must be noted that the current density is less for thinner fuel layers, so the emitter area must increase as fuel-layer thickness is decreased. This increase in emitter area will result in larger electrogenerator size, and in a more massive containment vessel.

Minimum system weight can be achieved only by an optimization procedure[22], and this optimization must include all components such as the electrogenerator and its containment vessel, the thruster, the cabling and controls, and the propellant and tank. The final optimized design will depend on a number of factors such as allowable field strength, so the primary function of this section is to provide information needed for the final optimization.

Mass of strontium-90-titanate electrogenerator components, the collector, the fuel, and the support foil, can be calculated from the information presented in previous sections. The total mass of these components for a 10-micropound cesium-contact ion thruster ACCENT system is shown in Figure 24 for a range of fuel-layer thickness and electrogenerator voltage. Internal support structure and containment vessel masses are not included in Figure 24. Although the thinner fuel-layer thickness would result in a lighter electrogenerator component mass, the electrogenerator current density would be reduced thereby causing an increase in electrogenerator size and an increase in containment-vessel mass.

Component masses of promethium-147 electrogenerators for 10-micropound thrust ACCENT systems are shown in Figure 25. The marked superiority of the charged-particle thruster is clearly shown by the very low component masses for q/m= 4000 coul/kg. This superiority is illustrated again in Figure 26 where component masses are shown for 350-micropound charged-particle thruster ACCENT systems for a range of q/m and electrogenerator voltage.

Propellant mass and tankage may be significant in assessing the total system mass. Propellant weight $W_{pr}$ is simply:

$$W_{pr}=Ft/I \tag{19}$$

Where $F$ is thrust in pounds, $t$ is propulsion time in seconds, and $I$ is specific impulse in seconds. Propulsion time may be related to mission time by specifying a duty cycle. Weight of propellant for charged-particle electrostatic thrusters is shown in Figure 27 for a range of specific impulse and thrust levels, all for a propulsion time of two years. For lower duty cycles, the propellant weight shown in Figure 27 may be multiplied directly by the duty-cycle fraction to obtain actual propellant weight. Also shown in Figure 27 are lines of constant q/m to relate specific impulse and net accelerating voltage.

Containment vessels probably will contribute a large share of the ACCENT system total mass. A detailed design analysis of aerospace safety features of the ACCENT system is beyond the scope of the present study, so a definite estimate of containment vessel mass cannot be made here. A conservative design for the vessel might be a 0.1-inch thick tantalum wall with an outer coating of ceramic, as discussed in a later section. To provide some means for making at least a rough estimate of system weight, it is assumed here that the containment vessel might be approximated with a 0.125-inch tantalum wall thickness. Masses of tantalum cylinders are shown in Figure 28 for a range of diameters and length/diameter ratios. These values will be used in the example system optimizations described in the next section.

System Optimization. Total mass of the ACCENT system is one of the most important performance parameters. System mass can be minimized by choosing optimum design parameters such as electrogenerator voltage. For example, the combined mass of the electrogenerator and the containment vessel can be minimized for ACCENT systems where propellant mass is negligible and where thruster mass can be assumed constant. Such an optimization will provide an optimum total system design with respect to mass.

The combined masses of promethium-147 electrogenerators and containment vessels for 10-micropound cesium-contact ion thruster ACCENT systems are shown in Figure 29 for a range of electrogenerator voltage, electric field strength, and for two vessel wall thicknesses. Internal support structure is not included, because the structure mass will depend strongly on the type of configuration. The structure mass, thruster mass, and electrical-system mass could be added to the values shown in Figure 29 to obtain the total system mass. Propellant mass is not included because it is negligible compared to the values shown in Figure 29.

The combined mass of promethium-147 electrogenerators and containment vessels for 350-micropound charged-particle thruster

ACCENT systems is shown in Figure 30 for a range of electrogenerator voltage and charge/mass ratio. Charged-particle thrusters with q/m=1000 coul/kg would provide the lowest mass shown in Figure 30. However, inspection of Figure 27 indicates that propellant mass may become appreciable, in fact may become more than the combined electrogenerator and containment vessel mass, if a 2-year 100% duty-cycle mission is specified. A lower duty cycle would reduce the propellant mass, but it still might be advantageous to operate at a higher specific impulse. This could be done either by increasing the charge/mass ratio at the expense of system mass, or by operating at a higher voltage.

Optimization of fuel-layer thickness can be important to total system weight, especially if thin support foils can be used. For example, the primary beta-current densities for promethium-147-oxide, 90% dense, electrogenerators with 0.5-mil aluminum support foils are shown in Figure 31. The contribution from rearward-emitted betas is included in Figure 31. From this information, the combined mass of the containment vessel and the electrogenerator for a 350-micropound, 1000 coul/kg charged-particle thruster has been calculated, and is shown in Figure 32. From this particular optimization study, it can be concluded that a fuel-layer thickness of 0.002 cm will provide minimum system mass. However, there is less than 1-lb difference between the 0.002-cm design and the 0.001-cm design, so the greatly reduced radioisotope inventory probably would dictate the 0.001-cm design.

As illustrated with these examples, the optimization procedure is straightforward if a mission is specified, and if the aerospace safety requirements for the containment vessel are specified.

A final observation can be made from these examples: the ACCENT system appears to be definitely competitive with other auxiliary propulsion systems[1], providing the electrogenerator can be developed with small inter-electrode spacings and with adequately high electric field strengths.

## AEROSPACE SAFETY CONSIDERATIONS

Aerospace safety has a great number of ramifications to the design of flight-prototype ACCENT systems. There are two primary factors involved in aerospace safety: nuclear-radiation shielding and radioisotope containment. Both of these factors can be strongly affected by environmental conditions, by interactions with the spacecraft, and by abnormal circumstances.

A comprehensive study of aerospace safety considerations is beyond the scope of the present work, primarily because of the preliminary nature of the ACCENT design study. When more definite designs are specified in the future, then a comprehensive aerospace safety analysis will be possible and in fact, mandatory. However, it is possible to define a few basic design parameters that have a direct influence on the present preliminary design study.

### Nuclear Radiation Shielding

Nuclear radiation dose rates from promethium-147 and strontium-90 radioisotope sources are shown in Figures 33 and 34 for various amounts of shielding.[24] These dose rate curves include the effect of self-shielding of the bremsstrahlung, except for the 1- and 10-thermal-watt curves in Figure 34 which are simple extrapolations from the 100-thermal-watt curve for strontium-90. The low-slope portions of the curves in Figure 33 are due to gamma radiation from the promethium-146. The steep-slope portions of the curves in Figure 33, and all of the curves in Figure 34 are due to bremsstrahlung.

When a beta particle leaves the nucleus in the decay process, radiation is spontaneously emitted and is called internal bremsstrahlung. When the beta particle is slowed down in passing through matter, radiation is emitted and is called external bremsstrahlung. The relative proportion of internal and external bremsstrahlung depends on the photon energy and on the material in which the beta is being slowed

down. For example, the spectral distribution[25] of radiation produced by the decay of strontium-yttrium-90 and by the slowing-down of betas in strontium titanate is shown in Figure 35. At the intermediate energies, from 0.1 to 1.0 Mev, external bremsstrahlung is about five times as intense as internal bremsstrahlung; while in the high energy range above 1.0 Mev, external and internal bremsstrahlung have about equal intensity.

Internal bremsstrahlung is a function of the nuclear decay process only, but external bremsstrahlung intensity is a strong function of the material in which the beta particle is slowing down[26]. This relation between external bremsstrahlung and the material is illustrated in Figure 36. If the beta particle slows down in beryllium, the external bremsstrahlung would be about 1/10 of that generated by the beta particle slowing down in strontium (atomic number, 38). While this ideal condition cannot be fully achieved in the ACCENT electrogenerator, it probably can be approached in practice to greatly reduce the external bremsstrahlung. For example, if 0.05-cm fuel layers were used, then inspection of Figures A7 and B4 shows that only a small portion of the yttrium-90-end-point beta energy would be lost in passing through the strontium-90-titanate fuel layer. If the remainder of the beta energy were absorbed in a beryllium collector, then the external bremsstrahlung would be considerably reduced in intensity.

Exact calculation of bremsstrahlung generation and self-shielding in ACCENT electrogenerators is beyond the scope of the present work. However, from the discussion so far, it can be concluded that the dose-rate curves in Figure 33 might be reduced by half an order of magnitude because of the thin-film configuration of radioisotope in ACCENT electrogenerators, and because of the additional self-shielding provided by the support and collector foils.

Estimates of shield-thickness requirements must be based on the radioisotope inventory, as shown by the

thermal-power parameter in Figures 33 and 34. Thermal-watts/microampere of electrogenerator current can be calculated from the physical properties[27] of the radioisotopes of interest. This and other parameters of interest are shown in Figures 37 and 38 for promethium-147-oxide and strontium-90-titanate electrogenerators respectively. The information in these figures can be related to thrust level through the information shown in Figures 4 and 5. For example from Figure 5, a 1000 coul/kg, 10-micropound, charged-particle thruster requires 4-microamperes of beam current at a net accelerating voltage of 60,000 volts. From Figure 38, a strontium-90-titanate electrogenerator with $\tau_f$=0.05-cm for such a thruster would have a radioisotope inventory of 8.3 thermal-watts, or 1220 curies. With the reduction in dose rate by beta-stopping in beryllium collectors, and by the additional internal shielding afforded by the collector and support-foil, the dose rate might be near the 1-thermal-watt curve in Figure 34. If this were the case, then strontium-90 ACCENT electrogenerators with containment-vessel walls of 125-mil tantalum would be restricted to applications having allowable dose rates above 100-mR/hr. In contrast, promethium-147 ACCENT electrogenerators with 125-mil (.32-cm) tantalum containment-vessel walls could be used for applications requiring as little as 1-mR/hr one meter from the source.

From this brief discussion of nuclear-radiation shielding, it is concluded that a 125-mil tantalum containment vessel would provide adequate shielding for promethium-147 ACCENT electrogenerators, but strontium-90 ACCENT electrogenerators might be restricted to applications where fairly high radiation dosage is allowable.

## Radioisotope Containment

For all isotopic space systems where safe return to the Earth surface and ultimate disposal is a requirement, the radioisotope fuel must be completely contained under all

foreseeable circumstances during the following mission phases or events:

a. launch-pad fires, explosions, etc.
b. launch and ascent aborts
c. re-entry from short-lived orbit
d. re-entry after orbit decay
e. impact and burial after re-entry

Extensive studies have been made of these aerospace safety requirements for various isotopic space system designs. For example, a comprehensive analysis has been made[28] of the burn-up of a promethium-147 fuel capsule for the radioisojet thruster. Studies such as these serve to emphasize the requirement for total containment of the radioisotope fuel under severely adverse conditions.

The requirement for total containment has been treated as well as possible in the present study with regard to containment-vessel mass. Total containment requirements also may be an important consideration in selection of dielectric type for the ACCENT electrogenerator. If vacuum dielectric is to be used, then two design philosophies are possible:

a. permanent evacuation of the electrogenerator during assembly, just before final sealing
b. opening of the electrogenerator to the vacuum of space after a successful injection into orbit, and permanent closing of the electrogenerator container after mission completion and before orbit decay and re-entry

The first of these design philosophies would require retention of the vacuum for the mission duration, which appears feasible under the hard-vacuum conditions of space. If the final sealing of the electrogenerator container were done shortly before launch, then there should be no appreciable loss of vacuum during the pre-orbit period. The second design philosophy would require complex mechanical and electronic-control devices and probably can be rejected on these grounds alone.

A gaseous dielectric appears to be compatible with the total containment requirement. In fact, a high-pressure $SF_6$ dielectric inside the electrogenerator containment vessel might add significantly to the impact strength of ACCENT electrogenerators. Reference to Figure 11 indicates that an $SF_6$ gas pressure of about four atmospheres would be required to support an electric field strength of $10^6$ volts/cm.

Solid dielectrics in the ACCENT electrogenerator would require either a vacuum or a gaseous environment, so the discussion above covers this case.

In conclusion, any of the dielectric types could be compatible with the radioisotope containment requirement, and it is possible that the gaseous dielectric would improve the impact strength of ACCENT electrogenerators.

## RECOMMENDED DESIGN FOR ACCENT PROTOTYPE SYSTEM

A design for a prototype version of the ACCENT system is described in the following sections. This design is a synthesis of the information presented in preceding sections and some additional considerations that are discussed at each decision juncture. A fundamental design philosophy is maintained throughout, that the prototype ACCENT system must have enough flexibility to allow economical changes in the development program. This design philosophy is followed because of the multiple choices available for a number of important design features, and because additional development data is needed to evaluate the multiple choices in design.

### Radioisotope Fuel Elements

General criteria such as availability, half-life, and nuclear-radiation properties have narrowed the radioisotope fuel to promethium-147 and strontium-yttrium-90. The choice between these two radioisotope fuels, and the recommended design of the fuel elements, depends on activity decay rate, nuclear-radiation shielding requirements, overall electrogenerator mass, and fabrication methods. These factors are discussed in turn, and a recommended design is presented in the following sections.

Radioisotope Fuel. On the basis of electrogenerator current density, which has a direct influence on system mass, promethium-147-oxide is satisfactory for missions up to about two years duration. For 5-10 year missions, strontium-90-titanate is superior because promethium-147-oxide electrogenerators would have an unacceptable degradation in performance.

In later sections on electrical design of the ACCENT system, it is shown that power-flattening probably will be needed for promethium-147-oxide electrogenerators in order to provide a constant thrust level. Because of this power flattening requirement, a voltage-regulation circuit is

needed, which introduces electronic complexity with attendant reduction in reliability. Even though the voltage-regulation circuit is very simple compared with other electric propulsion systems being developed, the reduction in reliability may be a significant consideration.

In contrast, the strontium-90-titanate electrogenerator could be operated without voltage regulation. The current/voltage characteristic of the electrogenerator provides a stable system when operated with an emission-limited thruster. Therefore the voltage-regulation circuitry could be replaced with a simple on-off electronic switch.

Nuclear-Radiation Shielding. This aspect of radioisotope fuels has been discussed in a previous section and can be summarized here. Promethium-147 electrogenerators can be easily shielded with the containment vessel to provide dose rates of 1-mR/hr or less. Strontium-90 electrogenerators will have higher dose rates, but with careful design the dose rate may be acceptable for many applications. Further development and/or study is needed to evaluate the nuclear-radiation shielding requirements for strontium-90 electrogenerators.

Electrogenerator Mass. Strontium-90 electrogenerators are basically heavier than promethium-147 electrogenerators. However, strontium-90-titanate has about twice the current density of promethium-147 initially, and this factor is about four at two years mission duration, and much higher for 5-10 year mission duration. For cylindrical electrogenerators, the diameter is proportional to the cube root of fuel-element surface area, so diameter is greatly dependent on fuel-element surface area when the area is relatively small. Charged-particle thrusters with large values of q/m have low current requirements, as shown by Figure 5. When the current requirement is small, the higher current density of strontium-90-titanate electrogenerators may provide significant reductions in ACCENT system mass. Furthermore,

strontium-90-titanate electrogenerators can be operated efficiently at much higher voltages than promethium-147-oxide electrogenerators, thereby providing higher specific impulse with charged-particle thrusters that have low q/m.

Whether charged-particle thrusters can be operated with low q/m at comparatively high voltage remains to be seen. Within the present context[1] of cesium-contact ion thrusters, or charged-particle thrusters with q/m=4000 coul/kg, promethium-147-oxide ACCENT systems appear to have promise of less mass than strontium-90-titanate ACCENT systems.

Fuel-Element Fabrication. Various possible methods for fuel-element fabrication are discussed in Appendix G. From the chemical or metallurgical standpoint, there appears to be no significant advantage to either promethium-147-oxide or strontium-90-titanate in any of the methods.

Fuel-layer thickness for promethium-147-oxide must be no more than 2-mils for efficient use of the radioisotope inventory. Fuel-layers for strontium-90-titanate are an order of magnitude thicker. From the purely practical standpoint of dimensional tolerance, it is clear that the thicker fuel layers with strontium-90-titanate offer a great advantage. However, this advantage is more than offset by the requirement for fabrication in a hot cell when strontium-90-titanate is the radioisotope fuel form. In contrast, promethium-147-oxide can be handled with much less radiation protection, thereby greatly reducing the cost of development of fabrication methods and the cost of prototype fuel elements.

Recommended Fuel-Element Design. It is recommended that promethium-147-oxide be the radioisotope fuel form for the ACCENT prototype design. This recommendation is primarily based on the economy of development of fabrication methods, and on the questionable possibility of reducing the dose rate from strontium-90 electrogenerators without unacceptable increases in system weight.

Of the four electrogenerator configurations shown in

Figure 6, only the circular-disc and the flat-plate configurations have sufficient flexibility to allow economical changes in design that are desirable during the development of the ACCENT system. Of these two, the flat-plate configuration is the more flexible with regard to support structure. If the circular-disc configuration were used, the support structure members would have to be annular discs; while the support structure members in the flat-plate configuration can be simple rectangular bars.

To provide a sufficiently rigid structure for the initial phases of the ACCENT system development, it is recommended that the fuel-support foil be 10-mil aluminum. From the information given in Appendix G, it appears that 1x6-inch cermets are about the largest that can be conveniently fabricated at present, so the recommended fuel-element design is as shown in Figure 39. A margin is provided along each long side of the fuel element to provide clamping area for the support structure. This margin also provides ample area for the transfer of heat from the fuel element. Bolt holes are provided for mounting in the support structure.

The fuel element shown in Figure 39 has a fuel layer on both sides. As shown in Figure 32, fuel-layer thickness does not have much effect on system mass of ultimate flight-prototype ACCENT systems with promethium-147-oxide electrogenerators. Thicker fuel layers will be much easier to fabricate in initial development phases, so a 2-mil (.005-cm) fuel-layer thickness is recommended for flame-sprayed, hot-pressed, or evaporated fuel layers. Cermets attached to the support foil may be somewhat thicker because of the cermet matrix.

### Dielectric Type

Vacuum, gas, and solid dielectrics are discussed in detail in Appendix E. Either vacuum or gas dielectrics have sufficient dielectric strength, and a small enough leakage current to provide good performance from ACCENT

electrogenerators. Most solid dielectrics suffer severe degradation of electrical properties when some value of total beta-ray dose is reached. It appears that this critical value of total dose will be more than reached in ACCENT electrogenerators, so solid dielectrics probably will not be found suitable.

Optimum designs of ACCENT electrogenerators will have voltages higher than the minimum-mass values shown in Figures 29 and 30 because the propellant mass will tend to drive the specific impulse to somewhat higher values. From this information, it can be estimated that electrogenerator voltages of more than 10,000 volts will be of interest for the ACCENT system. High values of electric field strength are required to provide small-volume electrogenerators and hence low-mass containment vessels. Electrode spacings for various voltages and electric field strengths are shown in Figure 11. For example, a voltage of 30,000 volts and a field strength of $10^6$ v/cm correspond to an electrode spacing of g=0.03 cm (11.8-mil). Maintenance of such small spacings between fuel-elements and collectors of any reasonable size does not appear feasible with vacuum or gas dielectrics alone, ie, some means of mechanical support will be needed to maintain the close spacings required.

Narrow spacers of solid dielectric material appear to be an answer to the problem of close spacing between the fuel-element and collector. A typical electrogenerator design with solid spacers is shown in Figure 40. Leakage currents resulting from the solid spacers will be comprised of current flowing through the volume of the spacer, and current flowing over the surfaces of the spacers. These two currents can be calculated if the volume resistivity $\rho$ and the surface resistivity $\rho_s$ are known.

Volume resistance R of the spacers is:

$$R=(g\rho)/(nwL) \qquad (20)$$

where $g$ and $w$ are the dimensions shown in Figure 40, $L$ is the length of the spacers, and $n$ is the number of spacers. Similarly, the surface resistance $R_s$ of the spacers is:

$$R_s=(g\rho_s)/(2nL) \tag{21}$$

Total leakage current $J_{lss}$ due to the solid spacers is:

$$J_{lss}=\phi/R + \phi/R_s \tag{22}$$

Using equations (20) and (21) in equation (22);

$$J_{lss}= \phi\left[(nwL)/(g\rho) + (2nL)/(g\rho_s)\right]$$

$$= \left[nL(\phi/g)\right]\left[(w/\rho) + (2/\rho_s)\right] \tag{23}$$

The number of solid spacers is

$$n=L/P \tag{24}$$

where $P$ is the distance between spacers as shown in Figure 40. Using equation (24) in equation (23), and defining a leakage current density $j_{lss}=J_{l,ss}/L^2$ :

$$j_{lss}=\left[(\phi/g)/P\right]\left[(w/\rho) + (2/\rho_s)\right] \tag{25}$$

Surface resistivity is typically smaller than volume resistivity, e.g., for Kapton H-film, $\rho=10^{18}$ ohm-cm and $\rho_s=10^{16}$ ohm. Since $w < 0.1$-cm, then the term $w/\rho$ will be much less than the term $2/\rho_s$ , and the solid-spacer leakage current density can be approximated by:

$$j_{lss}\doteq(2/\rho_s)(\phi/g)/P \qquad (w/\rho) \ll (2/\rho_s) \tag{26}$$

If $\rho_s=10^{16}$-ohm, $\phi/g=10^6$-volts/cm, and $P=.2$-cm, then $j_{lss}=10$-micro-amp/$m^2$ . A leakage current density of this order of magnitude is acceptable because it is much less than the electrogenerator current densities quoted in previous sections.

Because of the possibility of radiation damage to the

solid spacers it is not possible to state definitely that this design concept will be satisfactory. Solid dielectrics are known to suffer degradation of volume resistivity and dielectric strength. From equation (25) it can be seen that the volume resistivity of Kapton H-film could be degraded by three orders of magnitude before appreciable leakage occurred through the volume of the solid spacers. However, only more exact information on radiation damage to the various kinds of solid dielectric, or only after development tests of the ACCENT system, can a definite conclusion be reached with regard to the solid spacer design concept.

Because of the uncertainty regarding the effectiveness of solid spacers in the ACCENT electrogenerator, it is recommended that the prototype design be adaptable to testing vacuum dielectric, gas dielectric, solid dielectric, and solid-spacer vacuum- or gas-dielectric versions. This recommendation is reflected in the final mechanical design presented in a later section.

### Thermal Design of Electrogenerator

Heat produced in the ACCENT electrogenerator must be rejected either to the spacecraft structure, or must be rejected to space. Thermal efficiency of the ACCENT electrogenerator is less than 10% because of operation at voltages much less than those required for maximum efficiency. Because of the low thermal efficiency, there is not much difference in heat rejection between thrust-on and thrust-off conditions.

Solid dielectrics suffer appreciable reductions in volume resistivity and dielectric strength above about $150^{\circ}C$, as shown in Appendix E. For this reason, the ACCENT electrogenerator is designed for operation with fuel-element temperatures no greater than $150^{\circ}C$.

A typical heat-generation rate in the fuel layer of promethium-147-oxide electrogenerators is 90 watt/$m^2$ . This heat rate can be transferred by thermal radiation from a fuel

element at 150°C to a collector at 400°K. Temperature drop from mid-point to end of a 6-inch long 10-mil thick aluminum collector is less than 1°C, so heat may be rejected from the collector support structure or from a radiator at about 400°K (127°C). If the heat-sink temperature is 300°K (27°C), then the heat rejection rate from the radiator will be about 1000 watt/$m^2$ .

Ten micro-pound cesium-contact ion thrusters require less than 200 micro-amperes at net accelerating voltages above 20,000 volts, as shown in Figure 4. From Figure 37, it can be seen that at 20,000 volts, there is a thermal inventory of about 0.7 thermal-watts/microampere, so a promethium-147-oxide electrogenerator for a 10-micropound ACCENT system would generate less than 140 watts of heat. Radiator heat flux was estimated (above) at 1000 watt/$m^2$, so a radiator area of 0.14$m^2$ would be required. For example a radiator of dimensions 38x38-cm (15x15-inch) would be sufficient.

From this brief discussion, and from the information in Appendix F, it is evident that the thermal design of ACCENT electrogenerators is simple and that there should be no difficulty in striking a thermal balance with the spacecraft and space environment.

Electrical Design of ACCENT Prototype System

The ACCENT prototype system electrical circuitry must perform three distinct functions. During the pre-launch and launch phases of a mission the ACCENT system electrogenerator voltages must be limited to a low level. Once the mission is underway the circuitry must provide the desired operating conditions for the ACCENT thruster package in response to signals from the vehicle command logic circuitry. Current neutralization of the ACCENT system must be provided at all times by maintaining the neutralizer current equal to the thruster exhaust-beam current. All of these functions can be provided by the recommended electrical design of the ACCENT prototype system shown in Figure 41. Theory of operation, sub-system details, and dynamic characteristics

of this recommended design are described in the following sections.

Theory of Operation. Regulation of the high voltage available from the ACCENT system primary electrogenerator can be accomplished with a shunt regulator which utilizes the electrical impedance of the electrogenerator as its series-dropping resistor. For simplicity the shunting device shown in Figure 41 is a vacuum-tube thermionic diode of conventional design (eg: 1X2) operated with the cathode (filament) in a thermally-limited mode. The control of cathode emission is entirely by control of the filament current. Figure 42 shows a plot of diode current versus filament power for a 1X2. In the event that commercial vacuum diodes such as the 1X2 cannot be flight qualified the design and construction of a replacement with similar characteristics should not be too difficult.

During pre-launch, launch, and thruster shut-down periods, the filament current (and thus diode conductivity) will be at a maximum resulting in a potential difference across the diode (and thus across the electrogenerator and thruster) of a relatively small value. When a thrust-on command is received by the ACCENT system, filament current is decreased to a value that will result in the proper voltage drop across the diode (and thus across the thruster package) to assure proper thruster operation. Thruster high voltage is actively regulated by continuous adjustment of the diode filament current in response to an error signal generated by a comparison of the high voltage with a reference signal. The control range of the regulation circuitry will adequately compensate for the decay in activity of the radioisotope fuel over the total mission time which is illustrated in Figure 3.

Current neutralization of the ACCENT system package can be accomplished by means of an electron gun regulated so that the current of electrons ejected into space is sufficient to maintain the package at a potential no more than a volt or so different from the vehicle itself. The electron gun contains a control grid that is referenced to the vehicle through a

suitable isolation resistance. Electron current depends upon the potential difference between this grid and the electron gun cathode which is electrically connected to the ACCENT system ground. Thus the electron current can be controlled by the potential difference between the vehicle and the ACCENT system package. If the thruster ion current $J_i$ exceeds the magnitude of the electron current $J_e$, then the electron-gun cathode will appear more negative with respect to the control grid thus resulting in an increase in $J_e$. The reverse will also be true, thereby providing for automatic maintenance of overall current neutrality with respect to the vehicle. A bias supply will provide the proper design point value of grid potential to assure proper autogenous operation.

Operation of the ACCENT system thruster will be in the emission-limited mode thus allowing control of ion beam current $J_i$ through control of propellant flow. In the liquid-spray charged-particle thruster, propellant flow is determined by the propellant temperature within the propellant-feed tube, so an electronically controlled heater can be used to ultimately control the beam current.

The 600-volt bias for the thruster extractor electrode can be derived in a number of different ways since the current which must be provided is so small. In the present design the extractor potential is derived from a secondary electro-generator shunted by a suitable resistance to provide a nominal 600-volt source. To avoid the requirement for active regulation of this bias voltage, a small strontium-90 electro-generator could be used in this role.

Details of the various components of the overall electrical circuitry are discussed in the following sections.

Electrical Inverter. A main power inverter is required to provide the necessary operating power to the various components of the system. The input to the inverter in the present design is the vehicle 28-volt direct-current power buss. If the propellant heater power could be supplied from

the thermal power being rejected from the electrogenerator, and if the neutralizer filament could be heated by a radioisotope heater, then the small amount of remaining power for the electrical circuitry might be supplied by thermoelectric generators operating on heat rejected from the electrogenerator. Such refinements in design were considered to be too advanced for the present state of development of the ACCENT system, but are included in the recommended development program described in a later section.

The design of the inverter shown in Figure 43 is along conventional lines and provides for two different electrical outputs; a 100 volt, 10 kHz square wave, and a 5-volt direct-current output to power the control circuitry.

Main Voltage Regulator. The main voltage regulator consists of the shunt vacuum diode and the diode -filament current regulator shown in Figure 44. A constant-voltage supply consisting of T1, CR1-4, L1, R1, C1, and VR1 provide power to the diode filament through the series resistance R2. This resistance is chosen so that the filament power is low enough to assure approximately zero diode conduction due to the lack of thermally-generated cathode electrons. For the 1X2 diode this filament power level is approximately 0.02 watts. Transistor Q1 when in a conducting state serves to shunt current around R2 thus increasing the diode filament power and resulting in a higher diode conductivity. The control of Q1 is obtained from a comparison of the magnitude of the thruster high voltage with a reference voltage provided by R5 and VR2. The voltage divider formed by R7 and R8 reduces the high voltage signal to the level of the reference. The two signals are compared in a conventional integrated circuit operational amplifier, AMP, whose output is the control signal to Q1 through R3. A command logic signal acting through R4 will overide the effect of the reference voltage when it is desired to shut down the thruster.

Propellant Heater Supply. This supply is shown in Figure 45 and includes transformer T1 which matches the propellant

heater impedence to that of the main inverter square-wave output, and provides high-voltage isolation for the heater. The current input to T1 is controlled by a series magnetic amplifier device which is in turn controlled by transistor Q1. The control signal to Q1 is derived from a comparison of the desired thrust level, as defined by a signal from control logic, with a signal proportional to the neutralizer current, $J_e$ . Since propellant flow, and thus thruster beam current $J_i$ , is determined by heater power, and since $J_e$ and $J_i$ will be equal (on a net basis) the effect will be that of beam current regulation.

The signal representing $J_e$ is derived by passing all ejected electrons through R4 thus developing a voltage equal to R4 x $J_e$ and of the order of 1 volt at design beam current. The function of AMP is to compare the beam current signal with the command logic signal and then adjust the conduction of Q1 accordingly. Electrical damping must be provided in this circuitry to prevent excessive oscillation of the propellant heater power. The amount of damping and the method used to provide it will depend heavily on the thermal characteristics of the heater and the propellant tube.

Diodes CR1 and CR2 provide protection for Q1 by shunting out any stray transient signals that might otherwise damage it.

If it is desirable to monitor the heater-current, then transformer CT1 can be included to provide a signal proportional to this current.

Neutralizer Filament Supply: Figure 46 shows the circuitry that supplies power to heat the neutralizer filament. This circuit operates in the same manner as the propellant heater supply with the exception that the control is simply on/off as determined by the command logic control signal.

Neutralizer Grid Bias Supply. This supply is a simple zener-regulated bias source as shown in Figure 47. The

design voltage is chosen to match the characteristics of the neutralizer electron gun and to make up for the voltage drop across R4 in the propellant heater supply. The value of the bias voltage will only be a few volts for any conventional electron gun design. The supply is referenced to the vehicle ground through R2 which provides sufficient isolation to assure that essentially no current will flow between the vehicle and the ACCENT system package, and thus assuring that the overall vehicle potential will not be affected through operation of the ACCENT system thruster.

Power Requirements. A listing of the power required for the ACCENT system circuitry is as follows:

1. Main voltage regulator:
   control power ≃ 0.1 watt
   filament power ≃ 0.08 watt (max)
   electrical efficiency $\eta \simeq .95$
   $P_{in}=(0.1+0.08)/.95+0.19$ watt
2. Neutralizer filament supply:
   filament power ≃ 0.4 watt
   control power ≃ 0.1 watt
   $\eta \simeq 0.95$
   $P_{in}=(0.4+0.1)/0.95=0.53$ watt
3. Neutralizer grid bias supply:
   regulator power ≃ 0.01 watts
   $\eta = 1$
   $P_{in}=0.01/1=0.01$ watt
4. Propellant heater supply
   heater power 0.9 watt
   control power 0.1 watt
   $\eta=0.95$
   $P_{in}=(0.9+0.1)/0.95=1.05$ watt

5. Command Logic power

control power ≈ 1.0 watt

$P_{in}$=1.0 watt

Total power from inverter = 2.72 watts

Inverter losses = 0.15 watts based on the following:

nominal $\beta$ = 50

$V_{sat}$ = 0.3 volts

$V_{BE_{sat}}$ = 1.3 volts

Switching time = 100 nsec (eg: 2N2538)

Frequency = 10kHz

Transformer loss = (2.72+0.15)/0.98 = 0.06 watt

Total input power to inverter = 2.93 watts

ie: = 107ma x 28 volts

Overall Dynamic Characteristics of Electrical System. The time response of all parts of the ACCENT system electrical circuitry is orders of magnitude faster than that of the electrogenerator. This is due to the large electrical capacity and relatively high impedance inherent in the design of the electrogenerator.

Because of the large shunting capability of the voltage regulator, turn-off of thruster voltage can be accomplished almost instantly. However, the turn-on time will be completely controlled by the charging time of the electrogenerator capacitance. Figure 48 shows a simplified equivalent circuit of the electrogenerator, voltage regulator, and thruster. The total surface charge Q in the electrogenerator is (for plane parallel electrodes):

$$Q=\varepsilon S(\phi/g) \tag{27}$$

where $\phi$ is electrogenerator voltage, g is the inter-electrode spacing, S is the fuel-element surface area, and $\phi/g$ is the electric field strength. Charging time t is:

$$t=\varepsilon(\phi/g)S/\dot{Q}=\varepsilon(\phi/g)/j \tag{28}$$

where $\dot{Q}$ is the rate of charge accumulation, and $j$ is the electrogenerator current density. Charging rate $\dot{\phi}$ is:

$$\dot{\phi}=j/(\varepsilon g) \qquad (29)$$

For example, an electrogenerator with a current density of 100 micro-amp/$m^2$ and an electrode spacing of 10-mils will have a charging rate of about 3.5 kilovolts/sec. For the 100 micro-amp/$m^2$ current density, an electrogenerator with an electric field strength of $10^6$ volts/cm will have a charging time of 8.9 seconds. With a field strength of $10^5$ volts/cm, the charging time will be 0.89 seconds.

In normal operation thruster voltage (and thus the charge on the electrogenerator capacitance) will be maintained at a constant value, thereby eliminating the effects of circuit time-constant as a consideration. However, in the event of an electrical breakdown in the thruster the electrogenerator capacitance must be discharged to reduce the voltage to a low enough level to clear or extinguish the breakdown. Since arc breakdowns are low-impedance phenomena the discharge time will be quite short ($\tau$<100ms.) despite the relatively large value of capacity (C≃.05$\mu$fd/$m^2$). If the arc discharge does not extinguish until the electrogenerator charge is reduced to essentially zero then the recharging time will be as given by equation (28). In cases where the arc is cleared at a voltage somewhat greater than zero the recharge time will be commensurately shorter.

Of further concern is the effect on thruster performance of losing high-voltage regulation. Because of the simplicity of the shunt regulator, parallel vacuum diodes can be included to provide regulation in the event of primary diode failure. The possibility still remains that all redundant diodes might fail, in which case there will be no high-voltage regulation. The type of failure to be expected in the case of vacuum diodes should be filament failure resulting in a loss of diode conductivity. With this type of failure, the upper limit on the value of the high voltage will depend on

electrogenerator characteristics, or on the characteristics of the thruster. Figures 49 and 50 show plots of typical operating conditions for both the cesium-contact ion thruster and the charged-particle liquid-spray thruster operated both normally and with complete regulator failure.

With emission-limited operation of the cesium-contact ion thruster, loss of voltage regulation will cause the thruster voltage to increase to the electrogenerator current/voltage characteristic curve. Some increase in neutral-atom fraction can be expected, which would tend to reduce the life of the thruster accel electrodes.[1]

With propellant-flow-limited operation of liquid-spray charged-particle thrusters, loss of voltage regulation will cause both the thruster voltage and current to increase to a point on the electrogenerators current/voltage characteristic curve. This trend is due to the reduction in q/m with increasing thruster voltage[29], thereby causing the current to increase as a consequence of the constant propellant mass-flow rate.

It is clear from these characteristics that gross failure of the regulation system will only result in operation at a somewhat higher thrust level. The amount of excess thrust will depend on the type of thruster and on the age of the mission (ie: on the remaining activity of the electrogenerator fuel).

Mechanical Design of ACCENT Prototype System

A recommended mechanical design of the electrogenerator for the ACCENT prototype system is shown in Figures 51 and 52. This design has five rectangular flat-plate fuel elements. Each face of the fuel element has a fuel layer 1-inch wide and 6-inch long, as shown in Figure 39. This amounts to a total fuel-layer surface area of 60 $in^2$ (387 $cm^2$). With a 2-mil (0.005-cm) promethium-147-oxide fuel layer, the total radioisotope inventory is 1.935 $cm^3$ which corresponds to 9710 curies and about 3.5 thermal watts. At a nominal operating

voltage of 20,000 volts, the primary beta current density should be about 170 micro-amperes/$m^2$; and accounting for 23% leakage current, the electrogenerator current would be about 5 micro-amperes.

Spacing between the fuel elements and collectors can be varied by changing the side and end spacers. The fuel-element assembly, and the collector assembly, are electrically isolated from local ground by insulators. After assembly, the fuel-elements and the collectors can be tensioned with the tension screws.

Assembly can begin with inserting the studs into the lower element plate and element insulators, and into the lower collector plate and collector insulators. Then the lower side pad and lower side block can be slipped over the studs, followed by a fuel element. Then the lower end pad and lower side pad can be slipped over the studs, followed by a collector. Then element spacers and another fuel element can be placed, followed by collector spacers and a collector, and so on until the assembly is completed. Final adjustments can be accomplished by tightening the stud nuts and the tension screws.

The rectangular flat-plate design probably would be the most economical in the early phases of development of fuel elements for the ACCENT electrogenerator. However, the circular-disc geometry has flat fuel elements and collectors, and may be sufficiently economical in fuel form development work. Rectangular flat-plate configurations are not desirable for packaging in a cylindrical containment vessel; flight-prototype electrogenerators probably will have either the coaxial-cylinder, spiral-wound, or circular-disc geometry as illustrated in Figure 6. If the recommended rectangular flat-plate electrogenerator design were chosen and used in the development program, the work in that program probably would not be truly realistic because the rectangular flat-plate geometry is unlikely to be used in flight-prototype systems. If a circular-disc electrogenerator geometry were

used in the development program, then the work would certainly be realistic. For these reasons, an alternate recommended design is included here.

The alternate recommended design is shown in Figures 53 and 54, and has the following design characteristics:

radioisotope fuel: promethium-147-oxide, 90% dense
fuel-layer thickness: 2-mil (0.005 cm)
thruster: 4000 coul/kg liquid-spray
thrust: 10-micropound
specific impulse: 1300 sec.
mission duration: 2-yr
voltage: 20,000 volts
beam current: 24 micro-amperes
electrogenerator j : 132 micro-amp/$m^2$
fuel-layer surface area: 1830 $cm^2$
fuel-element diameter: 5-cm
number of fuel elements: 40
radioisotope inventory: 9.15 $cm^3$ , 45,900 curies, 16.4 thermal-watt
thermal load: 16.4 watt, thrust-off; 15.9 watt, thrust-on
nominal inter-electrode spacing: 0.040-inch (1-mm)
fuel-support foil: 10-mil aluminum
collectors: 10-mil aluminum
radioisotope mass: 60.3 gram
support foil mass: 47.8 gram
collector mass: 49.0 gram
sub total: 157.1 gram (0.35 lb)
containment vessel: 125-mil tantalum
cont. vessel inside diam.: 5.2-cm
contain. vessel L/D: 2
contain. vessel mass: 1200 gram (2.65 lb)
TOTAL 1357 gram (3.0 lb)

If the inter-electrode spacing could be reduced to 0.008-inch (0.2-mm), then the cylinder L/D would be less than 1.0, and the containment-vessel mass would be only 700 gram (1.55 lb) and the total would be only 1.9 lb. A spacing of 8-mil and

a voltage of 20,000 volts results in an electric field strength of $10^6$ volt/cm.

The alternate recommended design is intended to be realistic in all regards. A containment vessel is provided that should be more than sufficient for radiation shielding, since the 125-mil tantalum walls are about twice as thick as necessary. Collector and fuel-element discs (shown in Figure 54) are mounted on studs, three studs for the collectors, and three studs for the fuel elements. Each stud is bottom-screwed into tantalum plugs, which in turn are mounted in insulators, which in turn are mounted through the tantalum containment vessel bottom plate. Collectors and fuel elements are alternately stacked onto the threaded aluminum studs. For example, each collector (see Figure 54) has three holes to receive the three collector studs. Each collector also has three relief slots through which the fuel-element studs and spacers can pass without contacting the collector. Spacers maintain the desired spacing between the collectors and the fuel elements. This spacing can be changed by using alternate sets of spacers. All spacers are made from aluminum tubing to fit easily over the studs, and have precision lengths to prevent accumulation of positioning error.

Electrical contact with the electrogenerator can be made by attaching electrical leads to the tantalum plugs.

Heat generated in the electrogenerator can be rejected from the surface area of the containment vessel, which is $\pi x6x11.3 + 2x\pi x3^2 = 270$ cm$^2$ . With an emittance of unity, the 16.4 watts of heat can be rejected to surroundings at $300^{\circ}$K ($23^{\circ}$C) if the containment vessel has a temperature of $319^{\circ}$K ($42^{\circ}$C). Heat generated in the electrogenerator can be transferred from the cylindrical array of collectors and fuel elements from the outer area of the array, which is $\pi x5x10 + 2x\pi x2.5^2 = 196$ cm$^2$ , to the containment vessel. With an emittance of unity, the 16.4 watts can be transferred if the fuel element and collector assembly is maintained at

425°K (152°C). This is an acceptable operating temperature, so additional heat rejection surfaces are not needed. It is notable that this operating temperature will be reached only when the containment vessel is thermally isolated in a high vacuum. If the vessel is mounted to a heat-conducting support structure, the operating temperature will be lower. Furthermore, conduction of heat along the aluminum studs and aluminum spacers to the tantalum plugs has not been included in the calculations, and this mode of heat transfer will also reduce the operating temperature.

For convenience in performing tests with the ACCENT prototype system, both the bottom plate and the cover plate of the containment vessel should be bolted to the cylindrical portion. Two cover plates should be provided, one with a fitting for attachment to a high-pressure $SF_6$ system, and the other with a fitting for attachment to a vacuum system.

## RECOMMENDED DEVELOPMENT PROGRAM FOR ACCENT SYSTEM

A two-phase program is recommended for the development of the ACCENT system to a flight-prototype status. The first phase of this recommended program would include the fabrication and testing of the prototype design described in the previous sections, with a simulated thruster. The second phase would include aerospace safety analysis and design, assembly of a total flight-prototype ACCENT system including a liquid-spray thruster, and performance testing.

Principal items in the first phase of the recommended development program are as follows:

a. fabrication and assembly of circular-disc electrogenerator without radioisotope fuel
b. construction of electrical system
c. construction of test console, with thruster simulator
d. electric tests of cold electrogenerator with vacuum, $SF_6$, solid dielectric, and solid spacers; with design changes and adjustments as required
e. vacuum-deposition of promethium-147-oxide onto fuel elements
f. performance tests of system with simulated thruster load, over a wide range of conditions

In the interest of obtaining realistic test results, it is recommended that the complete 40-element circular-disc design be planned for this phase of the development program. This is of particular importance in assessing the effectiveness of the thermal design of the electrogenerator, and in determining the influence of the total electrode surface area on leakage current and electric breakdown limits.

Upon the successful completion of the first phase of the development program, it is recommended that a flight-prototype development phase be initiated. This second phase would include the following principal items:

a. design of flight-prototype system, based on the results obtained in the first-phase tests
b. aerospace safety analysis, resulting in a firm design for the containment vessel
c. refinement of fuel-element design and fabrication methods to a satisfactory quality level
d. construction of a liquid-spray thruster
e. construction of flight-prototype system
f. test of flight-protoype system

Finally, it is recommended that other applications for the ACCENT electrogenerator, such as auxiliary power, should be considered wherever possible without undue expense to the ACCENT system development program.

## REFERENCES


1. Mickelsen, W.R.: Advanced Concepts in Electric Propulsion. AIAA Paper No. 67-426. (July, 1967).

2. Strutt: Phil. Mag., 6, 588, (1903).

3. Mosely, H.G.J.: The Attainment of High Potentials by the Use of Radium. Proc. Roy. Soc., 88, 471, (1913).

4. anon.: A New Electronic Battery. (a news report on an oral address by J.B. Kramer). The Electrician. p.497 (October 31, 1924).

5. Pool, M.L.: Potential Nuclear Monokinetic Electron Sources. J. Appl. Phys., 15, 716, (October 1944).

6. Lobanov, I.A., and Beliakov, A.P.: Comptes Rendus, Acad. Sci. USSR, 47, 332, (1945).

7. Miller, P.H., Jr.: A New Type of Electrostatic Generator. Phys. Rev., 69, 666, (1946).

8. Linder, E.G.: Nuclear Electrostatic Generator. Phys. Rev., 71, 129 (1947).

9. Linder, E.G., and Christian, S.M.: The Use of Radioactive Material for the Generation of High Voltages. Phys. Rev., 83, 233, (1951).

10. Linder, E.G., and Christian, S.M.: The Use of Radioactive Material for the Generation of High Voltage. J. Appl. Phys., 23, 1213, (1952).

11. Linder, E.G., and Rappaport, P.: Radioactive Charging through a Dielectric Medium. Phys. Rev., 91, 202,(1953).

12. Rappaport, P., and Linder, E.G.: Radioactive Charging Effects with a Dielectric Medium. J. Appl. Phys., 24, 1110, (1953).

13. Anno, J.N.: A Direct-Energy-Conversion Device Using Alpha Particles. Nuclear News, 5, 3, (December, 1962).

14. Plummer, A.M., and Anno, J.N.: Battelle Studies on the Triode Concept of Direct Energy Conversion. Paper presented at the Summer Institute on Direct Energy Conversion at the Universtiy of Illinois. (July, 1963).

15. Plummer, A.M., and Anno, J.H.: Conversion of Alpha Particle Kinetic Energy into Electricity. ANL-6802, pp.170-180, AMU-ANL Conference on Direct Energy Conversion. (November 4-5, 1963).

16. Plummer, A.M., Gallagher, W.J., Mathews, R.G., and Anno, J.N.: The Alpha-Cell Direct-Conversion Generator. Battelle Memorial Institute (NASA CR 54256), (30 Nov. 1964).

17. Low, C.A., Jr. and Mickelsen, W.R.: An Electrostatic Propulsion System with a Direct Nuclear Electrogenerator. Paper presented at IAS National Propulsion Meeting, Cleveland, Ohio, (March 9, 1962). Also published in Astronautics and Aerospace Engineering, 21, 58, (December, 1962).

18. Low, C.A., Jr. and Mickelsen, W.R.: A Radioisotope Electrostatic Propulsion System. Am. Nuclear Soc. Trans., 5, 429, (November, 1962).

19. Mickelsen, W.R., and Low, C.A., Jr.: Potentialities of the Radioisotope Electrostatic Propulsion System. AIAA Paper No. 63048A, (March, 1963). Also published in Astronautics and Aerospace Engineering, p.52, (October 1963).

20. Cohen, A.J. and Low, C.A., Jr.: A Parametric Study of Direct Nuclear Electrogenerator Cells Using a Beta Emitting Source. AIAA Paper No. 63048B. (March, 1963).

21. Cohen, A.J.: A Numerical Analysis of Direct Nuclear Electrogenerator Cells that Use Cerium 144 Beta-Emitting Radioisotope Sources. NASA TN D-2070. (November, 1963).

22. Interim Design Report for Preliminary Design Study for the ACCENT System. Contract NAS5-10366. (3 April 1967 - 2 August 1967).

23. Berger, M.J., and Seltzer, S.M.: Energy Spectra and Angular Distribution of Electrons Transmitted through Sapphire ($Al_2O_3$) Foils. NASA SP-3008. (1964).

24. Van Tuyl, H.H., Roberts, F.P., and Wheelwright, E.J.: Shielding Requirements for Promethium Sources. HW-77375. (April, 1963).

25. Van Tuyl, H.H.: Bremrad - A Computer Code for External and Internal Bremsstrahlung Calculations. HW-83784. (September, 1964).

26. Berger, M.J., and Seltzer, S.M.: Tables of Energy Losses and Ranges of Electrons and Positrons. NASA SP-3012. (1964).

27. Rohrmann, C.A.: Radioisotope Heat Sources. HW-76323, REV 1. (15 October 1963).

28. West, W.S., Parker, A.J., Jr., and Pyatt, D.W.: An Aerospace Nuclear Safety Analysis of a $Pm_2O_3$ Radioisojet Thruster. NASA Goddard Space Flight Center X-701-67-279. (June 1967).

29. Kidd, P.W.: Parametric Studies of a Single Needle Colloid Thruster. AIAA Paper No. 67-530. (September, 1967).

Table I - Component specific mass for some electrogenerator design concepts.

| component | material | Thickness, $\tau$ inch | cm | density $\sigma$,gm,cc | specific mass gm/cm$^2$ | kg/m$^2$ |
|---|---|---|---|---|---|---|
| collector | Al | .010 | .0254 | 2.4 | .061 | |
| support foil | Al | .010 | .0254 | 2.4 | .061 | |
| two fuel layers | $Pm_2O_3$ | .004 | .010 | 6.6 | .066 | |
| TOTAL | | | | | .188 | 1.88 |
| TOTAL FOR TWO SIDES | | | | | | .94 |
| collector | Al | .125 | .317 | 2.4 | .76 | |
| support foil | Al | .010 | .0254 | 2.4 | .06 | |
| two fuel layers | $SrTiO_3$ | .079 | .20 | 3.7 | .74 | |
| TOTAL | | | | | 1.56 | 15.6 |
| TOTAL FOR TWO SIDES | | | | | | 7.8 |

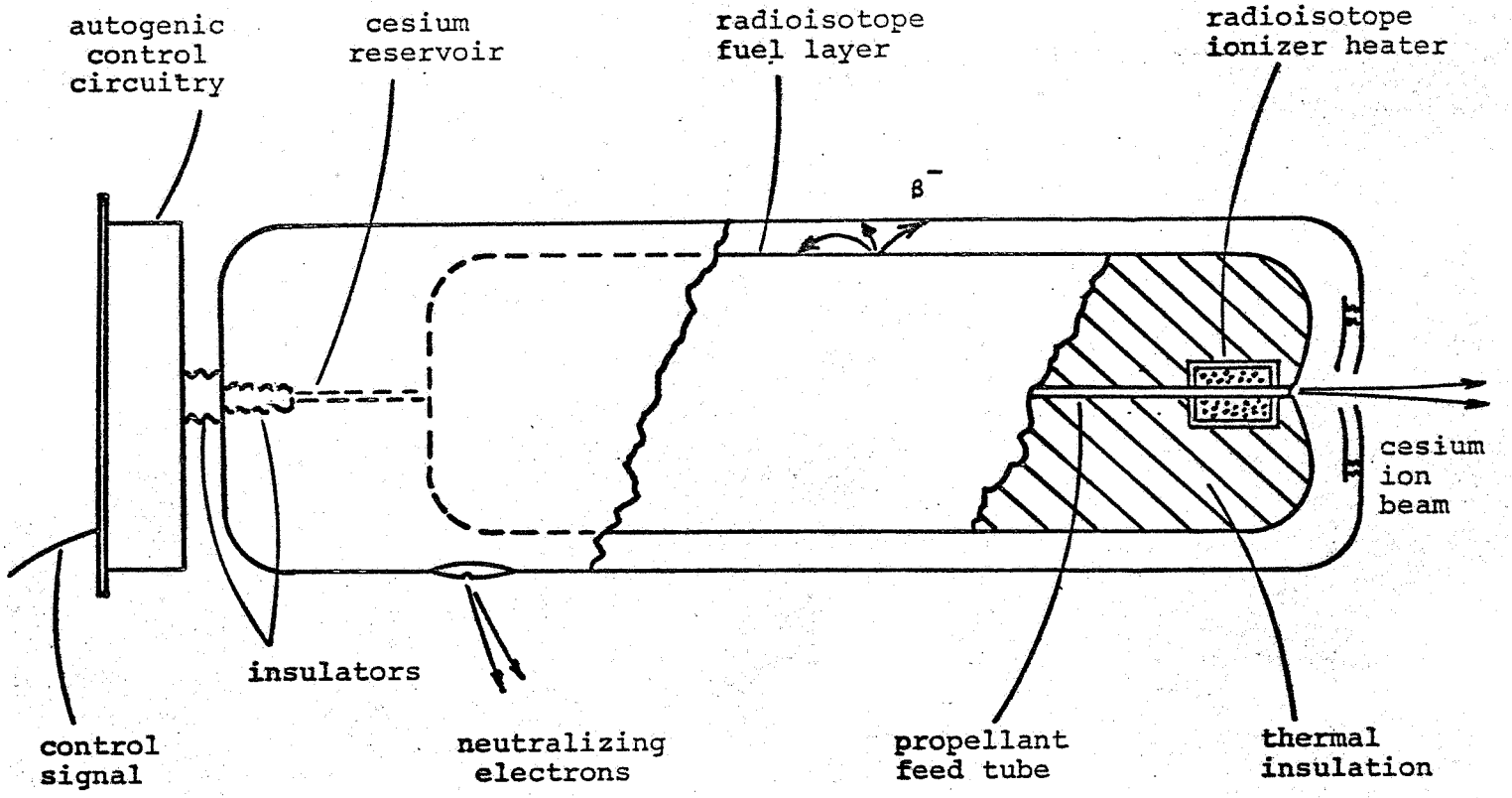


FIG. 1 - ACCENT System principles (autogenically-controlled-cesium-electro-nuclear-thrust system).

THE DANE COMPANY
FORT COLLINS, COLORADO 80521

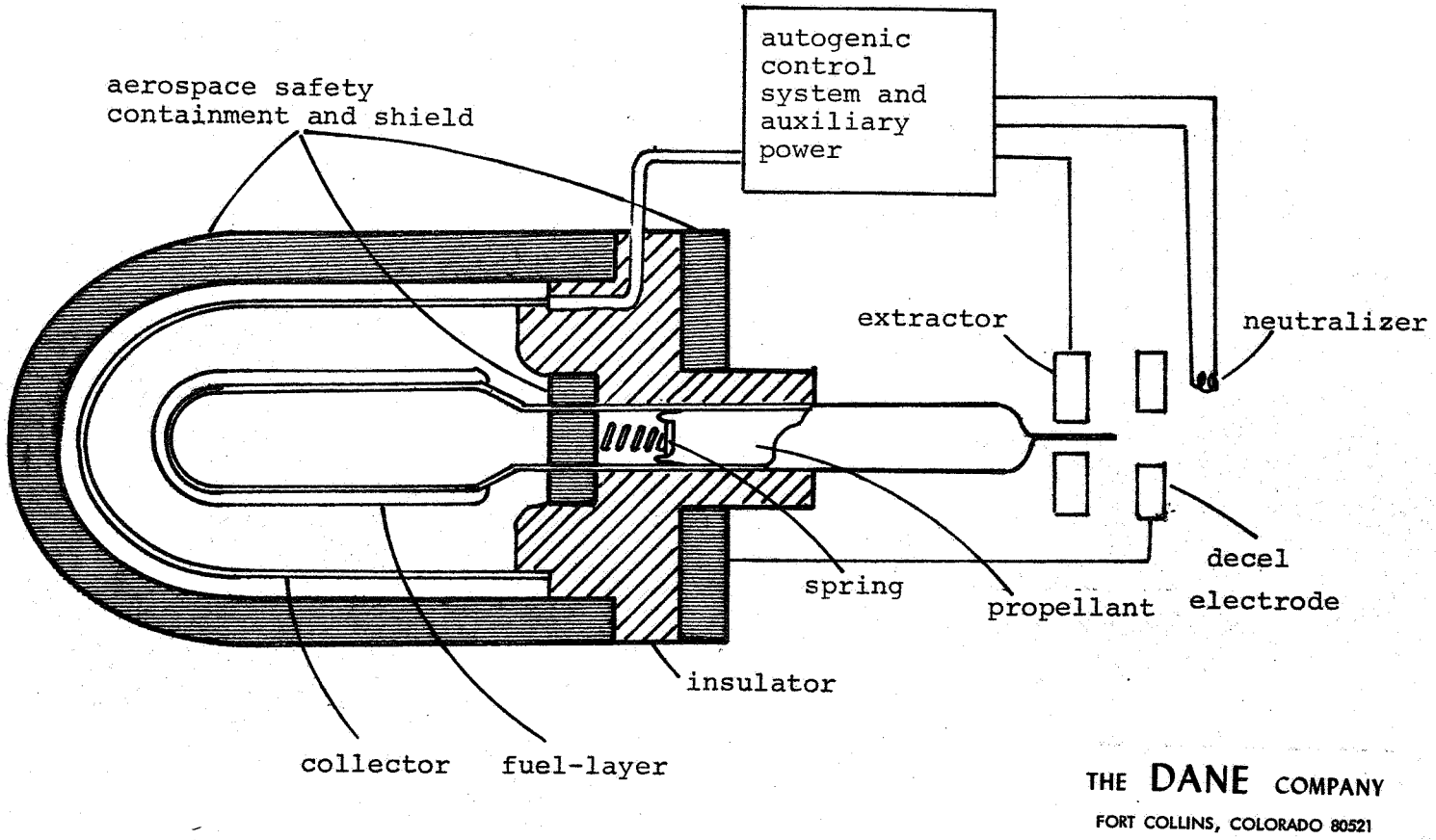


FIG. 2 - ACCENT system with liquid-spray thruster (autogenically-controlled-colloid-electro-nuclear-thrust system).

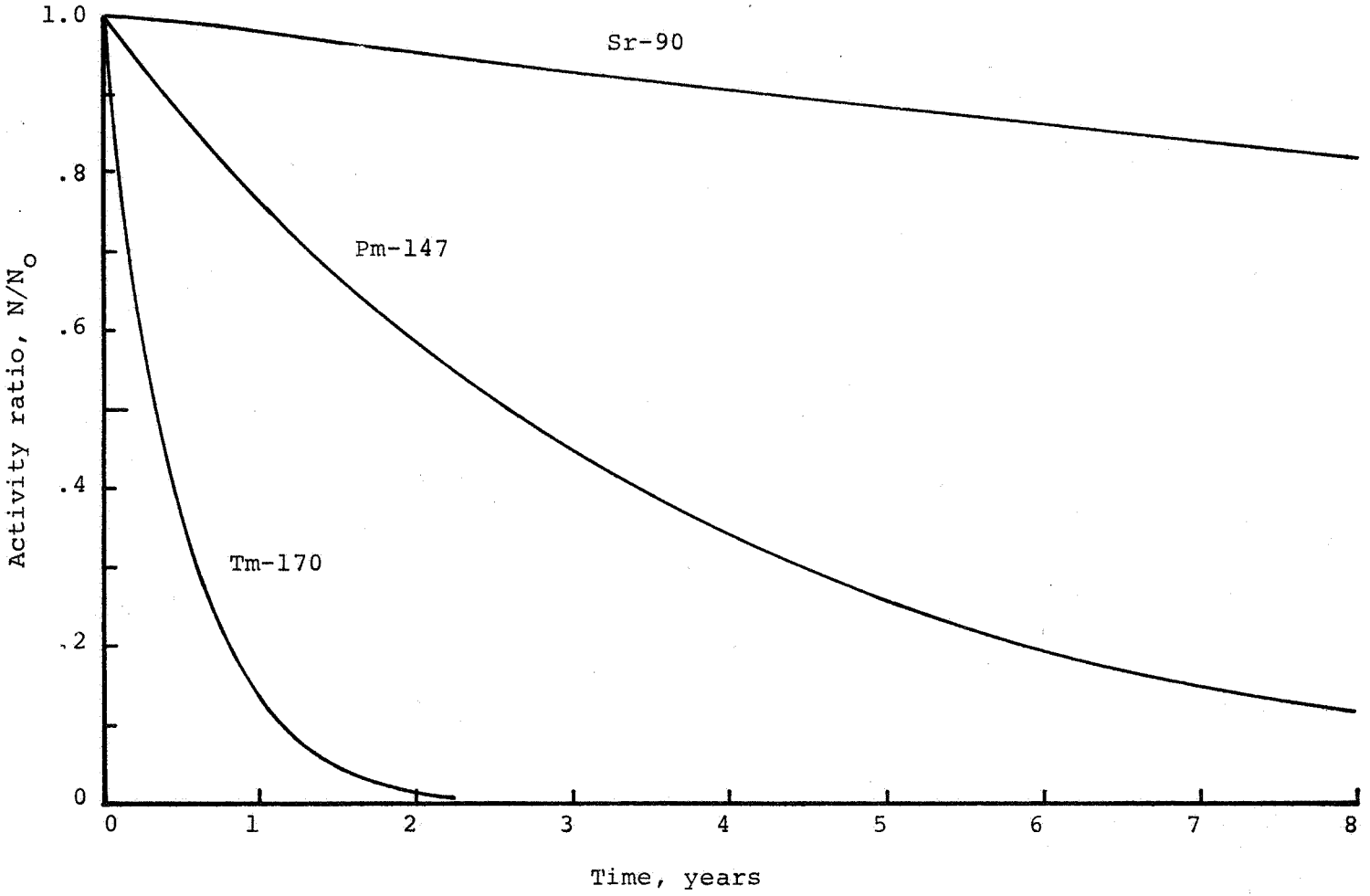


FIG. 3 - Decay of radioisotopes.

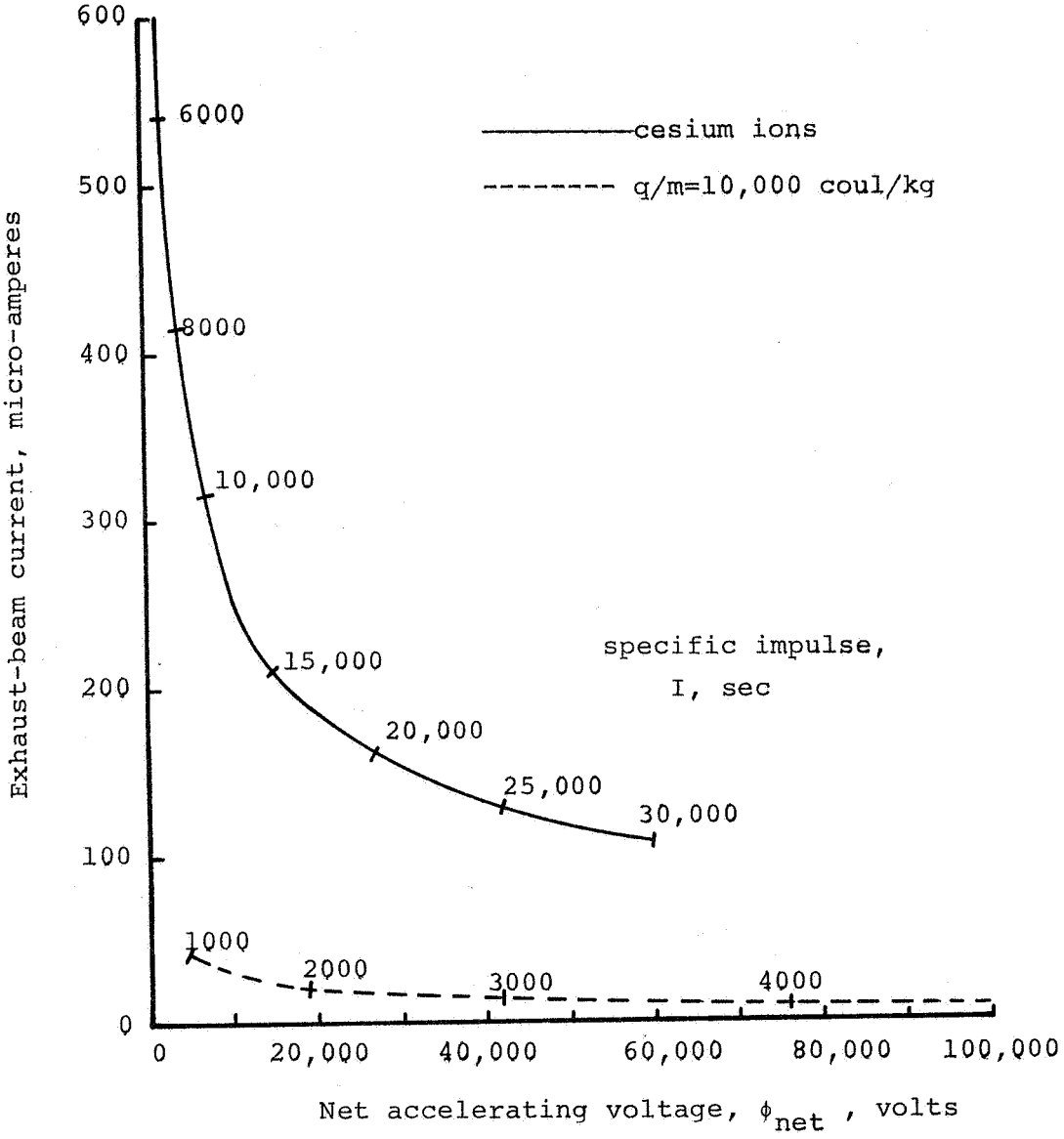


FIG. 4 - Thruster operating characteristics for 10-micropound thrust.

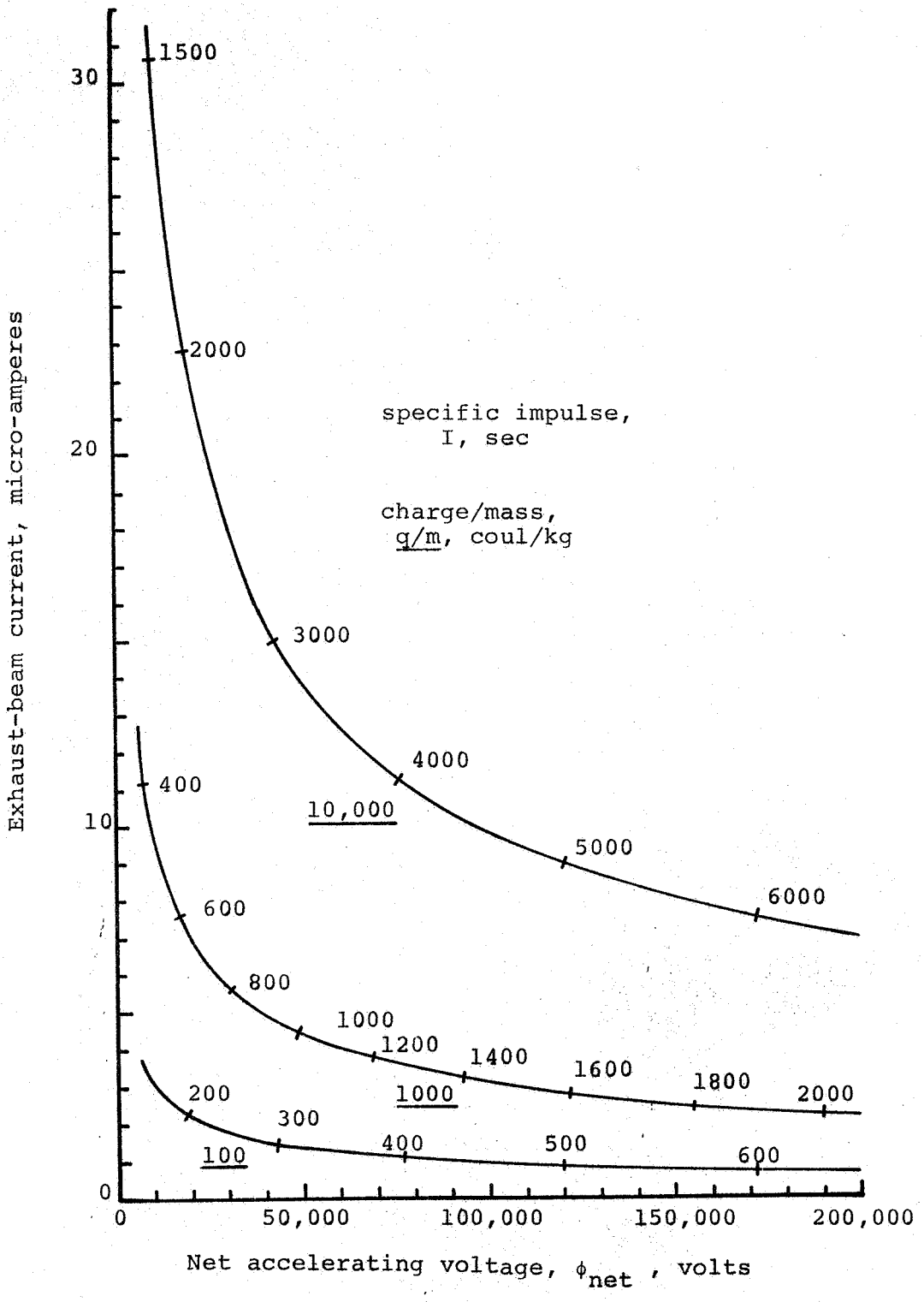


FIG. 5 - Charged-particle thruster operating characteristics for 10-micropound thrust.

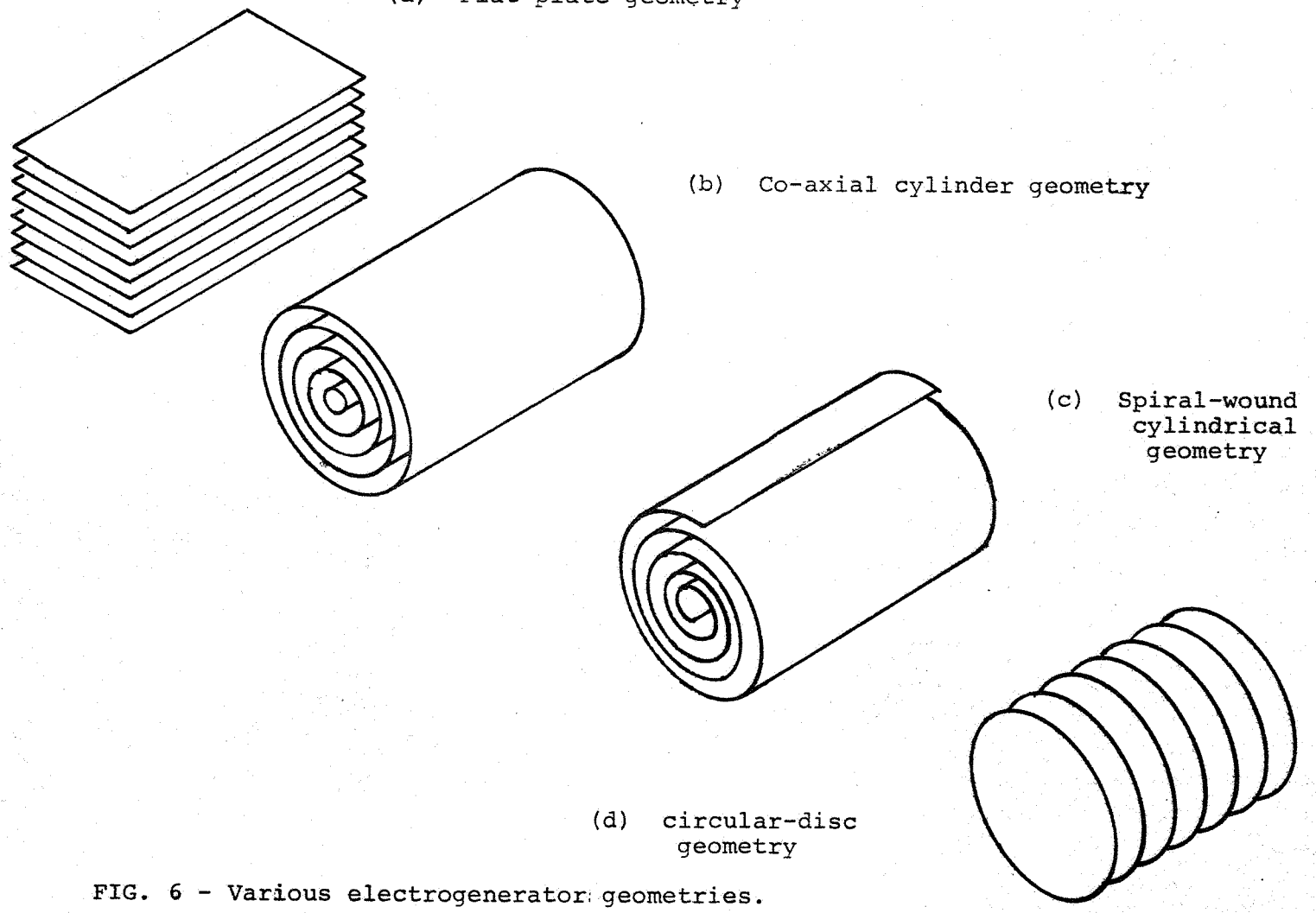


FIG. 6 - Various electrogenerator geometries.

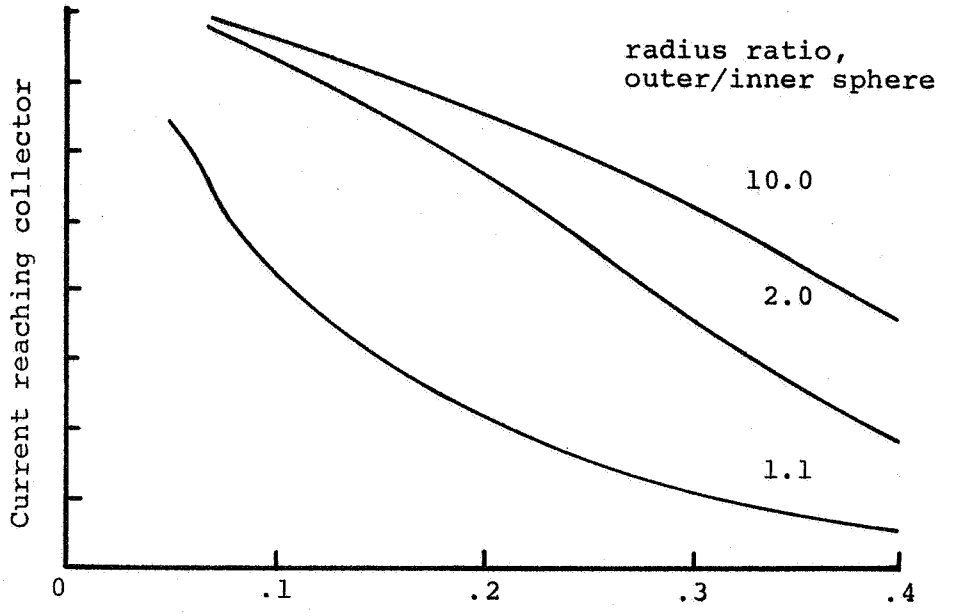


(a) concentric spheres

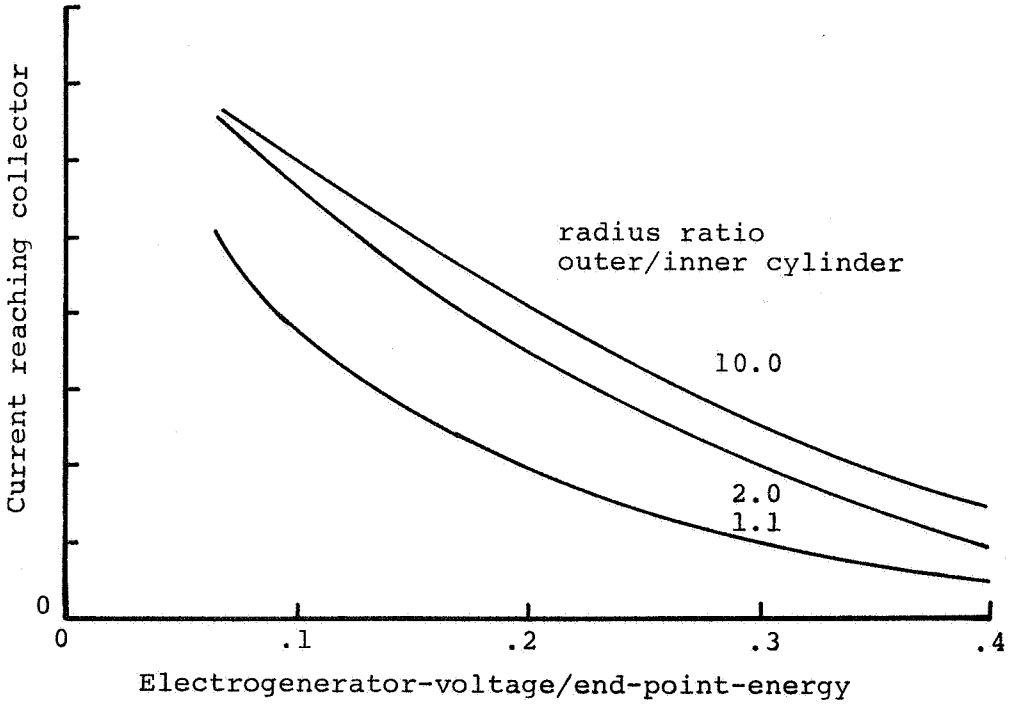


(b) coaxial cylinders

FIG. 7 - Relative currents reaching collector for concentric-sphere and coaxial-cylinder electrogenerator configurations.

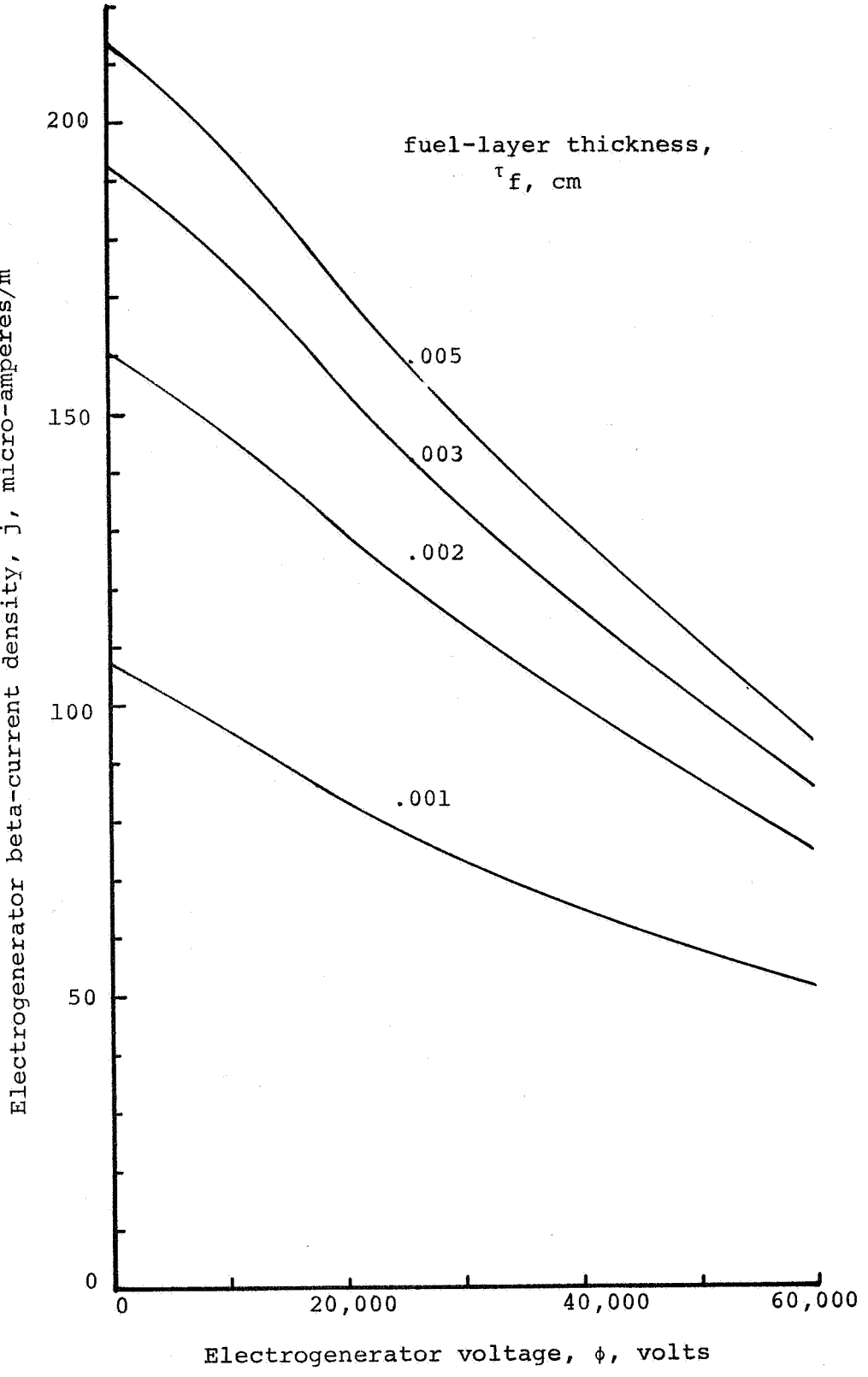


FIG. 8 - Primary beta current in $Pm_2O_3$, 90% dense, electrogenerator with thick support foil.

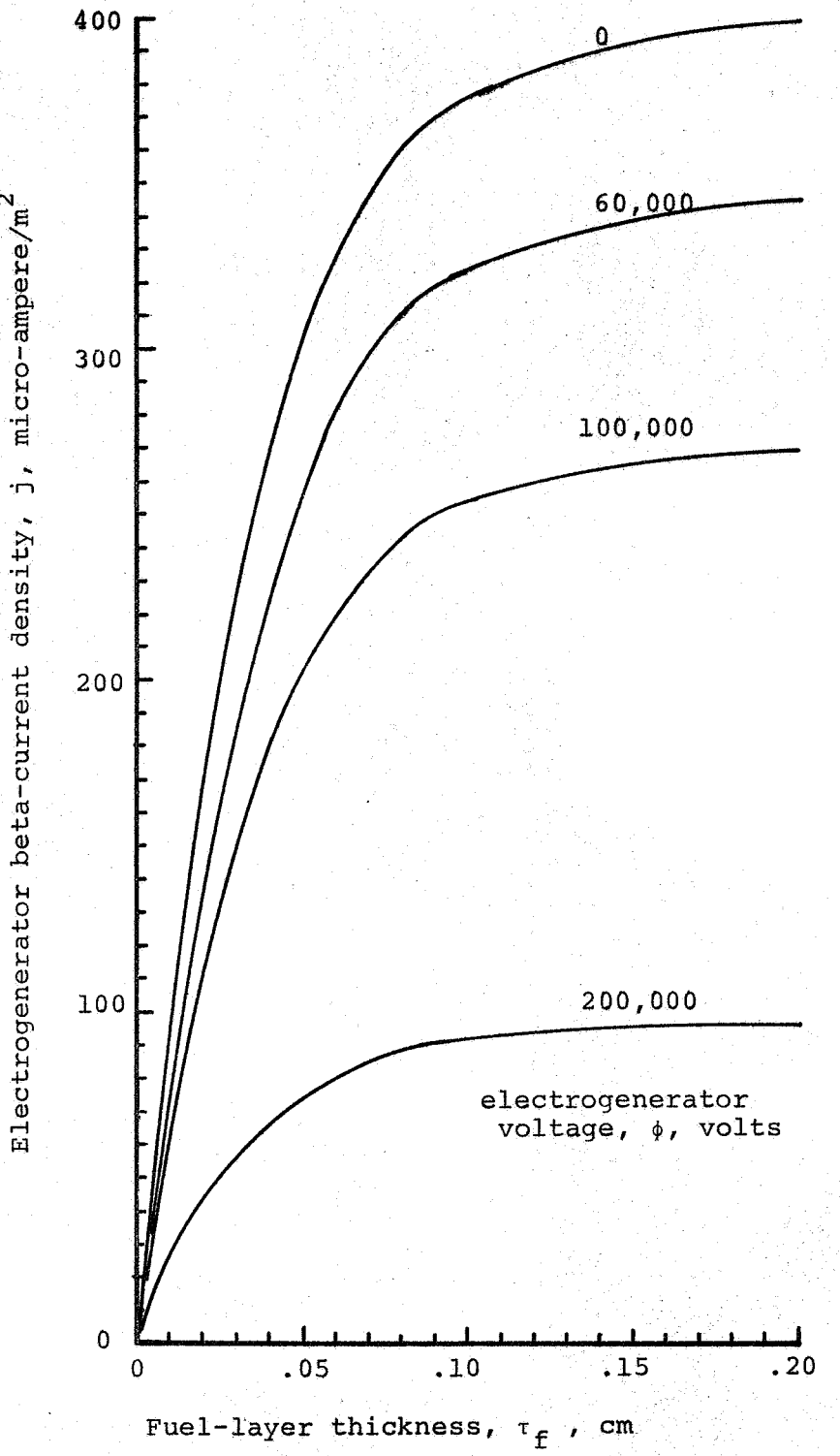


FIG. 9 - Electrogenerator current density for strontium-90-titanate, 90% dense, fuel layers, including contribution from fuel layer on other side of 10-mil aluminum support foil.

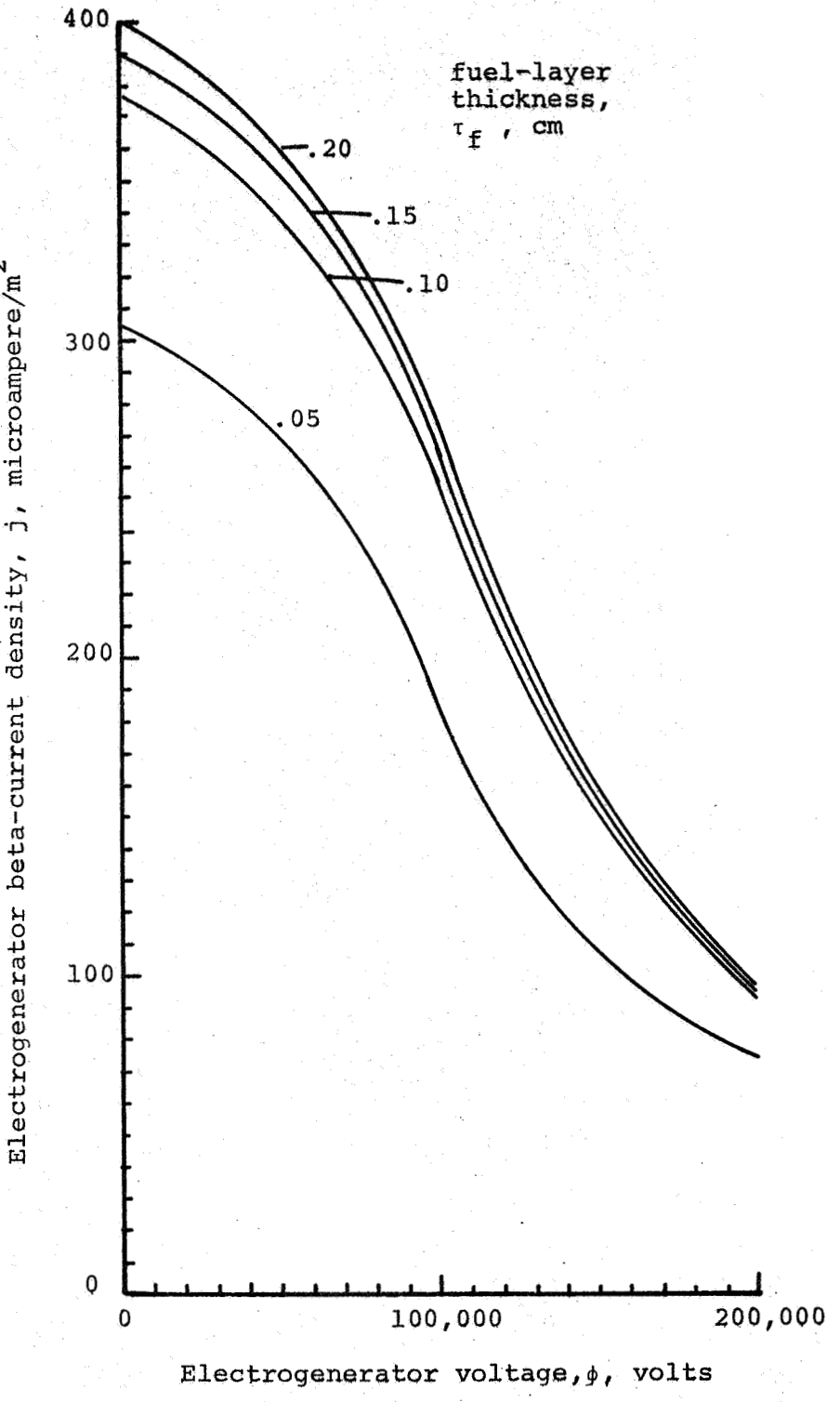


FIG. 10 - Electrogenerator beta-current density with strontium-90-titanate fuel layers on two sides of 10-mil aluminum support foil.

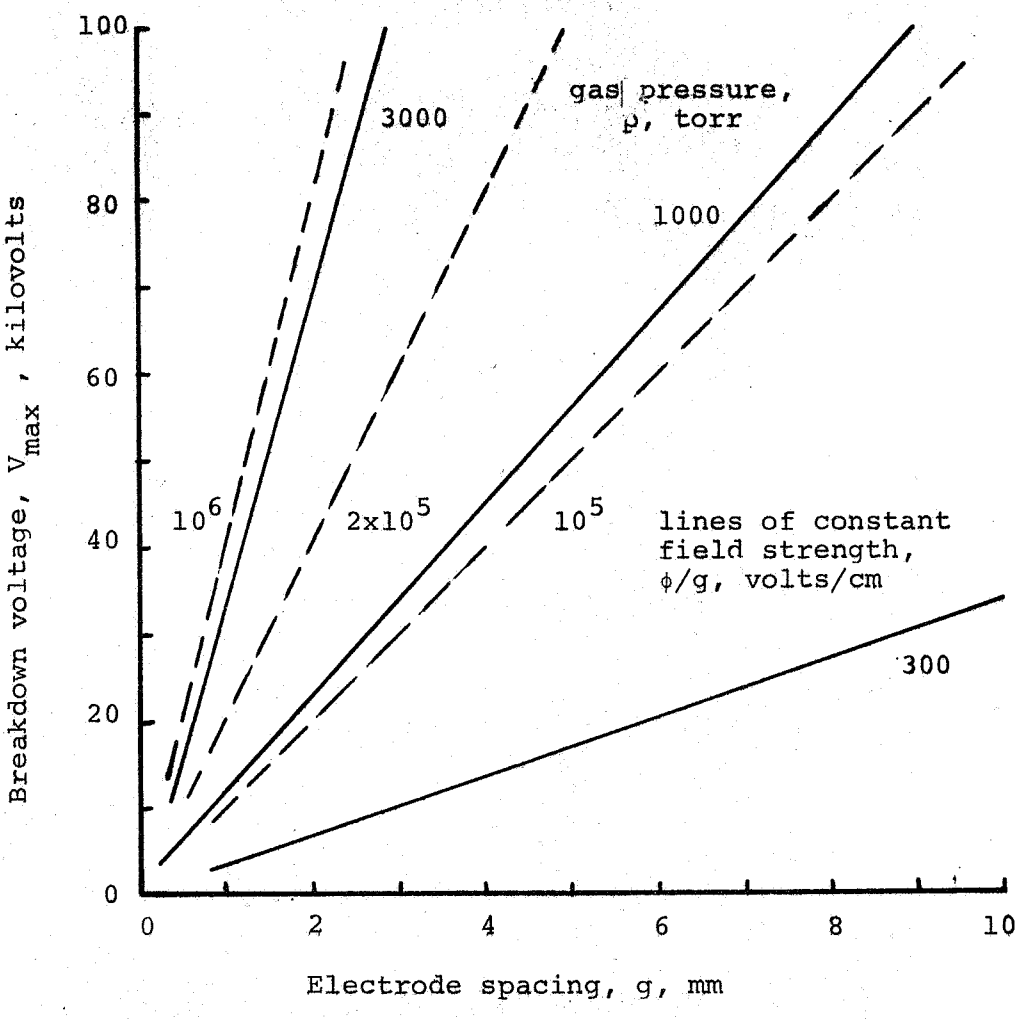


FIG. 11 - Electric breakdown voltage with $SF_6$ gas dielectric.

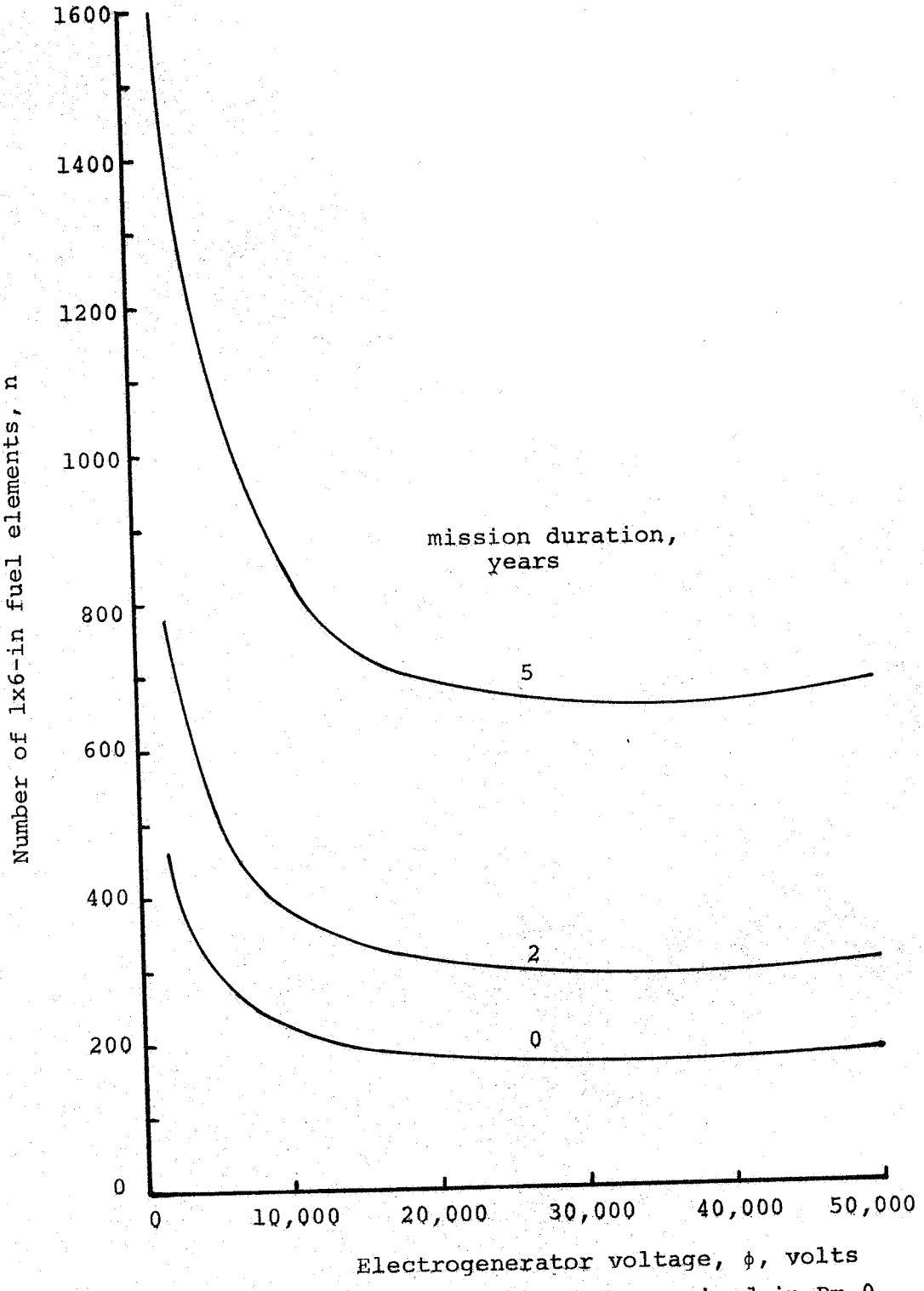


FIG. 12 - Number of 1x6-in fuel elements required in $Pm_2O_3$, 90% dense, electrogenerator for 10-micropound cesium-contact ion thruster. Fuel layer thickness $\tau_f$=.005 cm, two sides of 10-mil aluminum support foil.

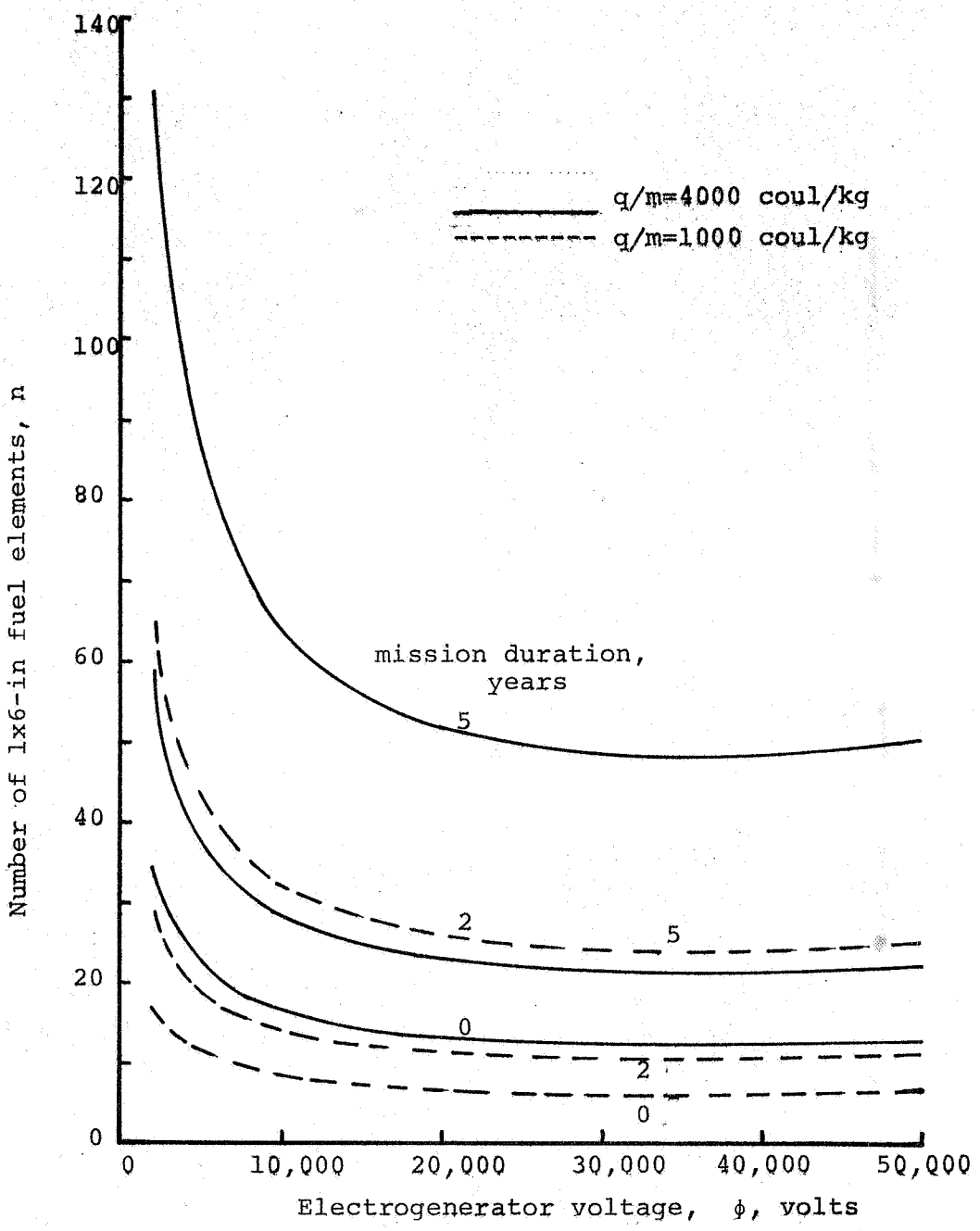


FIG. 13 - Number of 1x6-in fuel elements required in $Pm_2O_3$. 90% dense, electrogenerator for 10-micropound charged-particle thruster. Fuel-layer thickness, $\tau_f$=.005 cm, two sides of 10-mil aluminum support foil.

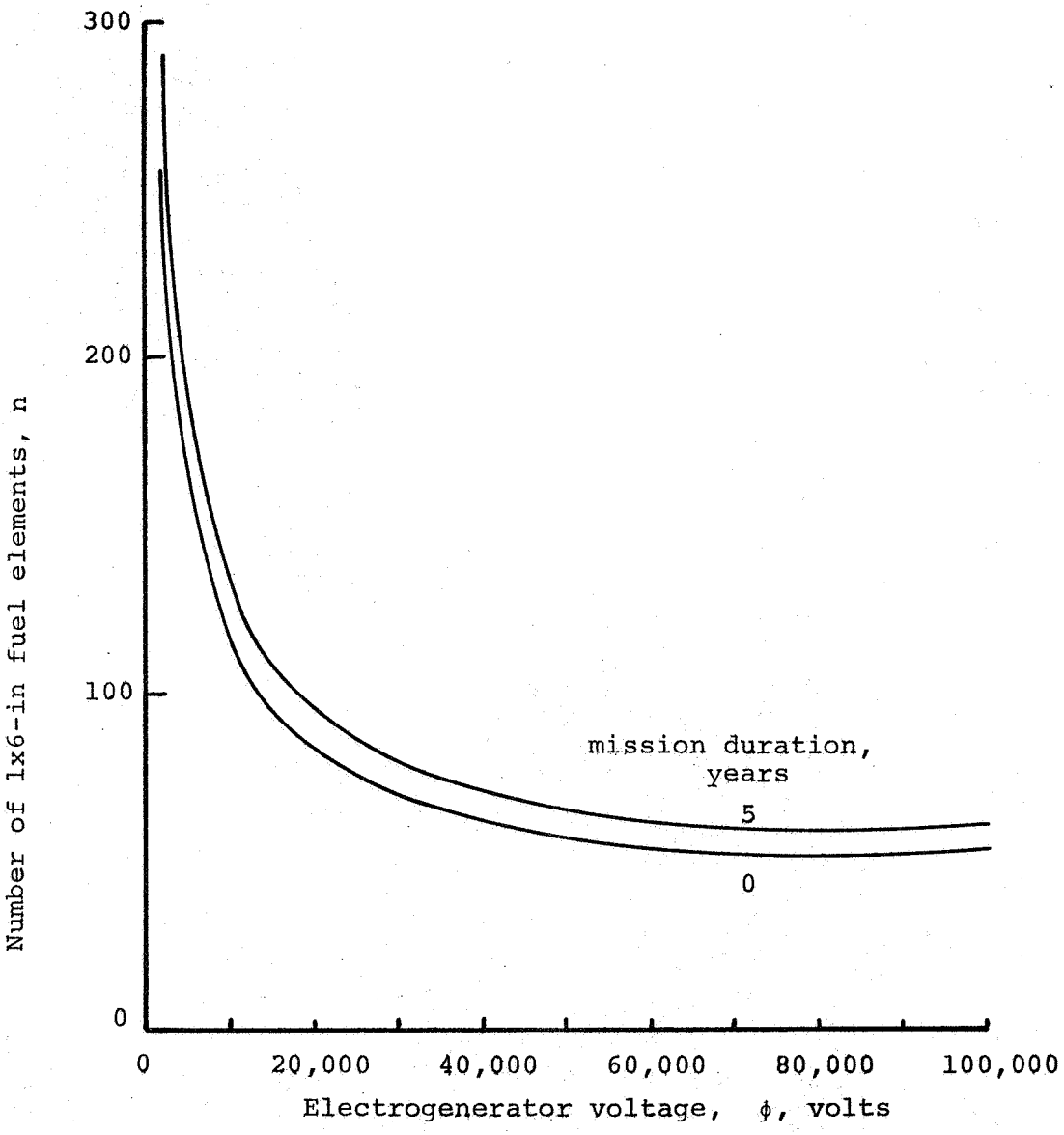


FIG. 14 - Number of 1x6-in fuel elements required in $SrTiO_3$, 90% dense, electrogenerator for 10-micropound cesium-contact ion thruster. Fuel-layer thickness, $\tau_f$=0.1 cm, two sides of 10-mil aluminum support foil.

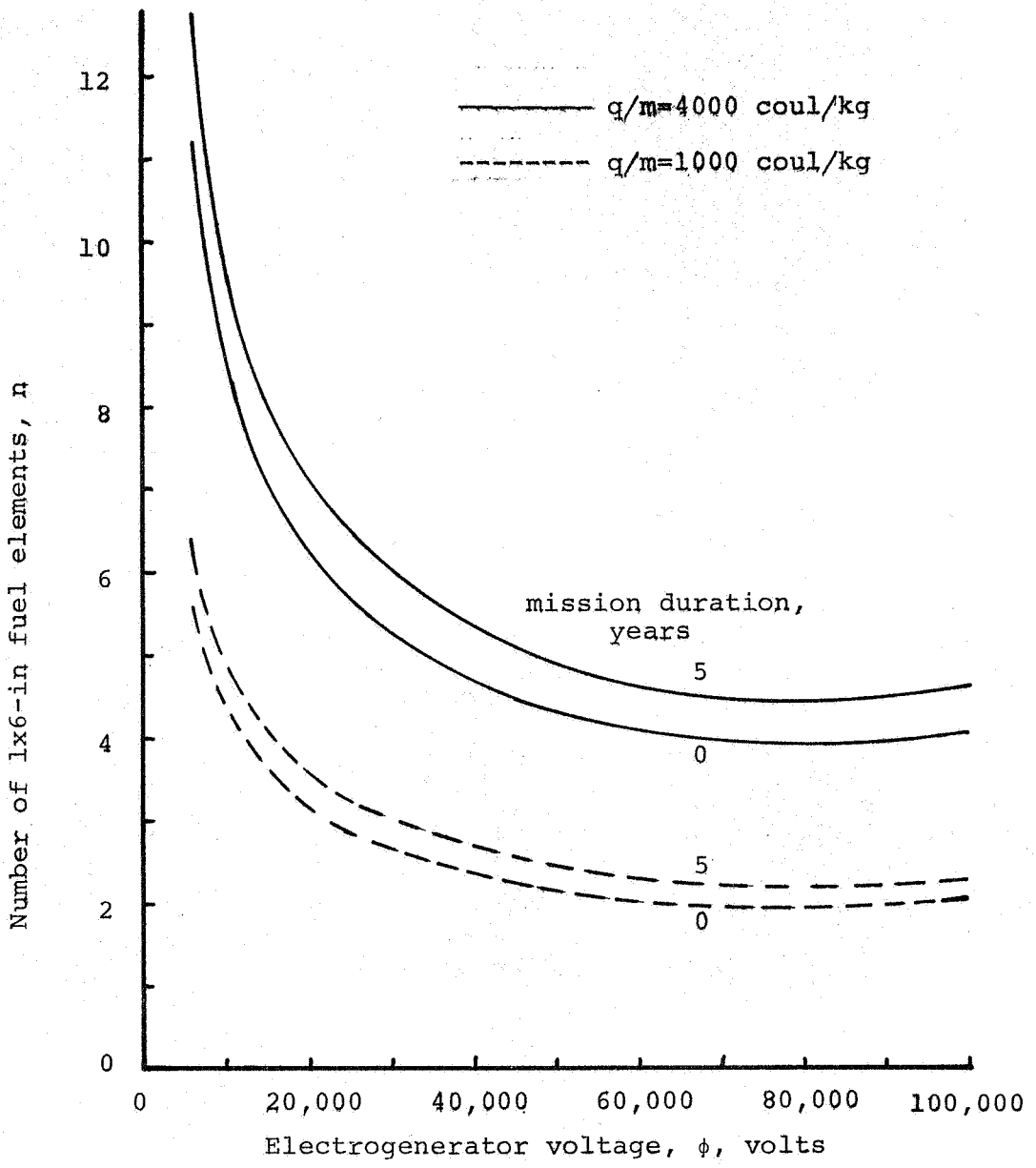


FIG. 15 - Number of 1x6-in fuel elements required in $SrTiO_3$, 90% dense, electrogenerator for 10-micropound charged-particle thruster. Fuel-layer thickness, $\tau_f$=0.1 cm, two sides of 10-mil aluminum support foil.

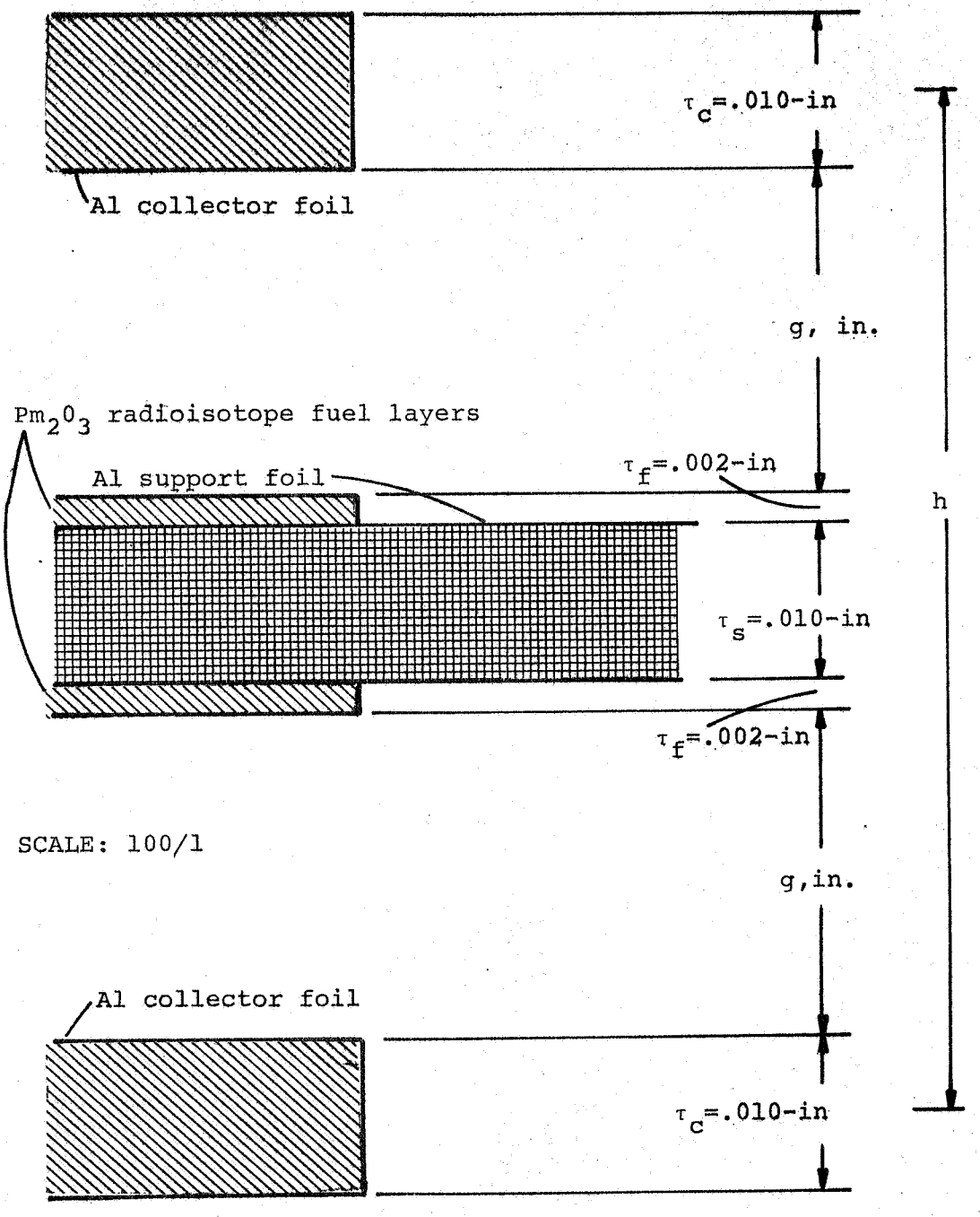


FIG. 16 - Design concept for promethium-147 electrogenerator with vacuum or $SF_6$ dielectric.

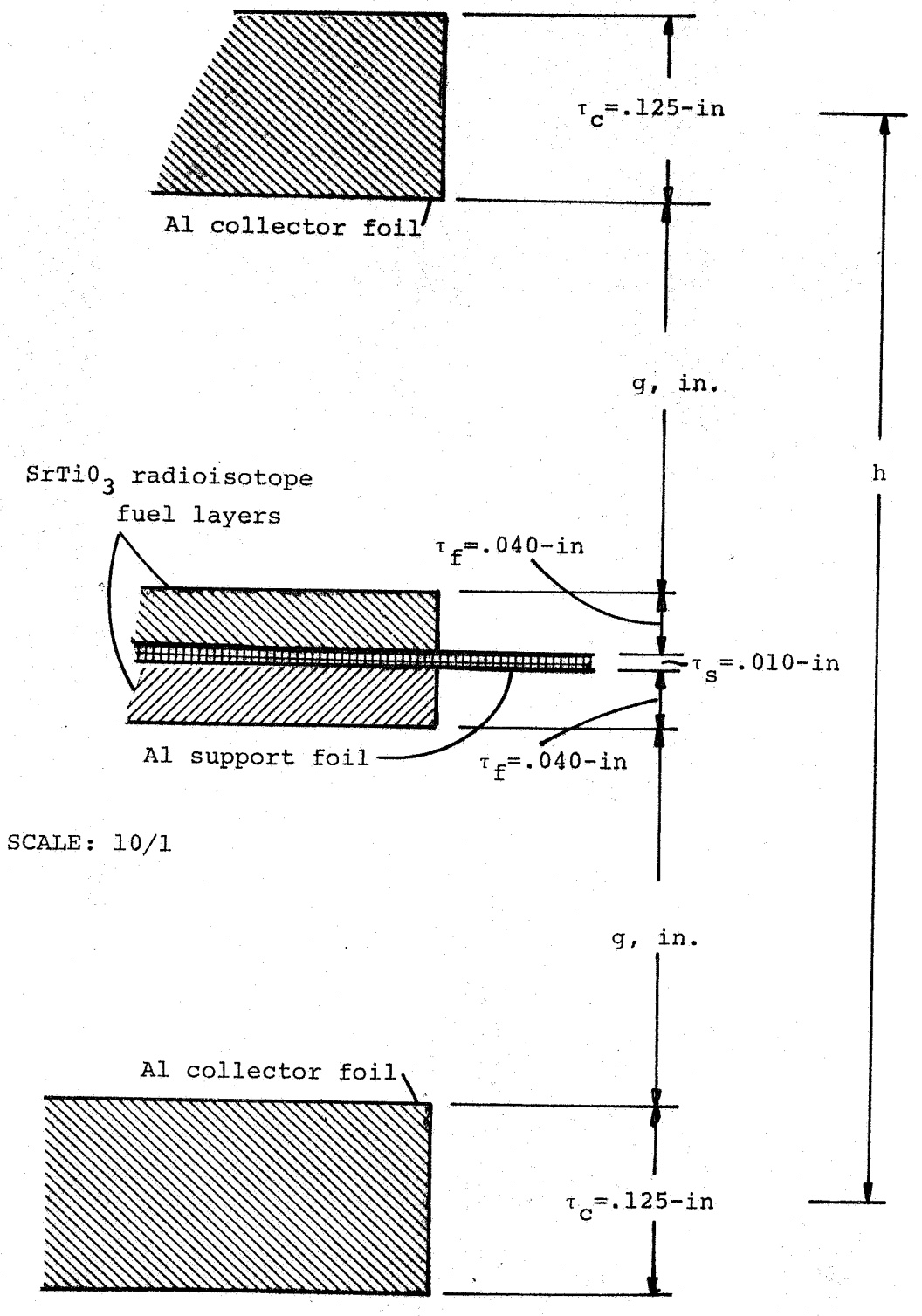


FIG. 17 - Design concept for strontium-90 electrogenerator with vacuum or $SF_6$ dielectric.

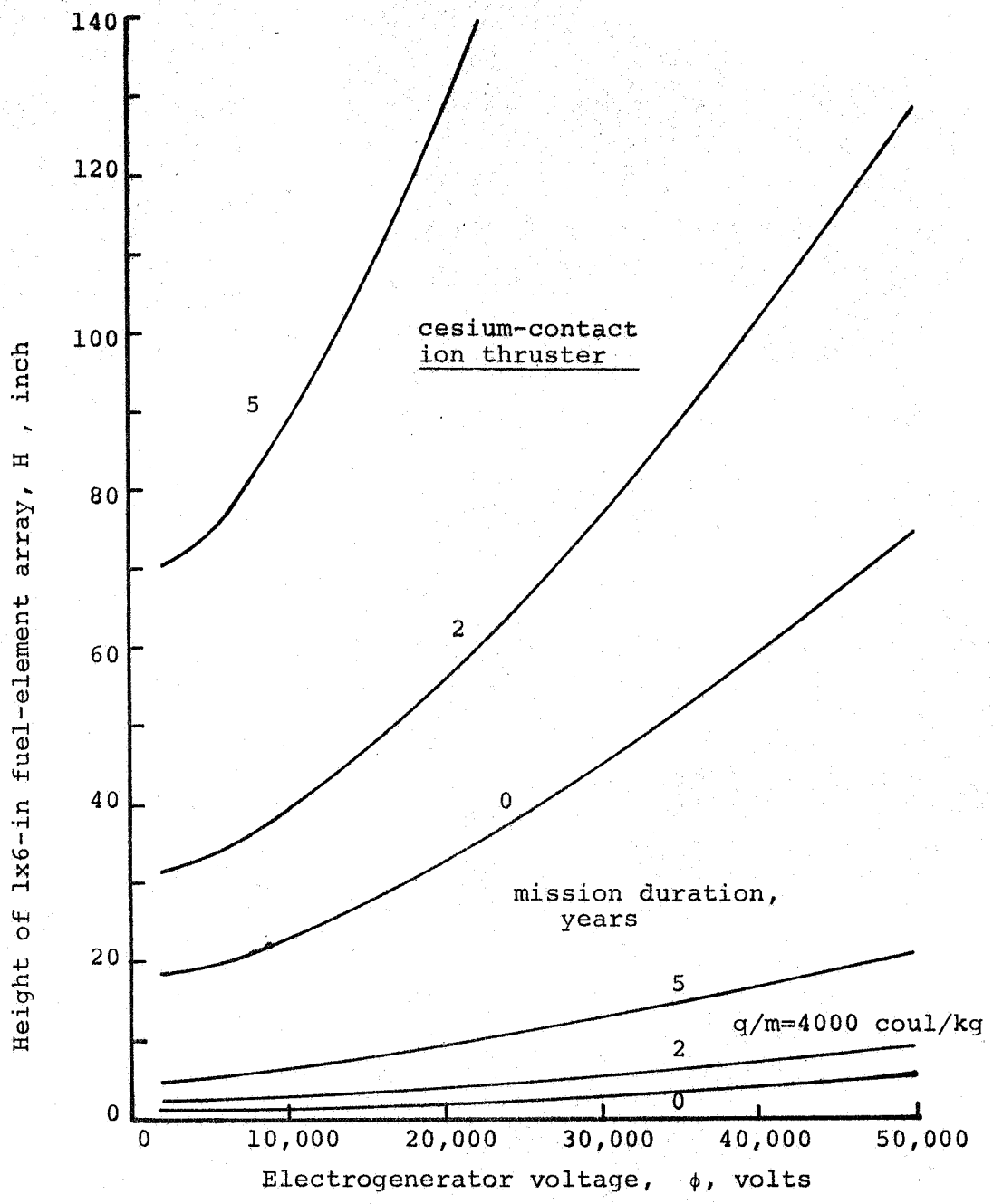


FIG. 18 - Total height of 1x6-in fuel-element arrays in $Pm_2O_3$ , 90% dense, electrogenerator for 10-micropound thrusters. Fuel-layer thickness, $\tau_f$=.005 cm, two sides of 10-mil aluminum support foil. Collector, 10-mil aluminum. Electric field strength, $\phi/g=10^5$ volts/cm.

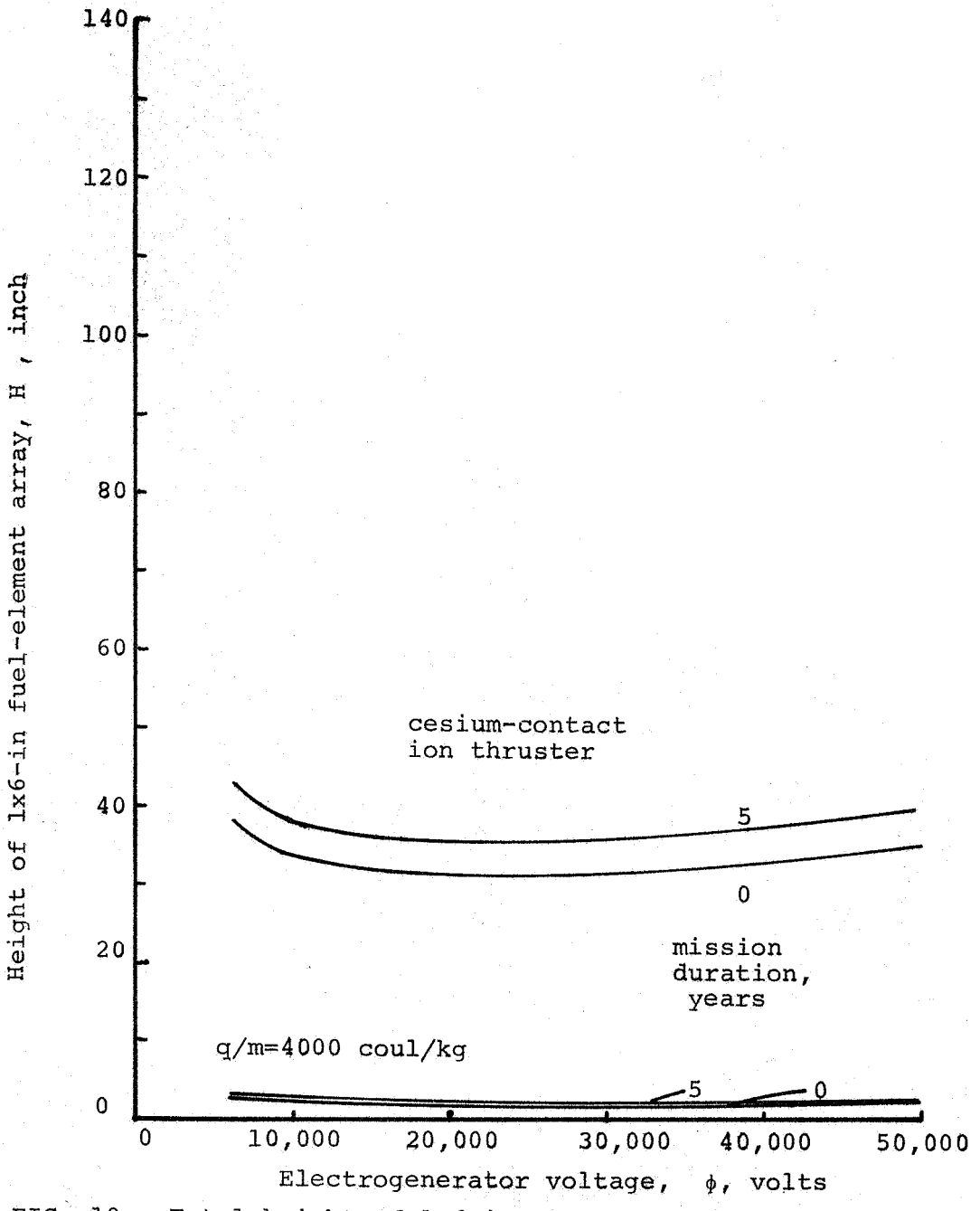


FIG. 19 - Total height of 1x6-in fuel-element arrays in $SrTiO_3$, 90% dense, electrogenerator for 10-micropound thrusters. Fuel-layer thickness, $\tau_f$=0.1 cm, two sides of 10-mil aluminum support foil. Collector, 125-mil aluminum. Electric field strength, $\phi/g=10^5$ volts/cm.

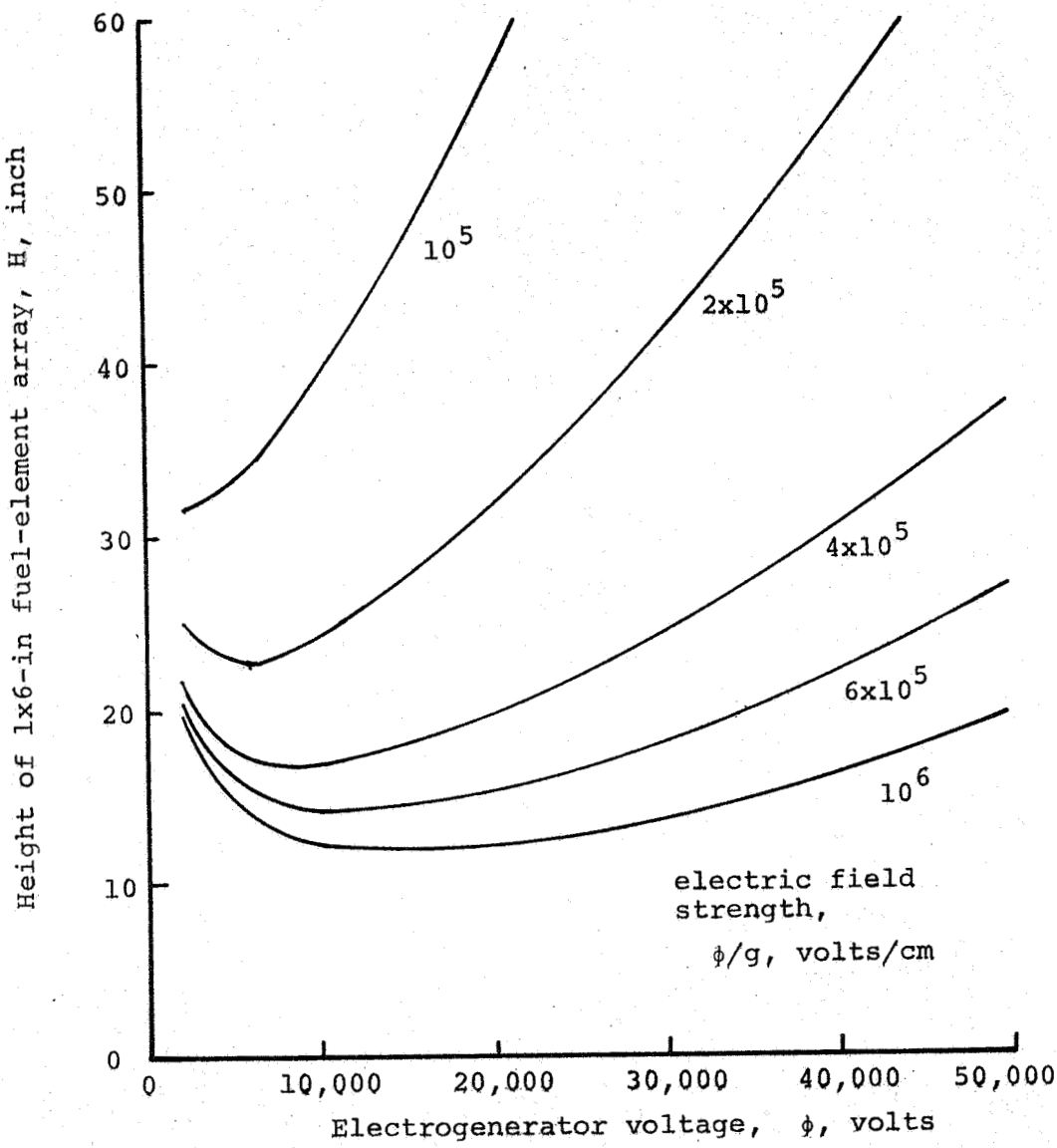


FIG. 20 - Total height of 1x6-in fuel-element arrays in $Pm_2O_3$, 90% dense, electrogenerator for 10-micropound cesium-contact ion thruster and 2-year mission duration. Fuel-layer thickness, $\tau_f$=.005 cm, two sides of 10-mil aluminum support foil. Collector, 10-mil aluminum.

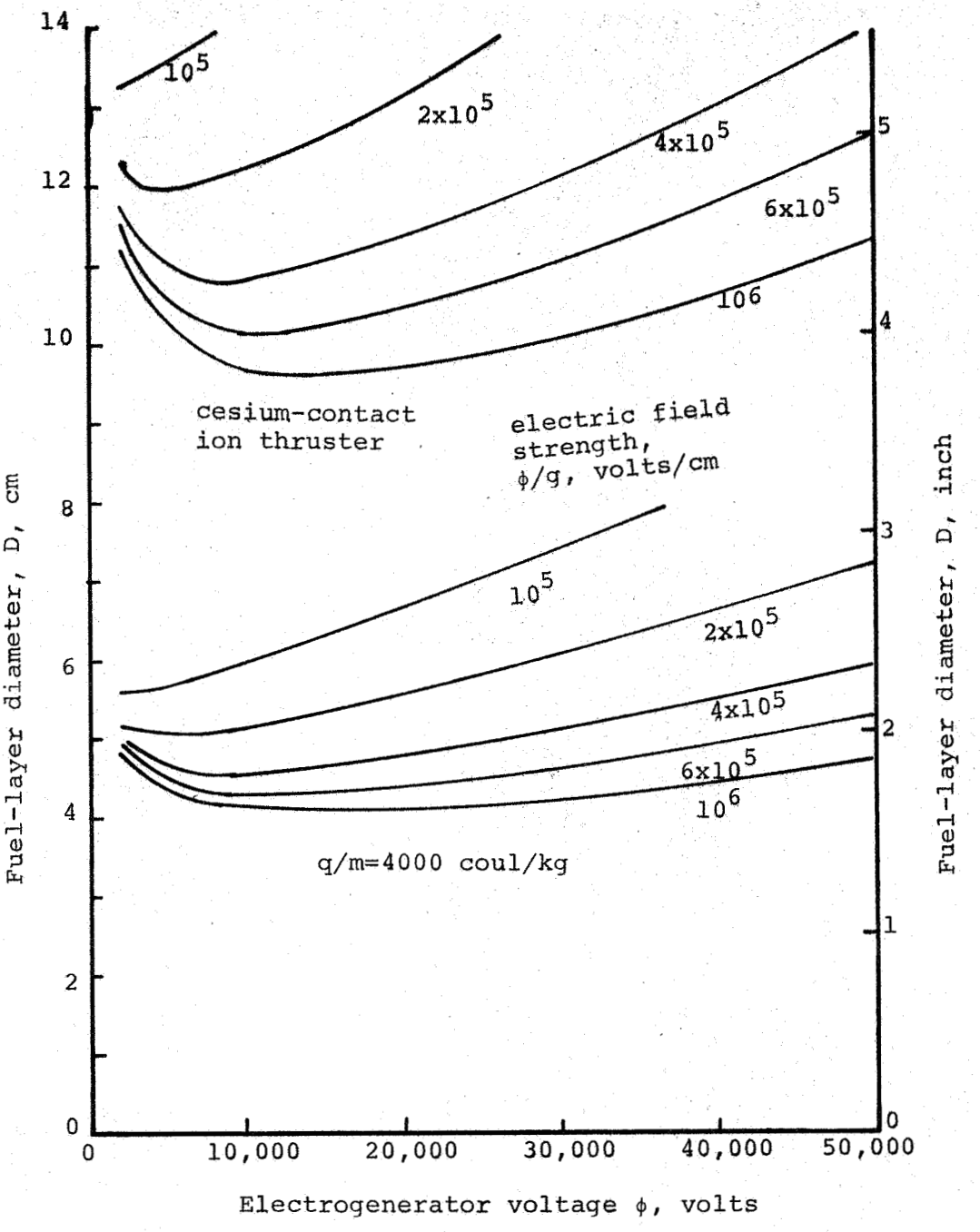


FIG. 21 - Diameter of fuel layers in $Pm_2O_3$, 90% dense, electrogenerator with circular-disc geometry and L/D=1.0 . Mission duration, $\ll$ 1-year. Fuel-layer thickness, $\tau_f$=.005 cm, two sides of 10-mil aluminum support foil. Collector, 10-mil aluminum.

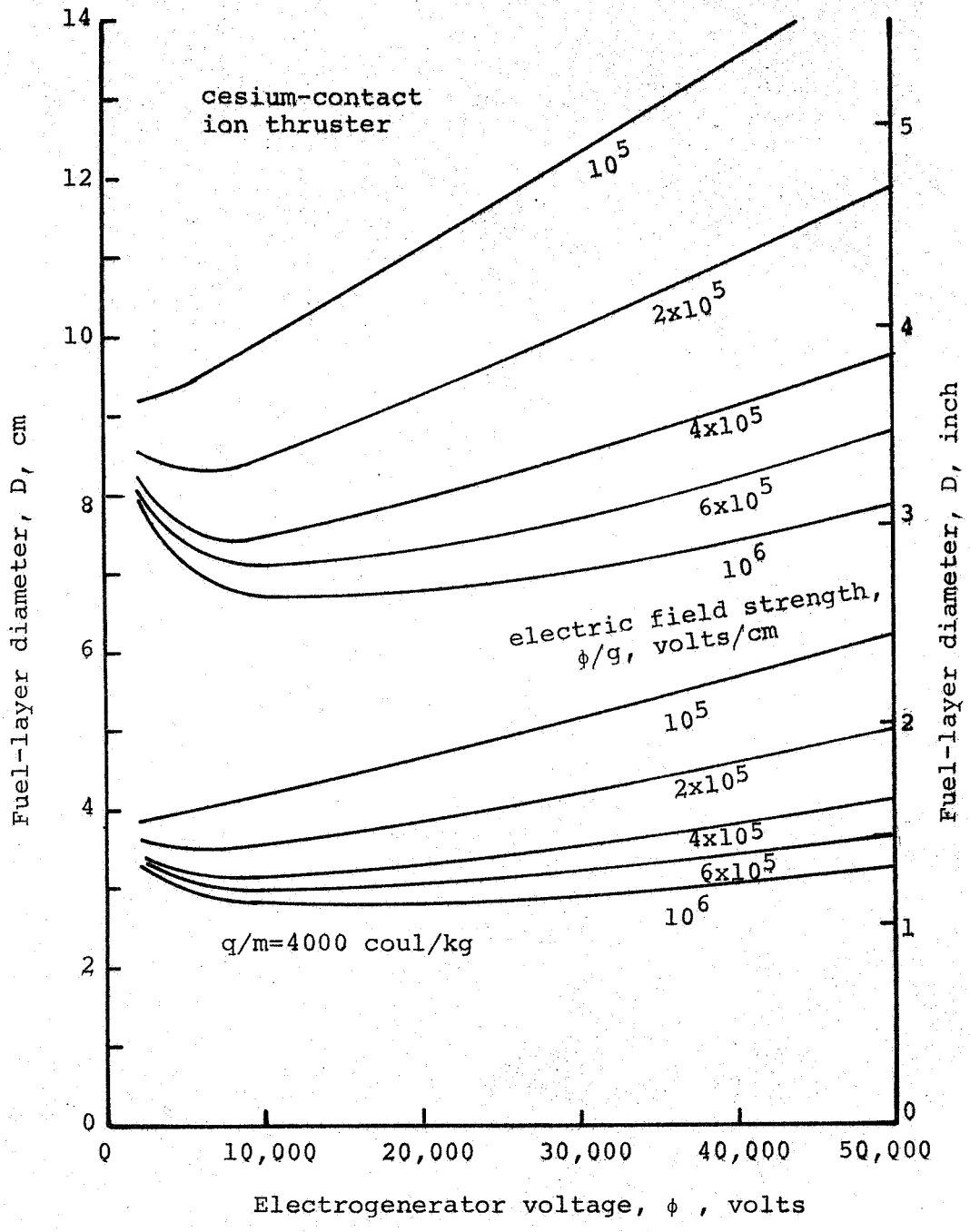


FIG. 22 - Diameter of fuel layers in $Pm_2O_3$, 90% dense, electrogenerator with circular-disc geometry and L/D=3.0 . Mission duration $\ll$ 1-year. Fuel-layer thickness, $\tau_f$=.005 cm, two sides of 10-mil aluminum support foil. Collector, 10-mil aluminum.

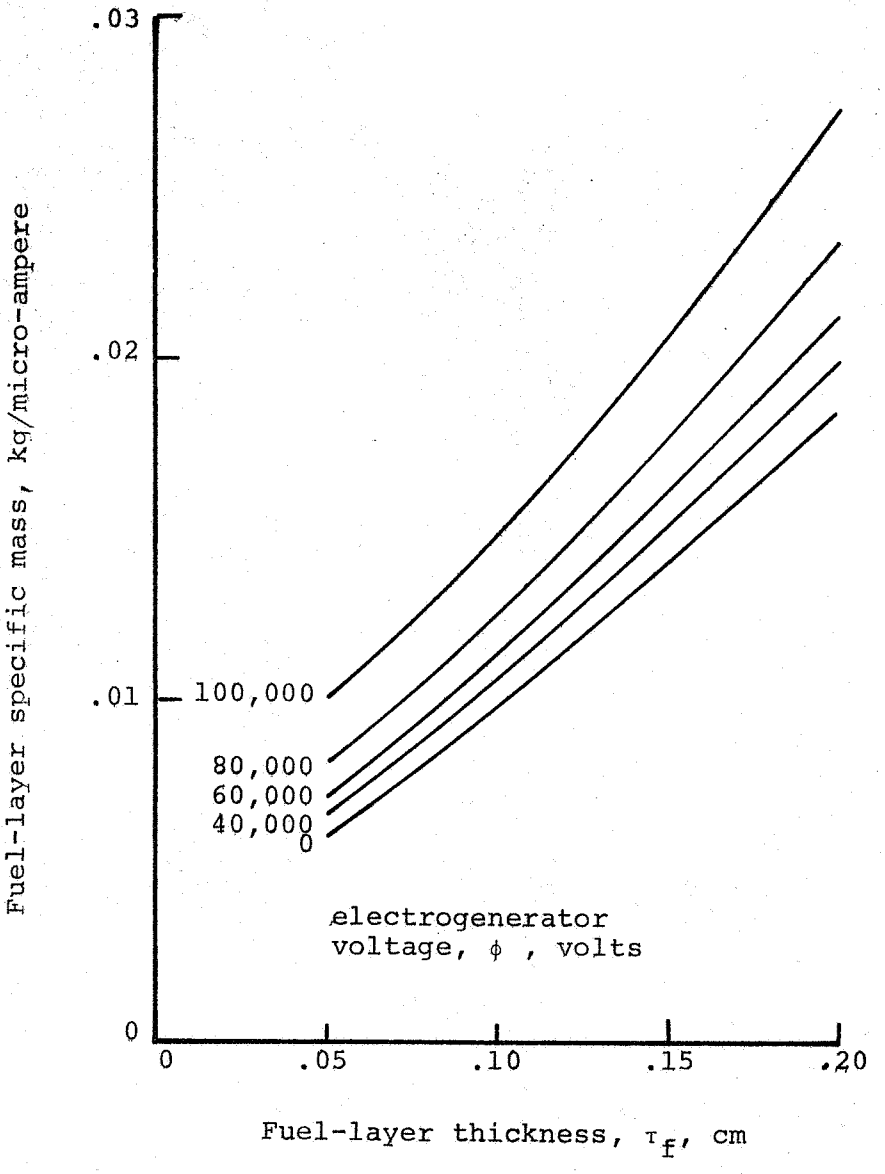


FIG. 23 - Specific mass, kg/micro-ampere, of strontium-90-titanate, 90% dense, fuel layers.

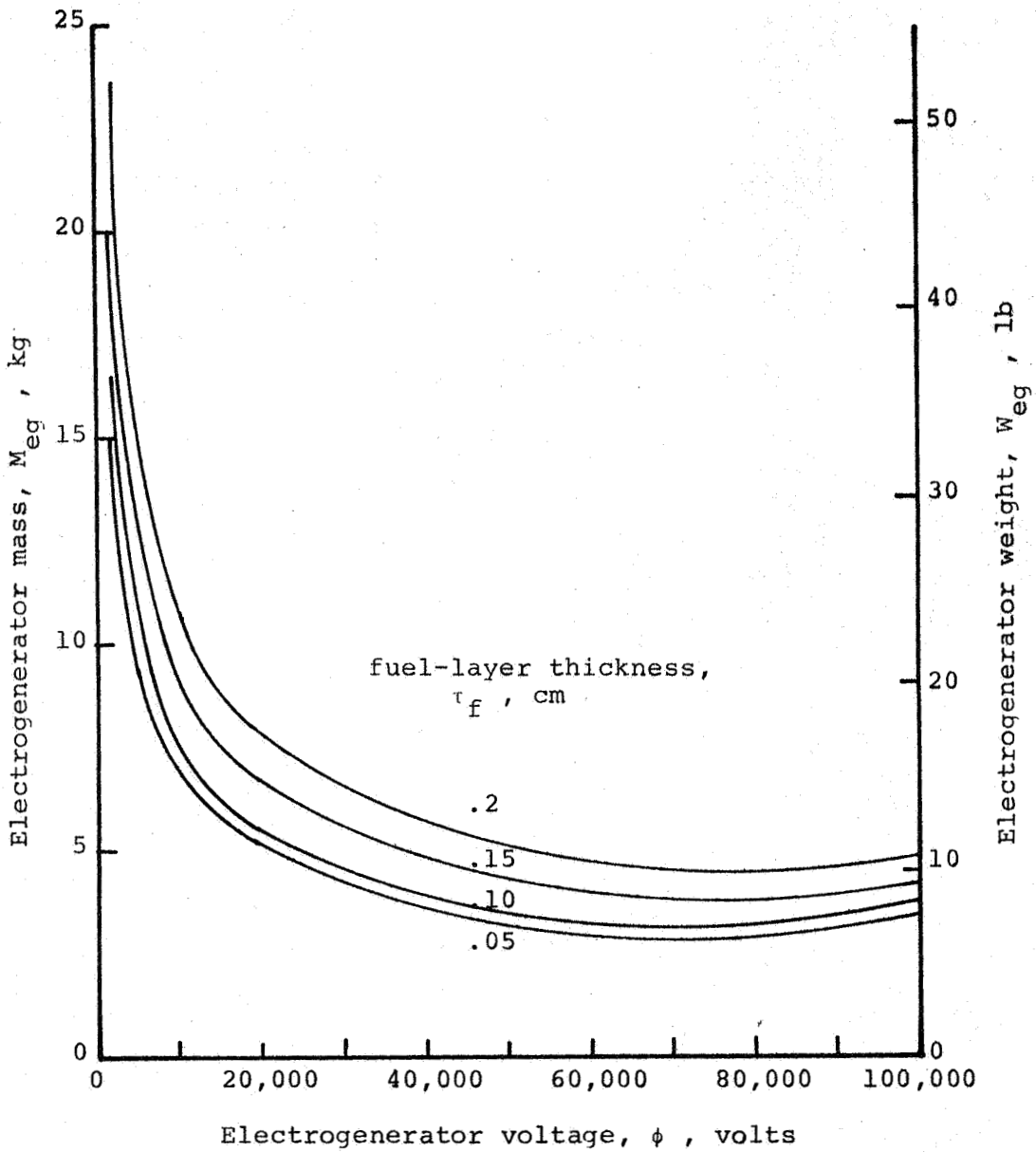


FIG. 24 - Mass of strontium-90 electrogenerators for 10-micropound cesium-contact ion thruster. Mission duration, 5-years. $SrTiO_3$, 90% dense fuel layer, both sides of 10-mil aluminum support foil. Collector, 125-mil aluminum. Support structure and containment vessel not included.

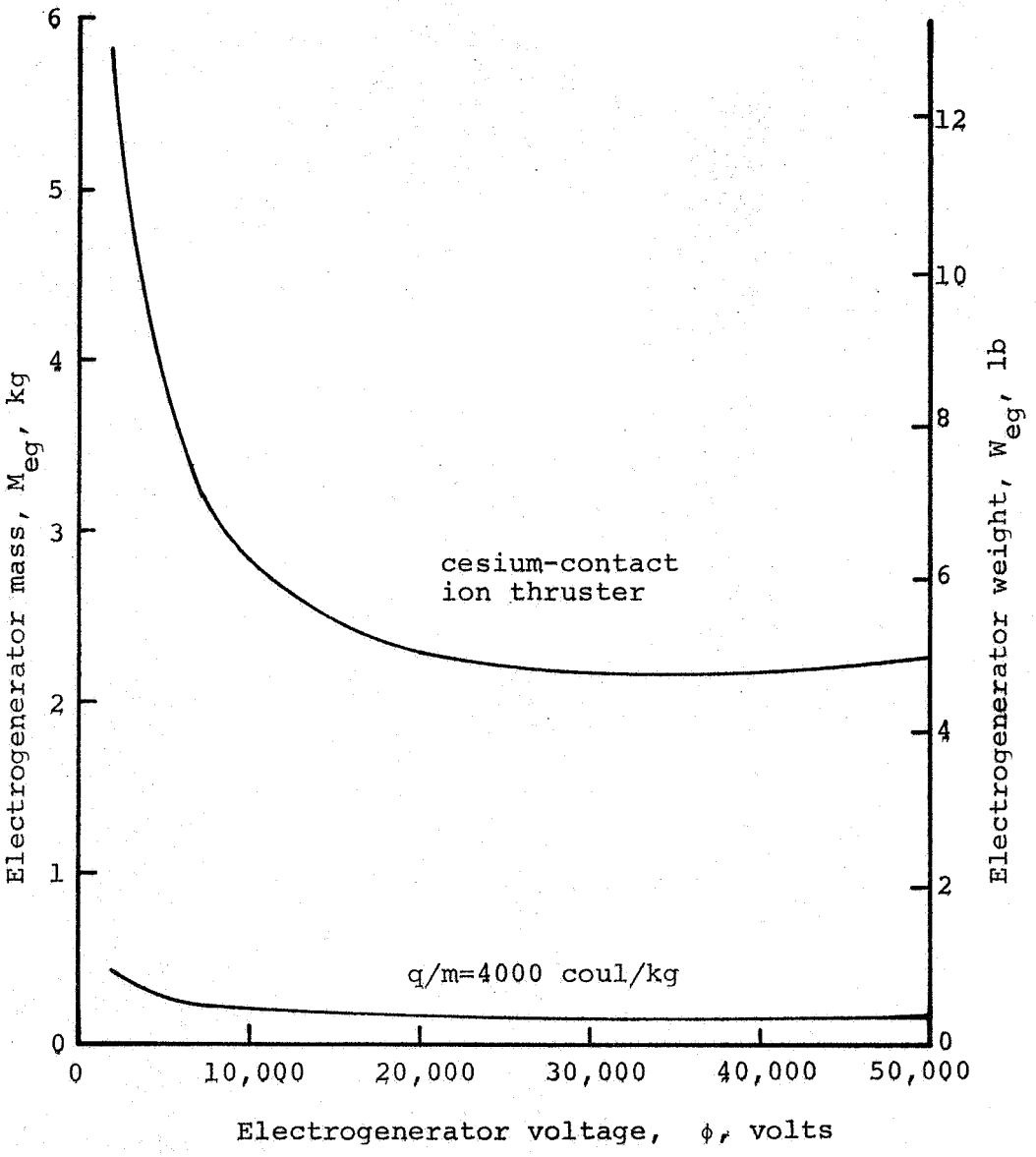


FIG. 25 - Mass of promethium-147 electrogenerators for 10-micropound thrusters. Mission duration, 2-years. $Pm_2O_3$, 90% dense fuel layer, $\tau_f$=.005 cm both sides of 10-mil aluminum support foil. Collector, 10-mil aluminum. Support structure and containment vessel not included.

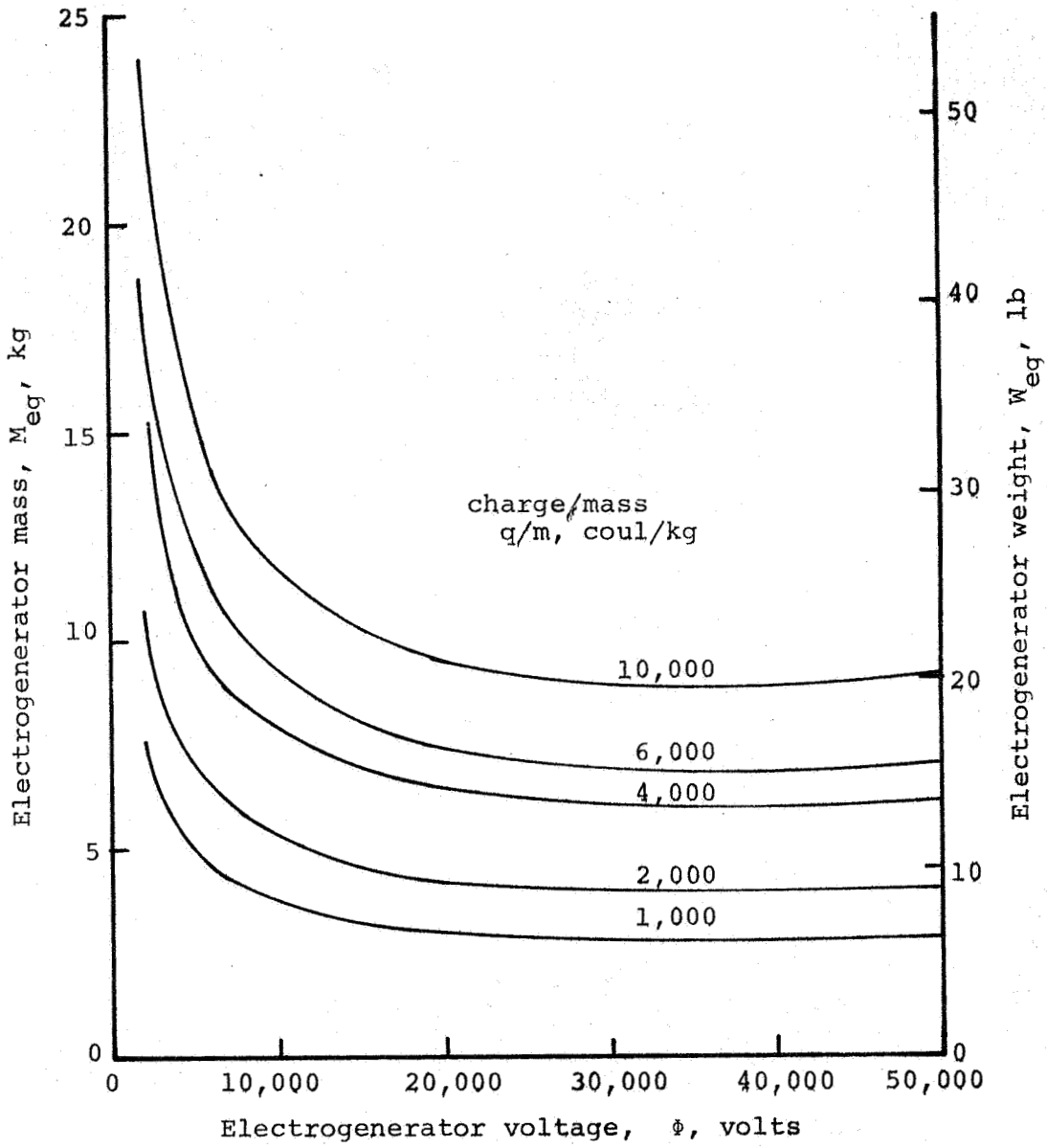


FIG. 26 - Mass of promethium-147 electrogenerators for 350-micropound thrusters. Mission duration, 2-years. $Pm_2O_3$, 90% dense fuel layer, $\tau_f$=.005 cm both sides of 10-mil aluminum support foil. Collector, 10-mil aluminum. Support structure and containment vessel not included.

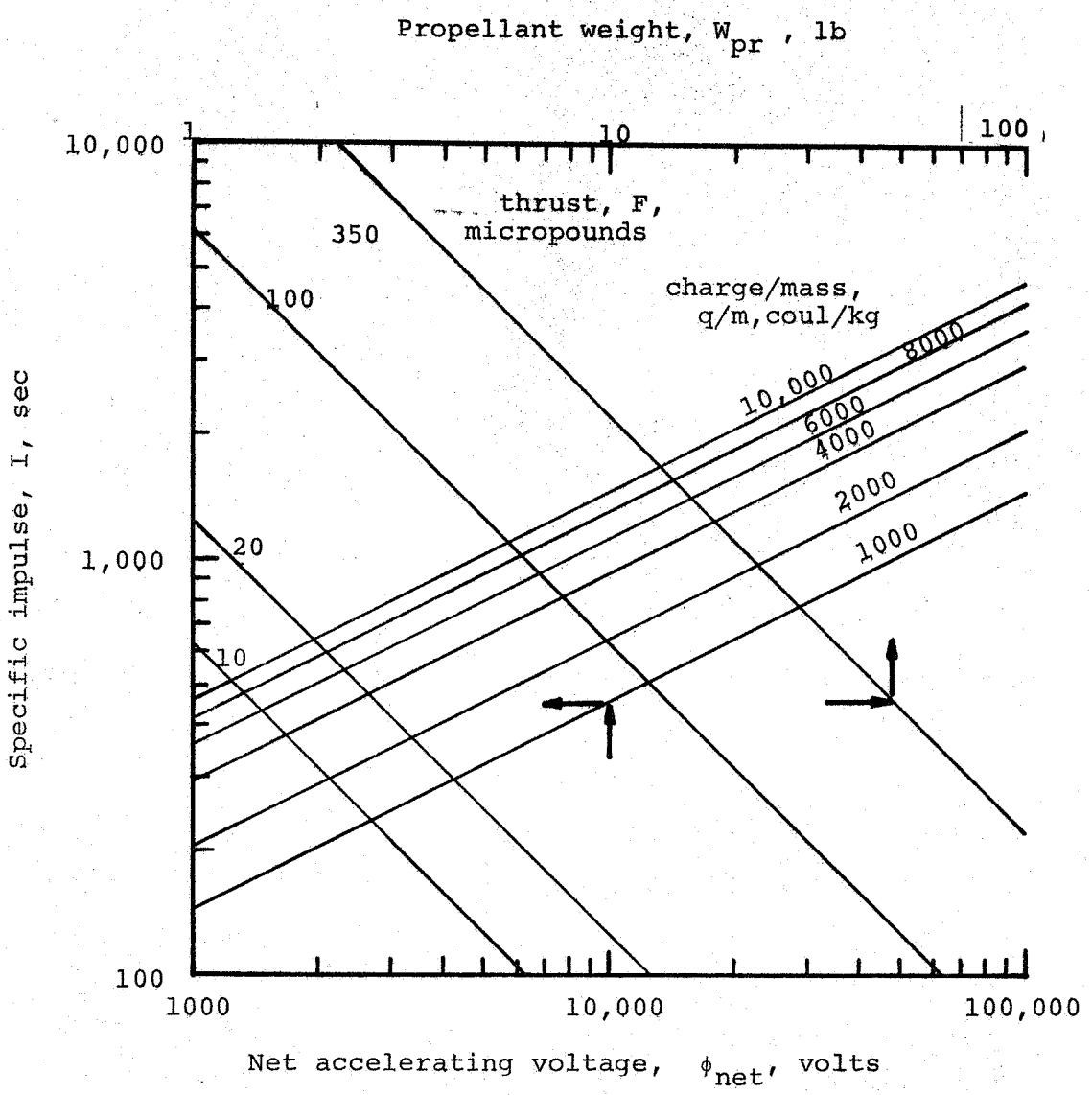


FIG. 27 - Propellant weight for charged-particle electrostatic thrusters. Mission duration, 2-years. Duty cycle, 100%.

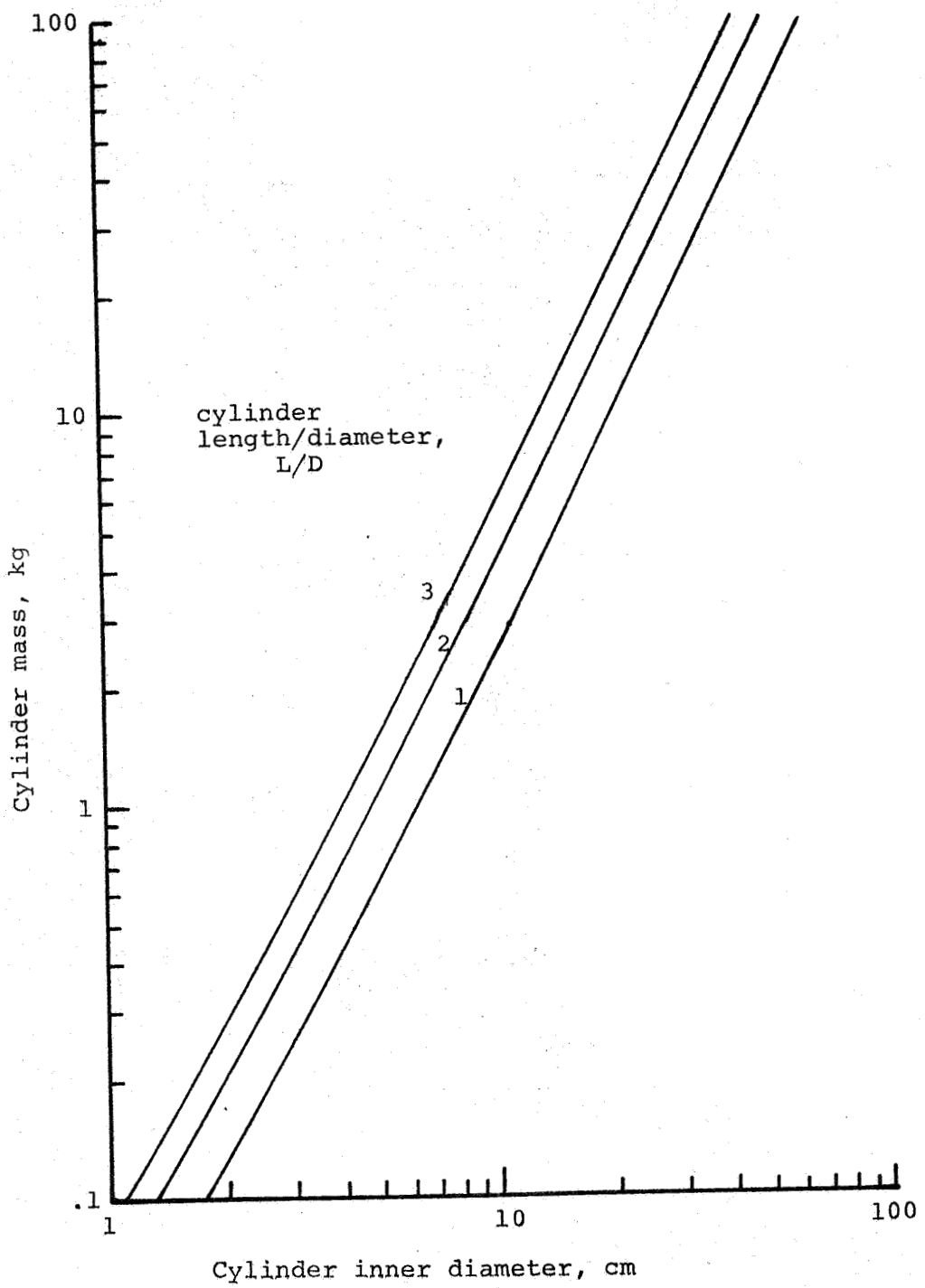


FIG. 28 - Mass of tantalum cylinder with 0.125-inch wall thickness.

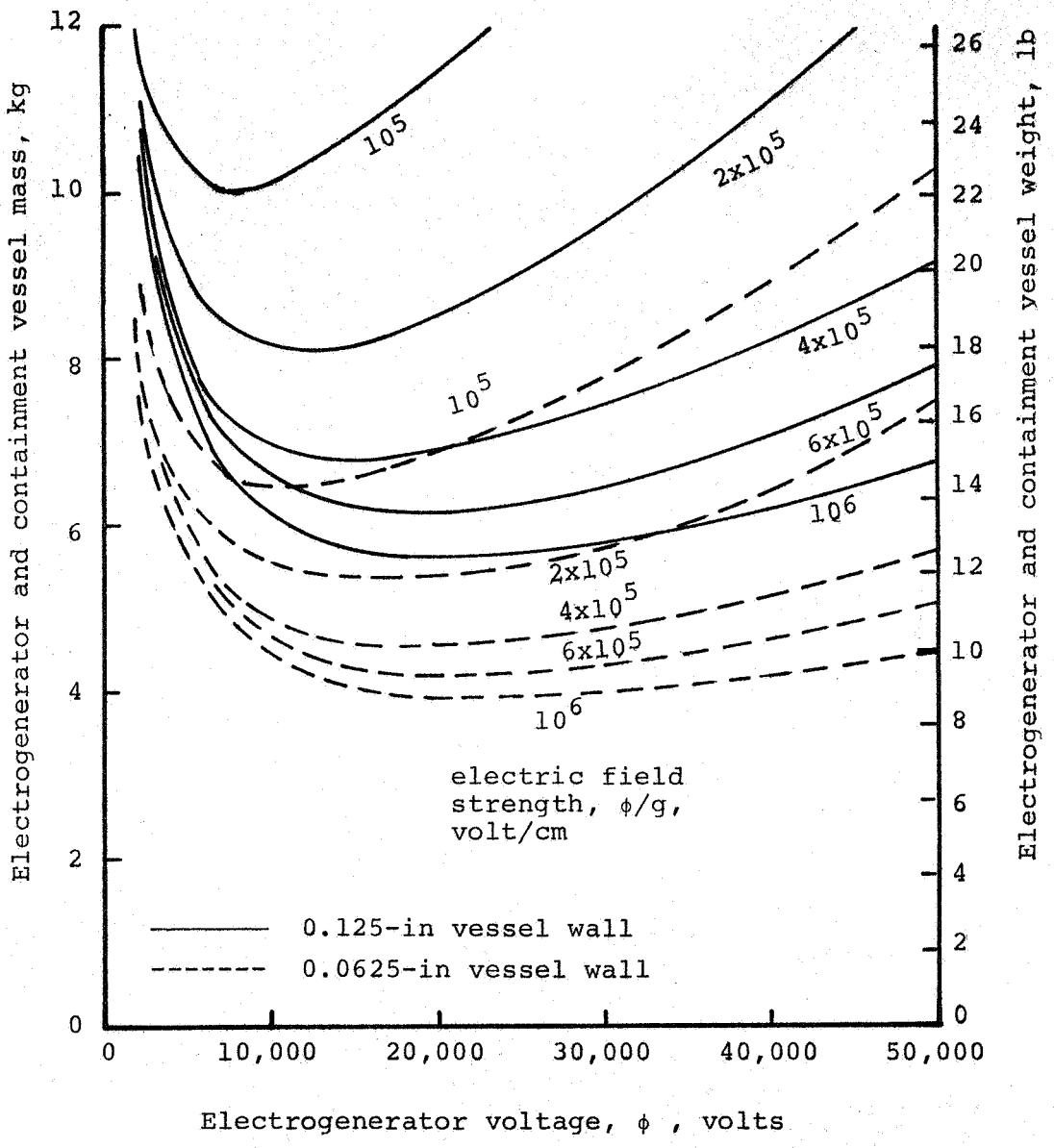


FIG. 29 - Combined mass of promethium-147 electrogenerators and tantalum containment vessels for 10-micropound cesium-contact ion thruster. Mission duration, 2-years. Vessel L/D=1.0. Support structure not included.

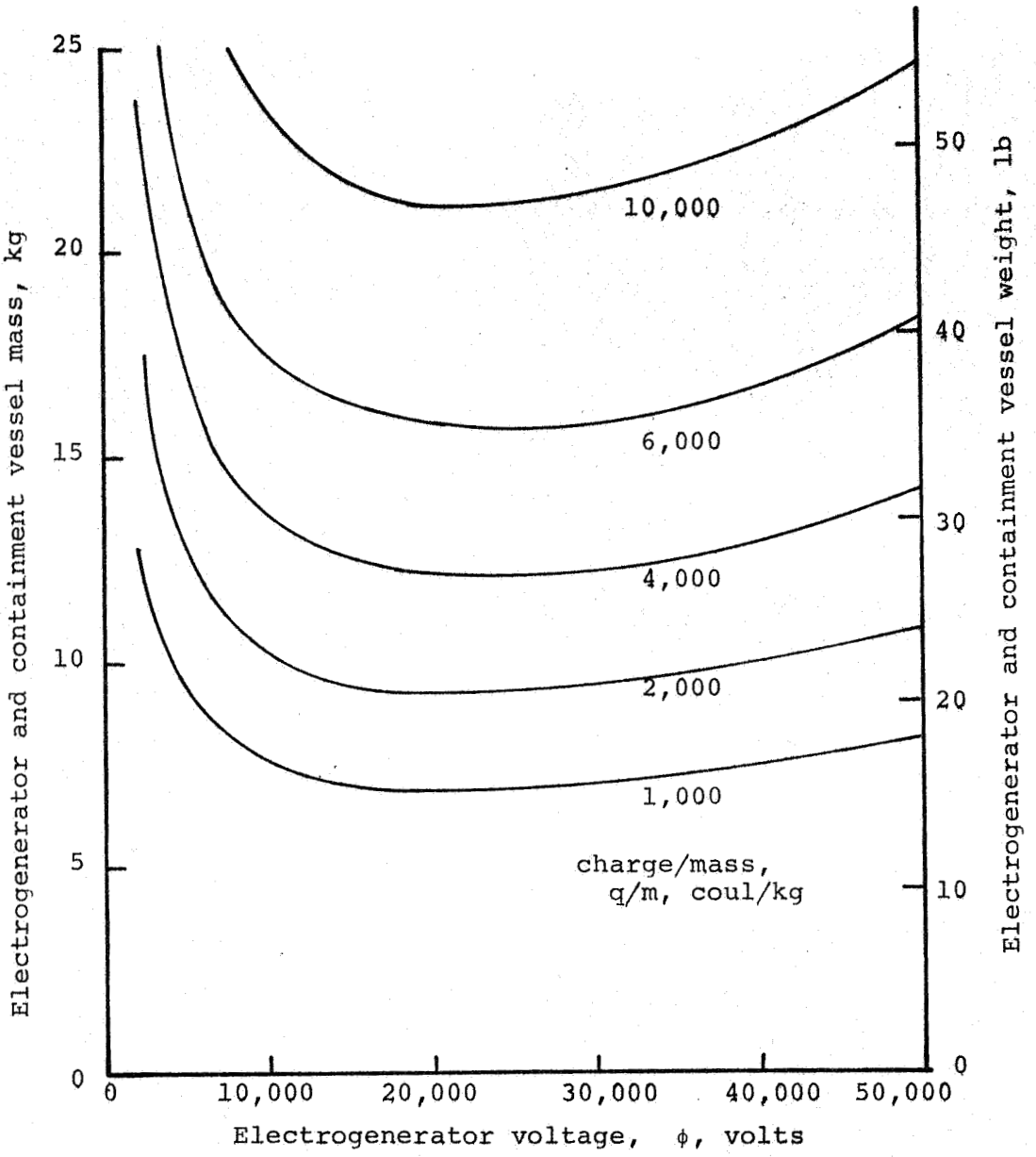


FIG. 30 - Combined mass of promethium-147 electrogenerators and tantalum containment vessels for 350-micro-pound charged-particle thruster. Containment-vessel wall thickness, 0.125-inch. Mission duration, 2-years. Vessel L/D=1.0. Support structure not included. Electric field strength, $\phi/g=10^6$ volts/cm .

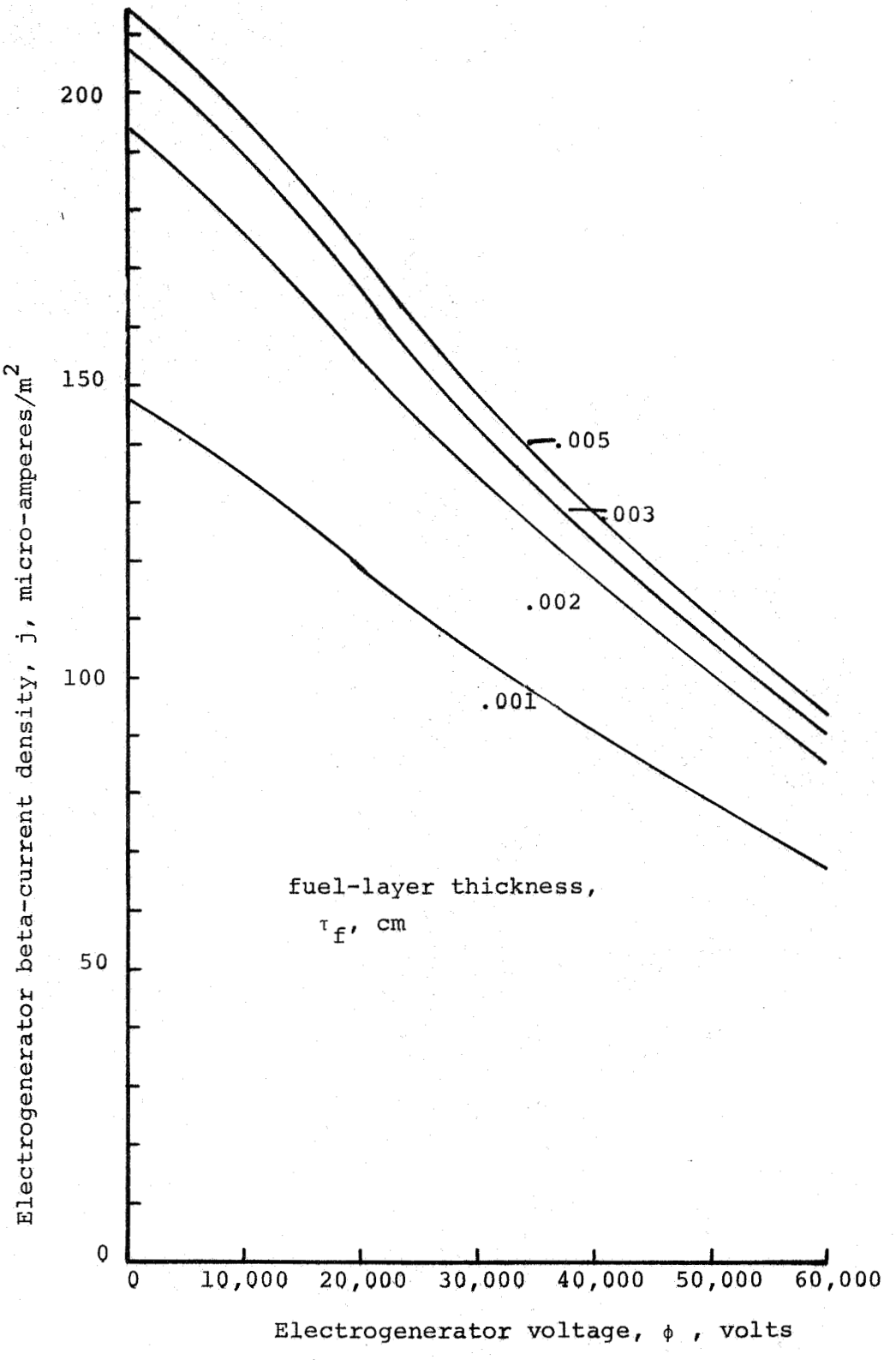


FIG. 31 - Electrogenerator beta-current density with promethium-147-oxide, 90% dense, fuel layers on both sides of 0.5-mil aluminum support foil.

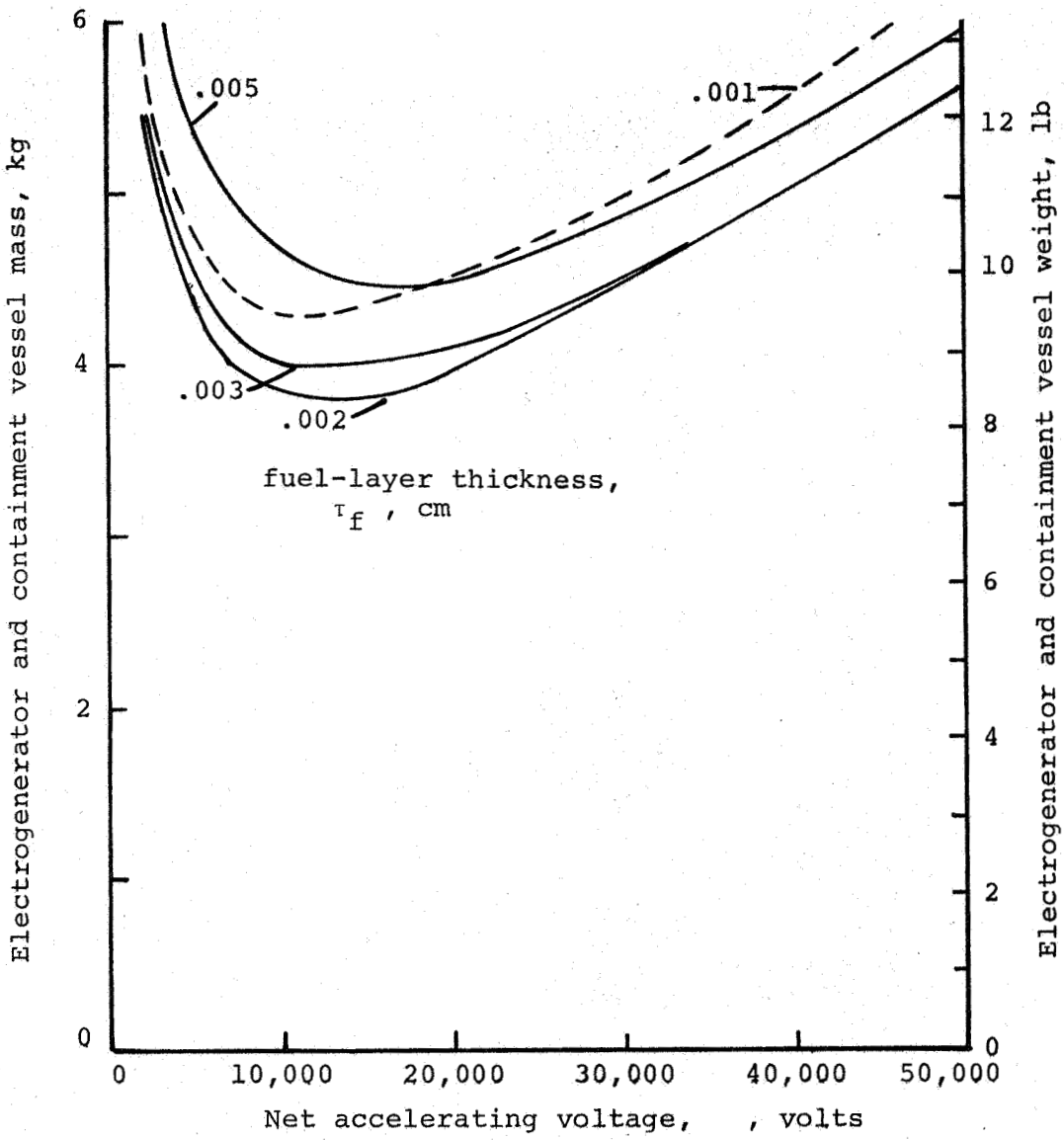


FIG. 32 - Effect of fuel-layer thickness on combined mass of 125-mil tantalum containment vessel and promethium-147-oxide, 90% dense, electrogenerators for 350-micropound, 1000 coul/kg charged-particle thruster. Mission duration, 2-years. Vessel L/D=1.0 . Collector, 5-mil aluminum. Support foil, 0.5-mil aluminum.

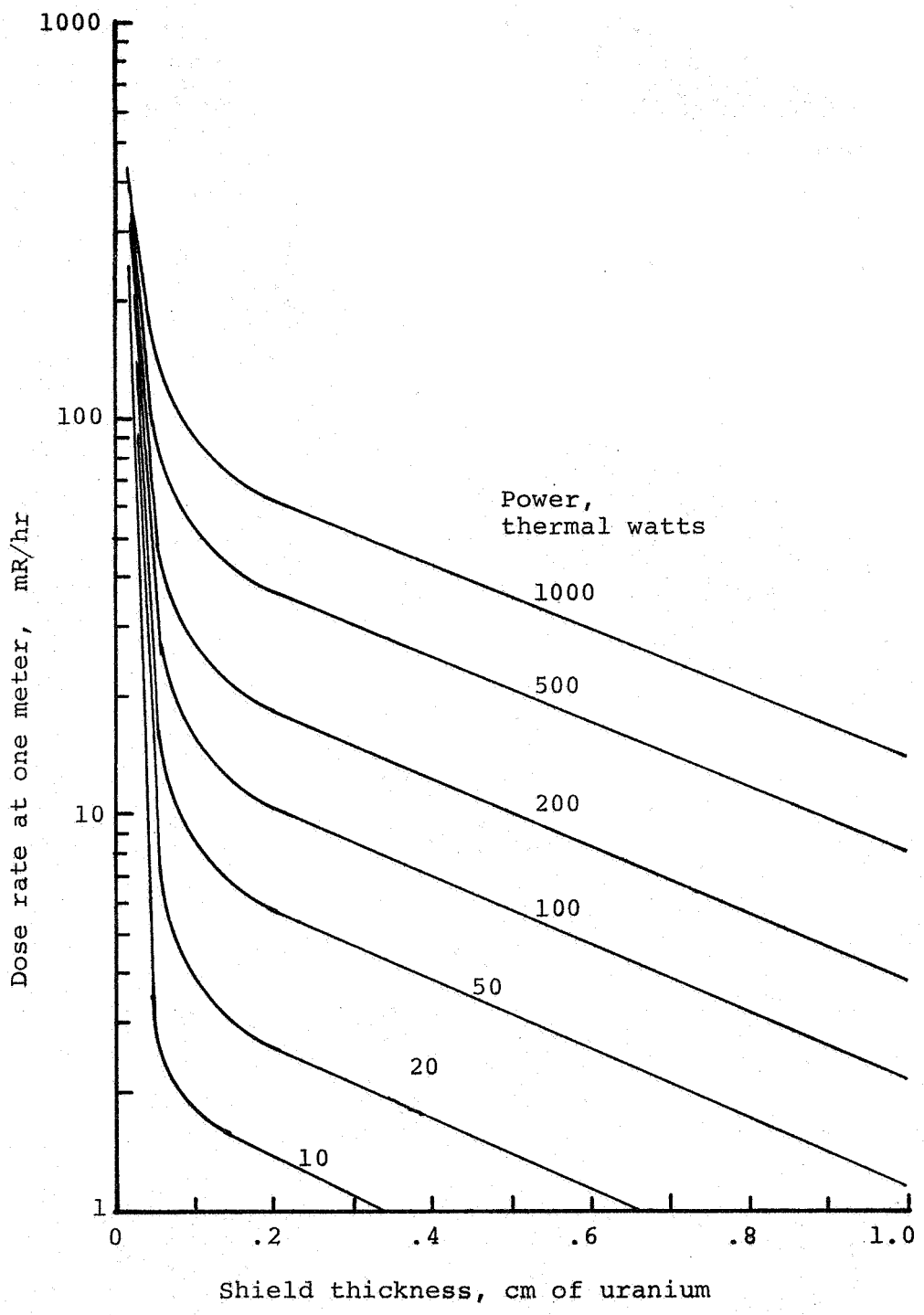


FIG. 33 - Dose rate one-meter from promethium-147 radioisotope containing 0.25 ppm Pm-146.

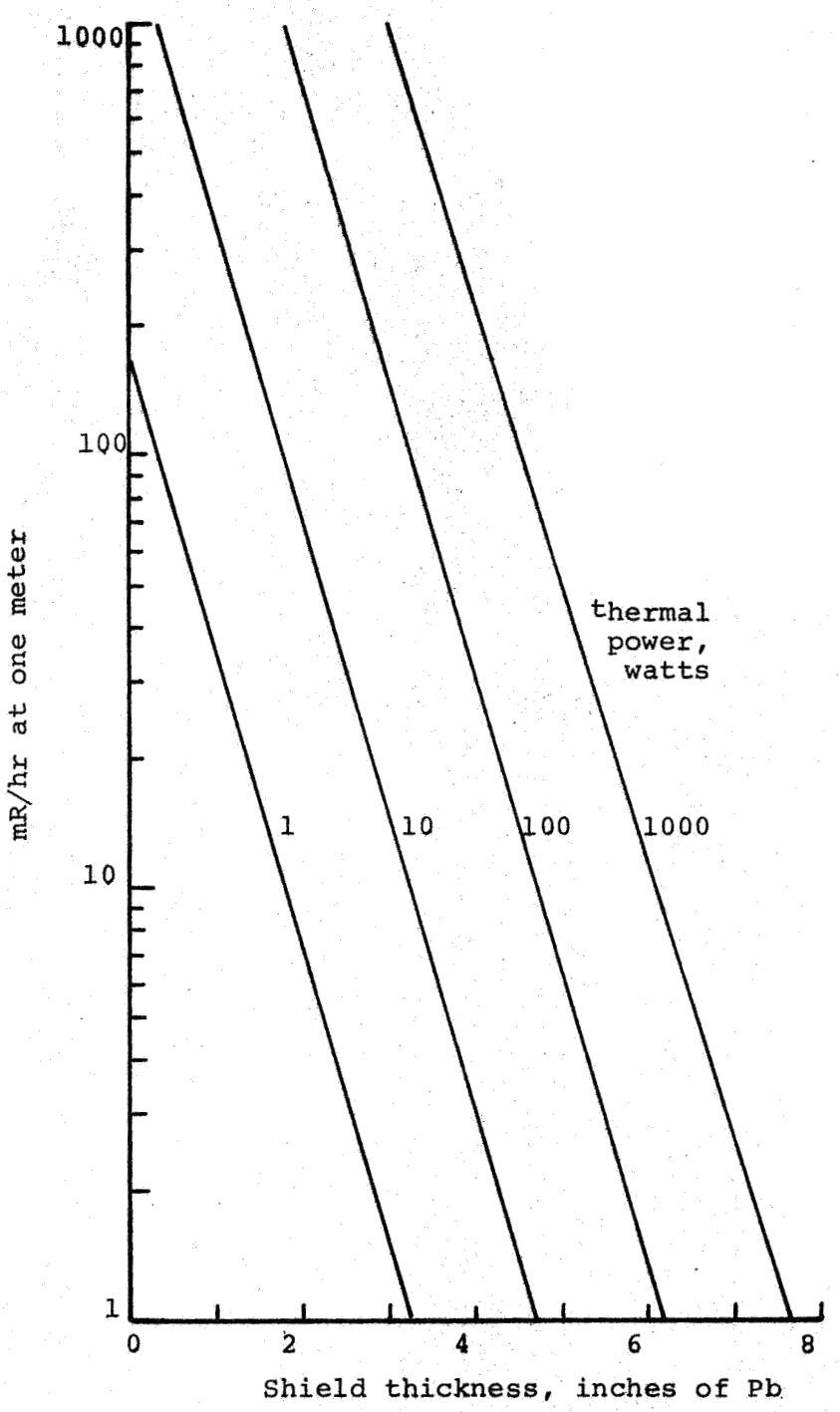


FIG. 34 - Dose rate one-meter from strontium-90 radioisotope.

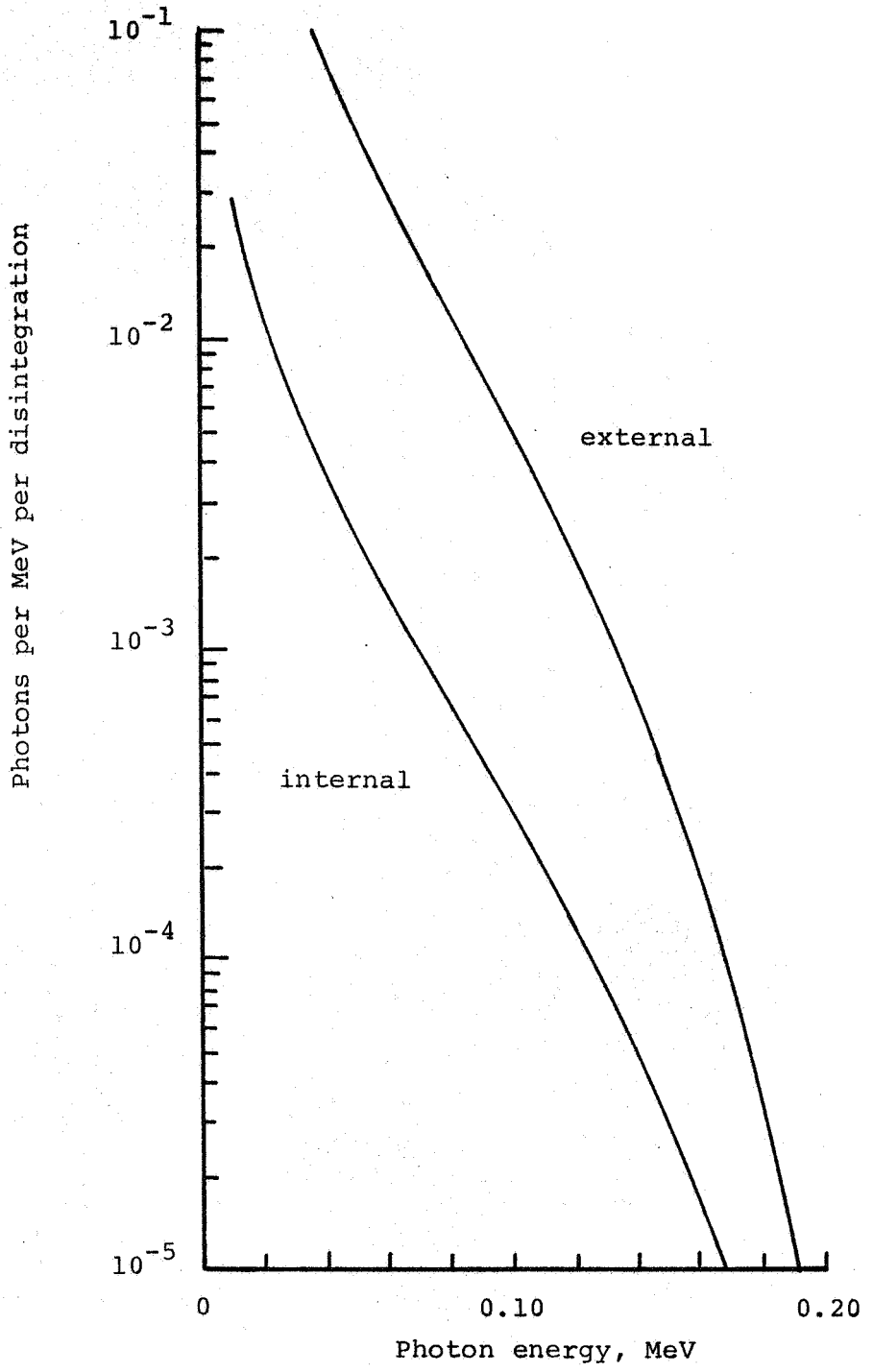


FIG. 35 - Bremsstrahlung from strontium-yttrium-90 beta particles stopped in strontium titanate.

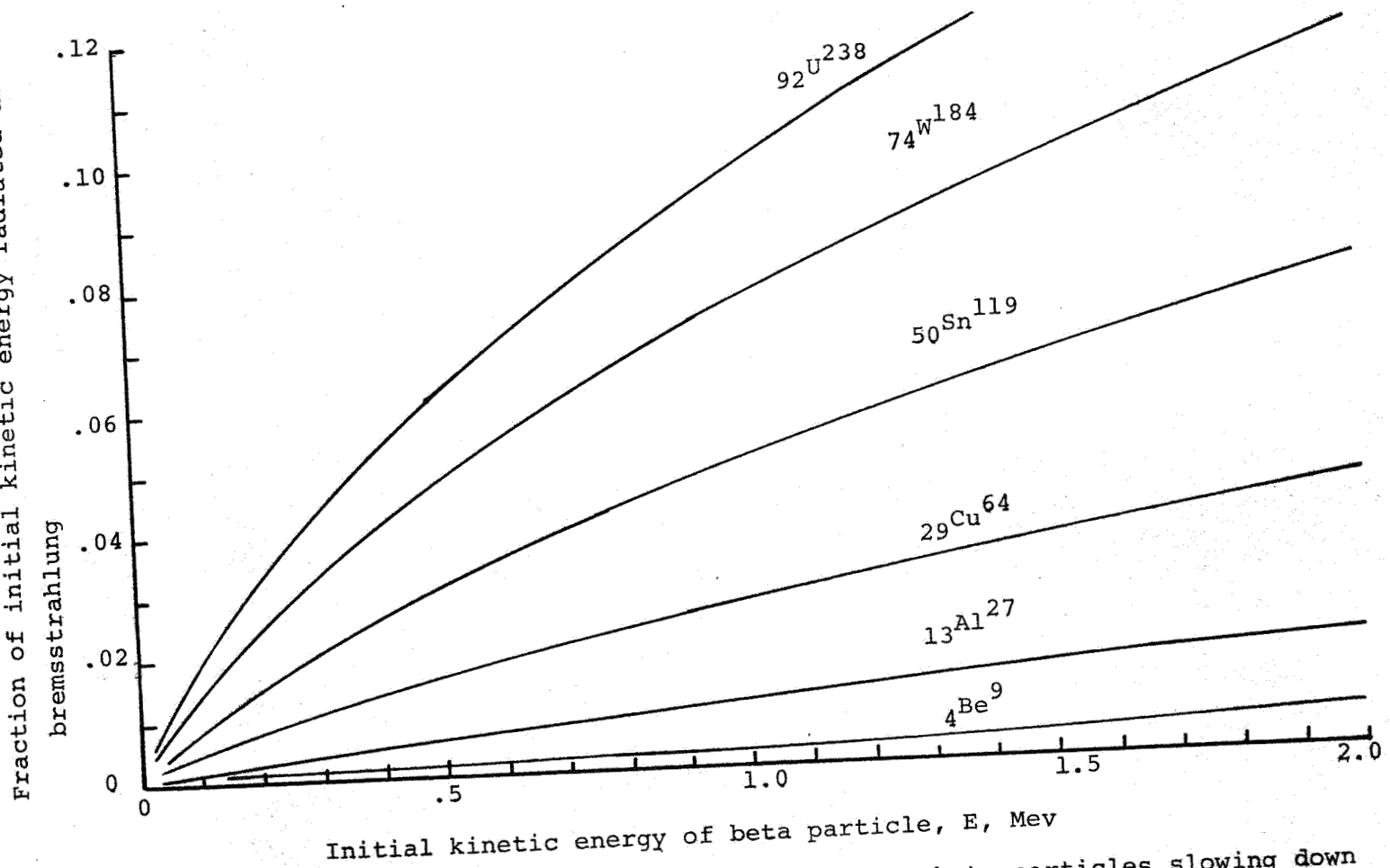


FIG. 36 - Relative production of bremsstrahlung by beta particles slowing down to a stop in various materials.

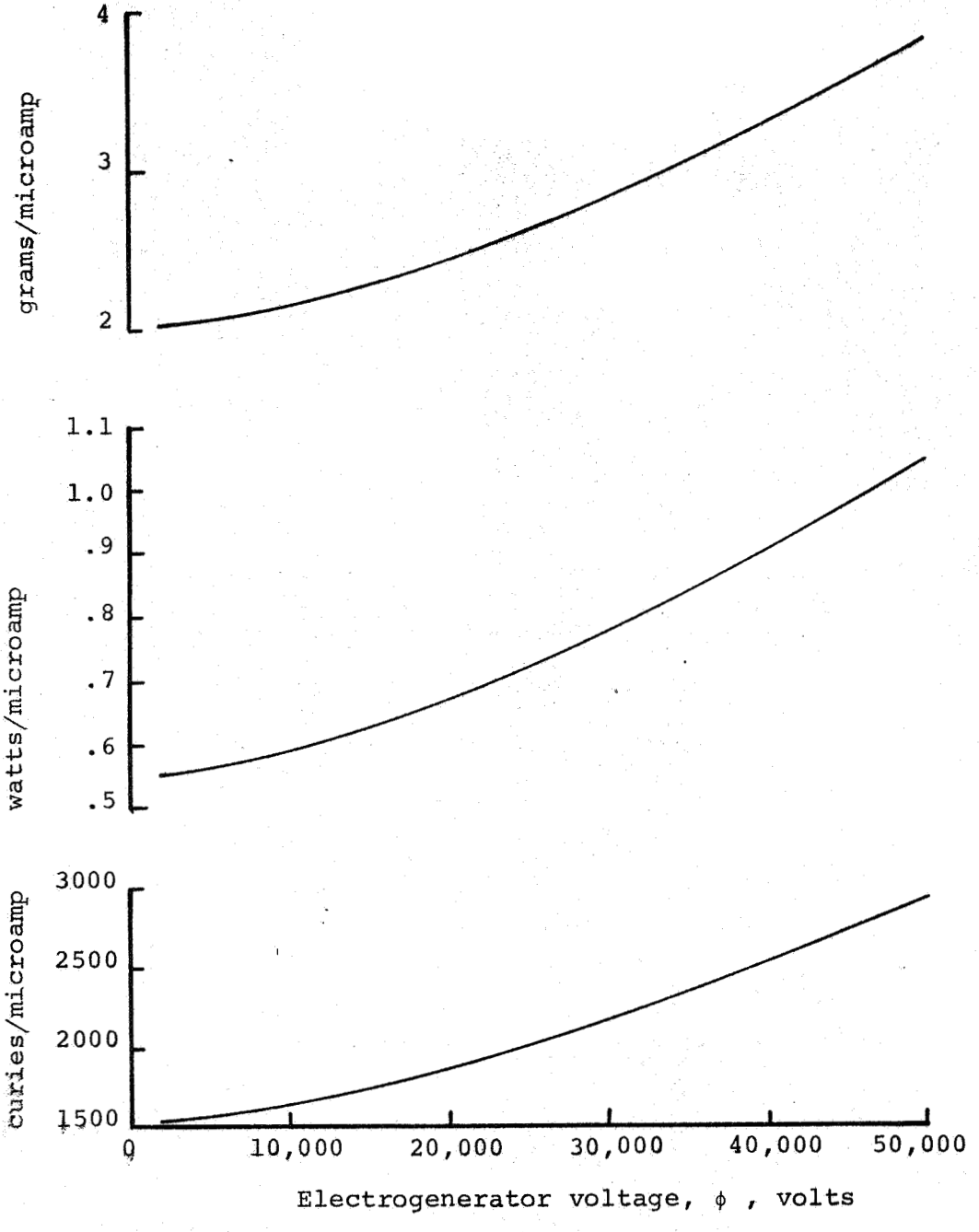


FIG. 37 - Characteristics of promethium-147-oxide electrogenerators. Fuel-layer thickness $\tau_f$=.005 cm, and 23% leakage current.

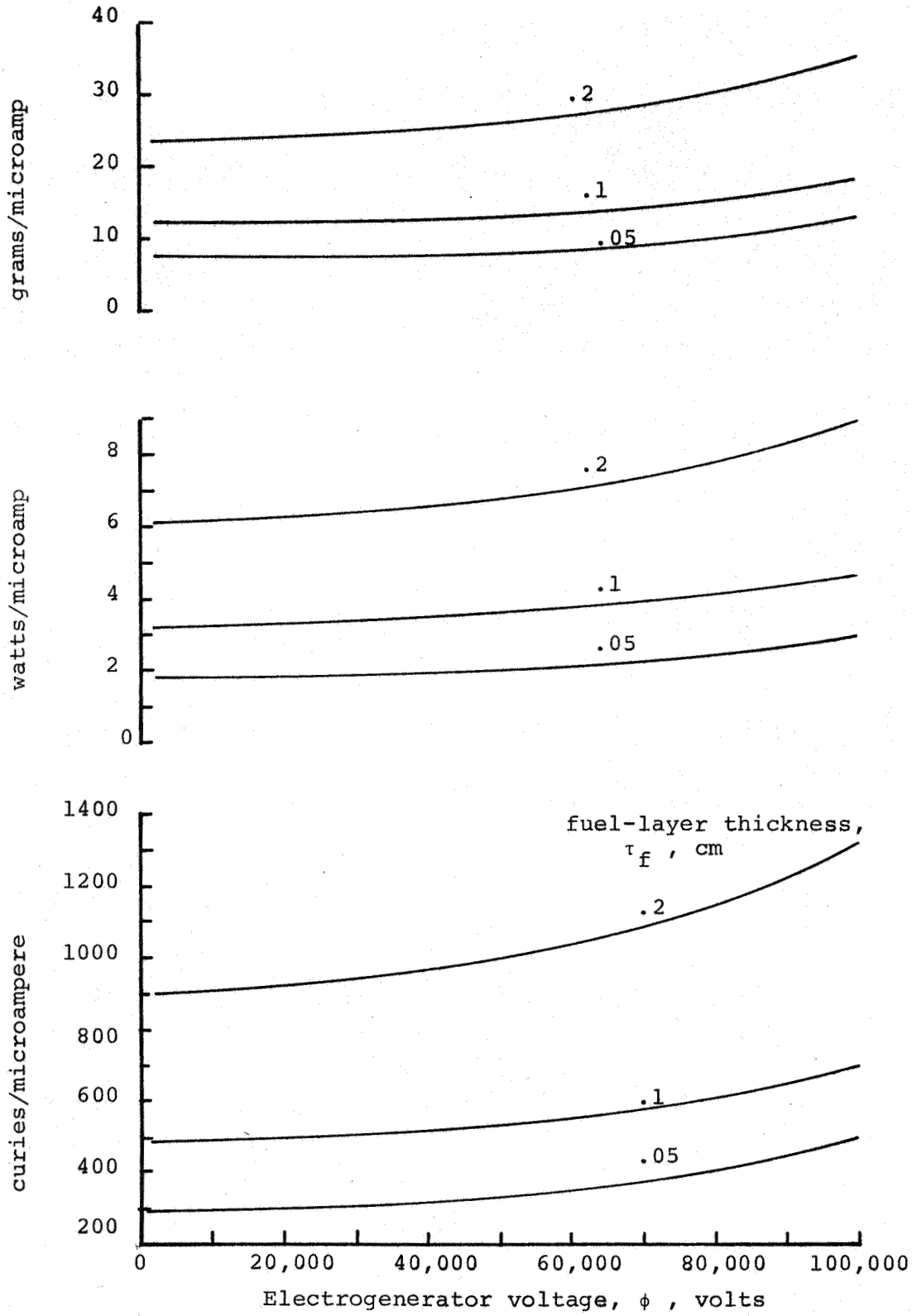


FIG. 38 - Characteristics of strontium-90-titanate electrogenerators. Leakage current, 23%

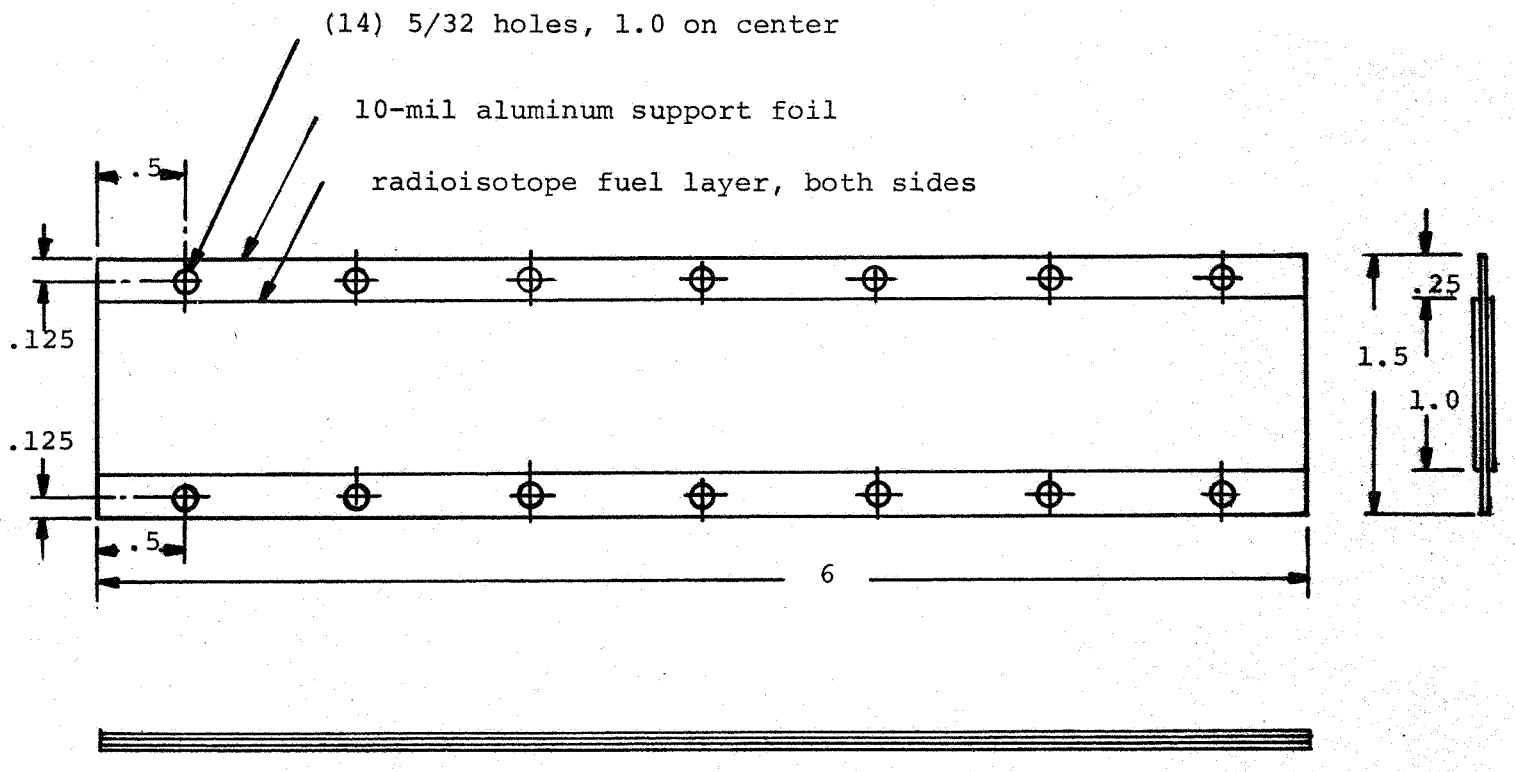


SCALE: 1/1

FIG. 39 - Recommended design of fuel elements for prototype ACCENT system.

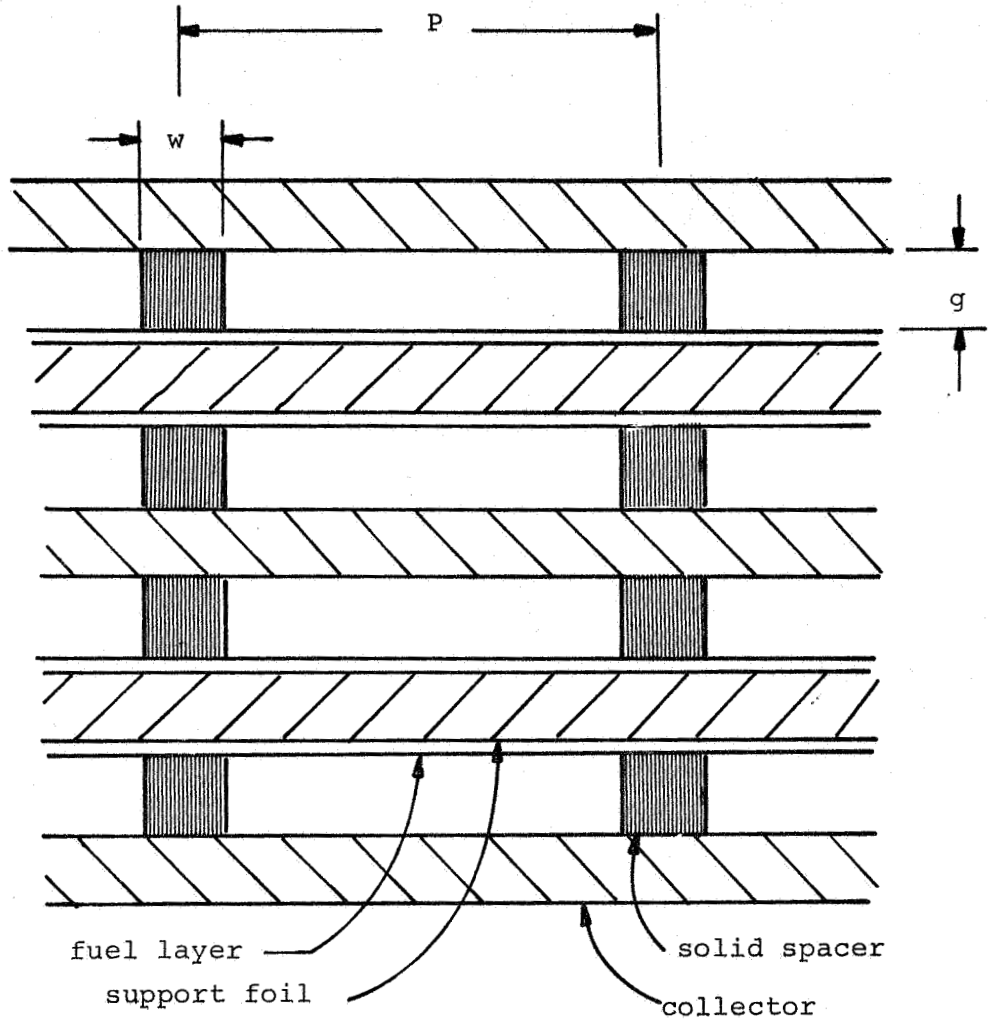


FIG. 40 - Typical design of ACCENT electrogenerator with solid spacers between fuel elements and collectors.

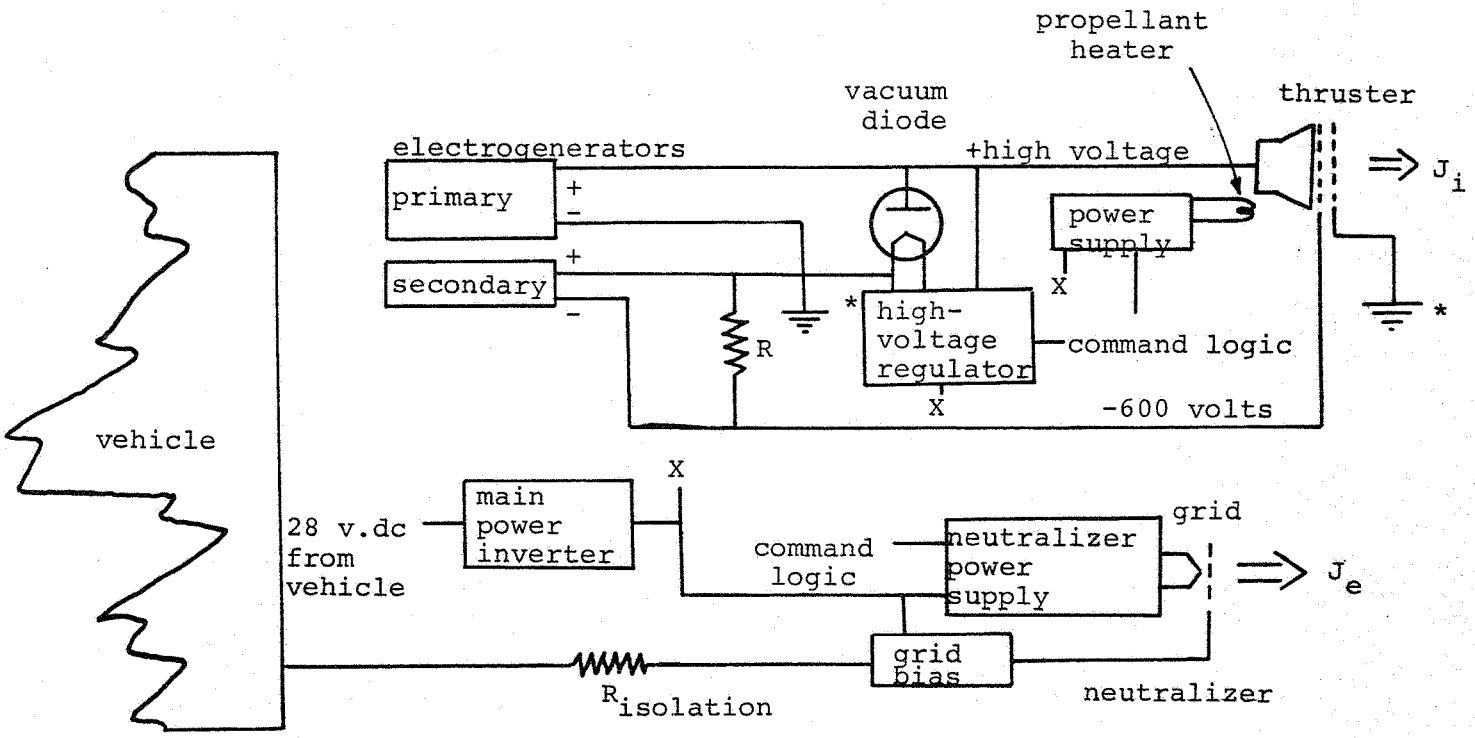


THE DANE COMPANY
FORT COLLINS, COLORADO 80521

FIG. 41 - ACCENT prototype system electrical diagram.

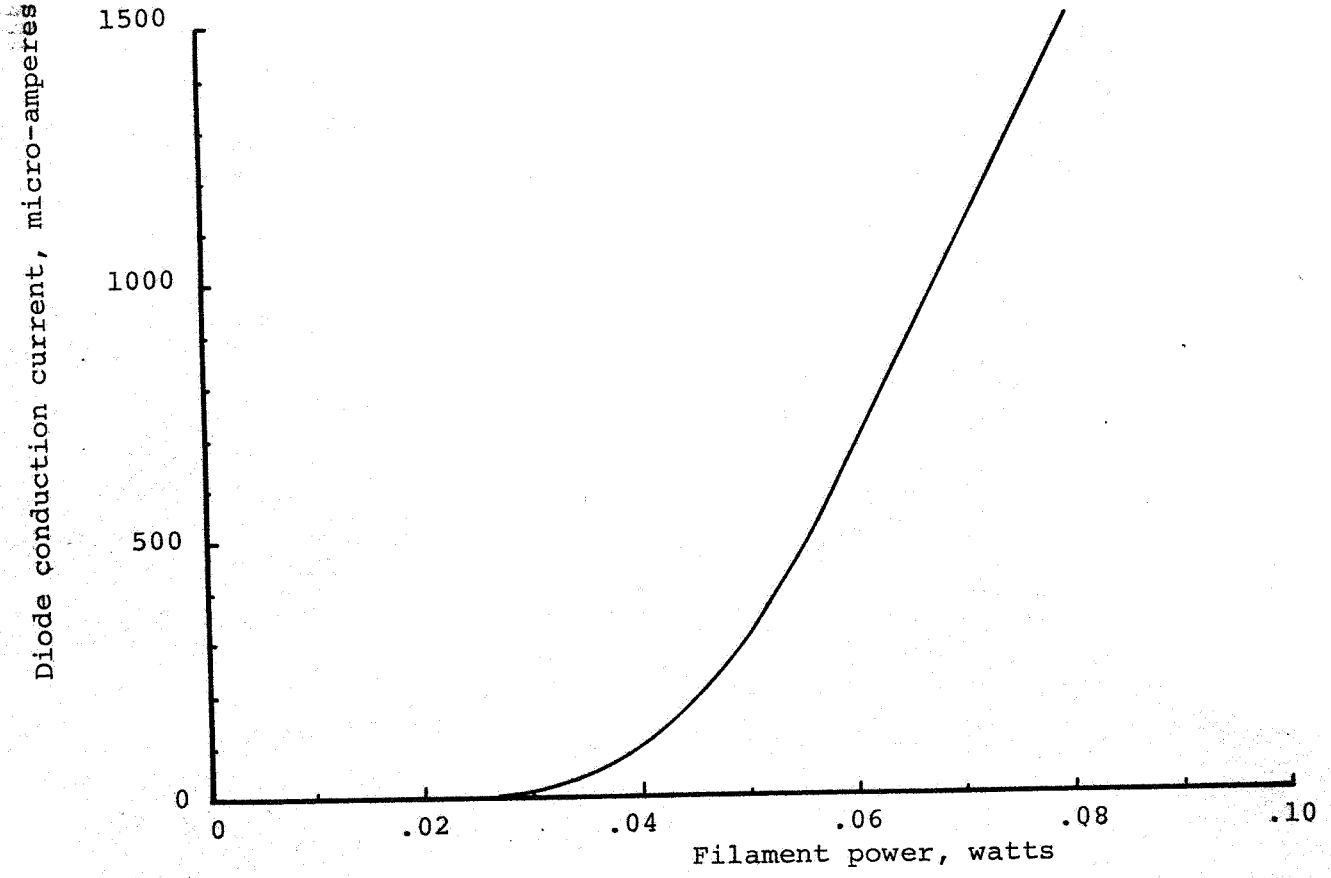


FIG. 42 - Current/filament-power characteristics of a typical 1X2 vacuum diode.

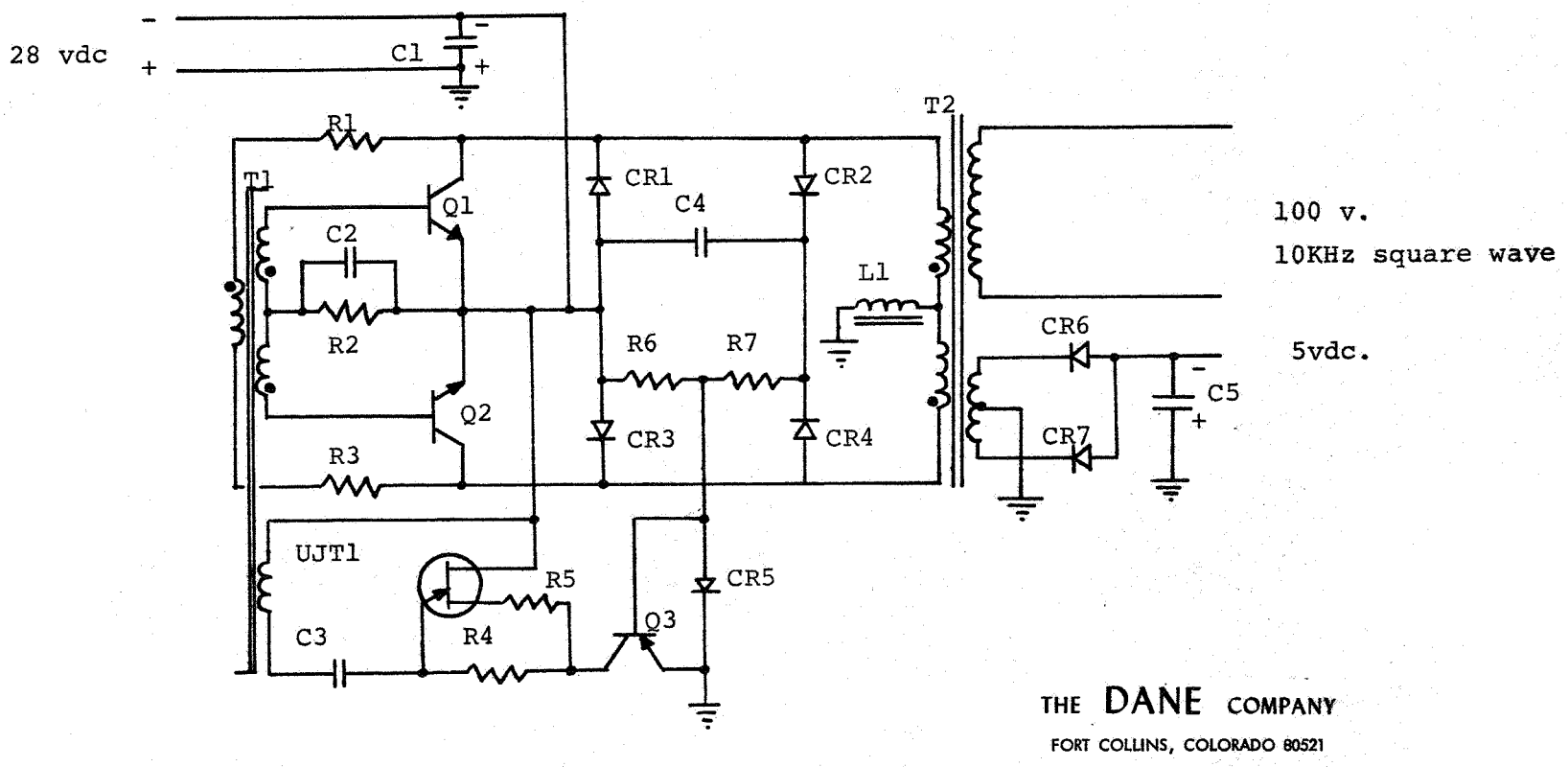


FIG. 43 - Main inverter for ACCENT prototype system.

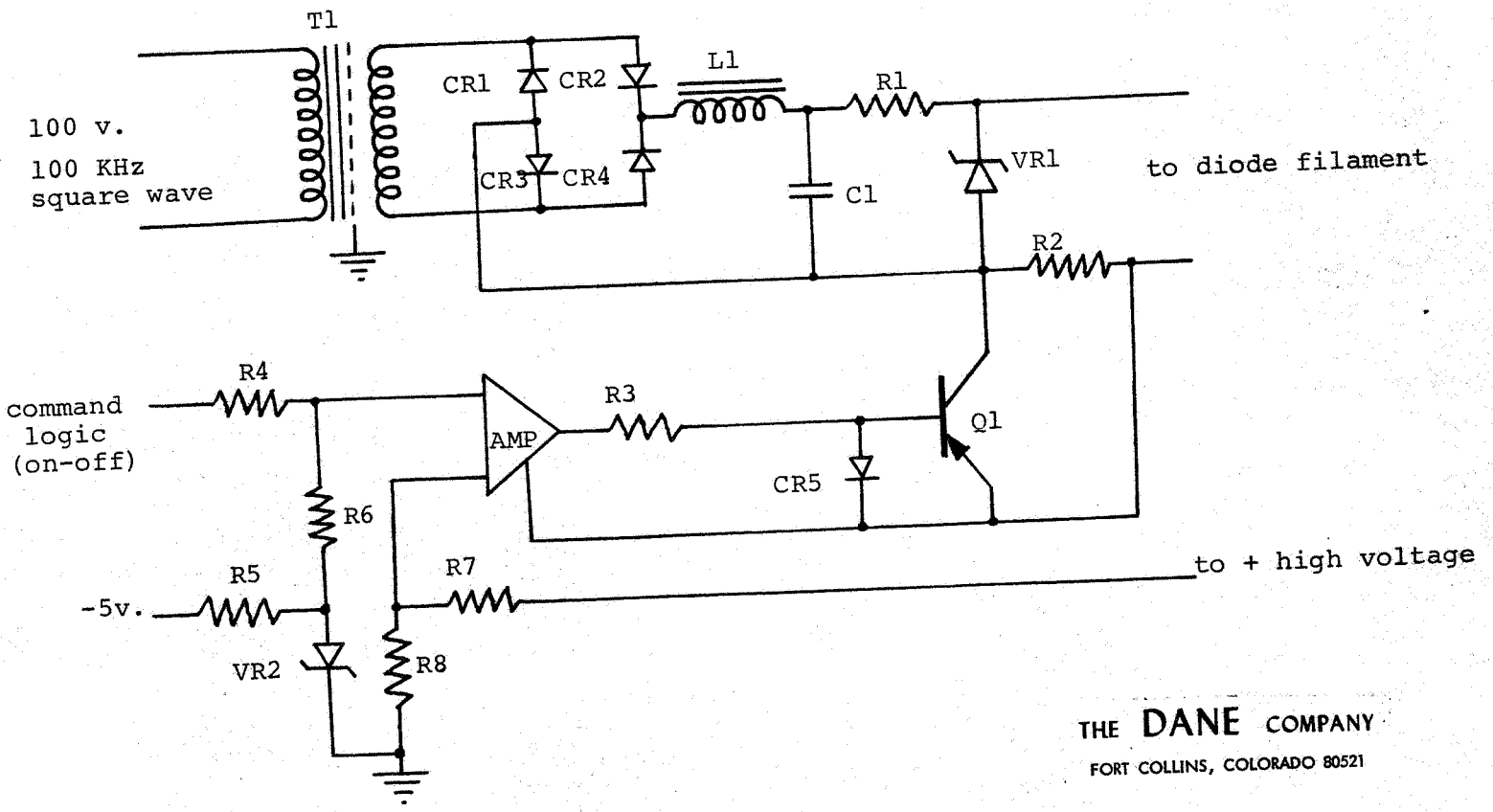


FIG. 44 - Main high-voltage regulator supply for ACCENT prototype system.

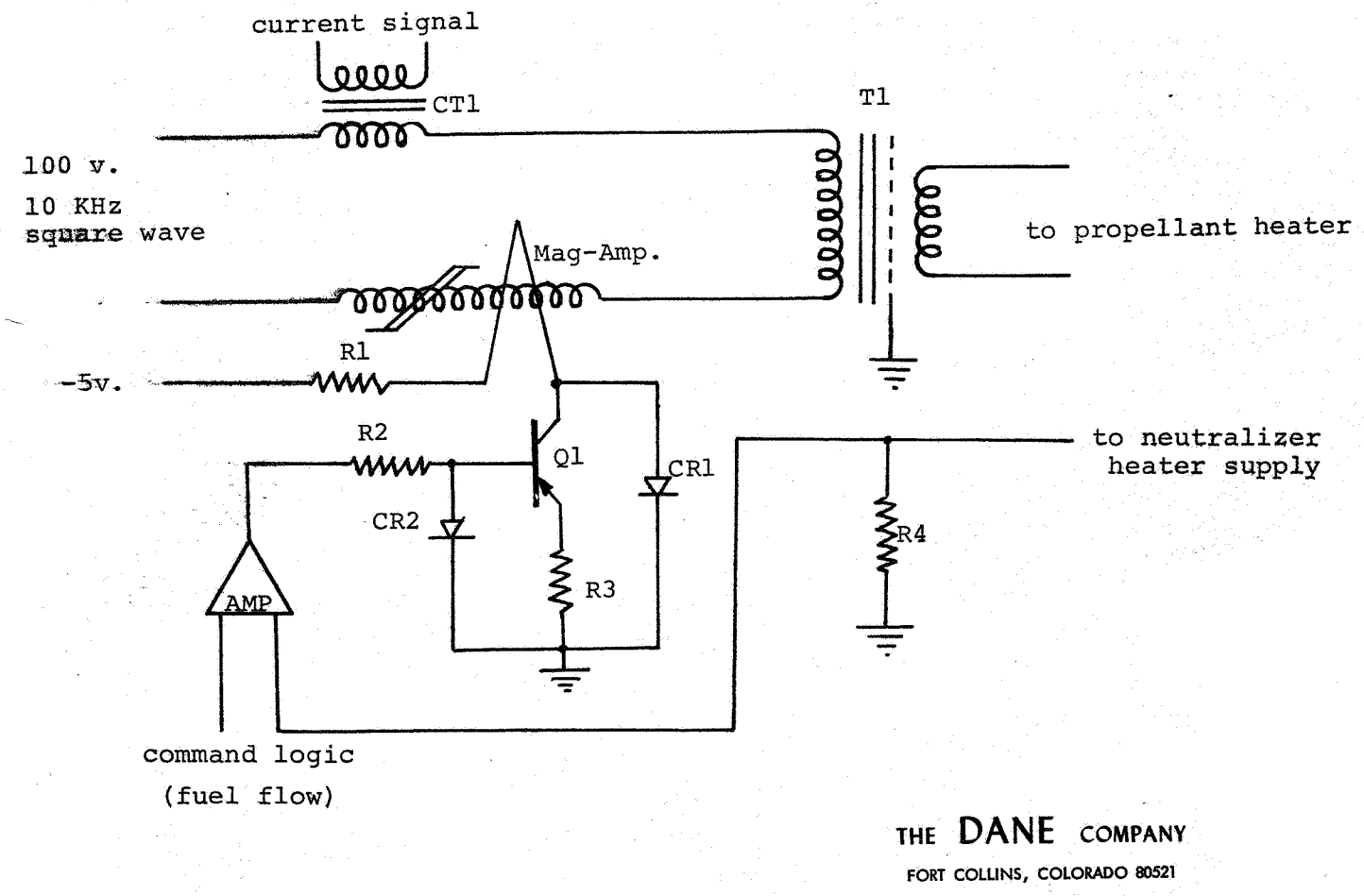


FIG. 45 - Propellant-heater power supply.

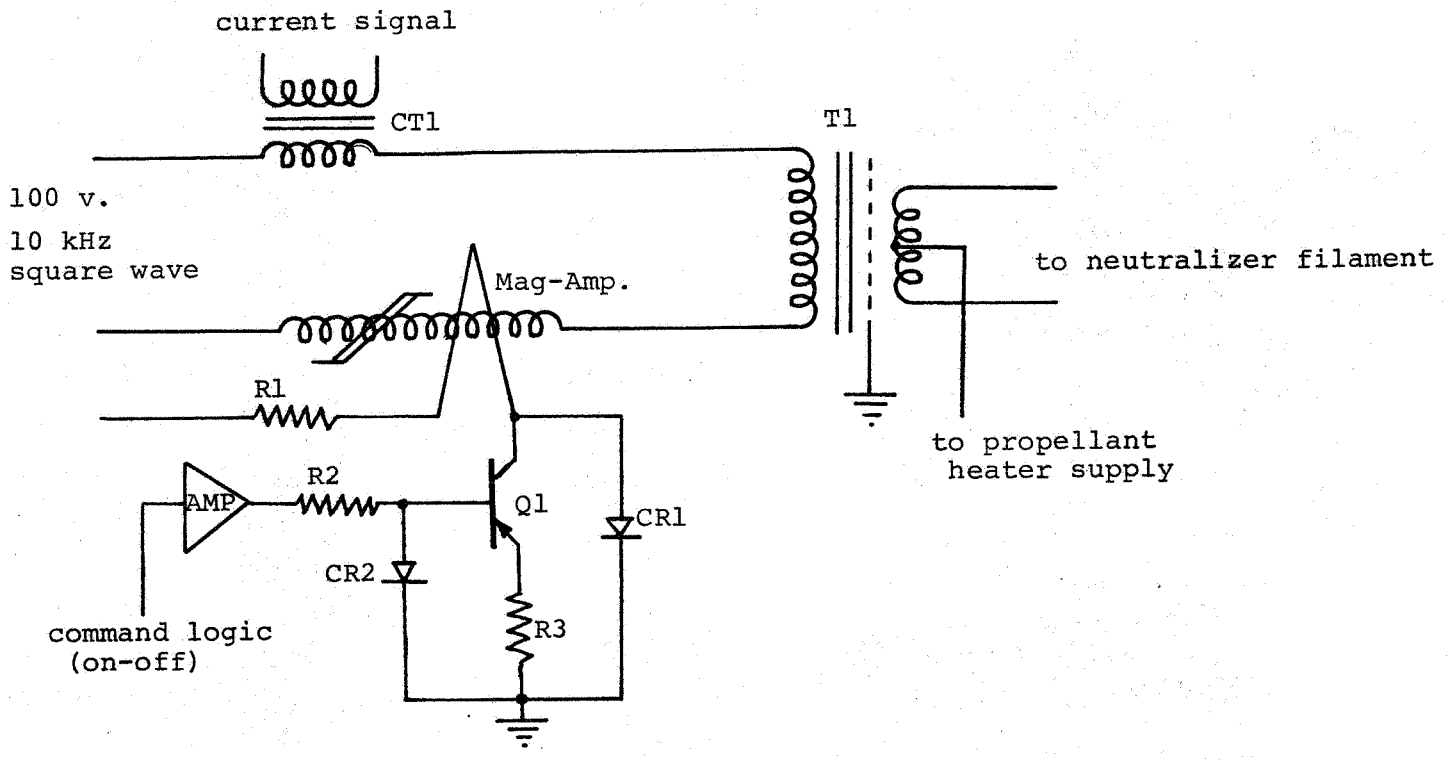


THE DANE COMPANY
FORT COLLINS, COLORADO 80521

FIG. 46 - Neutralizer-filament power supply.

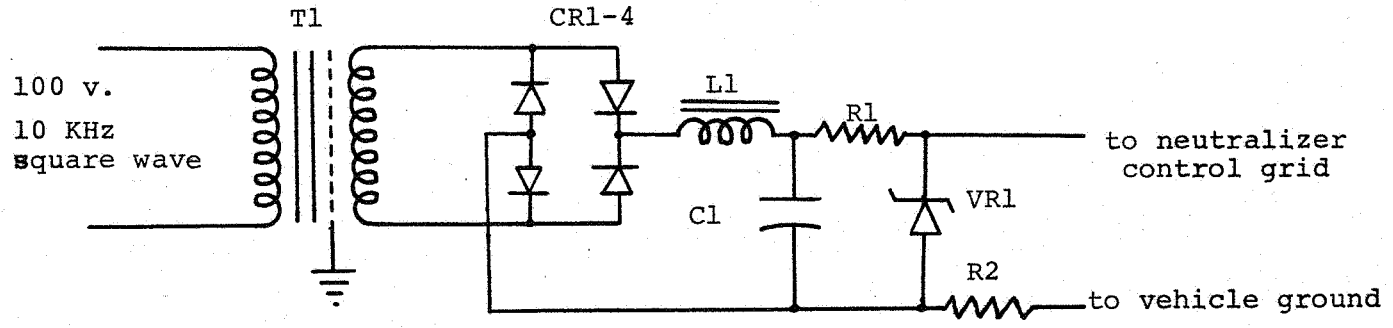


THE DANE COMPANY
FORT COLLINS, COLORADO 80521

FIG. 47 - Neutralizer-grid bias supply.

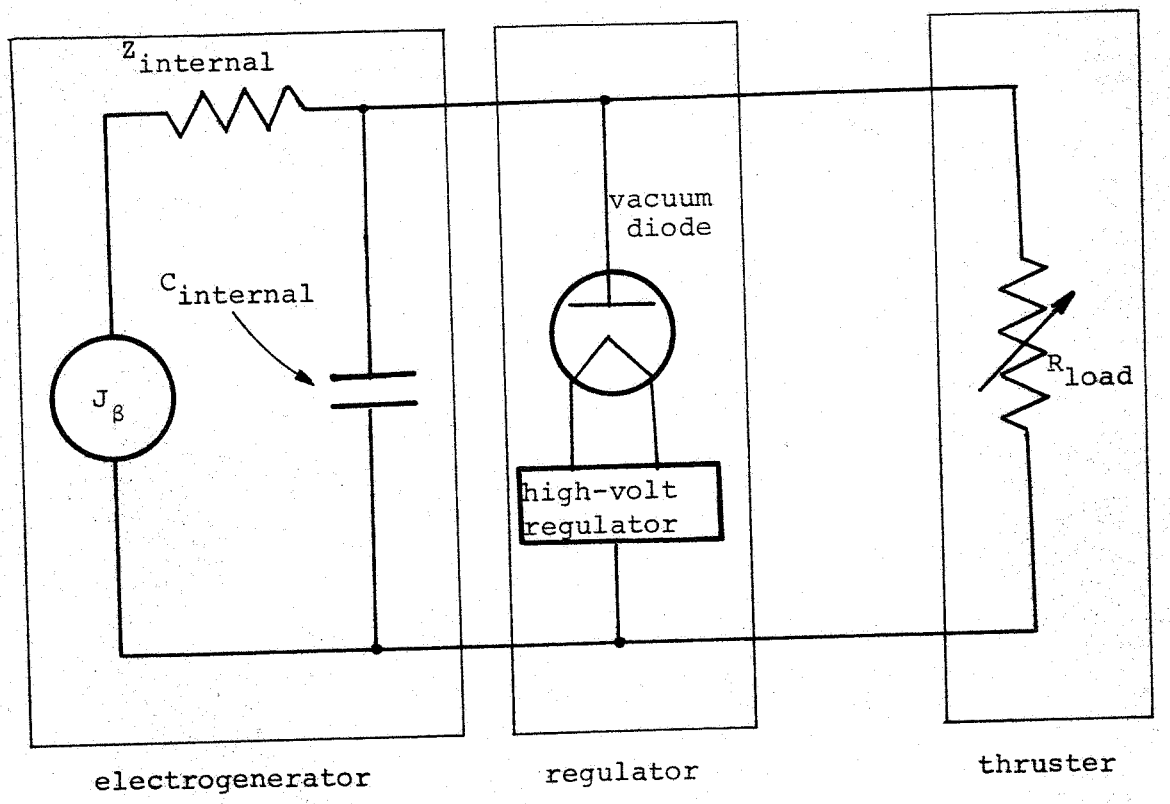


FIG. 48 - Equivalent circuit of ACCENT system electrogenerator, voltage regulator, and thruster.

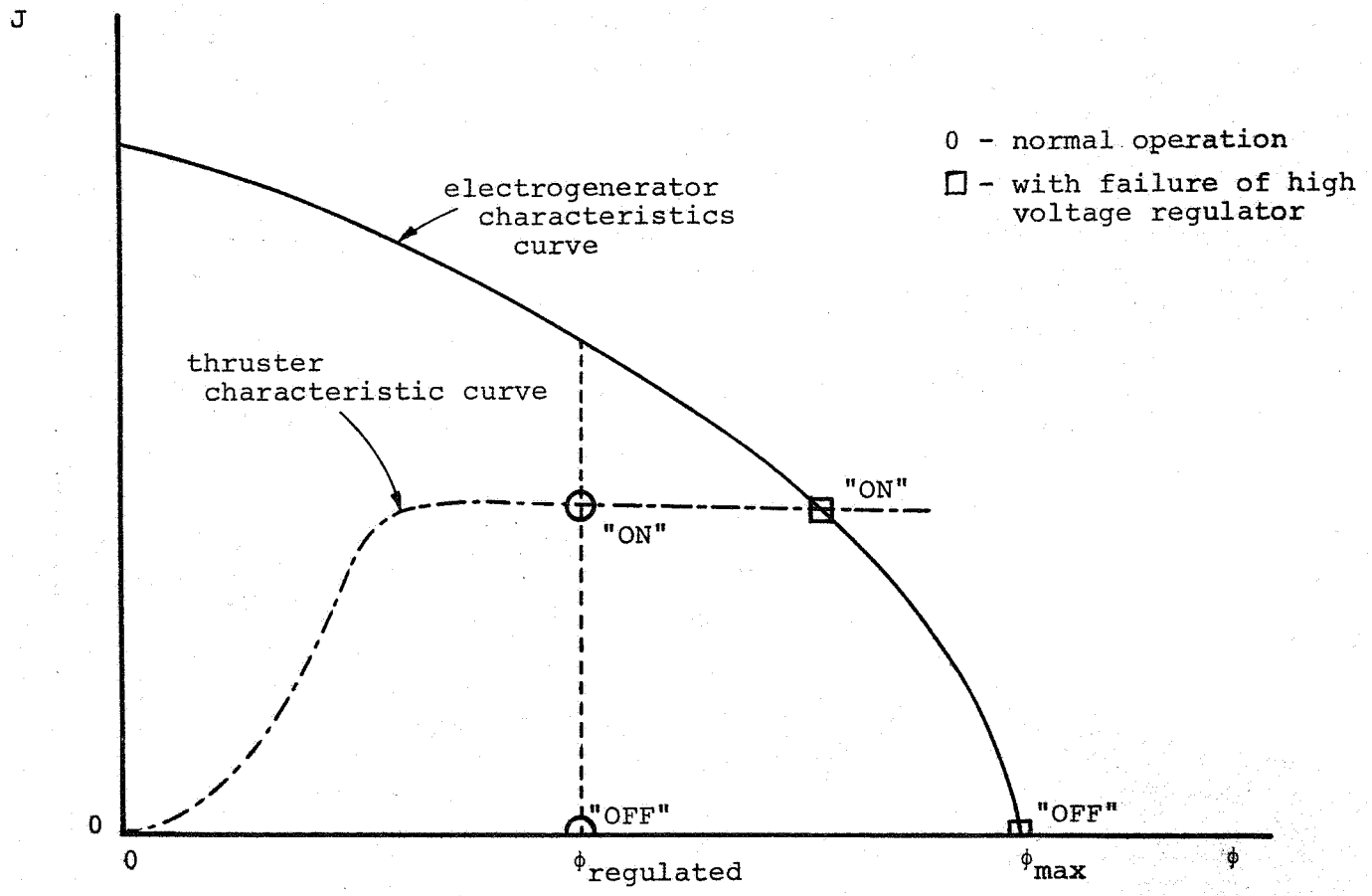


FIG. 49 - Operating modes of ACCENT system with cesium-contact ion thruster.

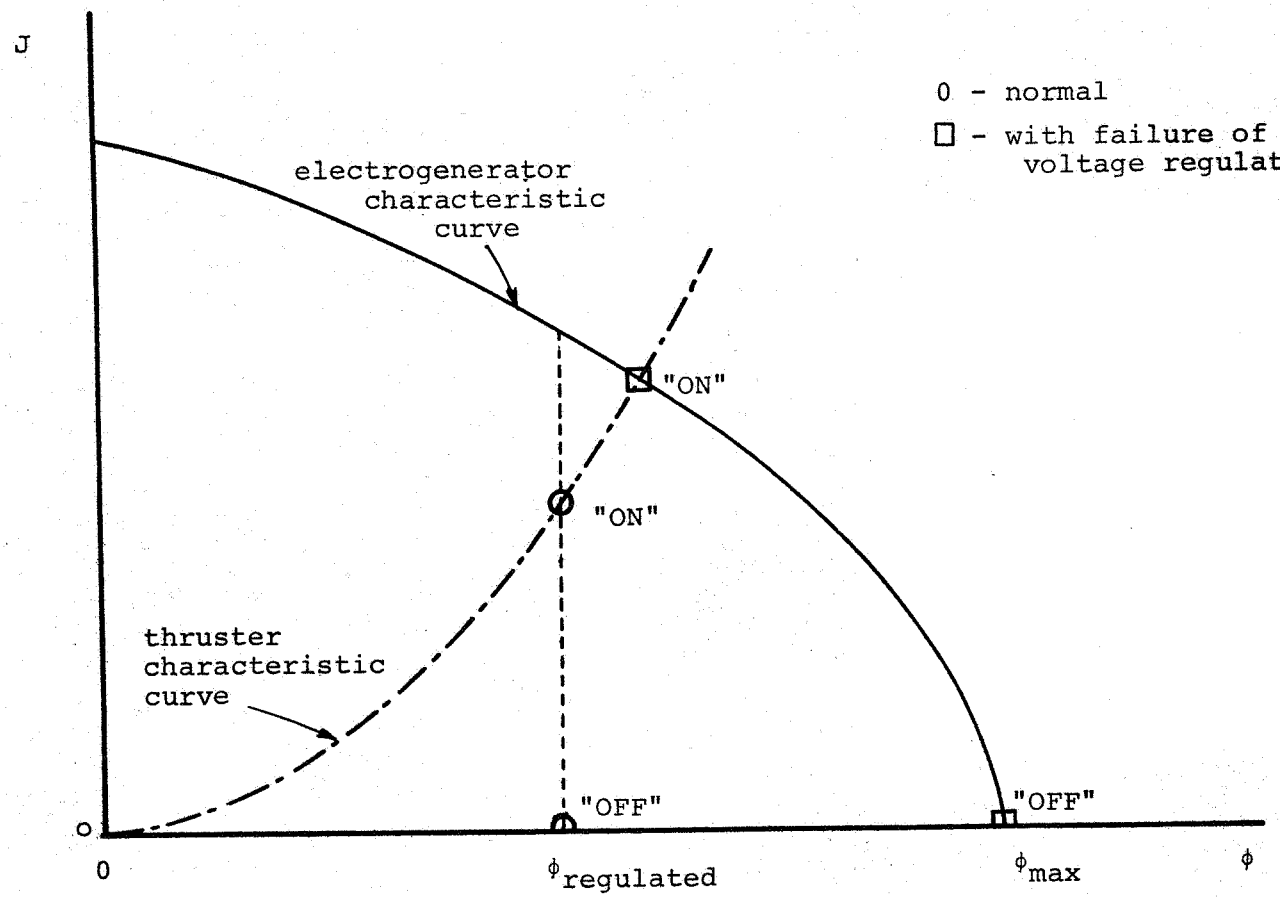


FIG. 50 - Operating modes of ACCENT system with liquid-spray charged-particle thruster.

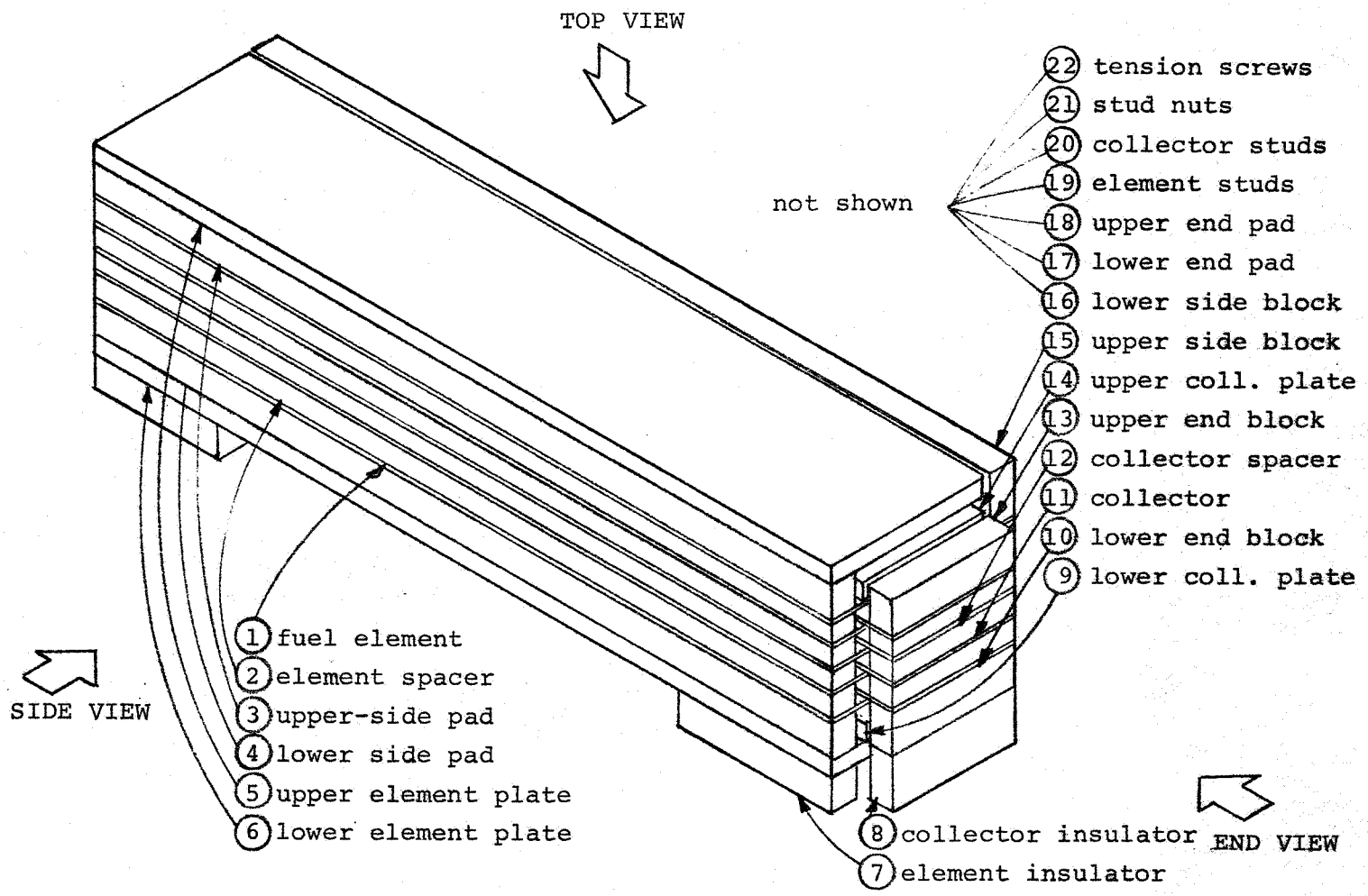


FIG. 51 - Recommended electrogenerator mechanical design with rectangular flat-plate fuel elements.

THE DANE COMPANY
FORT COLLINS, COLORADO 80521

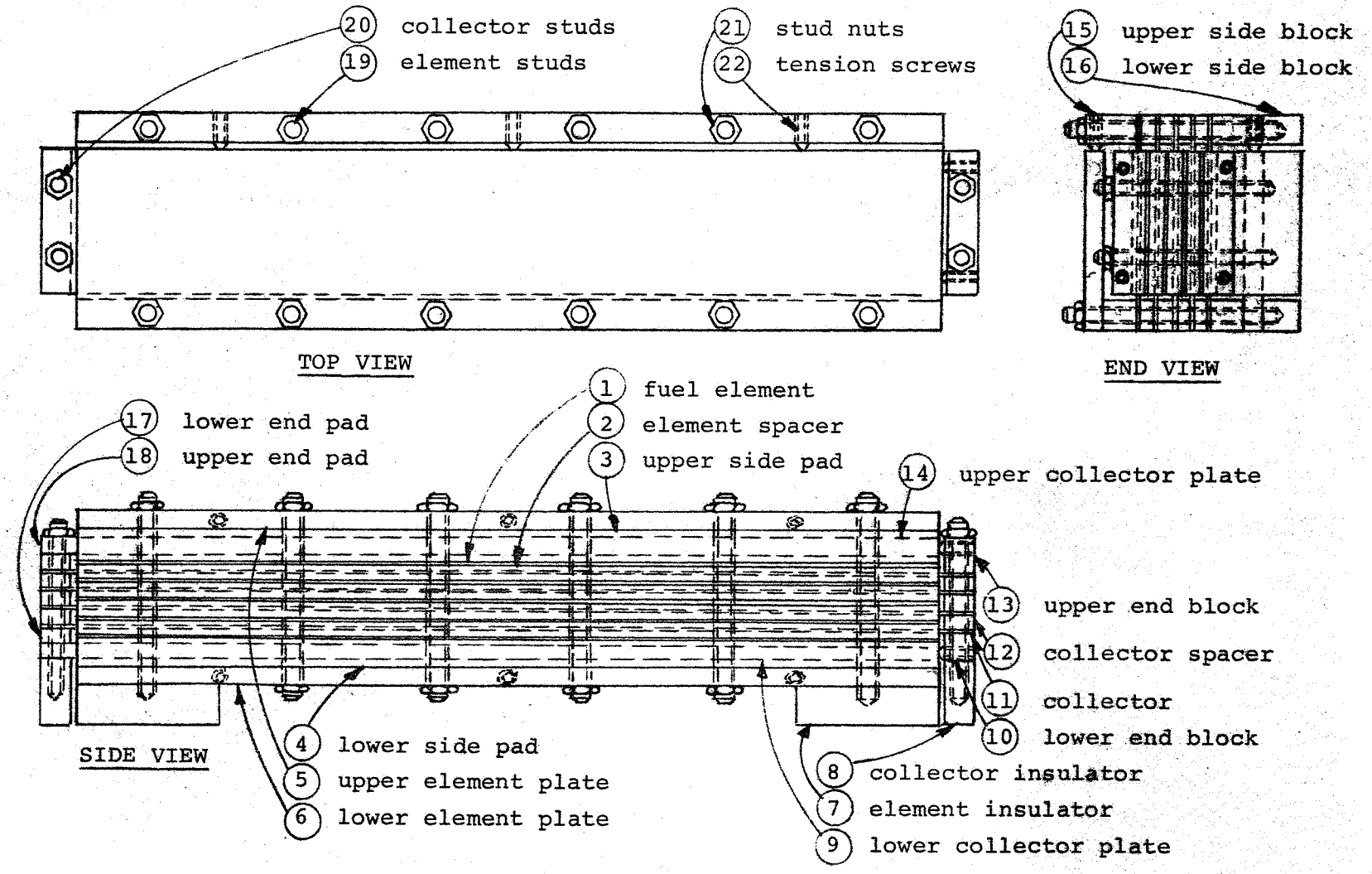


FIG. 52 - Assembly drawing of recommended electrogenerator mechanical design with rectangular fuel elements.

THE DANE COMPANY
FORT COLLINS, COLORADO 80521

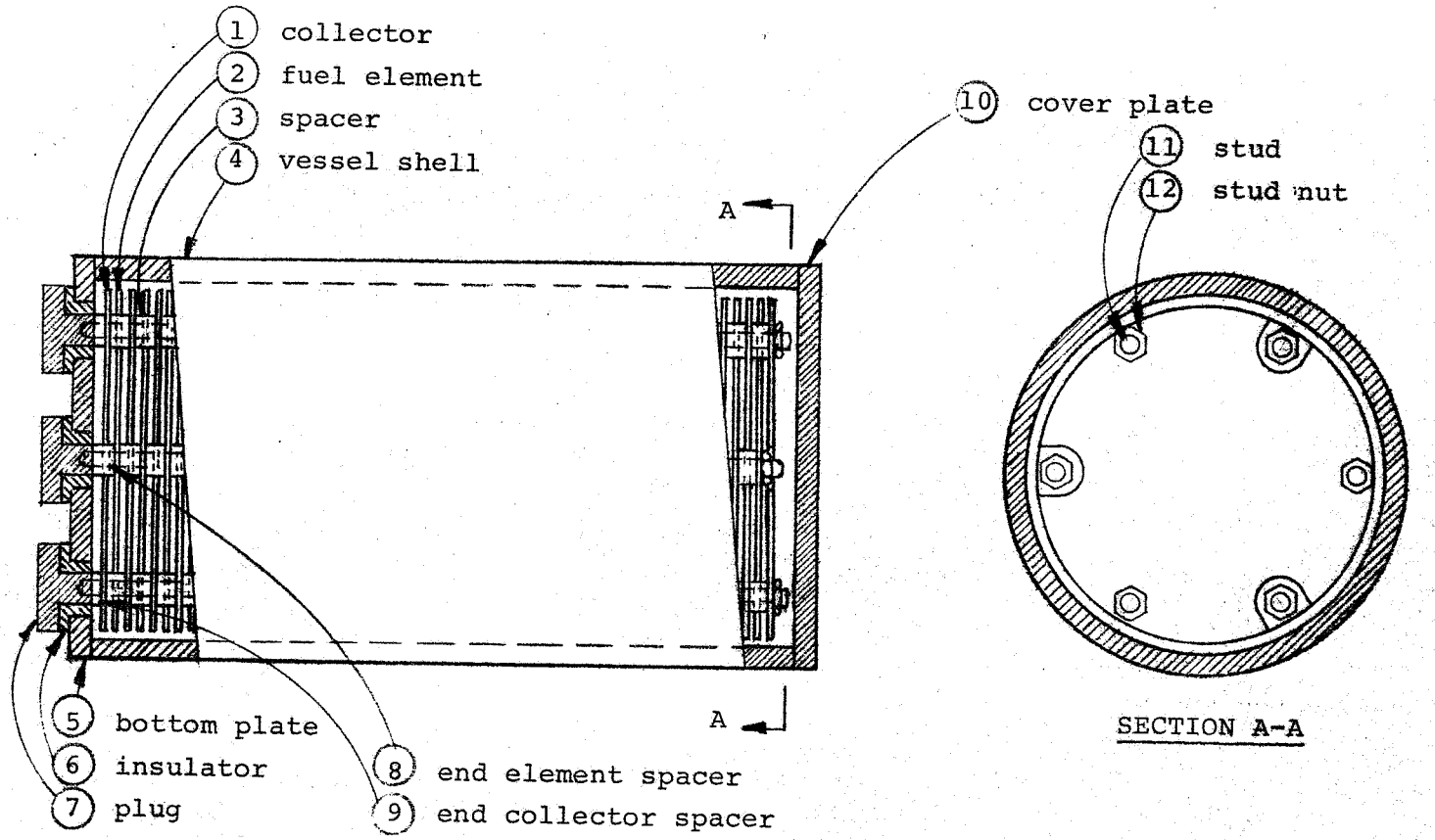


FIG. 53 - Alternate recommended electrogenerator mechanical design with circular-disc fuel elements.

THE DANE COMPANY
FORT COLLINS, COLORADO 80521

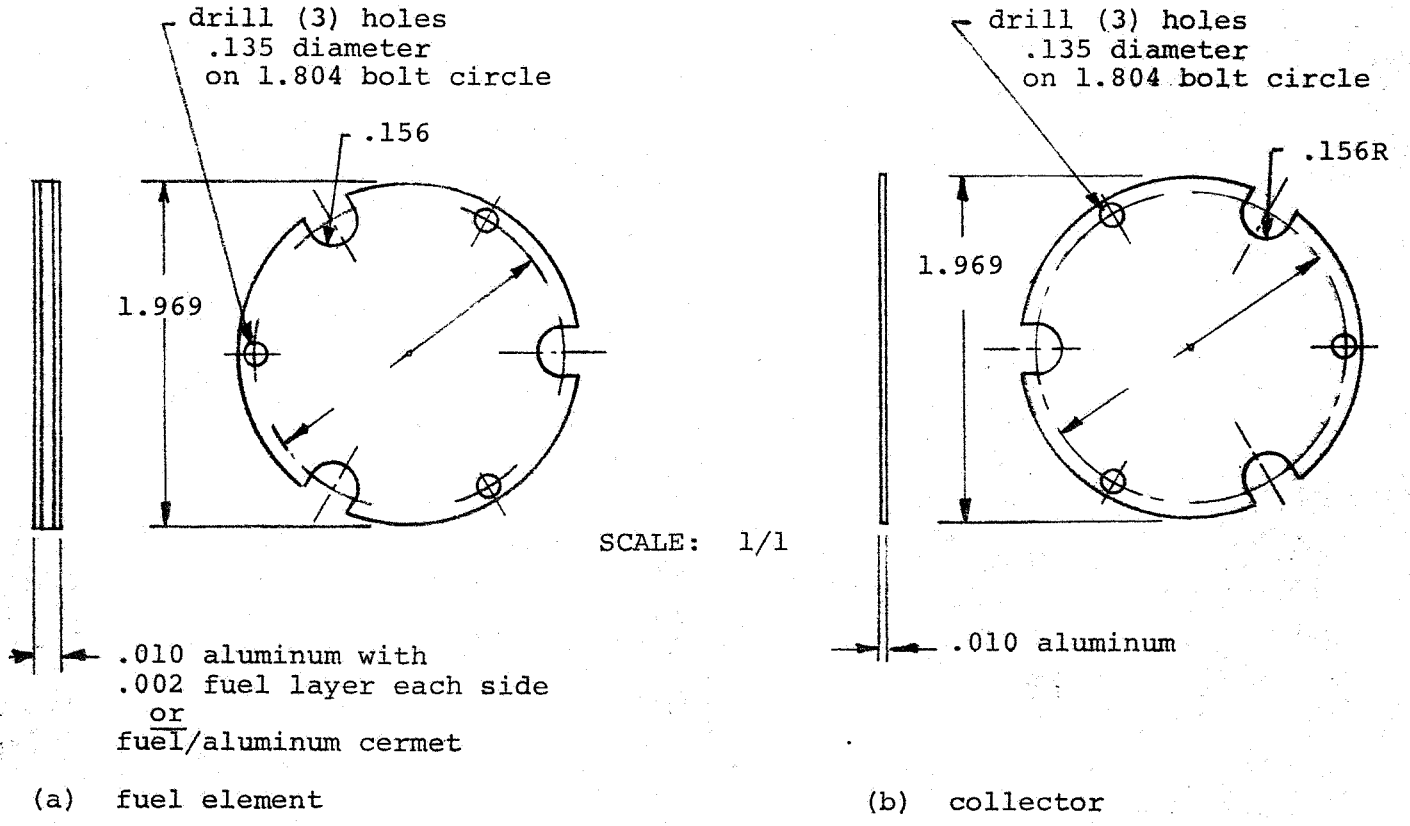


FIG. 54 - Fuel elements and collectors for circular-disc electrogenerator design.

# APPENDIX A

## BETA ENERGY SPECTRA

Beta-decay energy spectra are conventionally presented in Fermi-Kurie plots such as shown in Figure A1, where $N(\eta)$ is the number of betas per unit momentum interval, $\eta$ is the electron momentum after ejection from the atom in units of mc, m is electron mass, c is the speed of light, F is the Fermi function, and W is the total energy of the electron in units of $mc^2$. The following relations are of interest:

$$\eta^2 = W^2 - 1 \tag{A1}$$

$$E = mc^2(W-1) \tag{A2}$$

$$mc^2 = .5109 \text{ Mev} \tag{A3}$$

$$N(E) = N(\eta)/\left[1-(1/W)^2\right]^{\frac{1}{2}} \tag{A4}$$

With these relations, the shape of the energy spectrum, N(E) versus E, can be obtained. Then the spectrum function f(E) versus E can be obtained by normalizing the N(E) plot to conform to the identity:

$$\int_0^\infty f(E)\, dE \equiv 1 \tag{A5}$$

This method of obtaining the energy spectrum f(E) versus E is described in detail in the following paragraphs using the Fermi-Kurie plot (ref. A1) strontium-90 as an example.

Because of the final normalization of N(E) to obtain f(E), the units of the ordinate of the Fermi-Kurie plot need not be defined. For convenience in the analysis, arbitrary units of 0 to 7 can be assigned to ordinate of the Fermi-Kurie plot shown in Figure A1. Conversion from the Fermi-Kurie plot to N(E) is shown in Table A1. End-point energy in Table A1 was obtained from ref. A2, and the end-point values of W and $\eta$ were adjusted to this value of end-point energy. It should also be noted that the Fermi-Kurie plot

is nonlinear because the beta decay of strontium-90 is a forbidden transition.

Columns 1 and 2 of Table A1 are obtained directly from the Fermi-Kurie plot, and columns 3,4, and 5 are simple calculations as indicated. The Fermi function F listed in Column 6 was obtained for each value of $\eta$ from ref. A3. As described in the NBS Tables, F is a function of the electron momentum $\eta$ and the atomic number Z of the daughter atom. Strontium-90 decays to yttrium-90, so Z=39. The remainder of the columns, 7 to 11, are simple calculations as indicated. The resulting energy density function N(E) can be plotted against E as shown in Figure A2.

The plot of N(E) versus E can be normalized to obtain the spectrum density function f(E), which must conform to the identity expressed by equation (5). The energy density function f(E) for strontium-90 obtained in this way is shown in Figure A3.

Beta energy spectra for yttrium-90, promethium-147 (ref. A4), and thullium-170 (ref. A4), calculated by the same procedure and are shown in Figures A4-A6. A combined energy spectrum for the strontium-40, ytrrium-90 decay process is shown in Figure A7.

Beta-energy spectra can be calculated from semi-empirical relations such as described in ref. A5. These relations could be incorporated directly into a computer program. However, for the purposes of the present study the Fermi-Kurie-plot method was used in the interest of expediency, and clarity of detail for better fundamental understanding from the engineering viewpoint.

## REFERENCES


A1. Braden, C.H., Slack, L., and Shull, F.B.: The Forbidden Beta-Decay of $Sr^{90}$ and $Y^{90}$. Phys. Rev., 75, 1964, (1949).

A2. Daniel, H., Kaschl, G.Th., Schmitt, H., and Springer,K.: Shapes of Allowed and Unique First-Forbidden β-Ray Spectra: $In^{114}$, $K^{42}$, $Rb^{86}$, $Sr^{90}$, and $Y^{90}$. Phys. Rev., 136, 5B, B1240, (7Dec. 64).

A3. Tables for the Analysis of Beta Spectra. NBS Appl. Math. Series, 13, (June 2,1952).

A4. Agnew, H.M.: The Beta-Spectra of $Cs^{137}$, $Y^{91}$. $Pm^{147}$, $Ru^{106}$, $Sm^{151}$, $P^{32}$, and $Tm^{170}$. Phys. Rev., 77, 655, (1950).

A5. Van Tuyl, H.H.: Bremrad - A Computer Code for External and Internal Bremsstrahlung Calculations. AEC Research and Development Report HW-83784, (Sept. 1964).

TABLE A1. Conversion of Fermi-Kurie plot for strontium-90.

| 1 | 2 | 3 | 4 | 5 | 6 | 7 | 8 | 9 | 10 | 11 |
|---|---|---|---|---|---|---|---|---|---|---|
| W | $\left[\frac{N(\eta)}{\eta^2 F}\right]^{\frac{1}{2}}$ | $\eta^2$ =①$^2$-1 | $\eta$ =③$^{\frac{1}{2}}$ | E= .511(①-1) | F | N(η)= ②·③·⑥ | $1/W^2$ =1/①$^2$ | 1-(1/W$^2$) =1-⑧ | $\left[1-(1/W^2)\right]^{\frac{1}{2}}$ =⑨$^{\frac{1}{2}}$ | N(E) =⑦/⑩ |
| 1.05 | 6.4 | .102 | .32 | .0255 | 0.661 | 2.76 | .903 | .097 | .312 | 8.83 |
| 1.1 | 6.0 | .21 | .459 | .0511 | .993 | 7.51 | .827 | .173 | .416 | 18.03 |
| 1.15 | 5.7 | .323 | .569 | .0766 | 1.292 | 13.6 | .755 | .245 | .495 | 27.4 |
| 1.2 | 5.4 | .44 | .663 | .1022 | 1.577 | 20.2 | .695 | .305 | .552 | 36.6 |
| 1.25 | 5.2 | .563 | .75 | .1276 | 1.866 | 28.4 | .64 | .36 | .6 | 47.3 |
| 1.3 | 4.9 | .69 | .83 | .1531 | 2.160 | 35.7 | .592 | .408 | .639 | 55.9 |
| 1.35 | 4.65 | .823 | .908 | .1788 | 2.462 | 43.8 | .549 | .451 | .671 | 65.2 |
| 1.4 | 4.4 | .96 | .98 | .2045 | 2.756 | 51.2 | .51 | .49 | .699 | 73.3 |
| 1.45 | 4.2 | 1.025 | 1.012 | .23 | 2.904 | 52.5 | .493 | .507 | .711 | 73.9 |
| 1.5 | 3.85 | 1.25 | 1.12 | .255 | 3.405 | 63.0 | .445 | .555 | .745 | 84.6 |
| 1.55 | 3.6 | 1.403 | 1.186 | .281 | 3.730 | 67.8 | .416 | .584 | .765 | 88.5 |
| 1.6 | 3.35 | 1.56 | 1.25 | .307 | 4.065 | 71.3 | .39 | .61 | .78 | 91.4 |
| 1.65 | 3.1 | 1.723 | 1.313 | .332 | 4.405 | 73.0 | .367 | .633 | .795 | 91.7 |
| 1.7 | 2.8 | 1.89 | 1.375 | .358 | 4.758 | 70.5 | .346 | .654 | .809 | 87.3 |
| 1.75 | 2.4 | 2.063 | 1.44 | .383 | 5.143 | 60.9 | .326 | .674 | .821 | 74.3 |
| 1.8 | 2.1 | 2.24 | 1.497 | .409 | 5.489 | 54.1 | .309 | .691 | .831 | 65.1 |
| 1.85 | 1.75 | 2.423 | 1.56 | .434 | 5.893 | 43.7 | .292 | .708 | .841 | 52.0 |
| 1.9 | 1.4 | 2.61 | 1.616 | .46 | 6.260 | 32.1 | .277 | .723 | .85 | 37.7 |
| 1.95 | 0.9 | 2.803 | 1.676 | .486 | 6.670 | 15.2 | .263 | .737 | .857 | 17.6 |
| 2. | 0.5 | 3.0 | 1.723 | .511 | 6.998 | 5.25 | .250 | .75 | .865 | 6.05 |
| 2.07 | 0.0 | 3.29 | 1.814 | .546 | - | 0.0 | - | - | - | 0.0 |

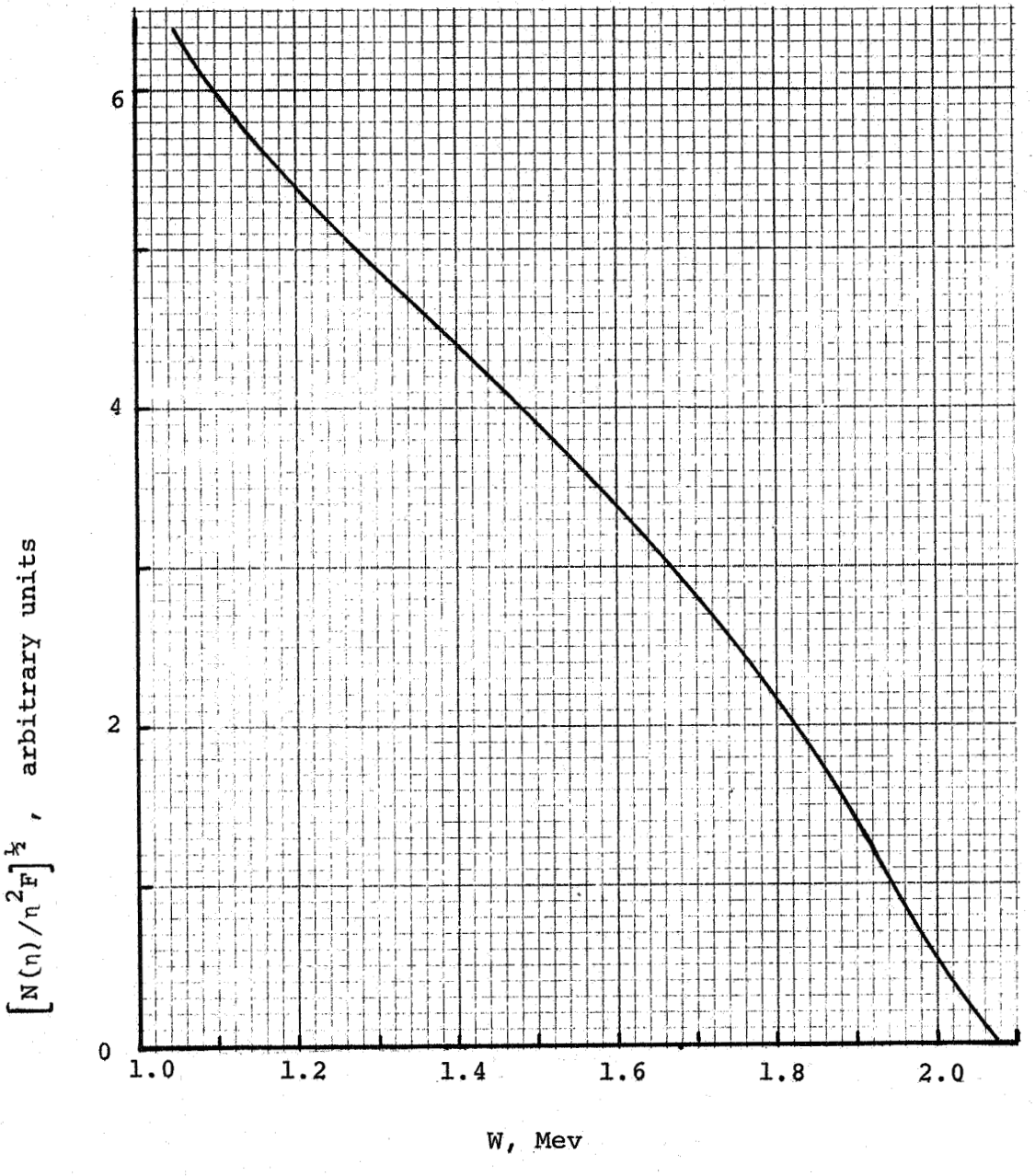


FIG. A1 - Fermi-Kurie plot for strontium-90.

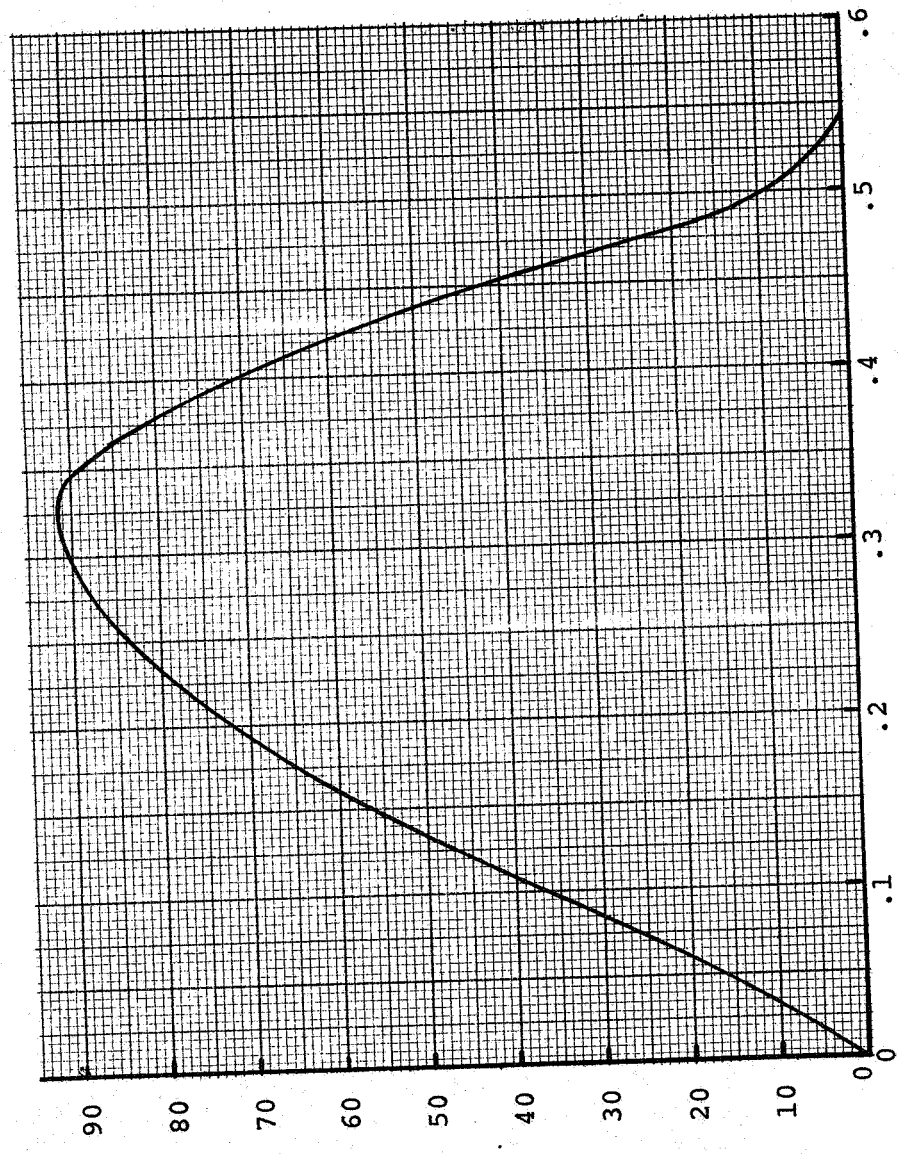


FIG. A2 - Shape of beta energy spectrum for strontium-90

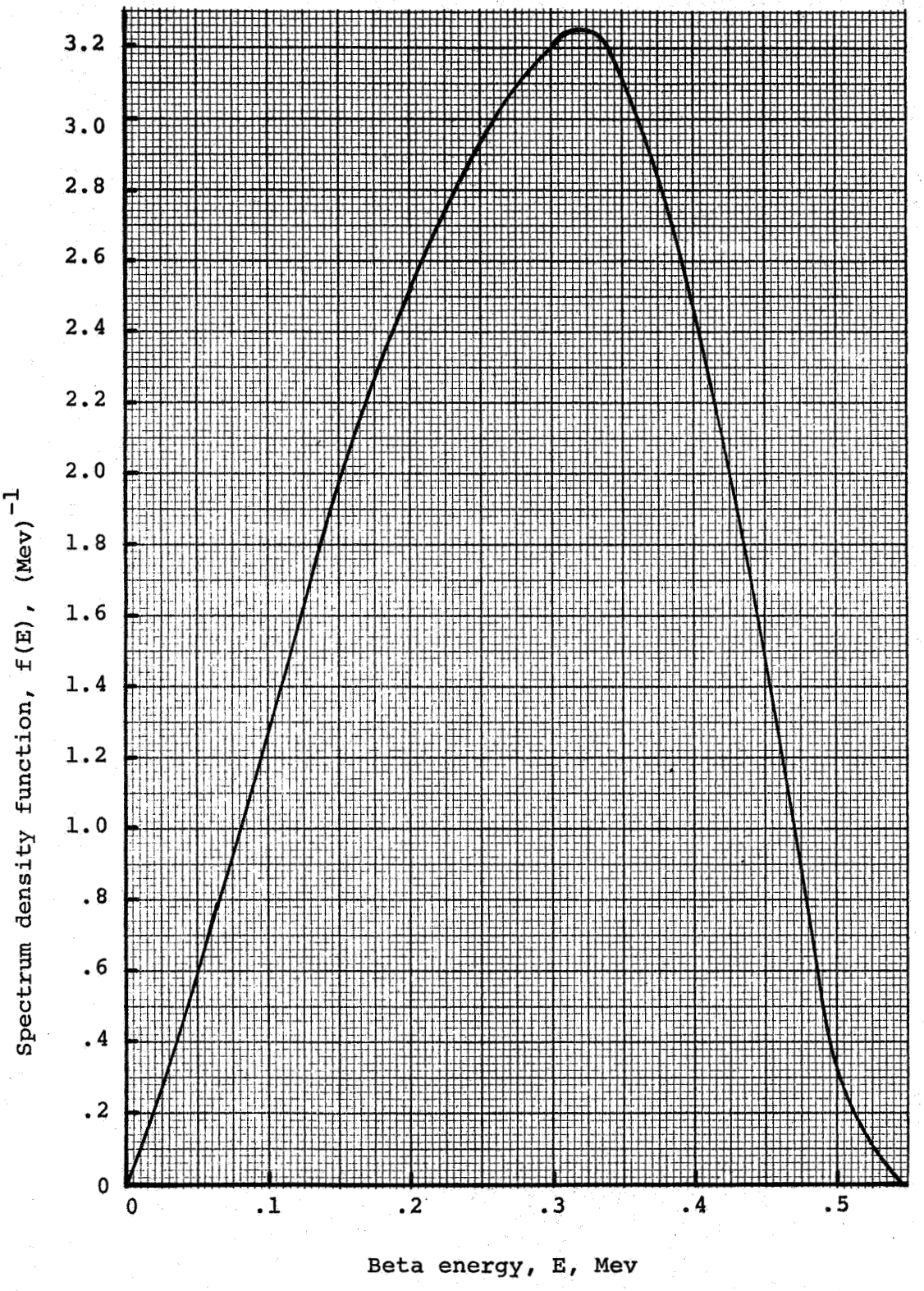


FIG A3 - Beta energy spectrum of strontium-90

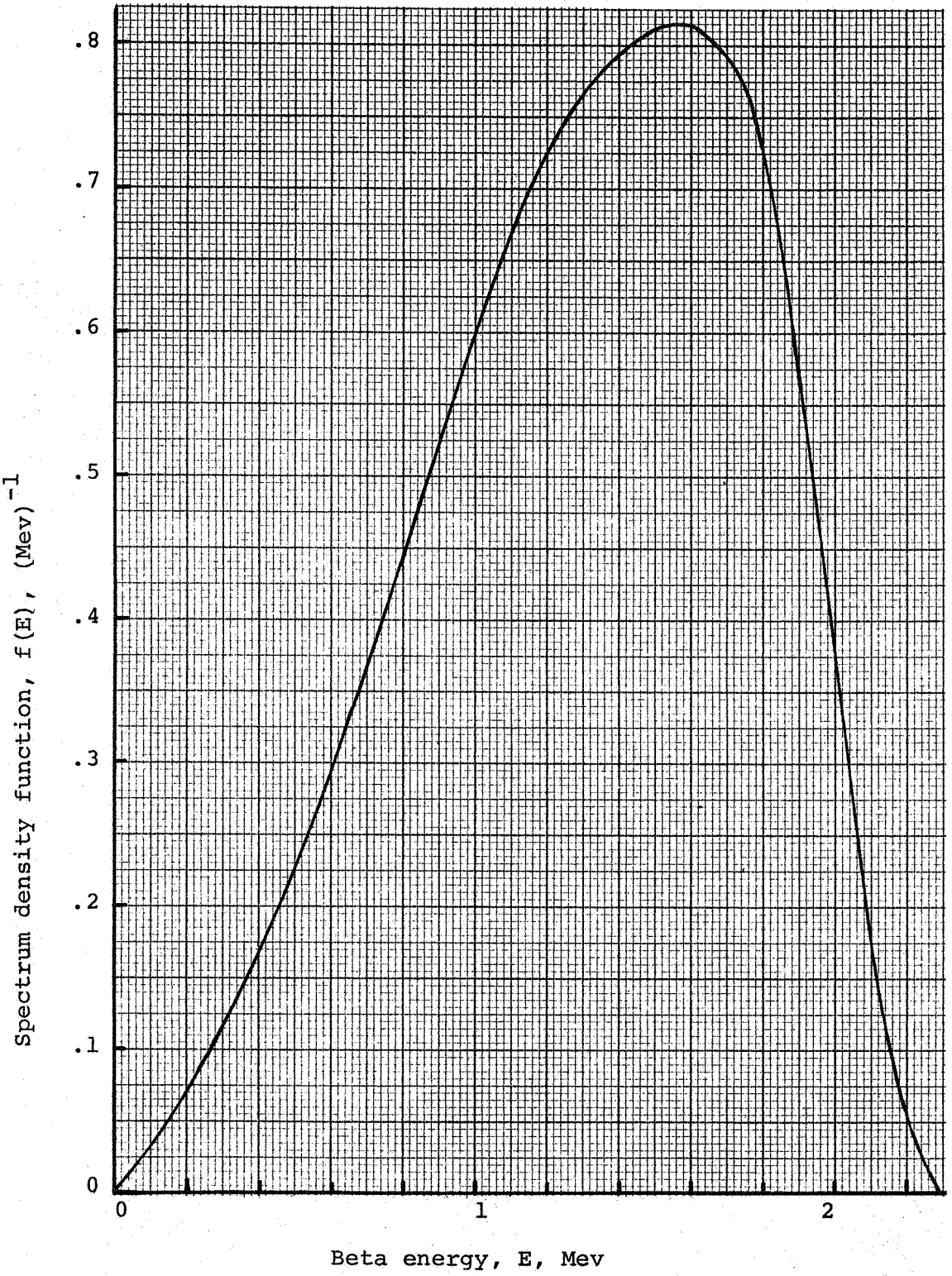


FIG. A4 - Beta energy spectrum of yttrium-90.

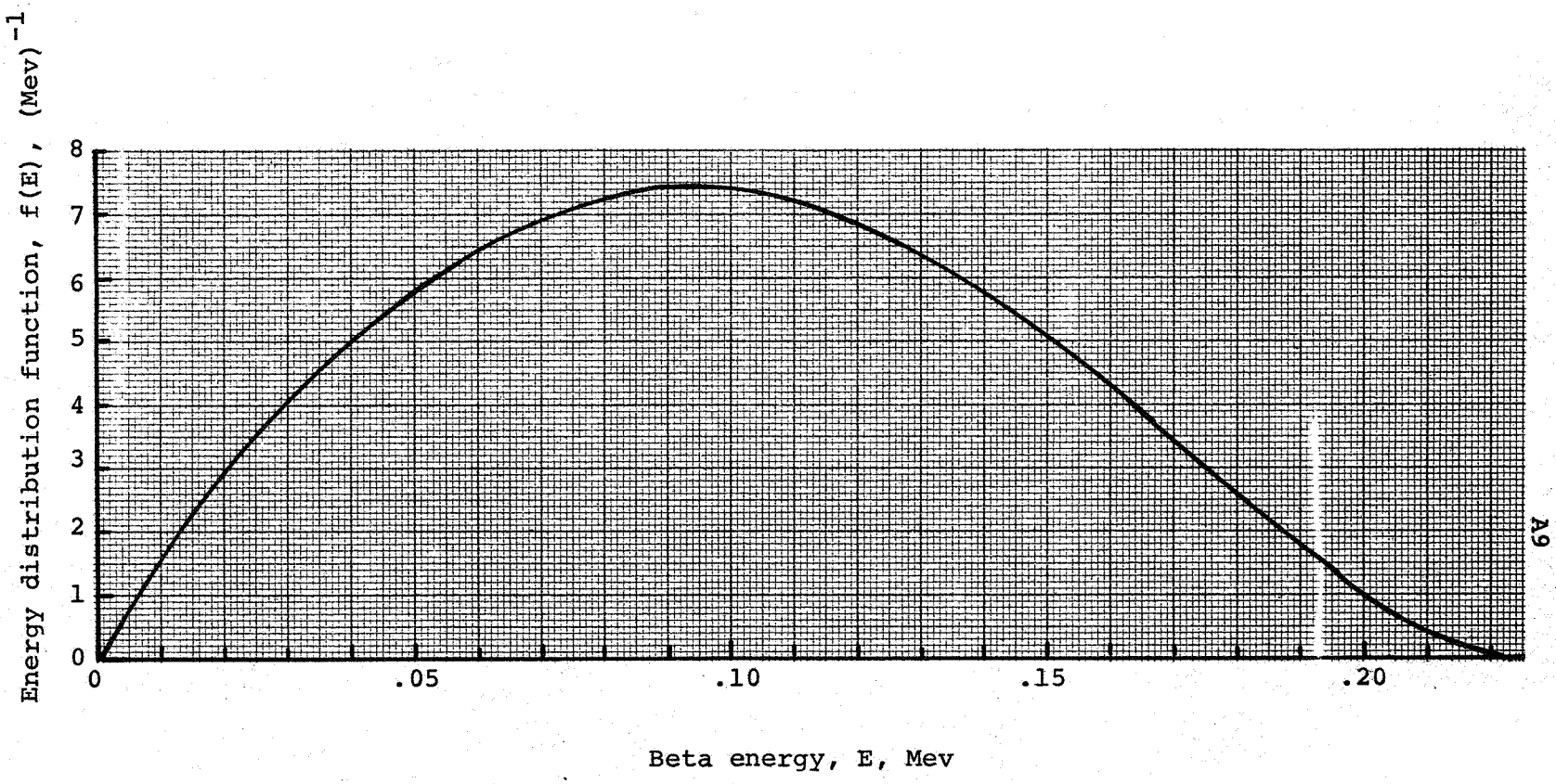


FIG. A5 - Beta spectrum of promethium-147.

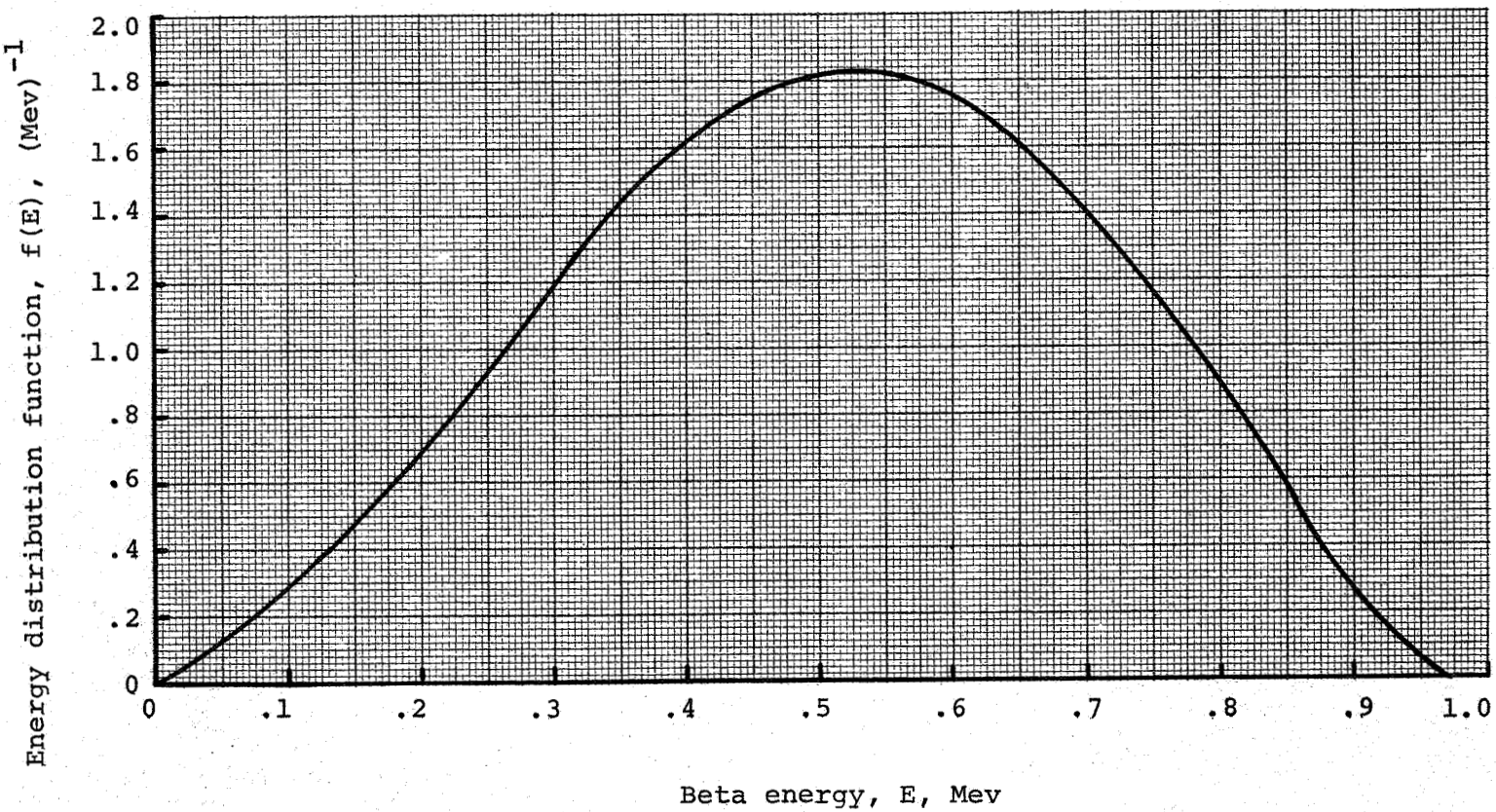


FIG. A6 - Beta spectrum of thulium-170.

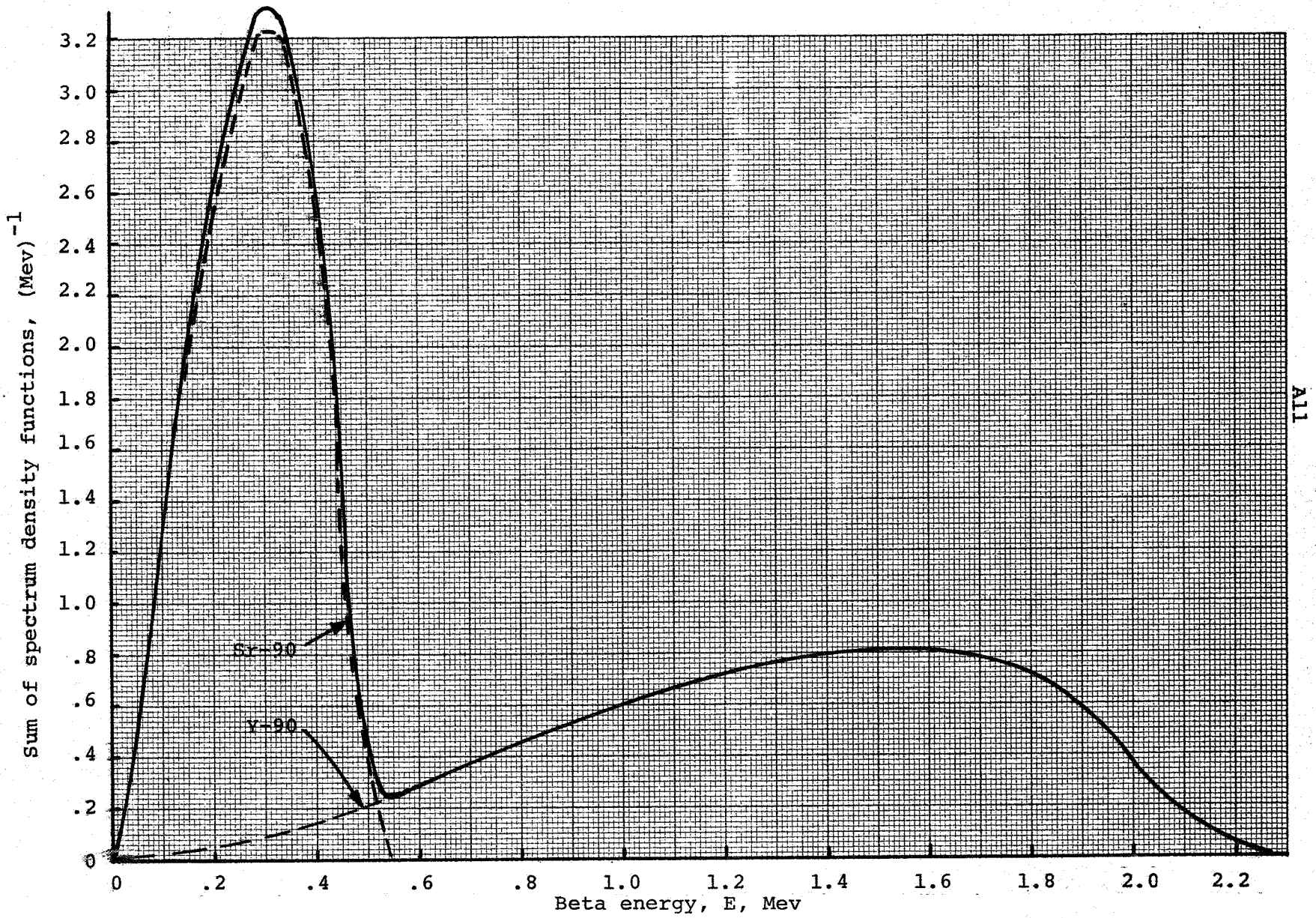


FIG. A7 - Beta spectrum of strontium-90-yttrium-90

# APPENDIX B

## BETA RANGE - ENERGY

Range-Energy data for beta particles passing through matter are conventionally presented in terms of range in milligrams/cm$^2$ as a function of beta energy. Data from refs. B1 and B2 are summarized in Figure B1.

For betas passing through materials other than aluminum, the correction factors given in ref. B3 can be used to obtain the range R in centimeters:

$$R = (1/\sigma)(13/27)(A/Z)(mg/cm^2)_{Al} \qquad (B1)$$

where $\sigma$ is the density in mg/cm$^2$ of the material, A is the average molecular weight of the material, and Z is the average atomic number of the material. The range equation (B1) can be expressed as:

$$R = C_R(mg/cm^2)_{Al} \qquad (B2)$$

where $C_R$ is the range coefficient. Values of the range coefficient for a number of radioisotope fuel forms and materials are listed in Table B1.

Beta range-energy plots for promethium-147-oxide, promethium-147-metal, thullium-70-oxide, and strontium-90-titanate are shown in Figures B2-B4. These range-energy relations were obtained from equation (B2), Figure B1, and Table B1. The range-energy relations shown in these figures must be treated as approximations only, since the paths of beta particles through material are not straight lines. However, the random paths probably average out, so that the range-energy relations can be used in electrogenerator performance calculations with confidence, particularly since the relations are based on experimental data.

## REFERENCES

B1. Willis, B.H.: High Energy Particle Data. AEC UCRL-2426, (October, 1953).

B2. Young, J.R.: Penetration of Electrons and Ions in Aluminum. J. Appl. Phys. 27, no. 1, 1, (January, 1956).

B3. Glendenin, L.E.: Determination of the Energy of Beta Particles and Photons by Absorption. Nucleonics, 2, 12, (Jan. 1948).

TABLE B1. Range coefficients for various radioisotope fuel forms, and materials.

| material or fuel form | $\sigma$, mg/cm$^3$ | (A/Z) | $C_R$, cm$^3$/mg |
|---|---|---|---|
| Pm(metal) | 7,300 | 2.41 | .000159 |
| $Pm_2O_3$(90% dense) | 6,600 | 2.34 | .000171 |
| $Tm_2O_3$(90% dense) | 8,600 | 2.39 | .000134 |
| $SrTiO_3$(90% dense) | 3,700 | 2.19 | .000284 |
| Al | 2,400 | 2.08 | .000417 |
| Be | 1,800 | 2.25 | .000600 |
| B | 2,300 | 2.16 | .000493 |
| Cd | 8,600 | 2.33 | .000131 |
| C | 1,620 | 2.00 | .000594 |
| Cr | 7,140 | 2.17 | .000149 |
| Cb | 8,400 | 2.27 | .000130 |
| Cu | 8,300 | 2.19 | .000127 |
| Au | 19,300 | 2.50 | .000062 |
| Fe | 6,900 | 2.15 | .000150 |
| Pb | 11,340 | 2.53 | .000107 |
| Mg | 1,570 | 2.03 | .000620 |
| Mo | 10,200 | 2.29 | .000108 |
| Ni | 8,900 | 2.10 | .000113 |
| Pt | 19,000 | 2.51 | .000066 |
| Si | 2,400 | 2.00 | .000401 |
| Ta | 16,600 | 2.48 | .000062 |
| Ti | 4,500 | 2.18 | .000233 |
| W | 19,300 | 2.49 | .000062 |
| Zn | 6,700 | 2.18 | .000157 |
| Zr | 6,400 | 2.28 | .000171 |

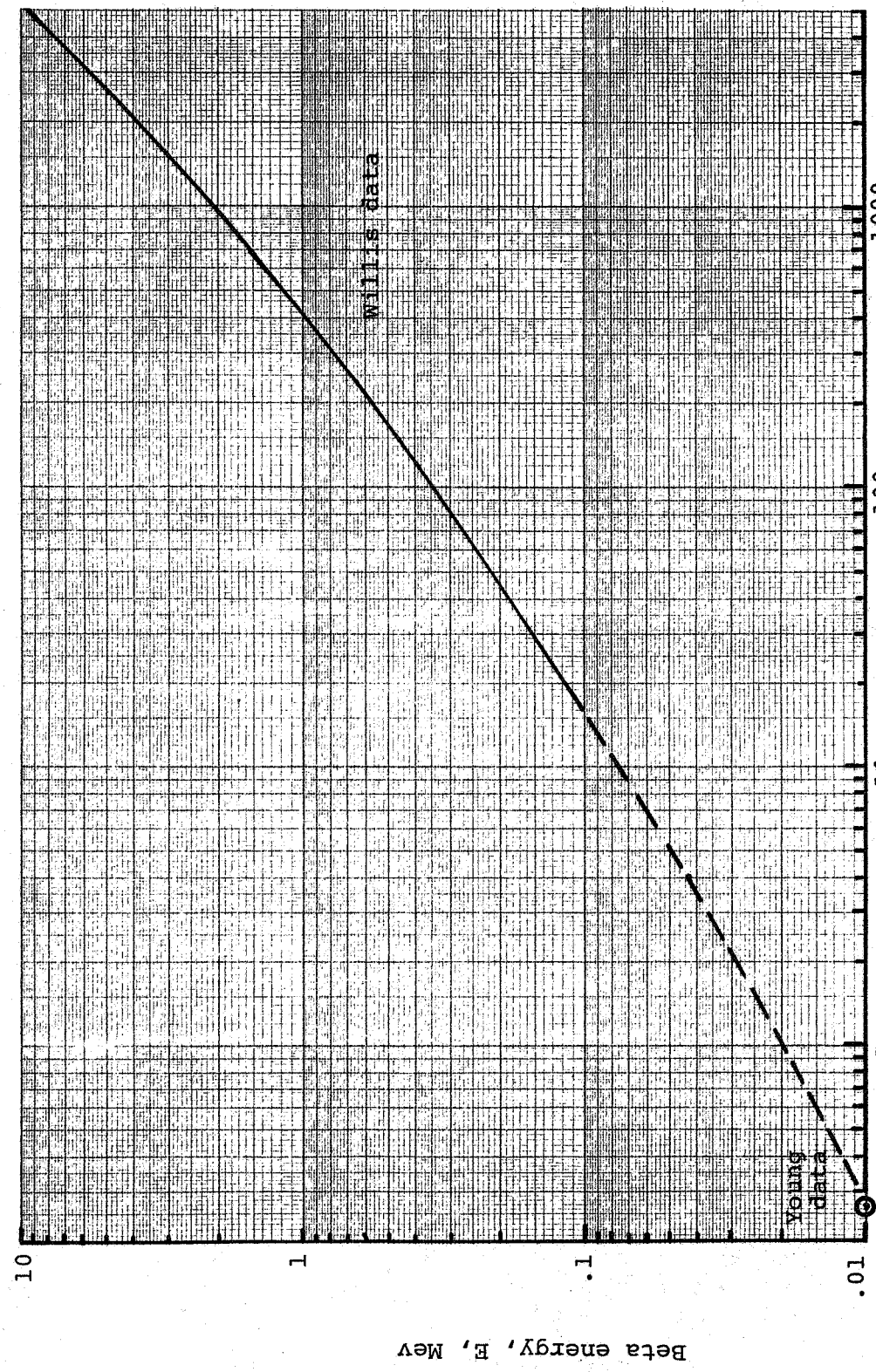


FIG. B1 - Range-energy of beta particles in aluminum.

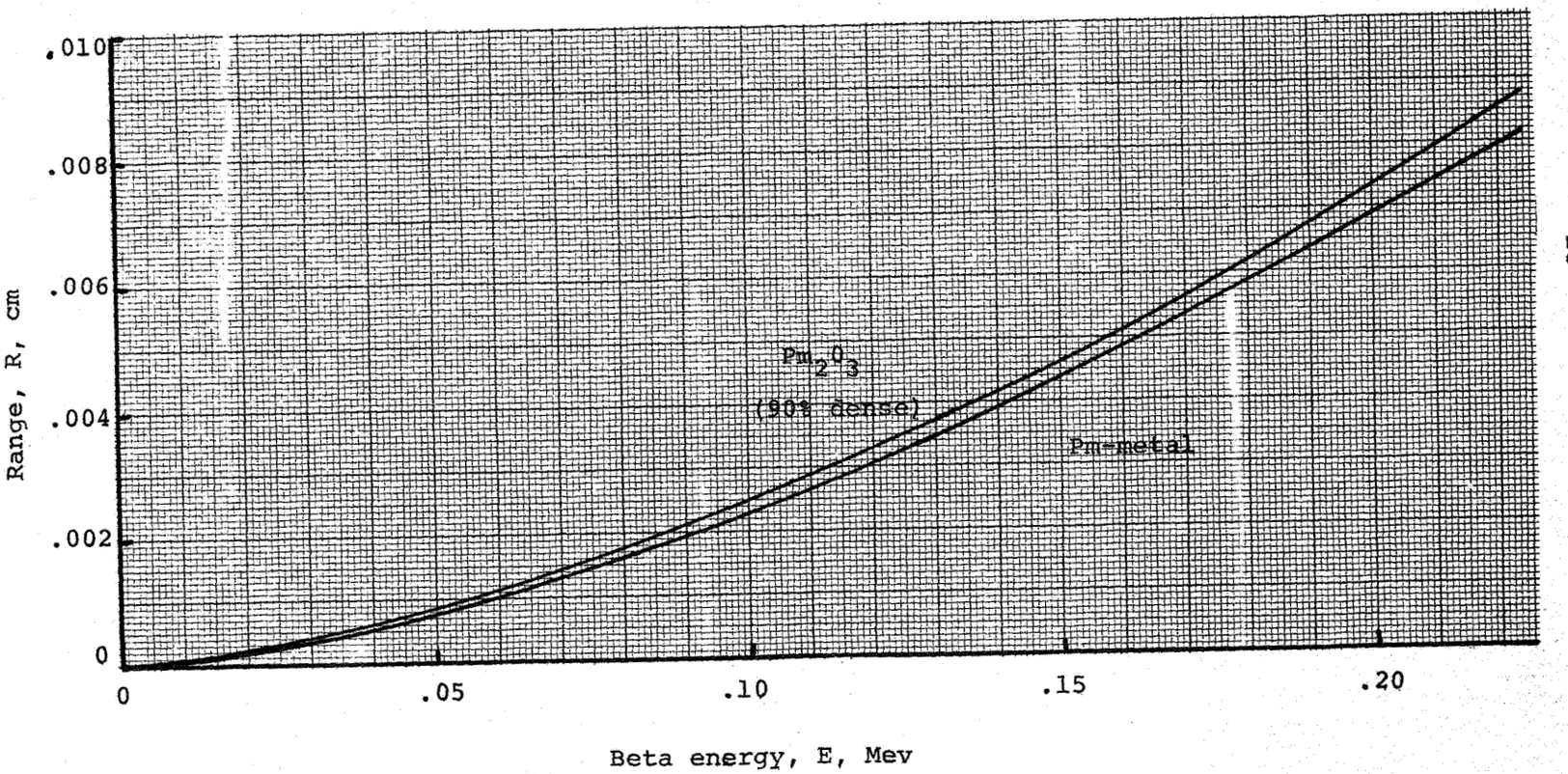


FIG. B2 - Range-energy of beta particles in promethium metal and promethium oxide. ($Pm_2O_3$, 90% dense).

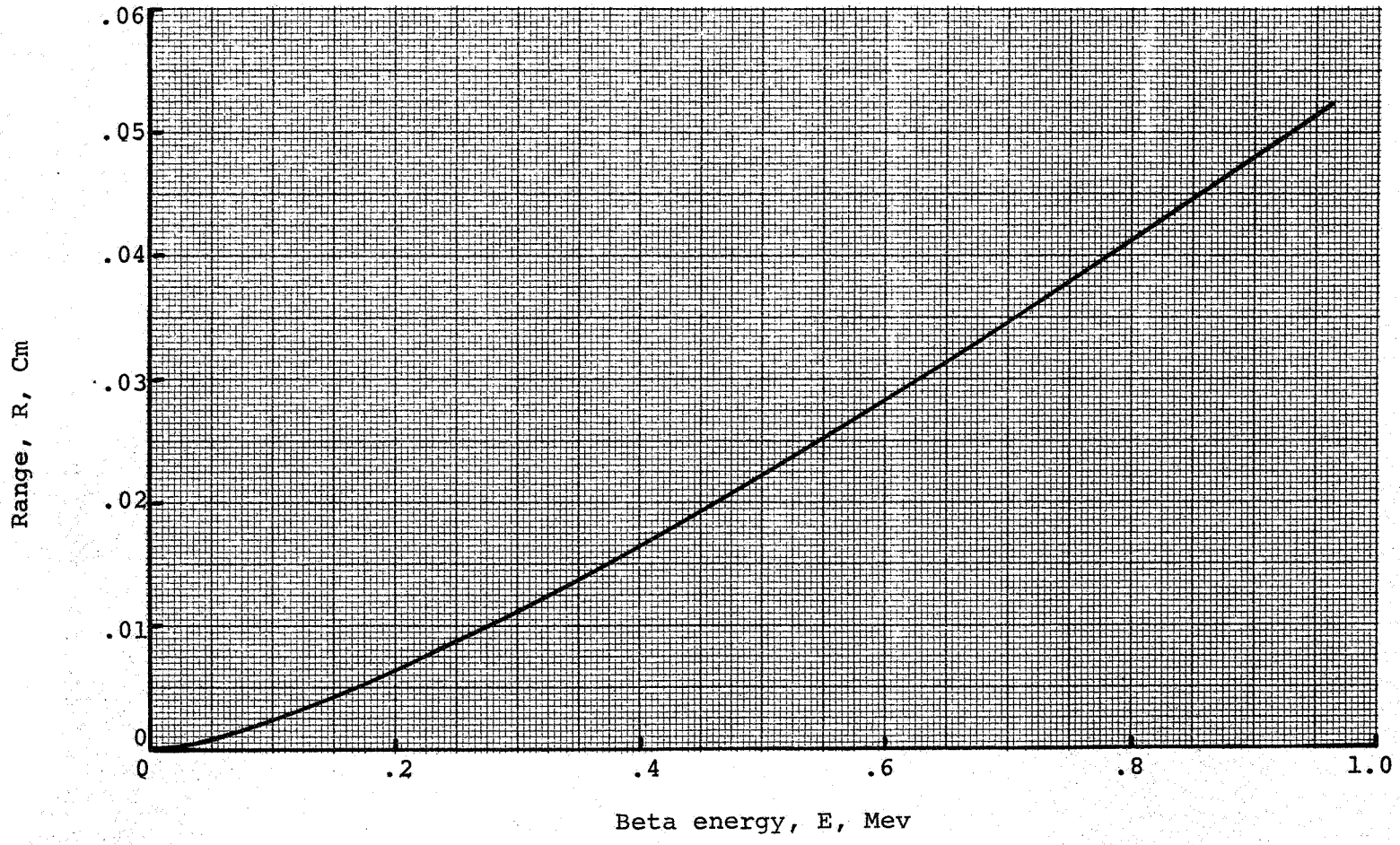


FIG. B3 - Range-energy of beta particles in thulium oxide. ($Tm_2O_3$. 90% dense)

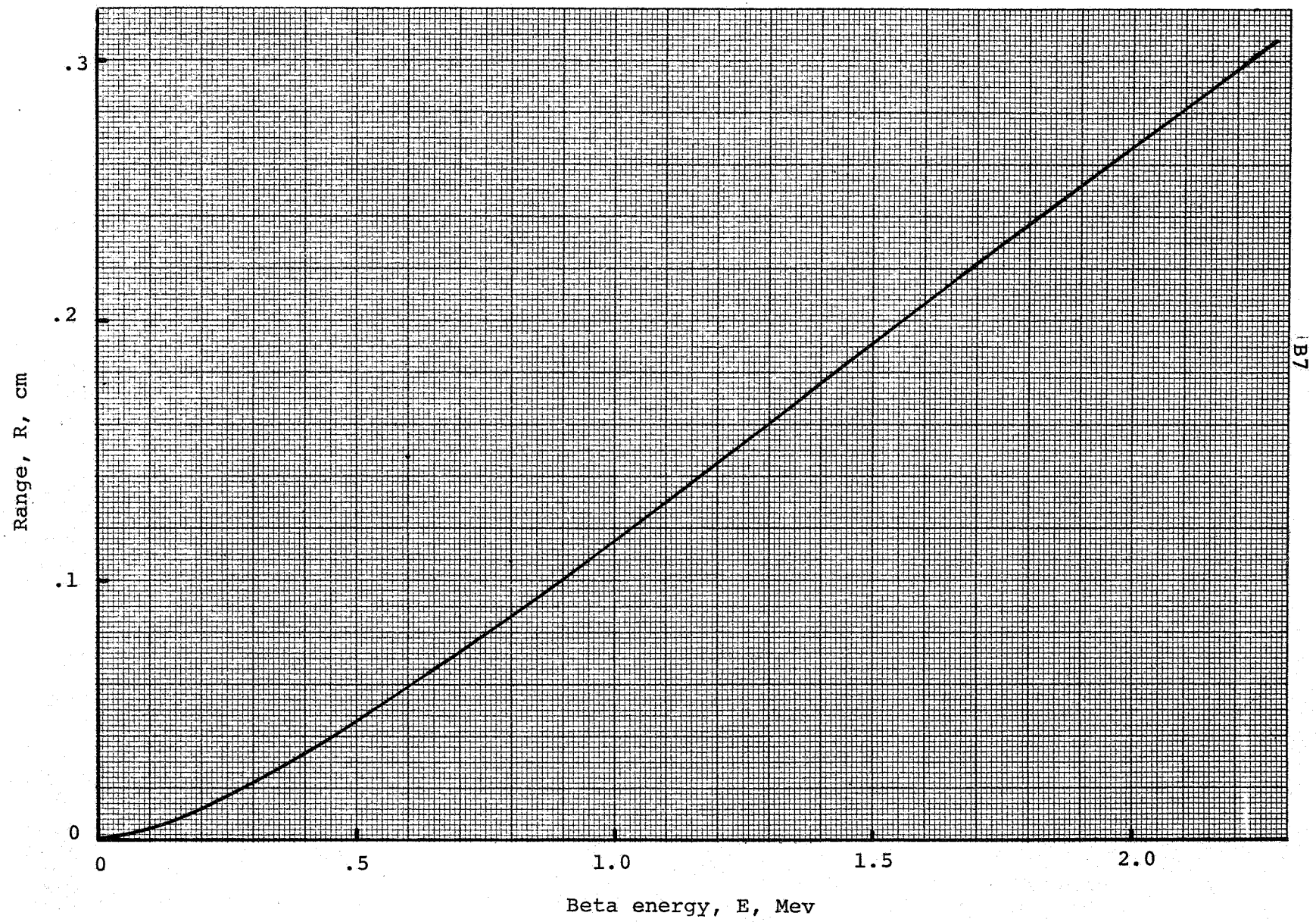


FIG. B4 - Range energy of beta particles in strontium titanate. ($SrTiO_3$, 90% dense).

 

# APPENDIX C

## ELECTROGENERATOR CURRENT

Electric current carried by the beta particles across a vacuum gap from the emitter to the collector, against an adverse potential field, can be calculated using the beta-energy spectra and the range-energy relations that were described in preceding sections.

Beta particles emitted from a differential unit volume within the fuel layer will have an isotropic distribution as shown in Figure C1. The fraction $N_s/N_o$ of beta flux that passes through the area $2\pi(r\sin\theta)(rd\theta)$ on the surface of an imaginary sphere of radius r is:

$$N_s/N_o = (2\pi r^2 \sin\theta d\theta)/4\pi r^2 = 1/2\sin\theta d\theta \qquad (C1)$$

where $N_o$ is the total beta flux leaving the differential unit volume.

Beta particles emitted from a unit volume located at a distance x below the surface, and emitted at an angle from the surface normal will travel a distance $x/\cos\theta$ to reach the surface, as shown in Figure C2. In passing through the material for this distance, the betas will lose energy and will have an energy $E_s$ at the surface. The energy $E_s$ can be found from the range-energy plots by entering the plot at energy $E_o$, finding the value of $R_o$ at $E_o$, and subtracting the increment in range $x/\cos\theta$ to find $R_s$ at $E_s$:

$$R_s = R_o - x/\cos\theta \qquad (C2)$$

The energy $E_s$ corresponds to the value of $R_s$ on the range-energy plot, as shown in Figure C3.

The fraction of total beta particles emitted from the unit volume between $\theta$ and $(\theta+d\theta)$ is $(1/2 \sin\theta\, d\theta)\, f(E)dE$. This fraction is a function of $\theta$ and of $E_o$, as shown in

Figure C4. The energy $E_{min}$ is related to the energy $E_o$ and the angle $\theta$ by range-energy condition $R_o=x/\cos\theta$ , as shown in Figure C5. In other words, betas with energy $E_{min}$ will reach the surface with energy $E_s=0$, having lost all their energy while passing through the distance $x/\cos\theta$ . There is an angle $\theta_{max}$ beyond which no betas will reach the surface, and this maximum angle is related to the end-point energy $E_{max}$ by:

$$R_{max} = x/\cos\theta_{max} \qquad (C3)$$

where $R_{max}$ is the range corresponding to the end-point energy $E_{max}$ as shown in Figure C5.

With the preceding relations, the fraction of total betas emitted from the unit volume between $\theta$ and $(\theta+d\theta)$ can be determined as a function of $E$ as shown in Figure C4. When there is no potential difference between the emitter and collector, the contribution to electrogenerator current from betas emitted between $\theta$ and $(\theta+d\theta)$ is simply:

$$f(\theta)d\theta = (1/2\ \sin\theta d\theta)\int_{E_{min}}^{E_{max}} f(E)\,dE \qquad (C4)$$

and this contribution can be represented as a function of $\theta$ as illustrated in Figure C6.

When a (retarding) potential difference $\phi$ exists between the emitter and collector, then only the betas with surface energy $E_s>E_{s,min}$ can travel to the emitter, where:

$$E_{s,min} = \phi/\cos\theta \qquad (C5)$$

as illustrated in Figure C2. For each value of $\phi$ and of $\theta$ , there will be a particular value for $E_{min}$ as illustrated in Figure C7. For each value of $\phi$ , the contribution to electrogenerator current from betas emitted between $\theta$

and $(\theta+d\theta)$ will depend on the value of $E_{s,min}$ as shown in Figure C8. The contribution to electrogenerator current can be calculated from equation C4, with a different value of $E_{min}$ for each $\theta$ and $\phi$, with a result such as shown in Figure C9.

The portion of electrogenerator current contributed by unit volumes located at a distance $x$ below the fuel layer surface can be represented by:

$$f(x) = \int_{o}^{\theta_{max}} f(\theta)\,d\theta \qquad \text{(C6)}$$

which is merely the area under the curves shown in Figure C9. This integration can be performed for a range of values of $x$ to obtain the information illustrated in Figures C10-C12 for the radioisotope fuel forms promethium-147-oxide, thullium-170-oxide, and strontium-90-titanate, respectively. A digital-computer program for calculating the function $f(x)$ is presented in Appendix D.

Electrogenerator current density $j$ can be determined from the information presented in Figures C10-C12 by integration over the fuel-layer thickness $\tau_f$:

$$j = eN\int_{o}^{\tau_f} f(x)\,dx \qquad (amp/cm^2) \qquad \text{(C7)}$$

where $e$ is electronic charge ($1.6\times10^{-19}$ coulomb) and $N$ is the volume activity of the radioisotope fuel form (beta emissions/sec-$cm^3$). The current density $j$ is the electrogenerator current per unit emitter surface area. Volume activities of radioisotope fuel forms are listed in ref. C1: promethium-147-oxide, 5018 curies/$cm^3$; thulium-170-oxide, 4550 curies/$cm^3$; strontium-90-titanate, 139 curies/$cm^3$.

With these volume activities, the current densities are:

Pm-147
($Pm_2O_3$, 90% dense) $$j = 299 \times 10^3 \int_0^{\tau_f} f(x)\,dx, \ \mu amp/m^2 \qquad (C8)$$

Tm-170
($Tm_2O_3$, 90% dense) $$j = 2710 \times 10^2 \int_0^{\tau_f} f(x)\,dx, \mu amp/m^2 \qquad (C9)$$

Sr-Y-90
($SrTiO_3$, 90% dense) $$j = 827 \times 10 \int_0^{\tau_f} f(x)\,dx, \mu amp/m^2 \qquad (C10)$$

Beta-current densities computed from these equations are shown in Figures C13-C15.

## REFERENCES

C1. Rohrmann, C.A.: Radioisotopic Heat Sources. AEC Research and Development Report HW-76323, REV 1, (15 Oct. 1963).

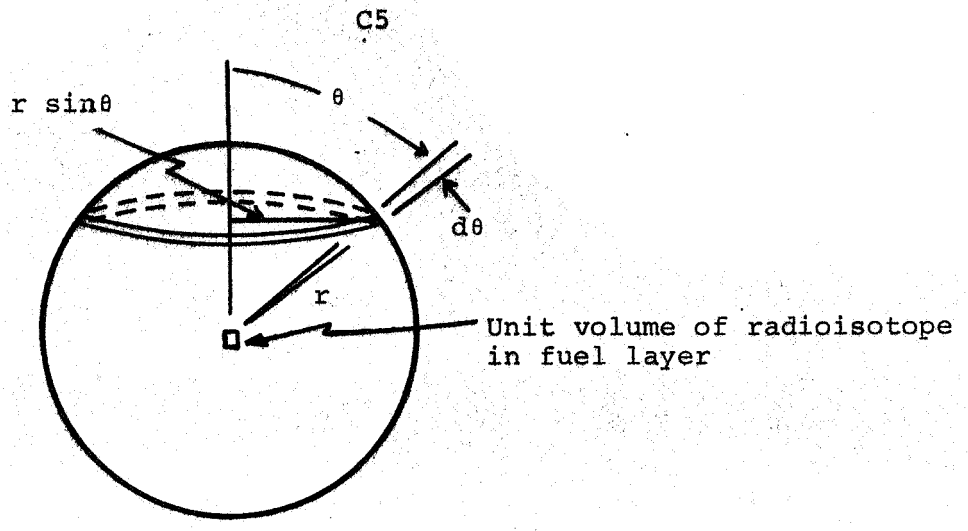


FIG. C1 - Isotropic emission of beta particles from a unit volume of radioisotope in the fuel layer.

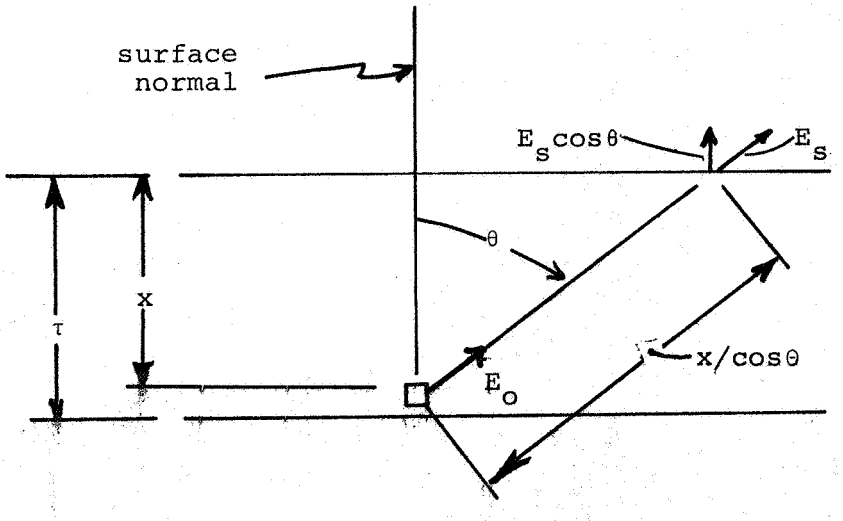


FIG. C2 - Energy loss of beta particles in fuel layer.

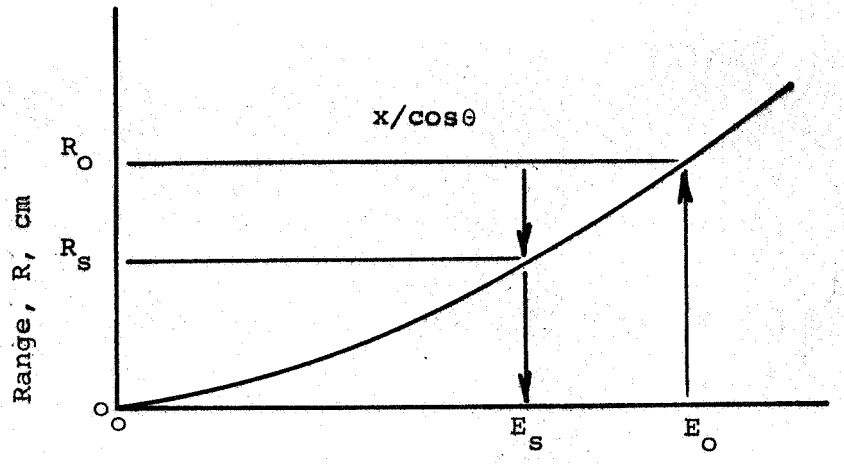


FIG. C3 - Determination of beta energy $E_s$ at fuel-layer surface.

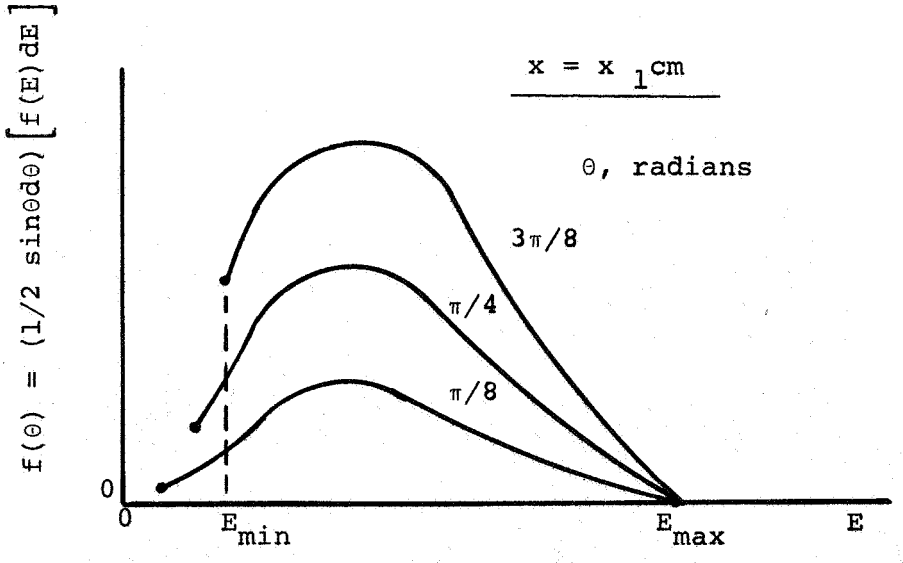


FIG. C4 - Fraction of total beta flux that is emitted from unit volume at energy E and at angles between θ and (θ+dθ).

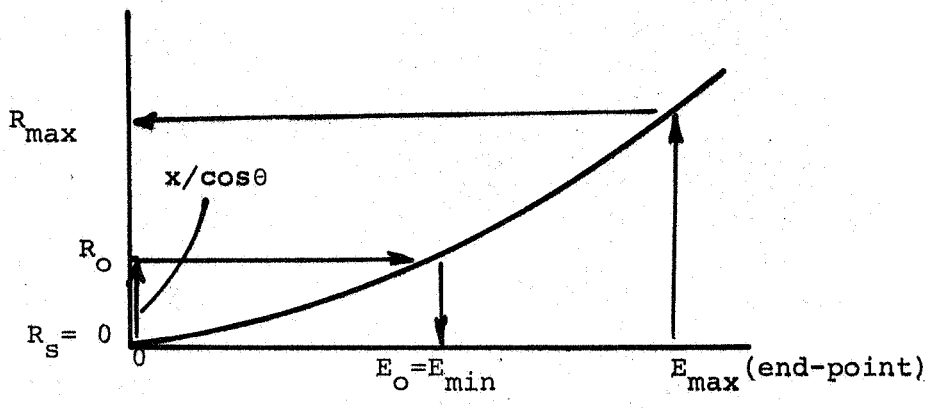


FIG. C5 - Range-energy condition for $E_{min}$

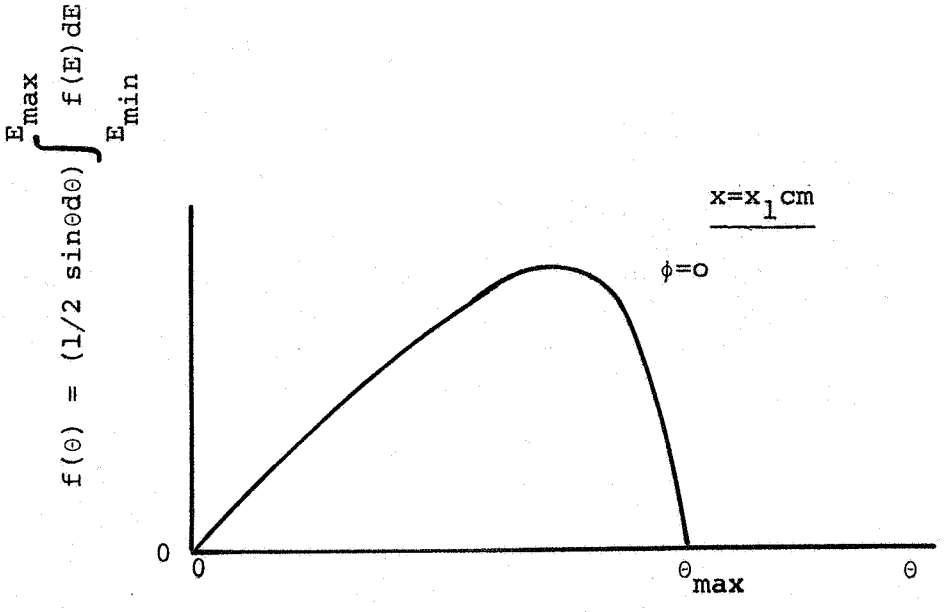


FIG. C6 - Contribution to electrogenerator current by betas emitted between θ and (θ+dθ).

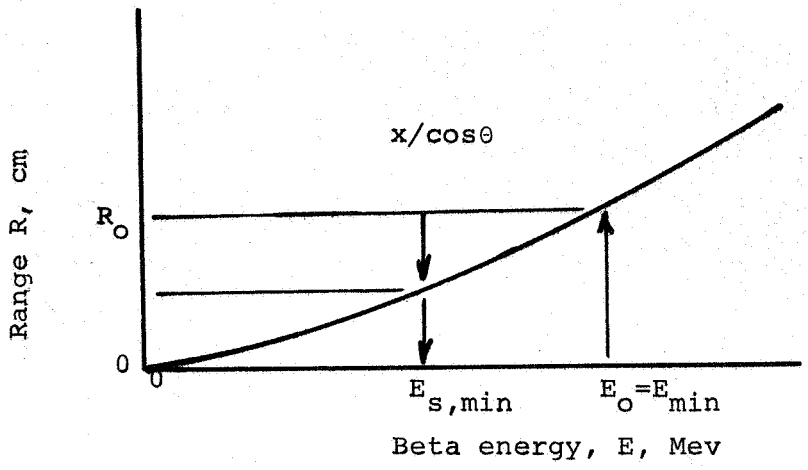


FIG. C7 - $E_{min}$ for a particular value of $E_{s,min}$ .

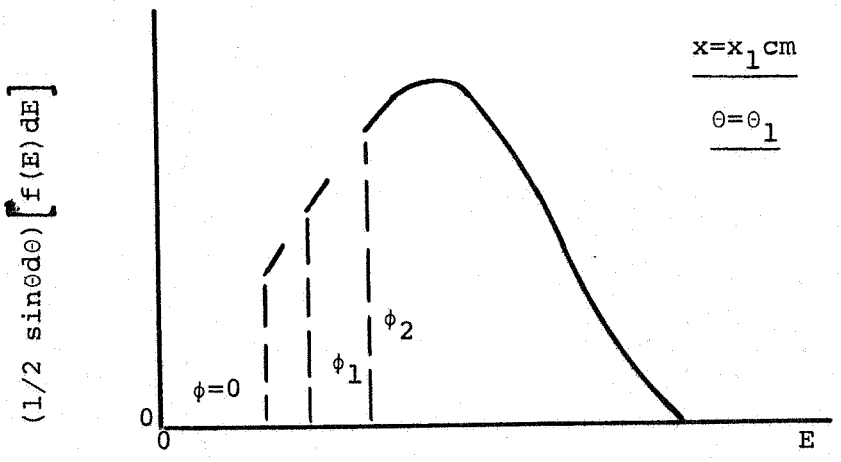


FIG. C8 - Fraction of total betas emitted at energy E and at angles between θ and (θ+dθ) for various values of electrogenerator voltage φ .

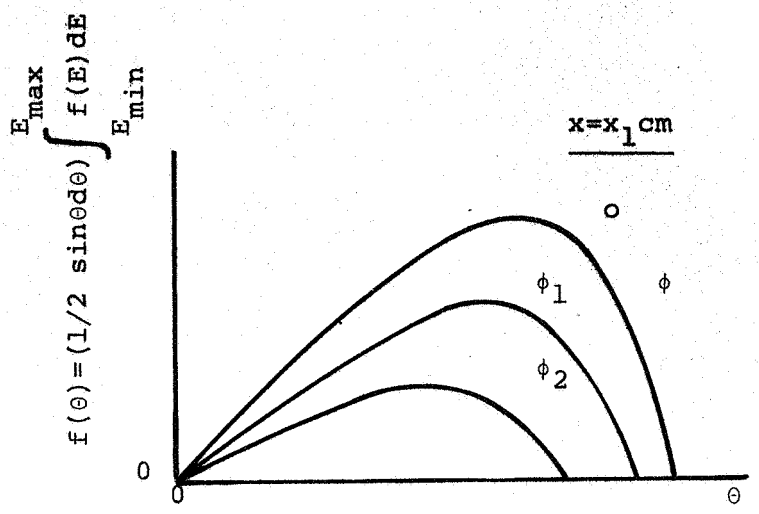


FIG. C9 - Contribution to electrogenerator current by betas emitted between $\theta$ and $(\theta+d\theta)$ for various electrogenerator voltages $\phi$ .

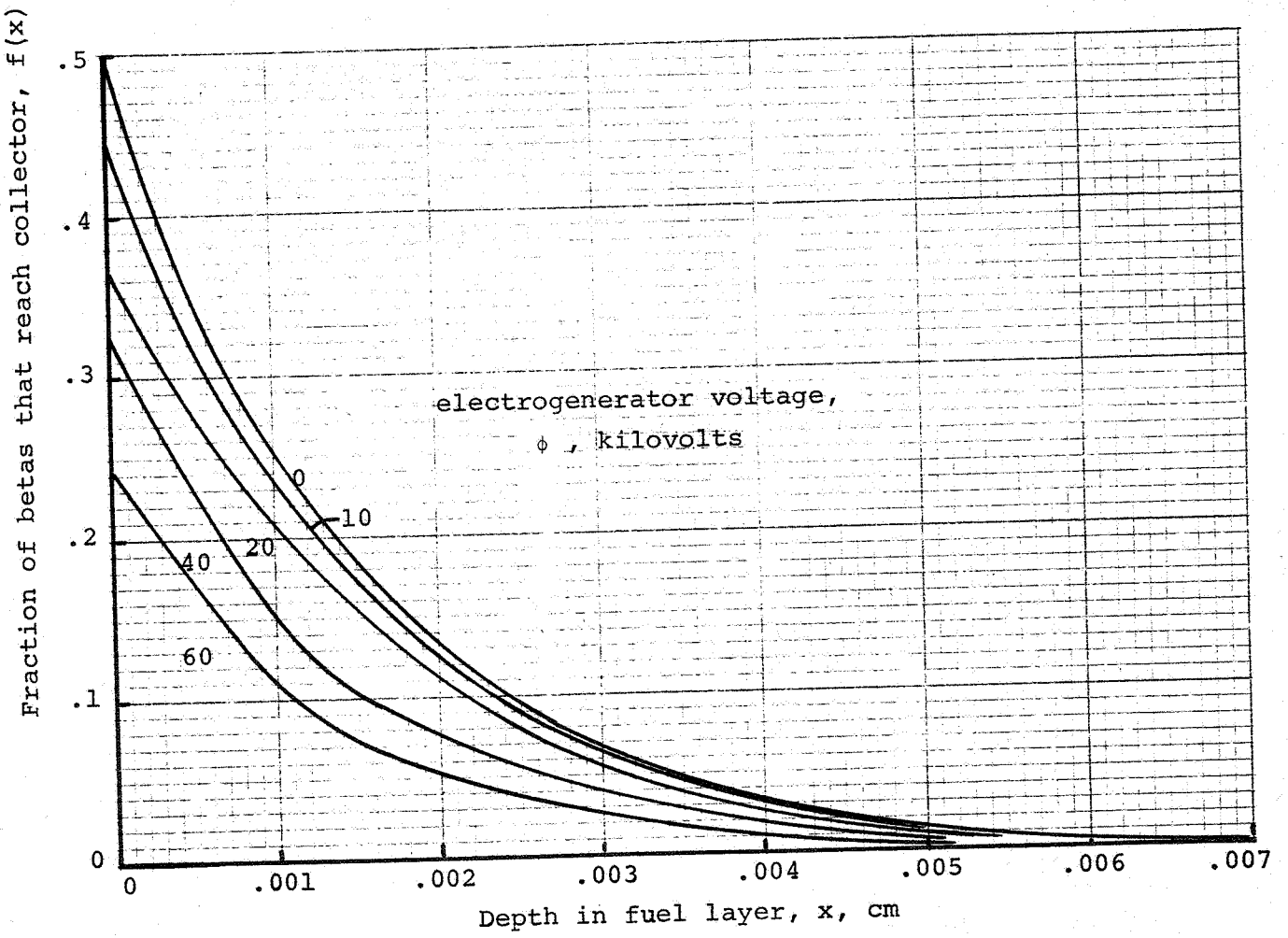


FIG. C10 - Contributions to electrogenerator current from various depths below the surface of a promethium-147-oxide fuel layer. ($Pm_2O_3$, 90% dense).

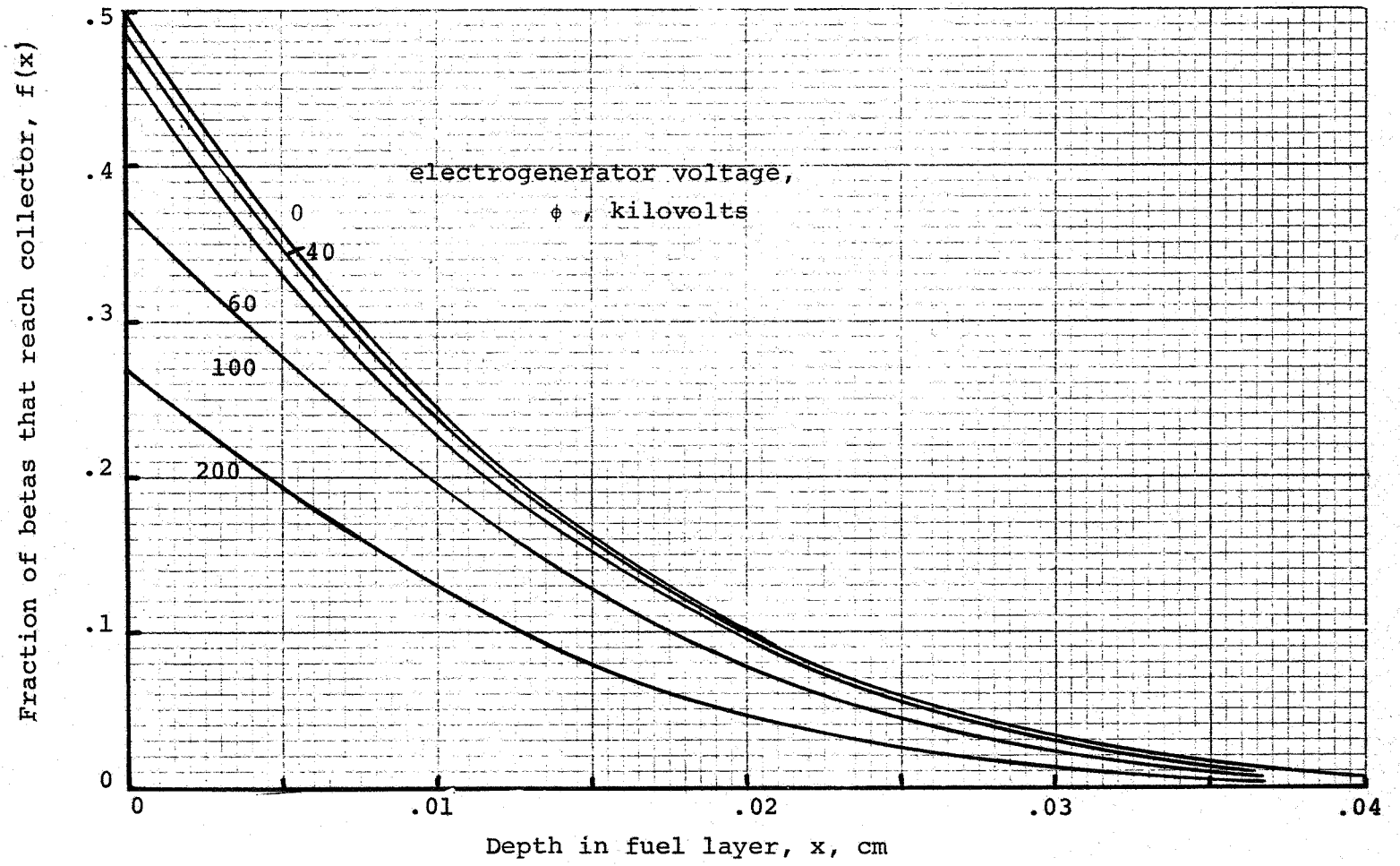


FIG. C11 - Contributions to electrogenerator current from various depths below the surface of a thulium-170-oxide fuel layer. ($Tm_2O_3$, 90% dense).

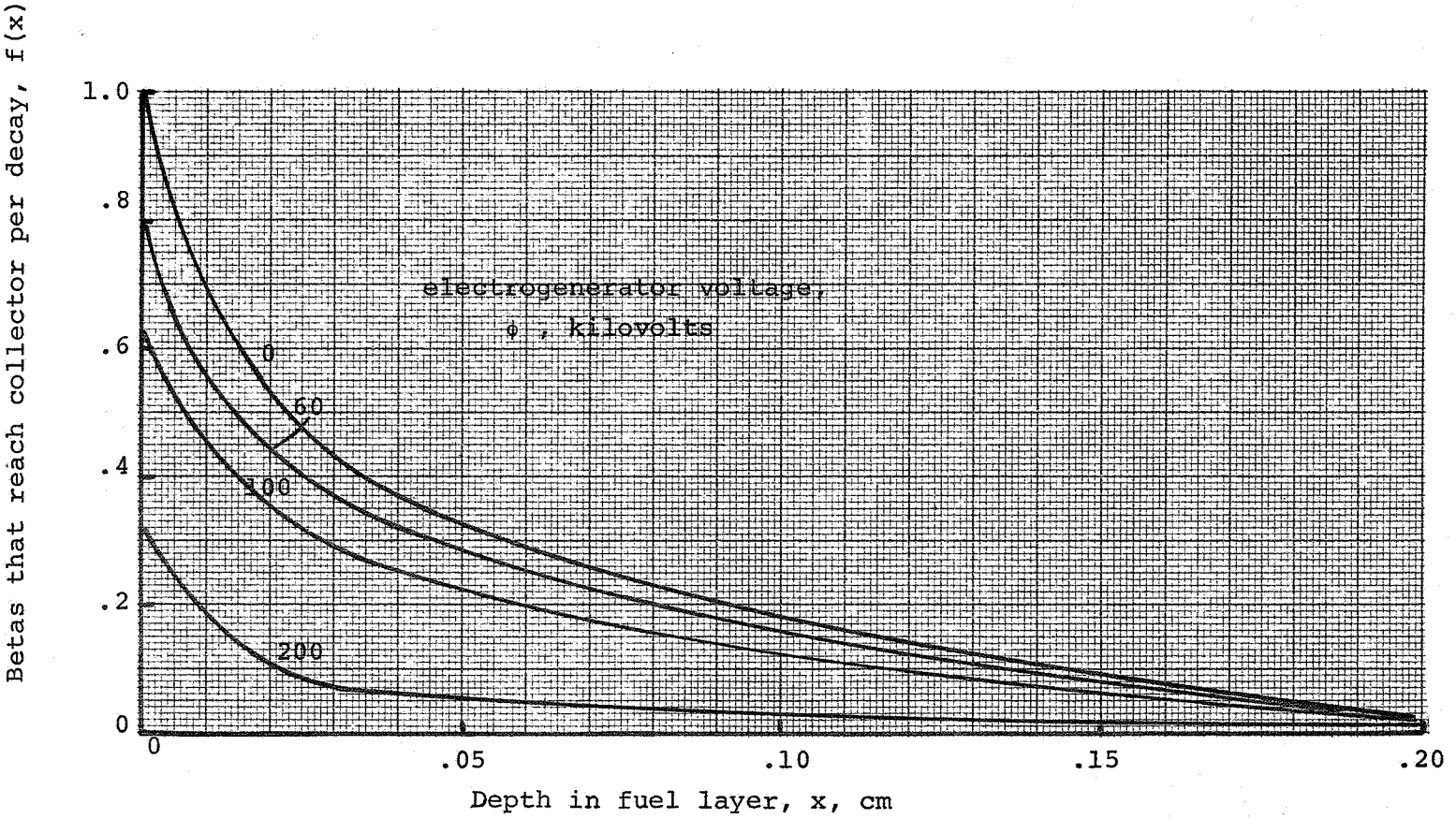


FIG. C12 - Contributions to electrogenerator current from various depths below the surface of a strontium-90-titanate fuel layer. ($SrTiO_3$.,90% dense).

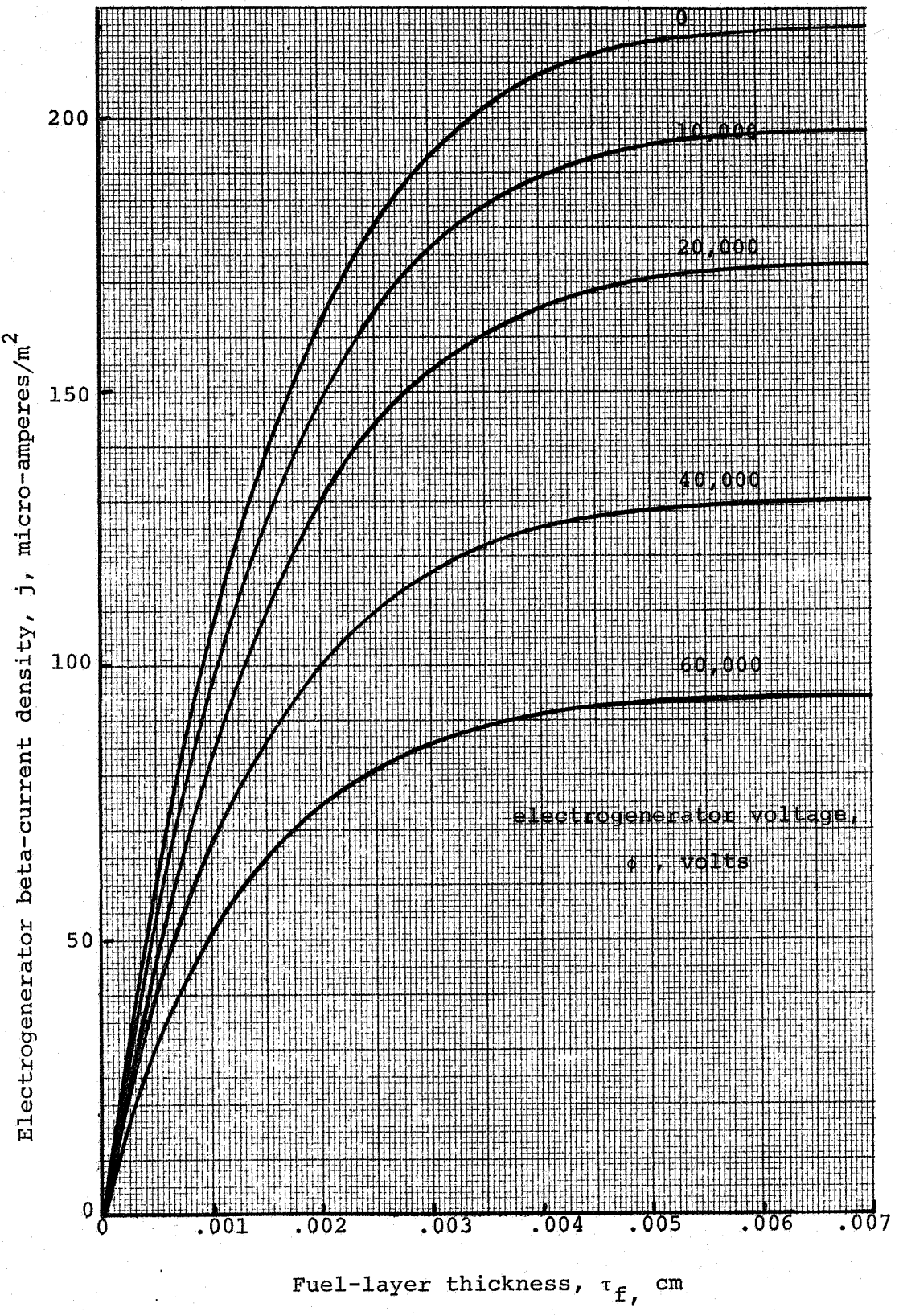


FIG. C13 - Electrogenerator beta-current density for Promethium-147-oxide fuel layers. ($Pm_2O_3$, 90% dense).

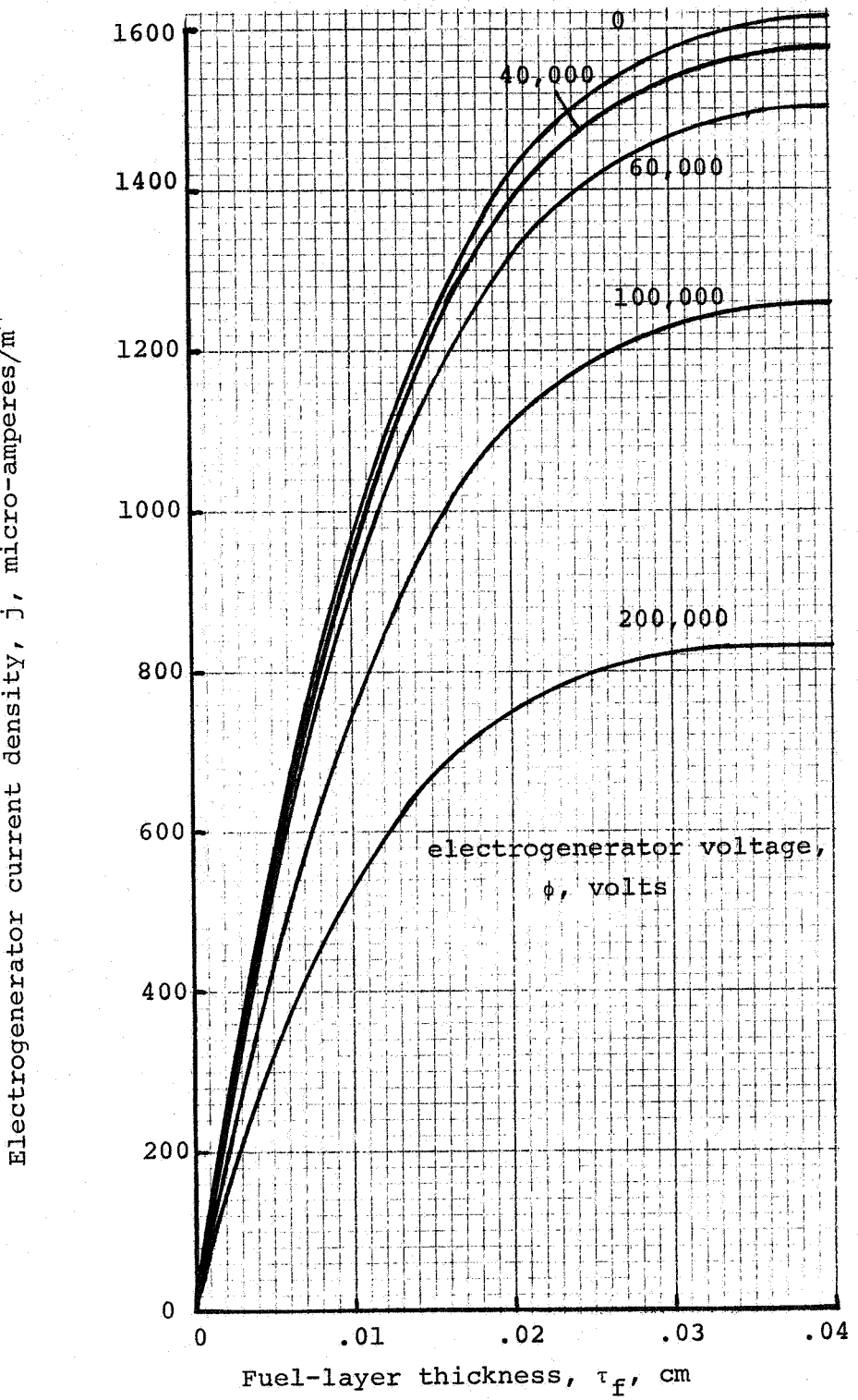


FIG. C14 - Electrogenerator beta-current density for thulium-170-oxide fuel layers. ($Tm_2O_3$, 90% dense).

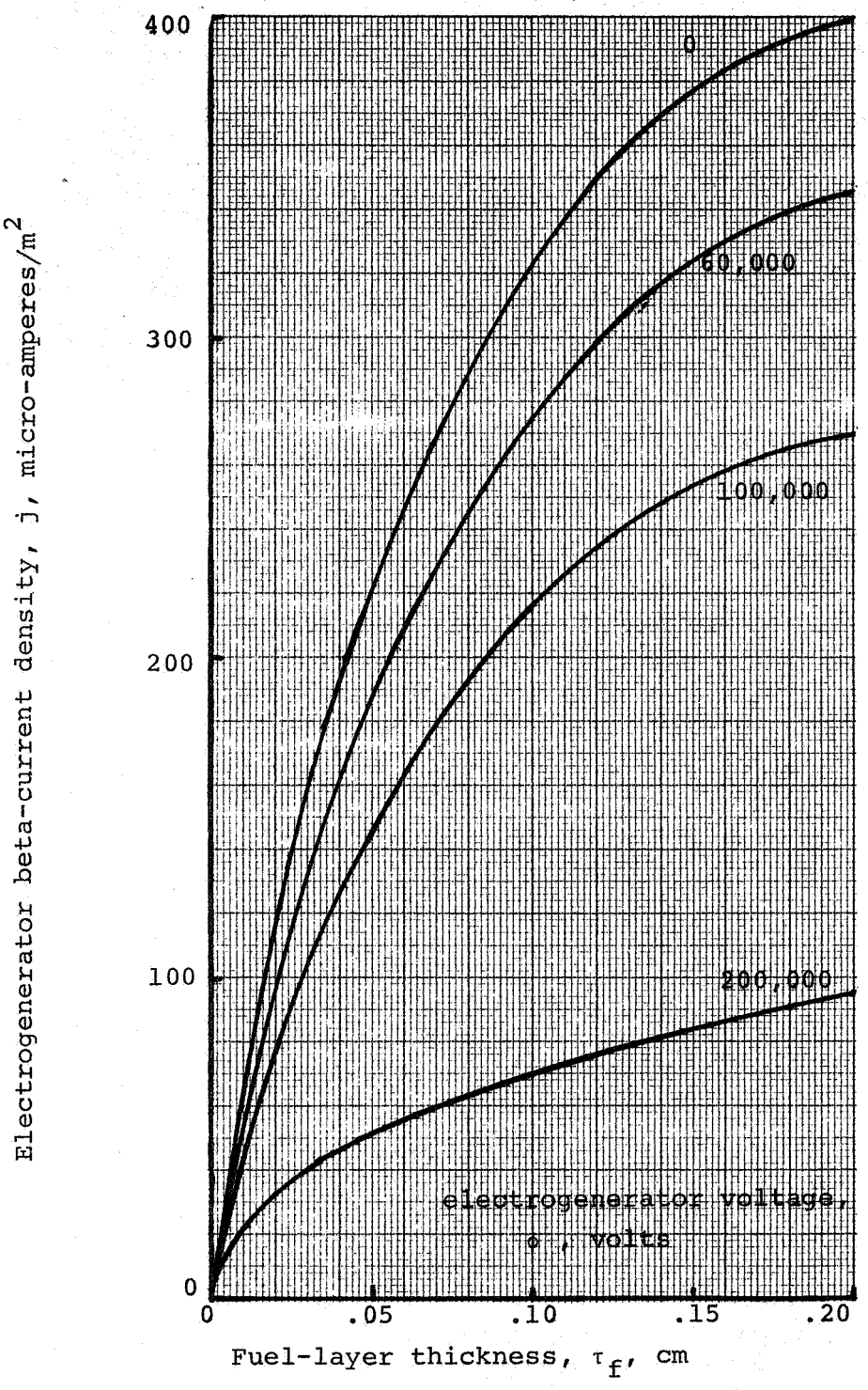


FIG. C15 - Electrogenerator beta-current density for strontium-90-titanate fuel layers. ($SrTiO_3$, 90% dense).

 

# APPENDIX D

## DIGITAL COMPUTER PROGRAM FOR CALCULATION OF ELECTROGENERATOR CURRENT

A digital computer program for calculation of electrogenerator current is presented in entirety in this Appendix. Essentially, the computer program calculates values of the definite integrals in equations (C8) to (C10) in Appendix C. Notations used in this program are related to the notations of Appendix C as follows:

REZ = tabulated values of range, R, cm

FEZ = tabulated values of spectrum density function, $f(E)$, $(Mev)^{-1}$

FXTE = $(\frac{1}{2}\sin\theta)\cdot f(E)$

ESA = beta energy, E, Mev

FXP = $f(x)$

FXTP = $f(\theta)d\theta$

EZS = end point energy in beta spectrum, Mev

DELEZ = increment in values of E in R and f(E) tabulations

X = depth in fuel layer, x, cm

PHI = electrogenerator voltage, $\phi$, Mev

THETA = angle from surface normal, $\theta$, radians

TH = angle from surface normal, $\theta$, radians

THMAX = maximum value of angle from surface normal, $\theta_{max}$, radians

ESMIN = minimum value of beta energy for given values of $E_o$ and $\theta$, $E_{min}$, Mev

DELR = increment in range, $R_o - R_s$, cm

RN = value of R at fuel-layer surface, $R_s$, cm

R = value of R at $E_o$, $R_o$, cm

ES = beta energy at fuel-layer surface, $E_s$, cm

FTH = $\frac{1}{2}\sin\theta$

The computer program is shown on the following pages.

```
*JOB,3020100,MIKK
*LIMIT,T=5,PR=300
*LIMIT,C=70000
*FORTRAN
      PROGRAM MIKK
      DIMENSION REZ(49),FEZ(49),FXTE(21,15,50)
      DIMENSION ESA(15,49),FXP(21,10),FXTP(21,15,10),XX(21)
    1 FORMAT (8F10.5)
    2 FORMAT (8F10.3)
    3 FORMAT(3I10,2F10.3)
  796 READ (5,3) NX,LN,NN,EZS,DELEZ
      READ(5,1) (REZ(L5),L5=1,NN)
      READ (5,2) (FEZ(L5),L5=1,NN)
      DO 200 I=1,NX
      READ (5,1)  X
C   START ALL OVER WITH A NEW PHI
      L=0
  892 L=L+1
      IF(L.GT.LN) GO TO 200
      IF(L.EQ.1) PHI = 0.0
      IF(L.EQ.2) PHI = 0.002
      IF(L.EQ.3) PHI = 0.005
      IF(L.EQ.4) PHI = 0.010
      IF(L.EQ.5) PHI = 0.02
      IF(L.EQ.6) PHI = 0.04
      IF(L.EQ.7) PHI = 0.06
      IF(L.EQ.8) PHI=0.1
      IF(L.EQ.9) PHI=0.2
      IF(L.EQ.10) PHI=0.4
     J = 0
C    START OVER WITH A NEW THETA FOR THE SAME  X  AND  PHI
   10 J = J + 1
      EZ = EZS
      IF (X.GT.0.0) GO TO 577
      THMAX=1.571
```

```
      GO TO 578
  577   THMAX=ACOS(X/REZ(NN))
  578 TH=(THMAX/15.)*J
C     START THRU WITH THETA
      ESMIN = PHI/COS(TH)
      IEZ=NN
      K = 0
      DELR = X/COS(TH)
      IF(ESMIN.GT.EZS) GO TO 116
      GO TO 118
  116   CONTINUE
      GO TO 335
  118 IF(DELR.GT.REZ(NN)) GO TO 125
      GO TO 30
  125 CONTINUE
      GO TO 335
  335 GO TO 892
  30    CONTINUE
C  TAKES CONSECUTIVELY DECREASING  R  VALUES R(49),  R(48)
      R = REZ(IEZ)
      RN = R - DELR
C  LOCATE ES WITH REFERENCE TO R(L5)
      IF(RN)34,34,33
   33 DO 31 M = 2,NN
      IF(RN.LE.REZ(M)) GO TO 32
   31 CONTINUE
   32 EZM = (M -1 )*(-DELEZ)
      EZMMW = (M - 2)*(-DELEZ)
C    CALCULATE   ES
      DELTA = (EZM - EZMMW)*(RN - REZ(M-1))/(REZ(M) - REZ(M-1))
      ES = EZMMW + DELTA
  34    IF(RN.LE.0.0)ES=0.
C  ESMIN IS AT FIRST ALSO EQUAL TO ZERO, K GOES 1,2,3,  TOWARD ZERO
```

```
      K = K + 1
      ESA(J,K) =(IEZ-1)*(-DELEZ)
      IF(ES    .LE.ESMIN) GO TO 451
      GO TO 452
  451  K1=K
C  COULD GET A DIFFERENT K1 FOR EACH THETA
 452  CONTINUE
      FTH = 0.5*SIN(TH)
      FXTE(I,J,K) = FTH*FEZ(IEZ)
  939 FORMAT(1H ,15F8.3)
C     DECREMENT  Z
      IEZ=IEZ-1
      IF(ES.LE.ESMIN) GO TO 106
C    GO THROUGH ALL REZ  VALUES,IE GO THROUGH ALL K VALUES
      IF(IEZ) 106,106,30
C    NOW GET AREAS
  106 DO 541 I2=1,NN,2
      IF(K1.EQ.I2  ) GO TO 542
  541 CONTINUE
      K2=K1+1
      FXTE(I,J,K2) =0.
      GO TO 543
  542  K2=K1
  543  CONTINUE
      SUMM=0.
      K6=K2-1
      DO 544  K=2,K6,2
      B=FXTE(I,J ,K)*4.
 544  SUMM=SUMM+B
      K3=K2-2
      SUMN=0.
      DO 545  K=3,K3,2
      BB=FXTE(I, J,K)*2.
  545  SUMN=SUMN+BB
      A=(-DELEZ/3.)* (FXTE(I,J,1)+SUMN+SUMM+FXTE(I,J ,K2 )    )
C     I  AND  X , J  AND THETA  , L AND   PHI   ,  K AND REZ
      FXTP(I,J,L)=A
```

```
      IF (J.LE.14) GO TO 10
C    GO THROUGH ALL REZ  FOR ONE X  AND  THETA, AND THEN AUGMENT THETA
C  NOW AUGMENT PHI  AND THEN AUGMENT X
      IF(L.LT.LN)  GO TO 892
  200 CONTINUE
      DO 500 I=1,NX
      READ (5,1) X
      IF(X.EQ.0.0) DELTA=1.570963/15.
      DELTA =(ACOS(X/(REZ(NN))))/15.
      DO 600 L=1,LN
      SMM=0.
      DO 700  N=2,14,2
      BX=FXTP(I,N,L)*4.
  700 SMM=SMM+BX
      SMN=0.
      DO 800 M=3,13,2
      C = FXTP(I,M,L)*2.0
  800  SMN=SMN+C
C   INTEGRATE CURVES OF PHIF VERSUS THETA FOR A PARTICULAR  X- PHI VS.X
  600 FXP(I,L)=(DELTA/3.       )*(SMM+SMN+FXTP(I,1,L)+FXTP(I,15,L)  )
  500 CONTINUE
      WRITE(6,994)
  994 FORMAT(1H1,38X,45HTHIS MATRIX IS G OF X WITH PHI AS A PARAMETER//)
      WRITE (6,115)
  115  FORMAT (17X,1HX,8X,7HPHI=0.0,1X,8HPHI=.002,1X,8HPHI=.005,1X,8HPHI=
     1.010,2X,7HPHI=.02,2X,7HPHI=.04,2X,7HPHI=.06,3X,6HPHI=.1,3X,6HPHI=.
     22,3X,6HPHI=.4/ )
      DO 501 I=1,NX
      READ (5,1) XX(I)
  501 WRITE(6,995)(XX(I),(FXP(I,L),L=1,LN))
  995  FORMAT (10X,F10.4,4X,10F9.4)
      GO TO 796
      END
*RUN,CLEAR
        10          9         49  0.96      -0.02
   .           .0002    .0005      .0009     .0014      .0020      .0027      .0033
  .0041       .005      .0059      .0068      .0077      .0087      .0097     0.0107
  .0118       .0128     .014       .0151      .0162      .0173      .0185      .0197
  .0209       .022      .0233      .0245      .0257      .027       .0282      .0294
  .0307       .032      .0332      .0344      .0356      .0371      .0384      .0397
```

| | | | | | | | |
|---|---|---|---|---|---|---|---|
| .041 | .0423 | .0436 | .045 | .0463 | .0477 | .049 | .0503 |
| .0516 | | | | | | | |
| . | 0.056 | 0.115 | 0.178 | 0.241 | 0.306 | 0.375 | 0.45 |
| .527 | 0.607 | 0.695 | 0.785 | 0.883 | 0.983 | 1.085 | 1.185 |
| 1.285 | 1.376 | 1.469 | 1.562 | 1.63 | 1.697 | 1.742 | 1.775 |
| 1.8 | 1.815 | 1.827 | 1.83 | 1.825 | 1.807 | 1.766 | 1.701 |
| 1.633 | 1.561 | 1.482 | 1.4 | 1.307 | 1.213 | 1.108 | 0.998 |
| .885 | 0.756 | 0.635 | 0.51 | 0.383 | 0.27 | 0.169 | 0.085 |
| .02 | | | | | | | |

.

.002
.005
.010
.015
.020
.035
.040
.045
.050

.

.002
.005
.010
.015
.020
.035
.040
.045
.050

.

.002
.005
.010
.015
.020
.035
.040
.045
.050

```
        10          7          46   .225     -.005
  .          .00006     .0001      .00017     .00024     .00032     .00041     .00051
 .00063     .00075      .00087     .001       .00115     .0013      .00145      .00161
 .00177     .00195      .00213     .00232     .00251     .0027      .0029       .0031
 .00331     .00353      .00375     .00398     .00422     .00446      .00471     .00497
 .00523     .0055       .00575     .00602     .00628     .00656     .00688      .00711
 .00739      .00768     .00796     .00824     .00852     .00883
  .          .65       1.42        2.21      2.90       3.52       4.08        4.58
  5.03       5.45      5.82       6.14       6.43       6.69        6.94       7.18
 7.34       7.44        7.49       7.50       7.45       7.37       7.23        7.03
 6.82        6.57      6.31        6.03       5.72       5.41       5.07        4.70
 4.32       3.92        3.50       3.06        2.69       2.26       1.88        1.50
  1.14      0.82       .53         .29        .12         0.
 .
.0005
 .001
 .002
 .003
 .004
 .005
 .006
 .007
 .008
 .
.0005
 .001
 .002
 .003
 .004
 .005
 .006
 .007
 .008
 .
.0005
 .001
 .002
```

.003
.004
.005
.006
.007
.008

21 10 47 .230 -.05

| | | | | | | | |
|---|---|---|---|---|---|---|---|
| . | .002 | .004 | .008 | .012 | .016 | .023 | .028 |
| .034 | .04 | .046 | .052 | .059 | .066 | .072 | .079 |
| .086 | .093 | .100 | .107 | .115 | .122 | .13 | .137 |
| .145 | .152 | .160 | .168 | .176 | .183 | .191 | .199 |
| .206 | .214 | .222 | .229 | .237 | .245 | .252 | .26 |
| .268 | .274 | .282 | .290 | .297 | .304 | .308 | |
| . | .57 | 1.26 | 2.07 | 2.61 | 3.02 | 3.33 | 3.2 |
| 2.63 | 1.58 | 0.47 | .25 | .29 | .34 | .38 | .43 |
| .47 | .51 | .54 | .58 | .61 | .64 | .67 | .70 |
| .72 | .74 | .76 | .78 | .79 | .81 | .82 | .82 |
| .81 | .8 | .78 | .75 | .71 | .65 | .58 | .49 |
| .37 | .26 | .18 | .11 | .05 | .02 | 0. | |

.

.002
.004
.008
.012
.016
.023
.028
.034
.04
.046
.06
.08
.1
.12
.14
.16
.18
.2
.22
.24

```
 .
.002
.004
.008
.012
 .018
.023
.028
.034
.04
.046
.06
.08
.1
.12
.14
.16
.18
.2
.22
.24
 .
.002
.004
.008
.012
 .018
.023
.028
.034
.04
.046
.06
.08
.1
.12
.14
.16
.18
.2
.22
.24
*END
```

# APPENDIX E

## DIELECTRIC BETA LOSSES AND LEAKAGE CURRENTS

Three types of dielectric can be considered for the ACCENT system electrogenerator: vacuum, gas, and solid. Each of these has certain advantages and disadvantages, as discussed in the following sections. The function of the dielectric is to preserve the potential difference between emitter and collector by preventing electric breakdown, and to perform this function with a leakage current that is small compared to the electrogenerator current. At the same time, the dielectric should have properties conducive to the design of a compact, light-weight electrogenerator. High dielectric strength, high resistivity, and high range coefficient are desirable characteristics. High range coefficients for gas and solid dielectrics are required in order to minimize beta energy loss in passing through the dielectric.

### Vacuum Dielectric

The phrase vacuum dielectric is probably misused in the literature because experiments usually have been done in partial vacuums (e.g. above $10^{-10}$ torr) where adsorbed gas films may have much to do with leakage current and breakdown voltage. For example, recent experiments (ref. E1) have shown that a residual gas pressure can provide more than an order of magnitude increase in the threshold voltage for significant pre-breakdown currents. These experiments indicated that the threshold voltage is much more than 600,000 volts when the "vacuum" dielectric contains about $10^{-4}$ torr of nitrogen gas, for electrodes with about one square meter of surface area spaced at 30 cm, for a pre-breakdown current threshold of 20 microamperes. (The electrode area of one square meter is of the order of ACCENT system electrogenerator electrode areas, and the leakage current of 20 microamperes/$m^2$

is fairly small compared with the electrogenerator current densities quoted in Appendix C.)

For high vacuum conditions where adsorbed gas films have negligible effect on pre-breakdown currents, the Fowler-Nordheim theory (refs. E2, E3) is in excellent agreement with experiment as shown by some recent work (refs. E4-E6). The Fowler-Nordheim theory is based on a model where microscopic protrusions from the electrode surface have high local electric field strength because of the very small radius of curvature of the tip of the protrusion. (Existence of such protrusions has been experimentally verified, and they are presumably present on the surface of all engineering materials, but their formation is not yet understood, ref. E7).

Considerable attention has been given to the Fowler-Nordheim theory, resulting in the following expression (ref. E5) for pre-breakdown leakage current $J_{l,p}$ (amperes):

$$J_{l,p} = 1.54 \times 10^{-6} \frac{S_e \beta^2 \phi^2}{\phi_w g^2 f_l} \exp\left(-6.83 \times 10^7 \frac{\phi_w g f_2}{\beta \phi}\right) \quad \text{(E1)}$$

where $S_e$ is the electrode area that actually emits electrons (ie, the emission area of the protrusions), $\beta$ is a field-amplication factor (typically 100 to 300), $\phi$ is the voltage between the electrodes, $\phi_w$ is the electrode work function, $g$ is the inter-electrode gap (spacing), and $f_l$ and $f_2$ are slowly varying functions of $E^{\frac{1}{2}}/\phi_w$. Values of $\beta$ for electrolytically polished copper electrodes have been found to vary between 140 and 247 over a range of electrode gaps from 0.3 to 1.9 mm, although this variation was not regular (ref. E5).

A typical variation of pre-breakdown leakage current with applied voltage is shown in Figure E1 (ref. E5). From the slope of this data, $\beta$ was calculated to be 248, and the (protrusion) emission area was determined from equation (E1)

to be $S_e = 4.8 \times 10^{-12}$ cm$^2$ . The measurements reported in ref. E5 were taken at pressures of $10^{-9}$ torr, so surface gas films should be absent or negligible and the data should be applicable to the ACCENT electrogenerator design. However, there is no known way of fabricating electrodes with a specified emission area $S_e$ .

In the absence of firm design criteria, recourse must be made to flexibility in the design. By inspection of equation (E1), it is evident that the pre-breakdown leakage current is strongly dependent on the applied field strength $\phi/g$ . For example, a 10% reduction in field strength in the upper-voltage range of Figure E1 results in an order-of-magnitude reduction of pre-breakdown leakage current. This implies that a 10% increase in the electrode spacing would achieve the same effect. In fact, this observation is borne out by the data of ref. E5 for copper electrodes with spacings from 0.3 to 2.0 mm, and there is every reason to believe that the same trend would be valid for aluminum electrodes since the work functions are nearly the same (Al, 4.08 ev; Cu, 4.2 ev; W, 4.5 ev). From this discussion, it is reasonable to design the electrogenerator with provision for changing the electrode spacing somewhat in order to achieve negligible pre-breakdown leakage currents.

In the light of the discussion so far, it is not surprising that firm design parameters are not available for vacuum electric breakdown. Applied field strengths of more than $10^6$ v/cm over an electrode-spacing range of 0.05 mm to 1.0 mm have been measured (ref. E8) after conditioning of electrode surfaces with low-energy electric discharges. Without conditioning, breakdown at field strengths of only $2.5 \times 10^5$ to $4.6 \times 10^5$ v/cm has been observed (ref. E5). Under the circumstances of such conflicting data, it seems advisable to design for the lower field-strength values, say, for $1 \times 10^5$ v/cm (e.g., 10,000 volts per mm) with provision for reducing electrode spacing by as much as a factor of ten during development of the ACCENT system.

Another source of leakage current in an electrogenerator with vacuum dielectric is secondary electron emission from the collector. Secondary electrons will be emitted as a result of beta particles incident on the collector, and it is evident that the secondary electrons will fall into the emitter (fuel element) thereby constituting a leakage current. There is sufficient data in the literature to form a basis for estimating the magnitude of electrogenerator leakage current due to secondary electron emission.

In the low-energy range of primary electron energy (i.e., beta energy at the collector in the electrogenerator), secondary electron emission can be quite large. A secondary electron coefficient $\delta$ is defined as the ratio of secondary electrons to primary electrons; and this coefficient is zero at zero primary energy, then rises to a maximum value $\delta_{max}$ at some primary energy $E_p$, and then decreases as primary energy is increased. Values of $\delta_{max}$ and $E_p$ are listed in Table E1 for a number of materials (refs. E8, E9).

At primary-electron energies above $E_p$, the secondary-electron emission coefficient falls rapidly to low values, as illustrated in Figure E2. The Sternglass theory is in agreement with much experimental data (ref. E9), and is considered to be more reliable than data such as from ref. E10, for the purposes of the present study.

At primary-electron energies well above $E_p$, the secondary-electron-emission coefficient becomes roughly constant as shown in Figure E3 (data from refs. E11, E12). It is notable that the data for aluminum in Figure E3 are in substantial agreement with the theory of Sternglass shown in Figure E2.

The data described so far have been for normal incidence, but the betas will reach the electrogenerator collector at all angles between normal and grazing incidence. Experimental data (ref. E12) indicates that the secondary-electron-emission coefficient at $60^{\circ}$ incidence (from normal) may be about twice the value for normal incidence.

From the available data, it appears that the secondary-electron-emission coefficient can be assigned a design value of 0.03, and that this value should prove to be conservative.

Beta particles arriving at the collector may be reflected (backscattered), and return to the emitter, thereby forming a third kind of leakage current. Electron-backscattering coefficients have been measured over a wide range of primary electron energy, as shown in Figure E4(refs. E12-E15). In general, the electron backscattering coefficient $\eta$ decreases with atomic number of the target material, so aluminum appears to be a good choice for a collector material on this basis. At low primary electron energy, carbon is reported to have $\eta=.08$ (ref. E15), and beryllium is reported to have $\eta=.08$ (ref. E10), so these also appear to be candidates for collector materials.

The data shown in Figure E4 are for normal incidence, and the electron backscattering coefficient increases with incidence angle of the primary electron, as shown in Figure E5 (refs. E12, E13). Some approximate theoretical calculations reported in ref. E13 indicate that the overall backscattering coefficient for electrogenerators with aluminum collectors may be $\eta=.20$ .

In summary there are three sources of leakage current in electrogenerators with vacuum dielectric:

1. pre-breakdown (field emission) leakage current $J_{l,p}$ , which can be made negligible by reducing the electrogenerator electric field strength.
2. secondary-electron emission current $J_{l,e}$ , which should be about 3% of the electrogenerator current, with aluminum collectors.
3. backscattered-electron current $J_{l,b}$ , which may be as great as 20% of the electrogenerator current, with aluminum collectors, and as great as 10% with beryllium collectors.

## Gas Dielectric

A gas with a large electron-attachment cross-section, such as $SF_6$, can be used as a dielectric. Capture of electrons by the gas dielectric results in the electric current being carried by slow-moving $SF_6$ negative ions, thereby reducing the current. In this way a discharge can be quenched before it becomes catastrophic. Furthermore, the leakage current is reduced. If total, complete, containment of the electrogenerator assembly is an absolute nuclear safety requirement, then a gas dielectric may be a very desirable design concept.

In leakage currents through a gas dielectric, the most important mechanism involved is impact ionization caused by electrons originating from the electrodes or from the gas itself in the interelectrode space, which are accelerated by the applied electric field to energy levels sufficient to cause ionization of the neutral gas atoms. When conditions in the interelectrode space produce electron energies greater than the ionization energy (15.7 ev for $SF_6$) an initial electron current will be amplified through a mechanism first described by Townsend who found experimentally that the amplified current $J$ could be expressed by:

$$J = J_o \exp(\alpha g) \qquad \text{(E2)}$$

where $g$ is the gap distance between the electrodes and $J_o$ is the initial electronic current. The coefficient $\alpha$ is known as Townsend's First Coefficient. Figure E6 is a plot of $\alpha/p$ against $E/p$ for sulfur hexaflouride (from ref. E16) where $p$ is the pressure, and $E$ is the electric field strength.

Although the above mechanism will result in an increase in electronic current (and thus increase leakage current) no complete breakdown will occur unless additional free electrons are produced by secondary processes which are more complicated than the primary electron-atom collision process. These

processes may include secondary emission of electrons by bombardment of the cathode by the returning positive ions, or by photoelectric action at the cathode or photoionization in the gas itself; the latter two caused by radiation from the initial ionization process.

The criterion for complete electrical breakdown can be expressed as:

$$\left[\gamma \exp(\alpha g)\right] - \gamma = 1 \qquad \text{(E3)}$$

where $\gamma$ is Townsend's Second Coefficient. For electronegative gases, a further process must be considered; that of electron attachment. An attachment coefficient $\eta$ can be determined for such gases and is defined as the mean number of attachments per unit length of electron travel in the direction of the electric field. A plot of $\eta/p$ against $E/p$ for $SF_6$ is shown in Figure E7.

The breakdown criterion for an electronegative gas is then given by:

$$\left[\gamma\alpha/(\alpha-\eta)\right]\left\{\exp\left[(\alpha-\eta)d\right] - 1\right\} = 1 \qquad \text{(E4)}$$

The term $(\alpha-\eta)$ is the net ions per cm of electron travel in the direction of the electric field. Figure E8 shows $(\alpha-\eta)/P$ plotted against $E/P$ for $SF_6$. In the region where $\eta$ is greater than $\alpha$ electrons are removed faster than they are produced resulting in a situation whereby electrical breakdown cannot occur.

Figure E9 is a plot of the maximum safe potential difference $V_{max}$ against gap distance (uniform plane electrodes) for various values of gas pressure for $SF_6$. If the value of $V_{max}$ is not exceeded the leakage current will not exceed values that would result for vacuum insulation of the two electrodes.

The following assumptions have been made in calculating the above information:

a. All of the relations hold at the pressure levels of interest.

b. No other mechanisms are present for the production of ionization.

If the passage of beta particles through the $SF_6$ gas produces an appreciable amount of ionization, then the operating voltage might be lowered to avoid electric breakdown (or the electrode spacing could be increased).

Because of the relatively low density of gaseous dielectrics, the interaction of betas with the collector can be expected to be essentially the same as with a vacuum dielectric; e.g., there will still be about 3% leakage current due to secondary electron emission, and as much as 20% leakage current due to electron backscattering from aluminum collectors and 10% with beryllium collectors. If the factor $(\alpha-\eta)$ in Figure E8 has a negative value, then the leakage current due to secondary electron emission might be suppressed, however,this current is only about 3% of the electrogenerator current so such a suppression would not appreciably improve the electrogenerator performance.

Backscattered electrons have an energy spectrum that is continuous from zero energy to the primary electron energy so most of the backscattered electrons will have energies of the order of the primary beta energy in the electrogenerator. Because of the relatively high energy of the backscattered electrons, it seems unlikely that the leakage current due to backscattered electrons will be suppressed appreciably even if the factor $(\alpha-\eta)$ is made negative.

In summary, it appears that the use of a gaseous dielectric such as $SF_6$ could provide much closer electrode spacings than possible with a vacuum dielectric, but that only a slight reduction in leakage current can be expected. For example, if the $SF_6$ pressure were 1000 torr, a 20-mil (.5mm) gap could support about 7000 volts, and a 100-mil (2.5 mm) gap could support about 30,000 volts. With slightly lower voltages, or slightly higher gaps, pre-breakdown and secondary-

electron leakage currents might be suppressed by the $SF_6$, leaving only the leakage current due to backscattered electrons.

## Solid Dielectric

Solid dielectrics offer the possibility of close-spaced electrodes, with a corresponding decrease in electrogenerator size. Properties of some solid dielectric materials are listed in Table E2.

Beta particles must pass through the solid dielectric in order to reach the collector. Therefore, the range coefficient $C_{R,d}$ of the dielectric, and the ratio of $C_{R,f}$ of the fuel form to $C_{R,d}$, are important parameters. Equivalent thickness $\tau_{eq}$ of the dielectric is simply:

$$\tau_{eq} = \tau_d(C_{R,f}/C_{R,d}) \qquad \text{(E5)}$$

where $\tau_d$ is the actual (physical) thickness of the dielectric. The current of betas reaching the collector can be estimated as shown in Figure E10.

In making this estimate it is assumed that the dielectric merely acts as a material obstruction to the passage of beta particles. This is equivalent to assuming that there is no electric field throughout most of the dielectric, e.g., the electric potential in most of the dielectric is the same as that of the fuel element. There is evidence that this assumption may be valid, for some data (ref. E17) show that essentially all of the potential drop in a solid dielectric between two conductors occurs near the cathode (which is the collector in the ACCENT electrogenerator). It is notable that this experimental observation is supported by detailed theoretical analysis. If there is a substantial potential drop near the emitter, then the betas would lose some of their energy in that region, and would travel through the remainder of the solid dielectric at the reduced energy; in this event the mthod used here would not be valid. However,

the present method should be a good first approximation even if there is an appreciable electric field at the beta emitter electrode (the fuel element).

The estimate of beta current illustrated in Figure E10 can be expressed as follows:

$$j = K \int_{\tau_{eq}}^{\tau_{eq} + \tau_f} f(x)\, dx \qquad \text{(E6)}$$

where the constant $K$ is given in Appendix C for each particular radioisotope fuel form. A further illustration of this estimate of beta current through a solid dielectric is shown in Figure E11. This figure is a portion of the beta-current density figures in Appendix C. Beta current lost by absorption in the dielectric is represented by $j_a$ corresponding to the equivalent thickness $\tau_{eq}$ of the solid dielectric. Beta-current density arriving at the collector is the difference between the current density at $(\tau_{eq} + \tau_f)$ and $j_a$, since this difference is identically the area under the shaded portion of Figure E10 multiplied by the constant $K$ as in equation (E6).

The approximate method described above can be used to obtain estimates of beta-current density arriving at the collector in electrogenerators with solid dielectrics, as shown in Figures E12 and E13. By comparison with the figures in Appendix C, it can be seen that a solid dielectric would decrease the beta current in a promethium-147-oxide electrogenerator by 40% or more, depending on the voltage. Reduction in beta current would be much less in a strontium-90-titanate electrogenerator. For example, a 5-mil thick polyimide dielectric would have an equivalent thickness of 0.0127 cm; and by inspection of the figure in Appendix C for strontium-90-titanate fuel layers, it is evident that the reduction in beta current-density by the dielectric would be about 70 micro-amperes/$m^2$ out of a total of more than 350 micro-amperes/$m^2$.

In using Figures E12 and E13, it must be remembered that the dielectric has an electric-breakdown limit. Dielectric strength is shown in Figure E14 for several dielectric materials. Below the electric-breakdown limit, leakage current through the dielectric can be characterized by a volume resistivity, and this property is shown in Figure E15 for several dielectric materials.

Whether these electrical properties will be affected by radiation damage from beta rays and bremsstrahlung is a moot question. Available information on radiation damage to dielectrics (ref. E18) indicates that the electrical properties are virtually unchanged until catastrophic breakdown occurs at high total doses such as $10^{18}$ n.v.t., equivalent to a gamma dose of at least $5x10^{8}$ rad. Tests of Kapton H-film irradiated with 2-Mev electrons indicate breakdown at about $5x10^{9}$ rad. The average energy of betas passing through the dielectric is probably of the order of .03 Mev, and about 40% of the beta current is lost in the dielectric as calculated above. But only about 10% of the total beta emission is involved, so only about 4% of the total activity could be lost in the dielectric. The rate of energy absorption in the dielectric is about:

$$dE/dt = (.03 \text{ Mev}) \times (.04x3.7x10^{10} \text{xcuries/cm}^2) \qquad (E7)$$

For a fuel-layer thickness of 0.005-cm (2-mil), there is about $.005x5020 = 25.1$ curie/cm$^2$ , so $dE/dt = 1.1x10^{15}$ (ev/cm$^2$)/sec. With a polyimide dielectric thickness of 1-mil (.00254 cm), there is about $1.42x.00254 = .0036$ gm/cm$^2$, so the energy absorption in the dielectric material is about $dE/dt = 0.31 \times 10^{18}$ (ev/gm)/sec. One rad corresponds to 100 erg/gm, which is $0.624x10^{14}$ ev/gm, so the beta dose rate in the dielectric is about $0.5x10^{4}$ rad/sec. At this dose rate, a total dose of $5x10^{9}$ rad would be reached in $10^{6}$ sec, or 280 hours. Even if this calculation were off by an order of magnitude, it would predict radiation damage problems with

the dielectric in promethium-147 ACCENT electrogenerators intended for long-life application. Strontium-90-titanate has a volume activity of only 139 curies/$cm^3$ , so the dielectric dose rate would be much less than in promethium-147 electrogenerators. Detailed calculation of beta energy loss in the dielectric could be made,but the value of such calculations would be questionable. Direct experimental evidence appears to be the most satisfactory way of answering the radiation damage question for solid dielectrics in the ACCENT electrogenerator. For the remainder of this discussion it is assumed that the electrical properties of solid dielectrics are not affected by the radiation environment of the electrogenerator.

Ohmic leakage current through the dielectric is simply:

$$j_{l,d} = \phi/(\rho\tau_d) \qquad \text{(E8)}$$

where $\phi$ is the electrogenerator voltage, $\rho$ is the dielectric volume resistivity, and $\tau_d$ is the dielectric thickness. Ohmic leakage currents through polyimide dielectrics of various thicknesses, and with various electrogenerator voltages are shown in Figure E16. From this figure, it is evident that for dielectric temperatures below 120°C, the ohmic leakage current will be an order of magnitude lower than the beta current arriving at the collector (see Figure E12 for comparison).

In summary, leakage current through solid dielectrics will be made up mostly of betas reflected from the collector. Secondary electrons emitted from the collector will be merely a part of the ohmic leakage current, which in turn can be maintained at a few percent of the electrogenerator current if the dielectric is at a temperature less than 100°C. The major loss in electrogenerator current will be beta absorption in the solid dielectric, which will be from a few percent to over 40% depending on the type of dielectric, dielectric thickness, and type of radioisotope. Whether radiation

damage to the dielectric will be a problem probably can be best resolved by direct experience in real electrogenerators.

## REFERENCES


E1. Koral, K.F.: High-Voltage Characteristics of A Large-Gap Coaxial-Cylinder Electrode. NASA TN D-3949. (May, 1967).

E2. Fowler, R.H., and Nordheim, L.W.: Electron Emission in Intense Electric Fields. Proc. Roy. Soc. (London), A119, 173. (1928).

E3. Nordheim, L.W.: The Effect of the Image Force on the Emission and Reflexion of Electrons by Metals. Proc. Roy. Soc. (London), A121, 626. (1928).

E4. Chatterton, P.A.: A Theoretical Study of Field Emission Initiated Vacuum Breakdown. Proc. Phys. Soc., 88, 231. (1966).

E5. Davies, D.K., and Biondi, M.A.: Vacuum Electrical Breakdown between Plane-Parallel Copper Electrodes. J. Appl. Phys., 37, no. 8, 2969. (July, 1966).

E6. Alpert, D., Lee, D.A., Lyman, E.M., and Tomaschke, H.E.: Initiation of Electrical Breakdown in Ultrahigh Vacuum. J. Vac. Sci. Technol., 1, 35. (1964).

E7. Little, R.P., and Smith, S.T.: Field Enhancing Projections Produced by the Application of An Electric Field. J. Appl. Phys., 36, 1502. (1965).

E8. McKay, K.G.: Secondary Electron Emission. Advances in Electronics, Vol. I. Academic Press. (1948).

E9. Dekker, A.J.: Secondary Electron Emission. Solid State Physics, Advances in Research and Applications, Vol. 6. Academic Press. (1958).

E10. Bronshtein, I.M., and Segal, R.B.: Inelastic Scattering of Electrons and Secondary-Electron Emission in Certain Metals. I. Soviet Physics Solid State, 1, no. 10, 1365, (April 1960).

E11. Schultz, A.A., and Pomerantz, M.A.: Secondary Electron Emission Produced by Relativistic Primary Electrons. Phys. Rev., 130, no. 6, 2135, (15 June 1963).

E12. Cohen, A.J., and Koral, K.F.: Backscattering and Secondary-Electron Emission from Metal Targets of Various Thicknesses. NASA TN D-2782. (April, 1965).

E13. Koral, K.F., and Cohen, A.J.: Empirical Equations for Electron Backscattering Coefficients. NASA TN D-2909. (July, 1965).

E14. Wright, K.A., and Trump, J.G.: Back-Scattering of Megavolt Electrons from Thick Targets. J. Appl. Phys., 33, no. 2, 687, (Feb., 1962).

E15. Sternglass, E.J.: Backscattering of Kilovolt Electrons from Solids. Phys. Rev., 95, no. 2, 345, (15 July 1954).

E16. Bhalla, M.S., and Craggs, J.D.: Measurement of Ionization and Attachment Coefficients in Sulfur Hexafluoride in Uniform Fields. Proc. Phys. Soc., 80, 151, (1962).

E17. Croitoru, Z.: Space Charges in Dielectrics. Progress in Dielectrics, Vol. 6. Academic Press (1965).

E18. Black, R.M., and Charlesby, A.: Irradiated Polymers. Progress in Dielectrics, Vol. 2. Academic Press (1960).

TABLE E1 - Maximum secondary-electron-emission coefficients for various target materials.

| target material | $\delta_{max}$ | $E_p$, Mev |
|---|---|---|
| Ag | 1.5 | .0008 |
| Al | 1.0 | .0003 |
| Au | 1.46 | .0008 |
| Be | 0.6 | .0002 |
| C | 1.0 | .0003 |
| Cu | 1.3 | .0006 |
| Fe | 1.3 | .00035 |
| Mg | 0.95 | .0003 |
| Mo | 1.25 | .000375 |
| Ni | 1.3 | .00055 |
| Pt | 1.6 | .0008 |
| Ti | 0.9 | .00028 |
| W | 1.4 | .0006 |
| Zr | 1.1 | .00035 |

TABLE E2 - Properties of some dielectric materials.

| property | Boralloy (pyrolytic boron nitride) | Teflon FEP (tetraflouro-ethylene) | Mylar (polyester) | Parylene N (poly-para-xylylene) | Kapton H-film (polyimide) |
|---|---|---|---|---|---|
| Max. useful temp., $^{o}F$ | 3000 | 550 | 460 | 430 | 750 |
| Density, $mg/cm^3$ | 2100 | 2200 | | 1120 | 1420 |
| vol. resist., ohm-cm (at 23°C) | $10^{14}$ | $10^{18}$ | $4x10^{15}$ | $1.4x10^{17}$ | $10^{18}$ |
| diel. strength, volt/mil (at 23°C) | 4000 | 500 | 5000 | 6500 | 7000 |
| range coeff., $C_{R,d}$ | .000474 | .000725 | | .000843 | .00061 |
| $C_{R,Pm_2O_3}/C_{R,d}$ | .361 | .236 | | .203 | .280 |
| $C_{R,Tm_2O_3}/C_{R,d}$ | .283 | .185 | | .159 | .220 |
| $C_{R,SrTiO_3}/C_{R,d}$ | .599 | .392 | | .337 | .466 |

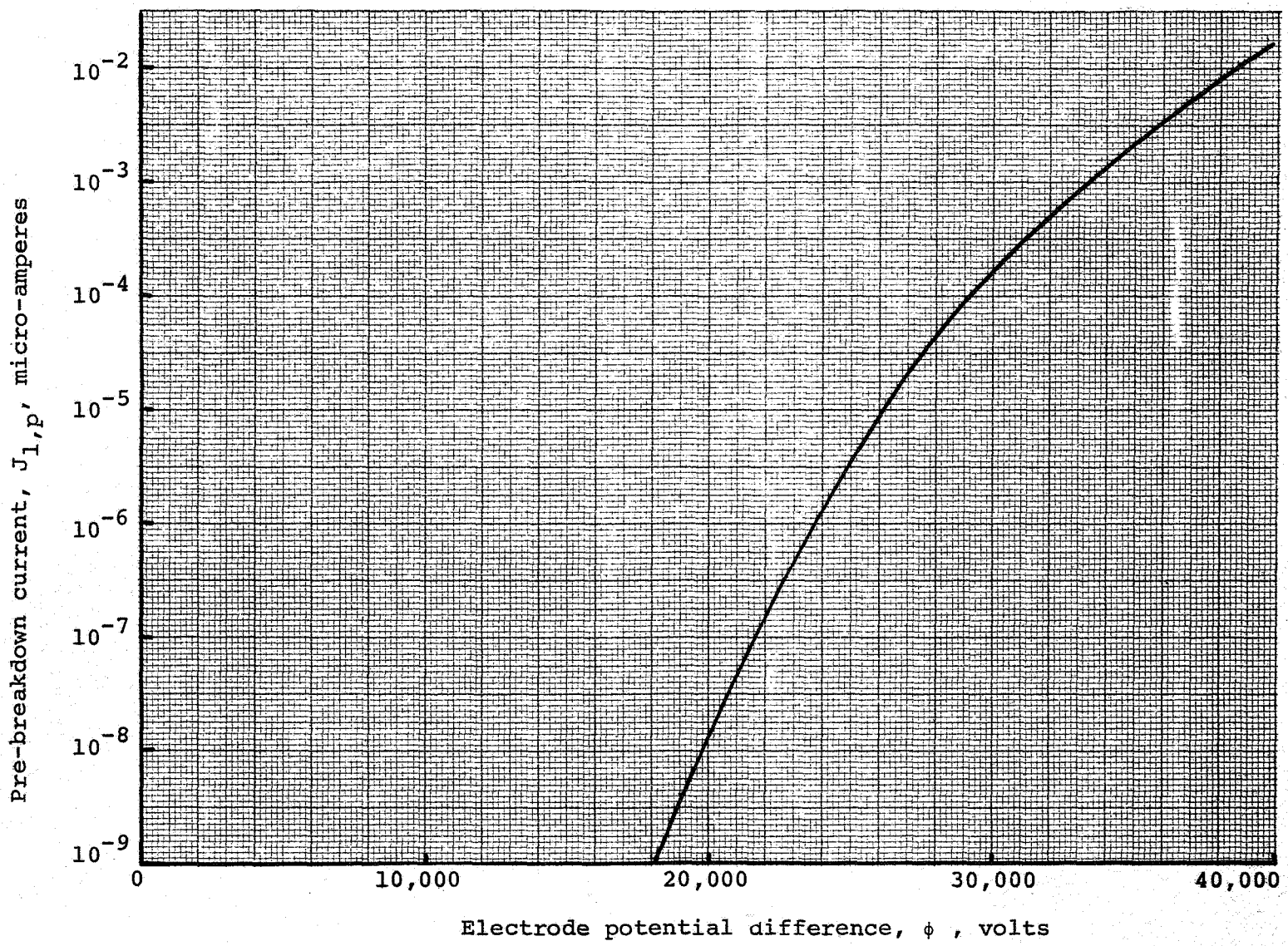


FIG. E1 - Typical pre-breakdown leakage current between parallel plane copper electrodes. Electrode area approximately 1 sq. cm.; electrode gap,2 mm.

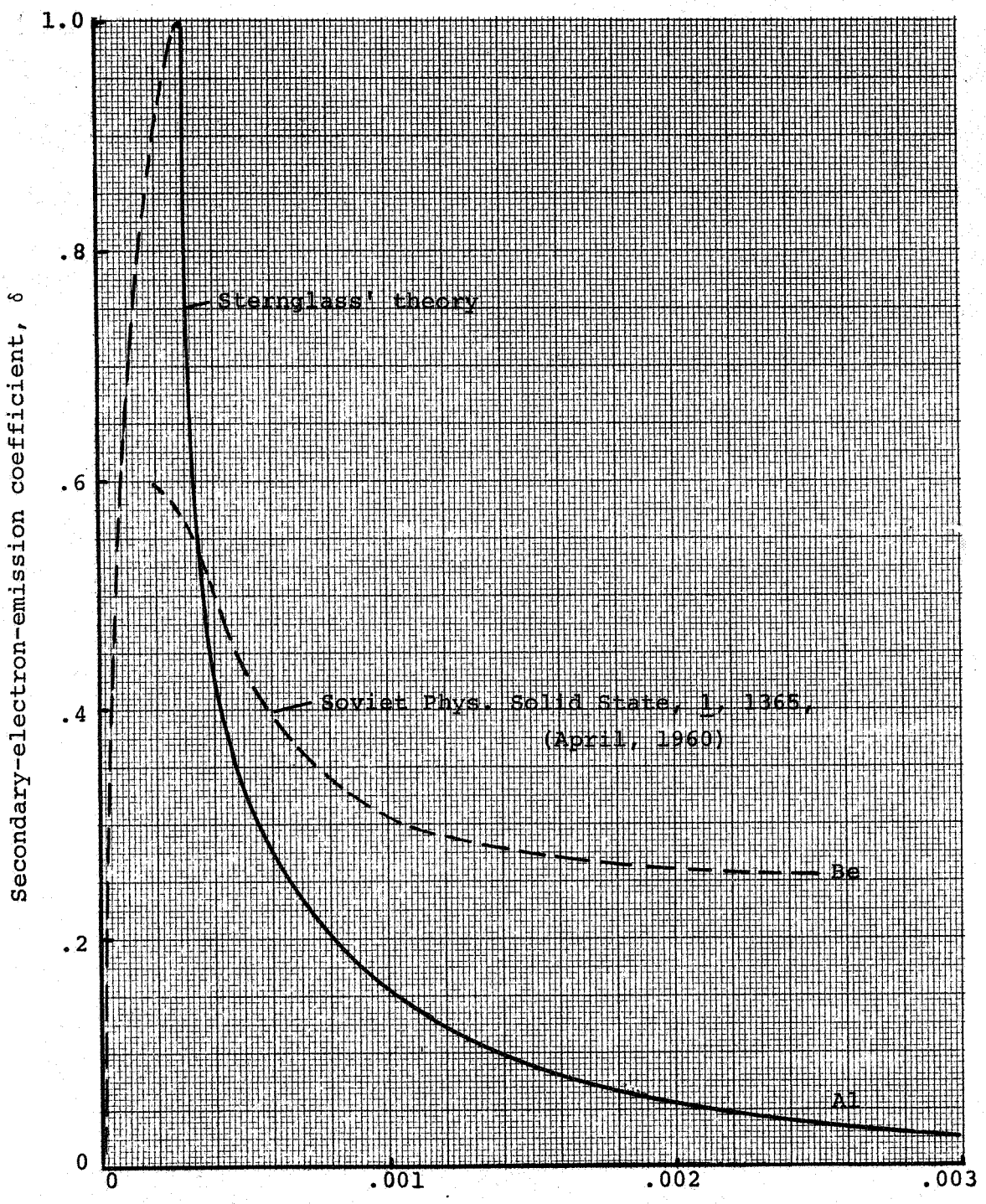


FIG. E2 - Secondary-electron-emission coefficients at low primary-electron energy, and normal incidence.

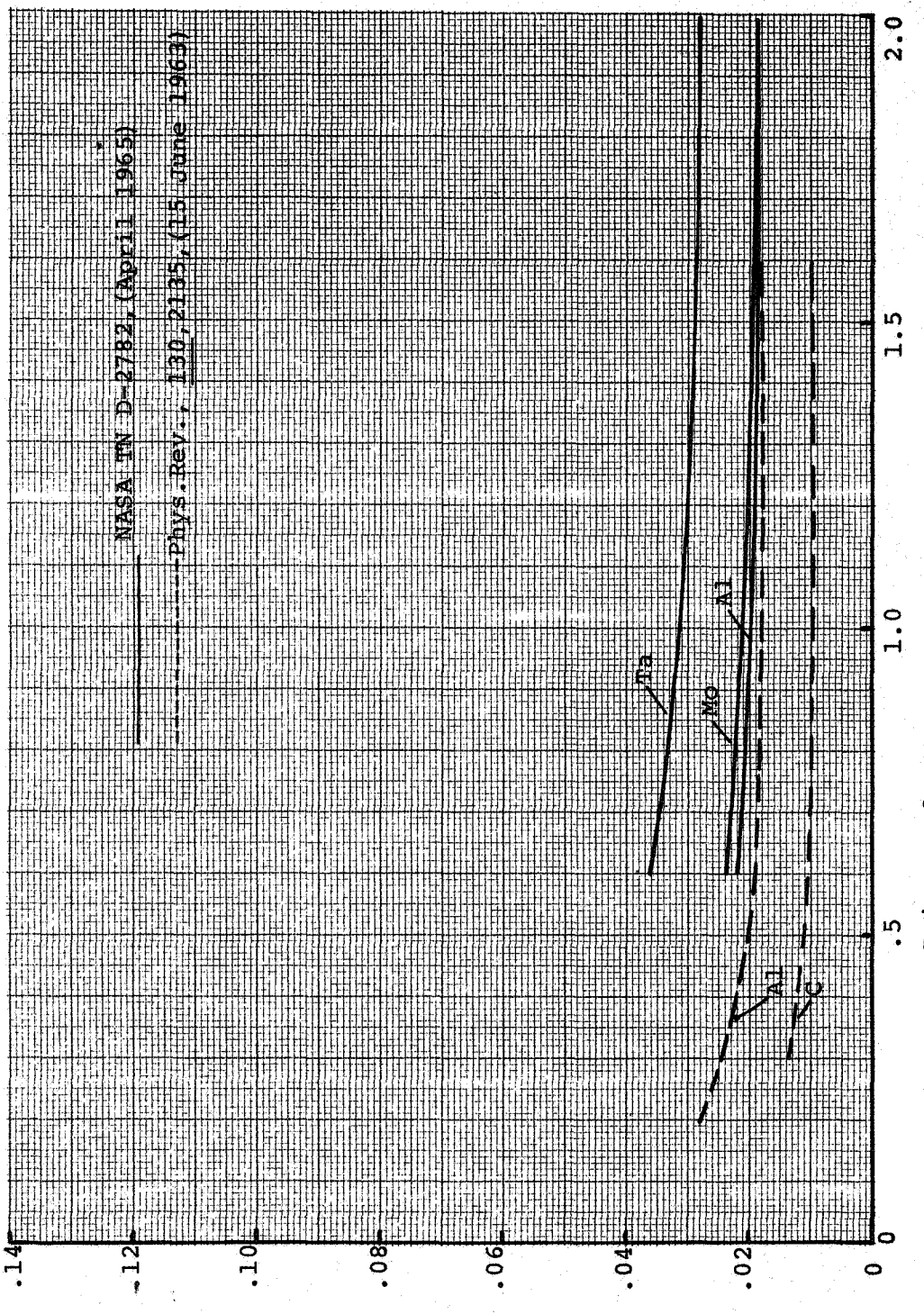


FIG. E3 - Secondary-electron-emission coefficients for various target materials at higher primary-electron energy, and normal incidence.

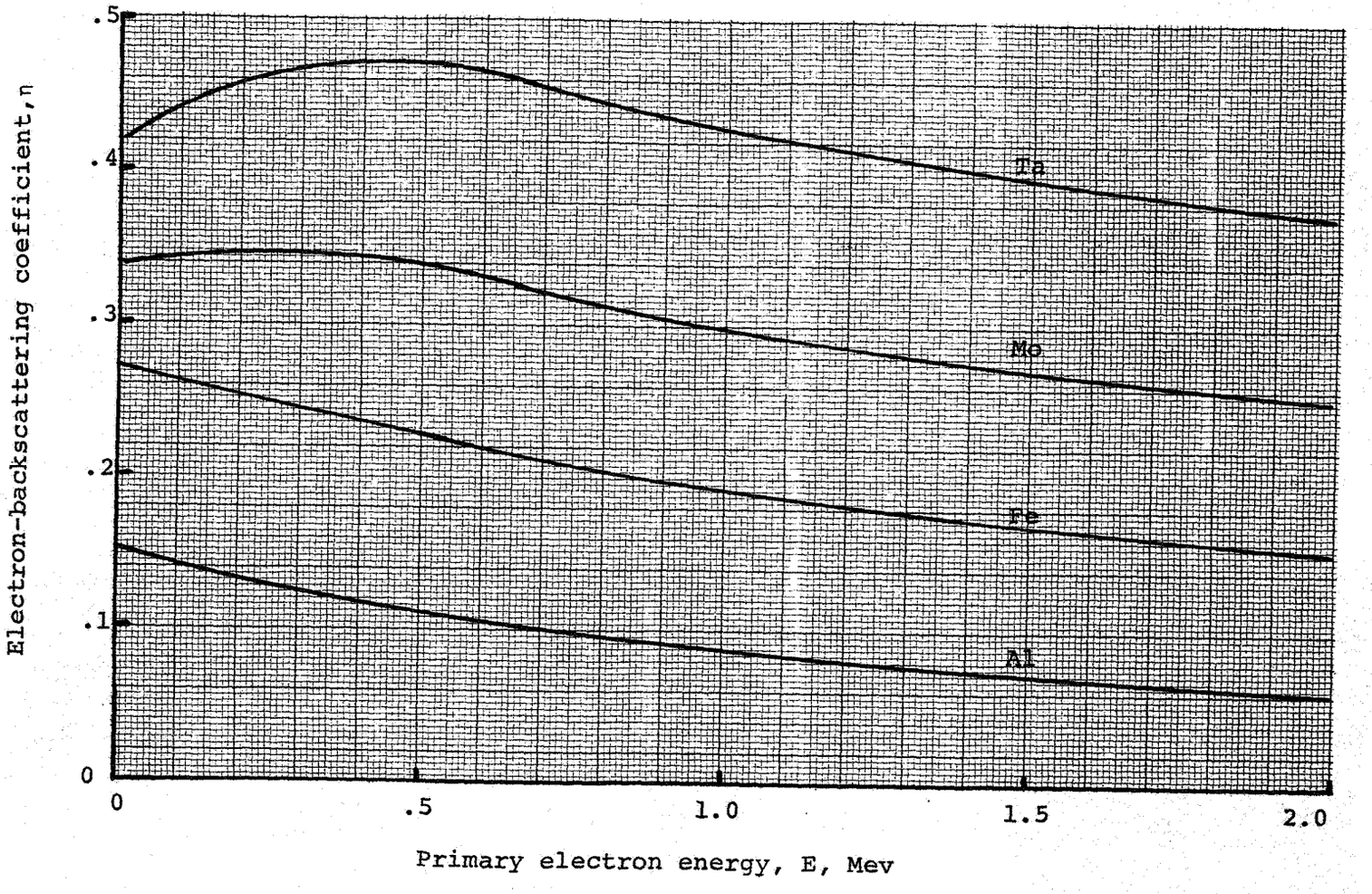


FIG. E4 - Electron-backscattering coefficient for various materials, with normal incidence.

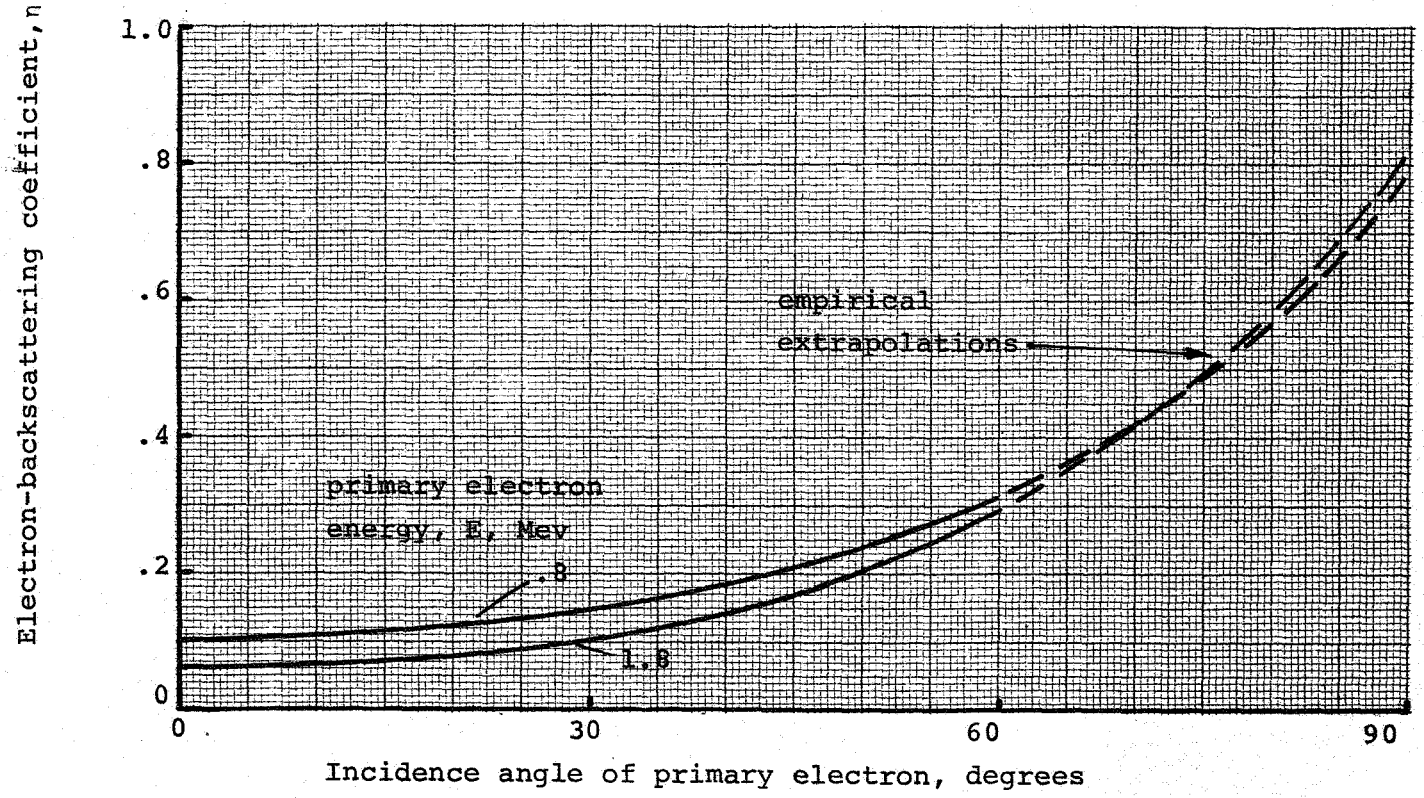


FIG. E5 - Effect of incidence angle on electron backscattering coefficient for aluminum.

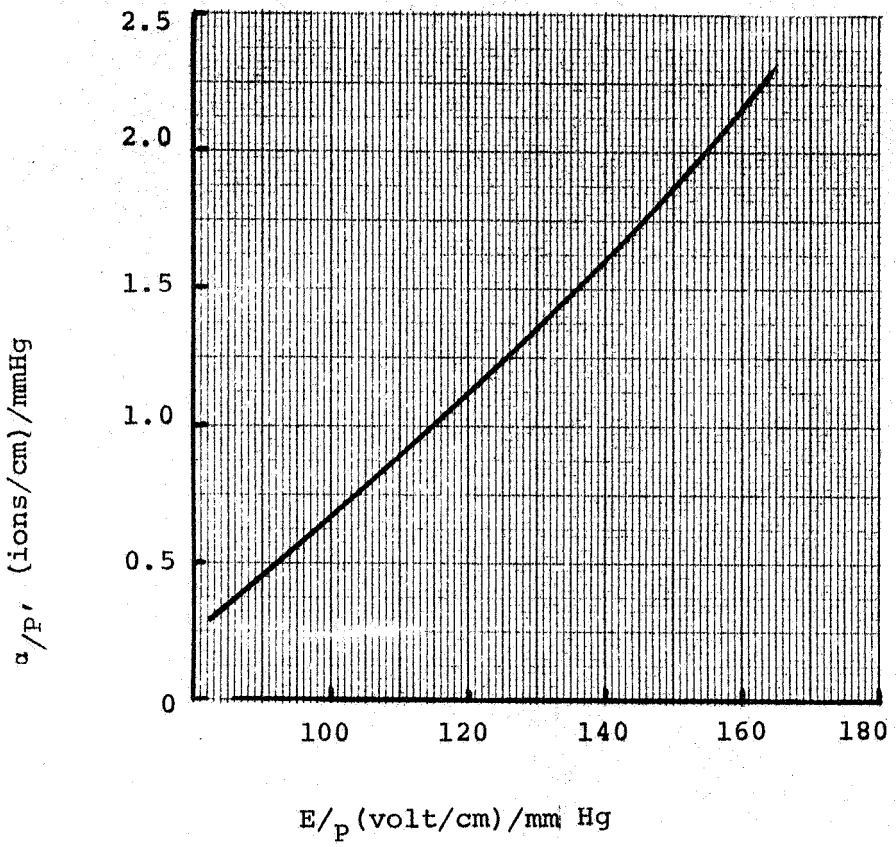


FIG. E6 - The first Townsend coefficient α for $SF_6$ gas.

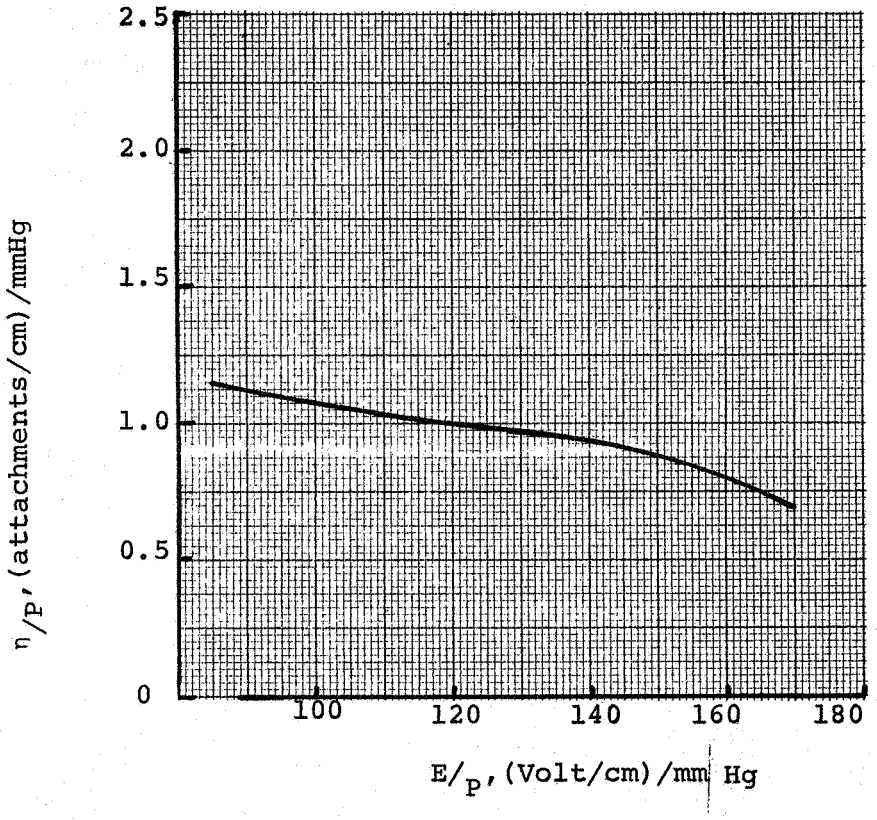


FIG. E7 - The second Townsend coefficient $\gamma$ for $SF_6$ gas.

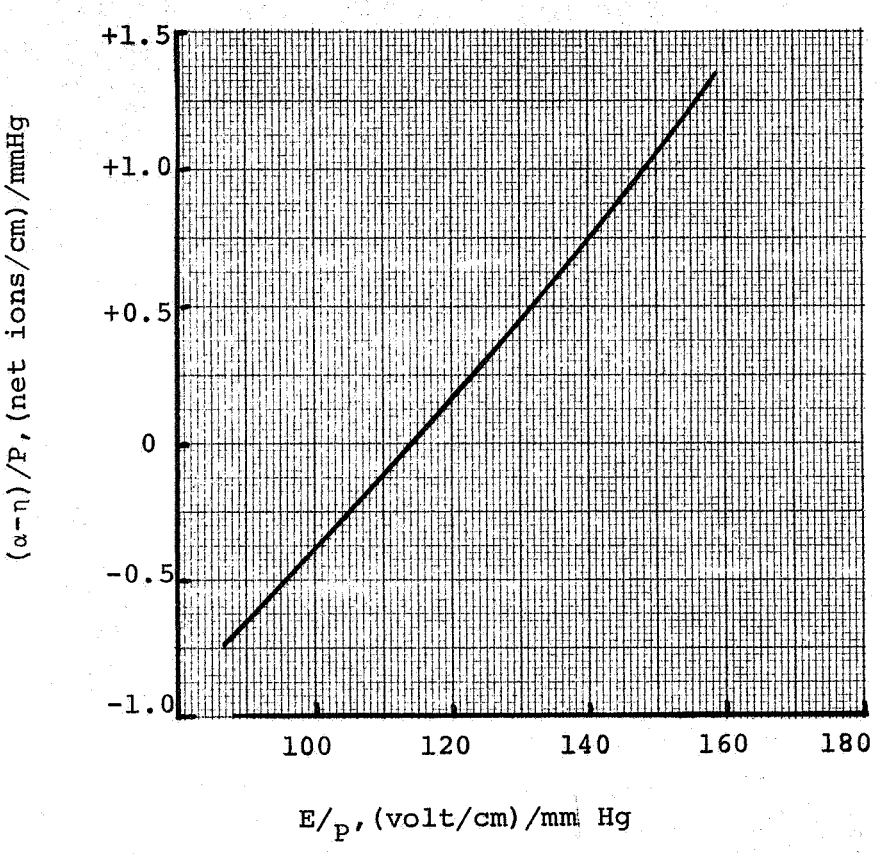


FIG. E8 - Electric breakdown criteria for $SF_6$ gas.

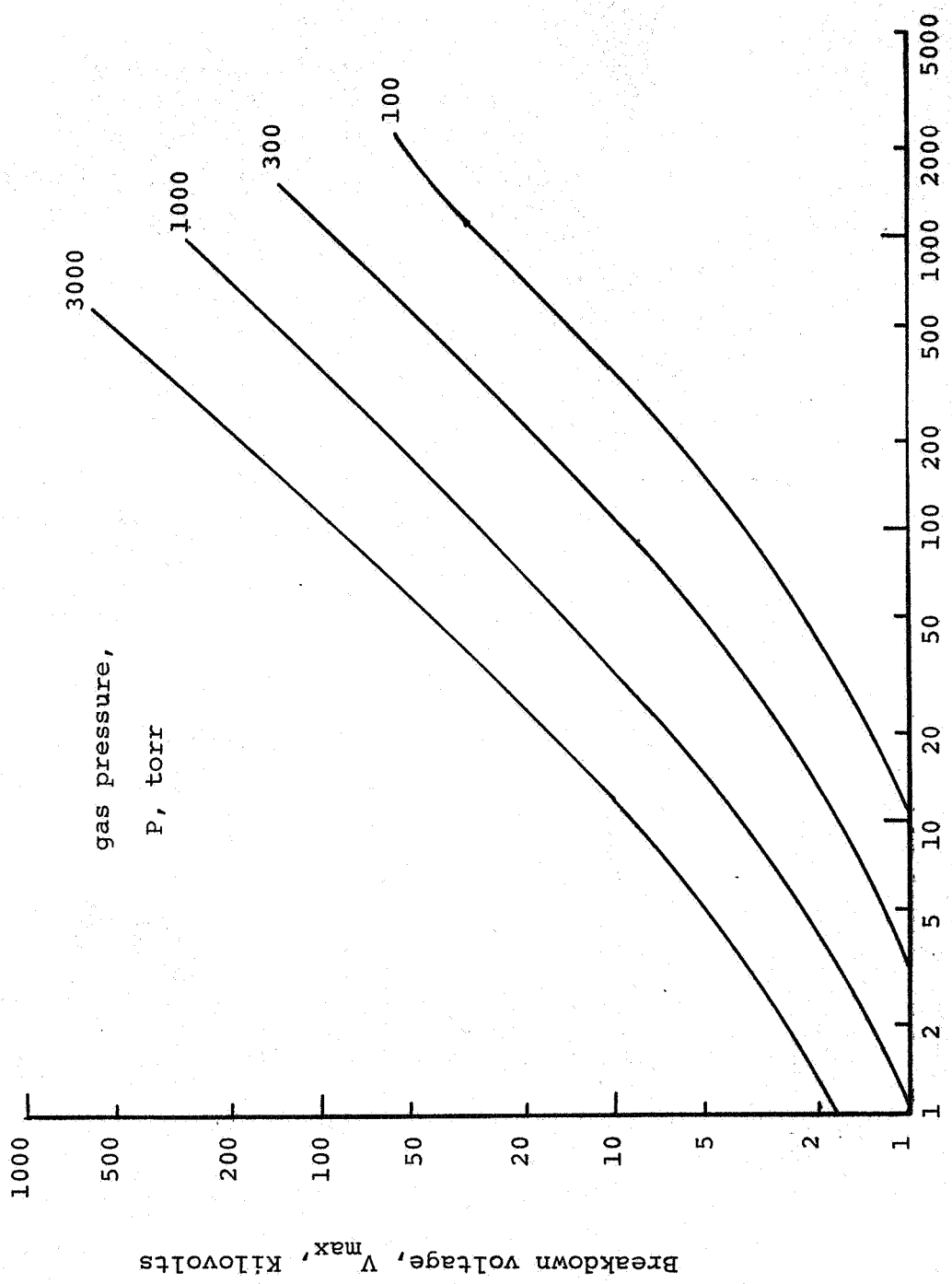


FIG. E9 - Theoretical electric breakdown voltage for $SF_6$ gas.

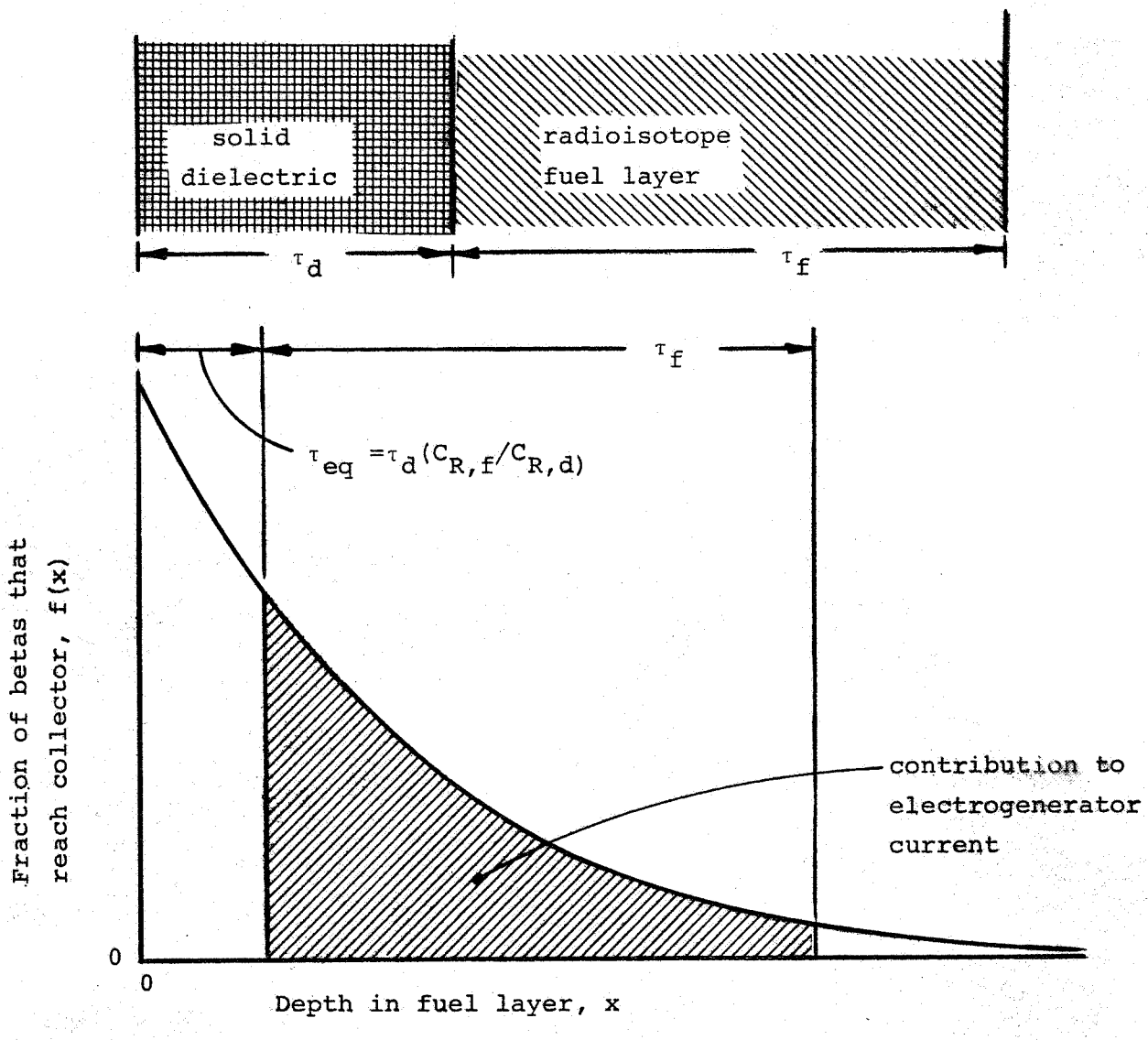


FIG. E10 - Estimate of beta current reaching collector after passing through solid dielectric.

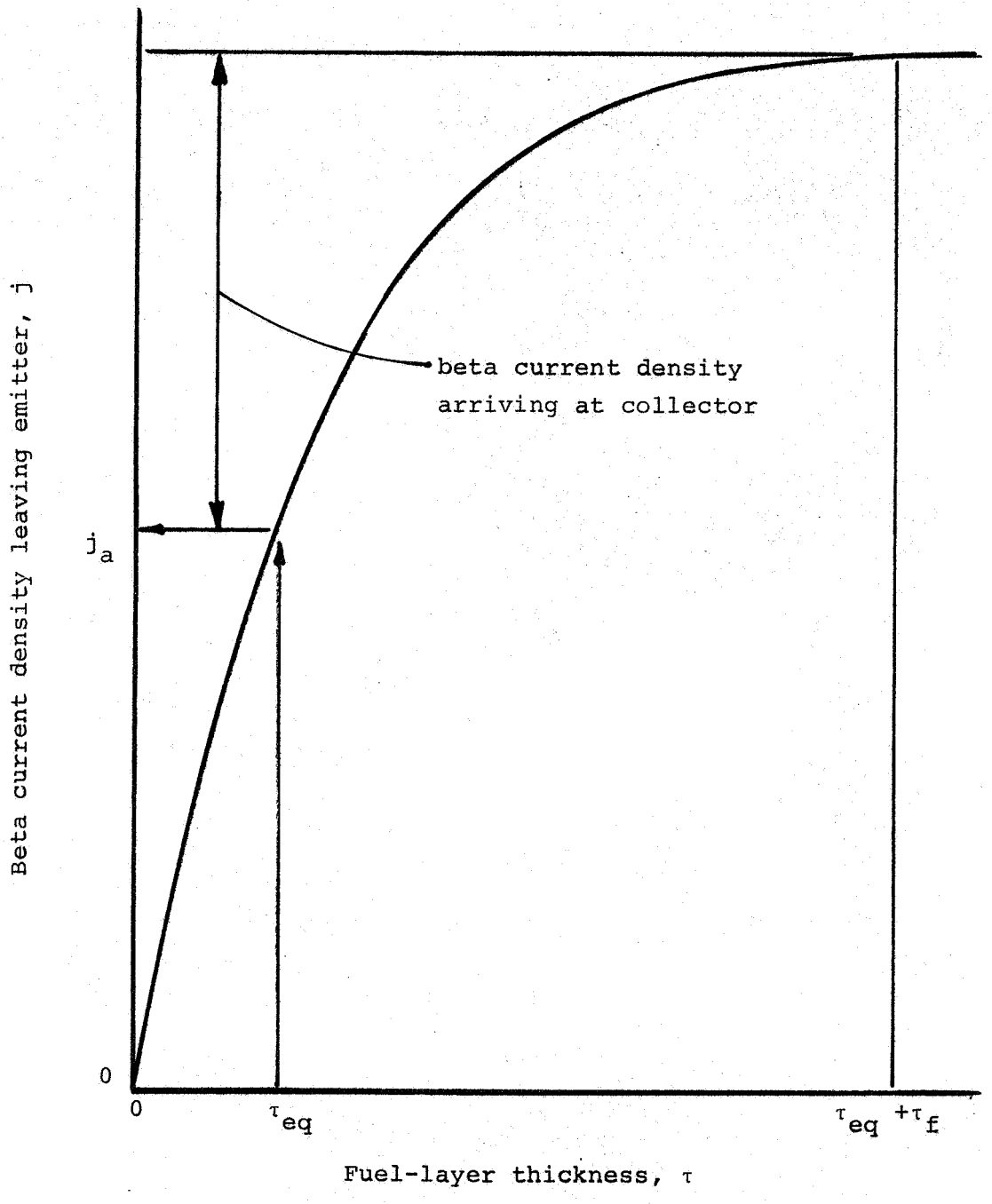


FIG. E11 - Method for estimating beta-current density arriving at collector in electrogenerator with solid dielectric.

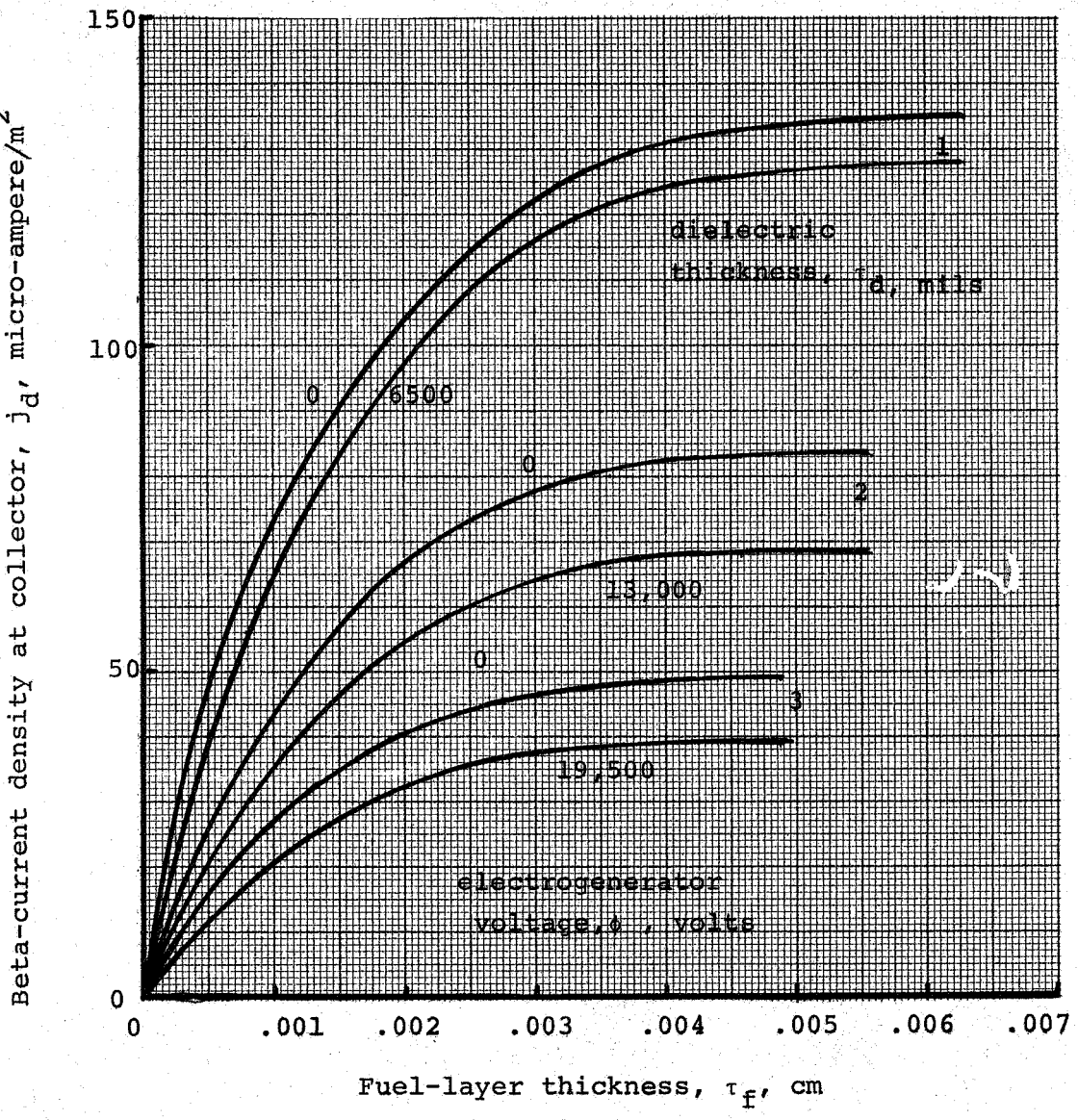


FIG. E12 - Beta-current density arriving at collector in promethium-147-oxide ($Pm_2O_3$, 90% dense) with polyimide solid dielectric.

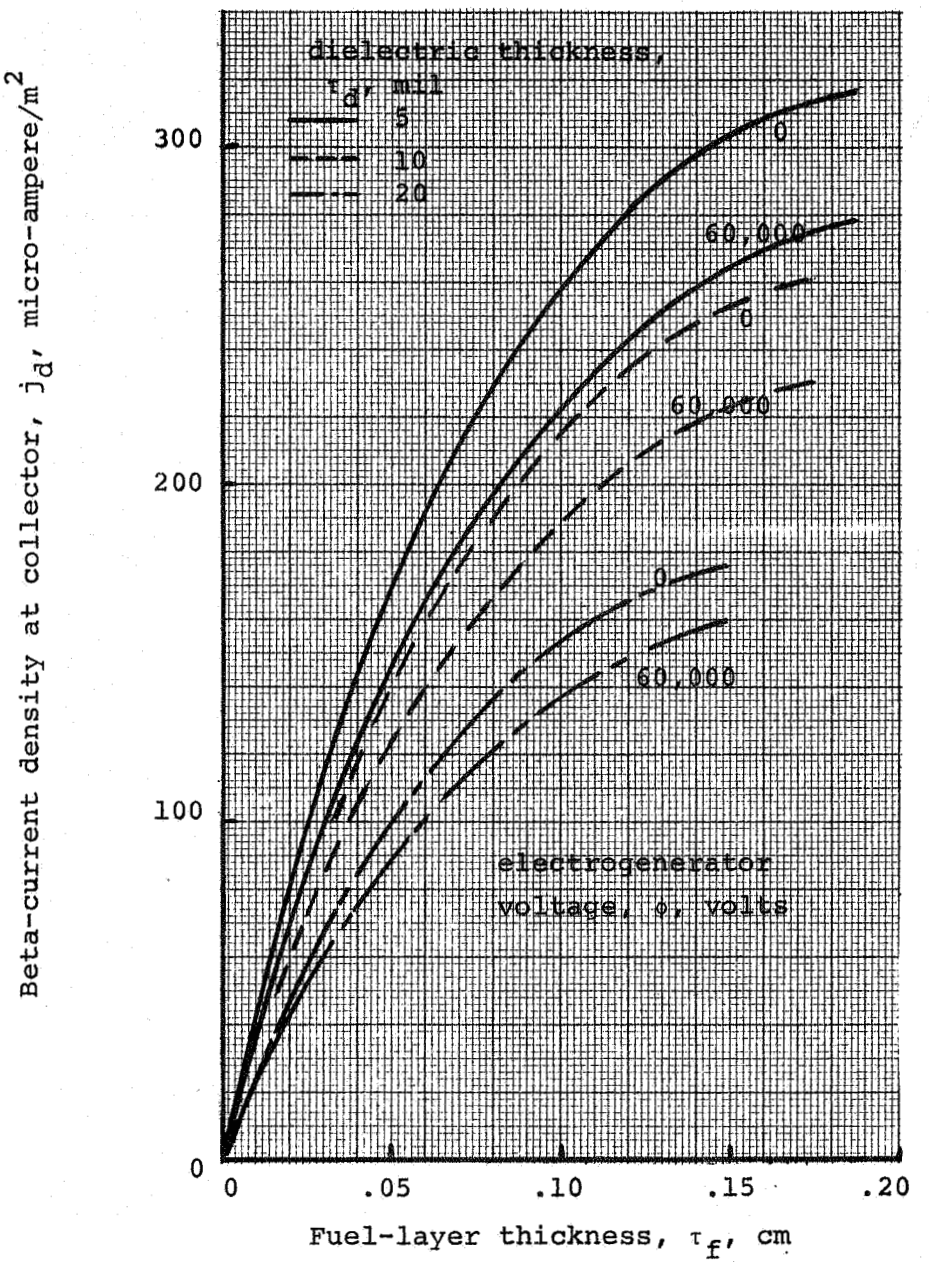


FIG. E13 -- Beta-current density arriving at collector in strontium-90-titanate ($SrTiO_3$, 90% dense) with polyimide solid dielectric.

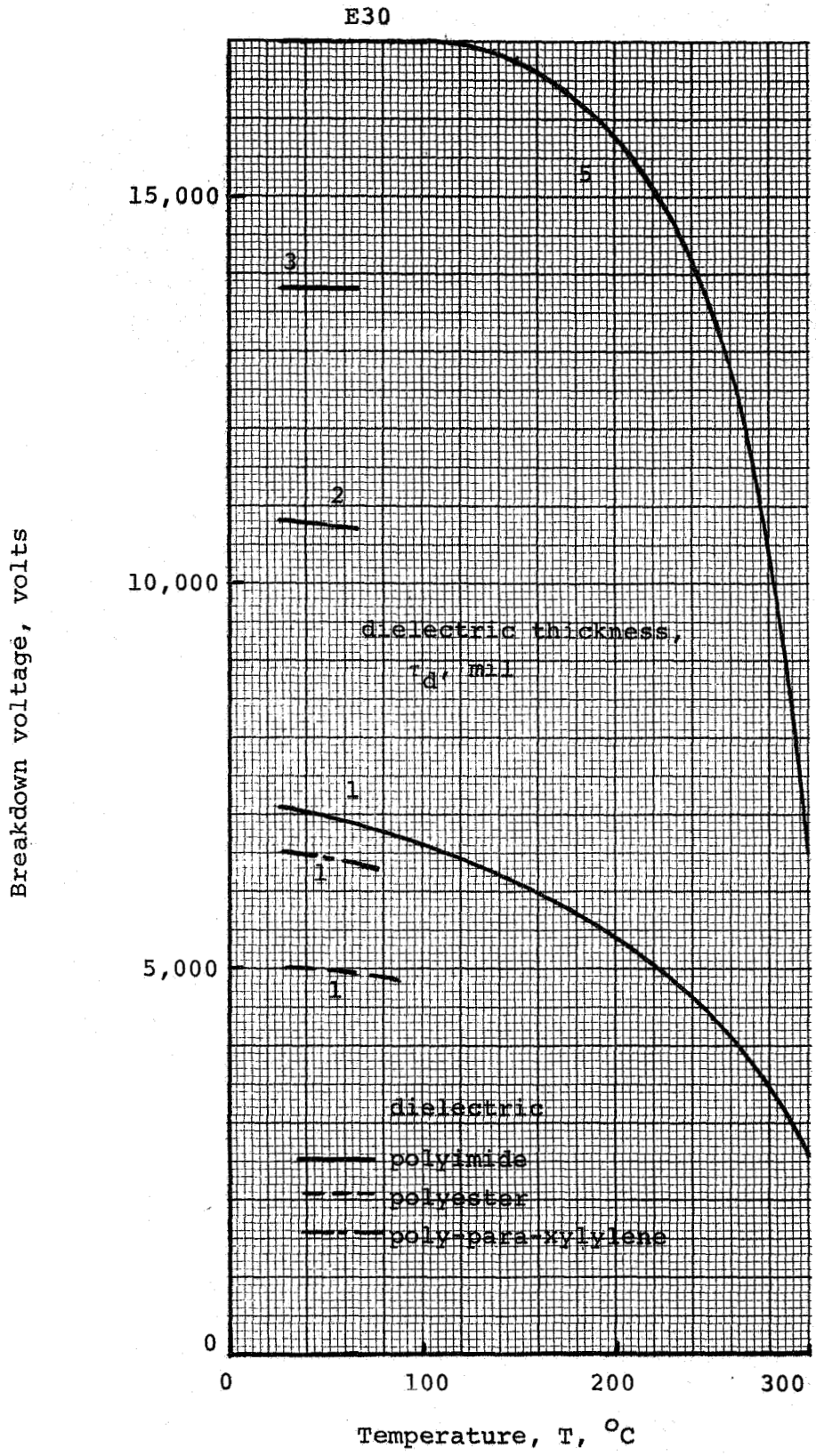


FIG. E14 - Breakdown strength of some dielectric materials

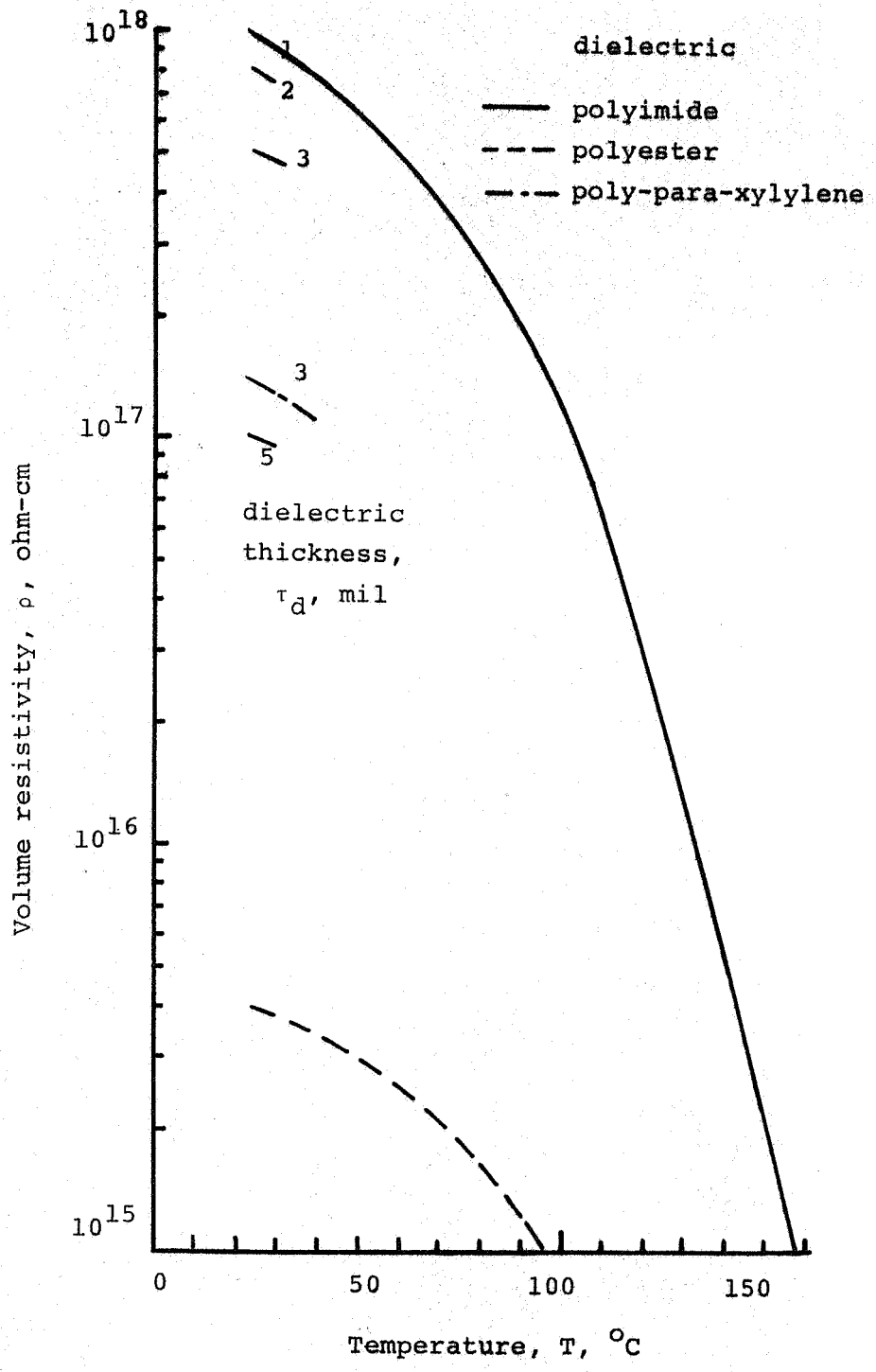


FIG. E15 - Volume resistivity of some dielectric materials

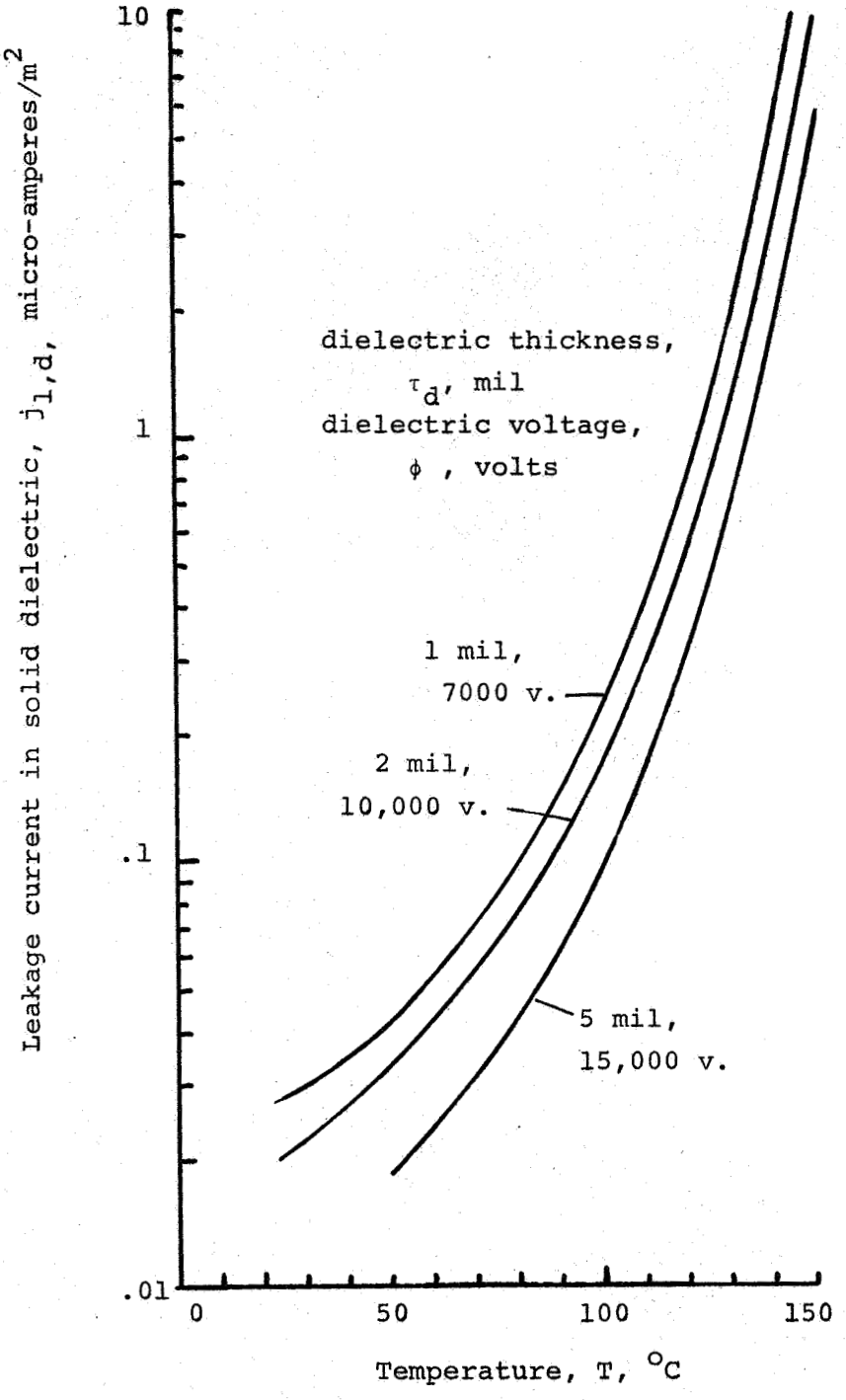


FIG. E16 - Ohmic leakage current in polyimide solid dielectric.

# APPENDIX F

## THERMAL DESIGN CONSIDERATIONS

Conduction of heat in the electrogenerator electrodes is of fundamental importance in establishing electrode dimensions that will provide a satisfactorily low peak temperature in the electrode. This is of particular importance for solid-dielectric electrogenerators where the resistivity of the dielectric decreases rapidly as temperature increases. Heat generation and heat flow in vacuum-dielectric electrogenerators is illustrated in Figure F1.

Heat generation and flow in the emitter of a vacuum-dielectric electrogenerator can be expressed (by reference to Figure F1) as follows:

$$-kA(dT/dx) = w_E \int_o^x (\dot{Q}_G/S - \dot{Q}_D/S)dx \qquad (F1)$$

where $k$ is thermal conductivity, $A$ is cross-sectional area, $w_E$ is emitter width, and $x$ is measured from the center of symmetry (ie, peak temperature location) of the emitter. A typical value for the heat generation term is $\dot{Q}_G/S = 90$ watt/m$^2$ for 2-mil thick layers of promethium-147-oxide (90% dense). Radiation heat transfer between the emitter and collector is:

$$\dot{Q}_D/S = \sigma(T_E^4 - T_C^4)/(1/\varepsilon_E - 1/\varepsilon_C - 1) \qquad (F2)$$

where $\sigma$ is the Stefan-Boltzman constant, and where $\varepsilon_E$ and $\varepsilon_C$ are emittances of the emitter and collector respectively. Radiation heat transfer rates determined from equation (F2) are shown in Figure F2. From inspection of this figure it is evident that the integrand in equation (F1) will be negligible when the emitter temperature is about 50$^o$C and the collector temperature is 300$^o$K. In other words, at 50$^o$C emitter temperature, all of the heat generated in the emitter can be transferred by radiation to the collector if the collector is maintained at 300$^o$K (27$^o$C). If the collector

must be operated at a higher temperature, then the emitter temperature would be higher also, for example, when the collector must be maintained at 400°K, the emitter temperature must be at about 130°C if the heat generated in the emitter is to be transferred by radiation to the collector.

Collector temperature must be high enough to provide adequate heat rejection to the spacecraft or to space. If the ACCENT system is integrated into the spacecraft in such a way that it is surrounded by the spacecraft structure, then the heat sink temperature is the spacecraft temperature. For example, if the spacecraft structure is at 300°K, then the collector temperature must be enough greater than 300°K to provide adequate transfer of heat. If the collector electrodes transfer heat by conduction to a collector support structure, and if the collector support structure must reject the heat to the spacecraft structure by thermal radiation, then a collector temperature of 100°C(373°K) would provide a transfer of 650 watt/$m^2$ to a 300°K spacecraft structure (see Figure F2). In turn, an emitter temperature of about 120°C would provide adequate radiation heat transfer to the collector. From this discussion, it appears that emitter temperatures of 150°C or less will be satisfactory.

For thermal radiation to be effective in transferring heat from the emitter to the collector, the collector must have a nearly uniform temperature profile. If it is assumed that the radiant heat arrives at the collector uniformly, then a simple analysis can be made of the collector temperature profile. This assumption is essentially that $\dot{Q}_D/S$ is the same everywhere on the collector surface shown in Figure F1, so the heat flow equation for the collector is:

$$-kA(dT/dy) = w_C \int_o^Y (\dot{Q}_D/S)\,dy \qquad \text{(F3)}$$

Since $\dot{Q}_D/S$ is assumed constant, then:

$$-kA(dT/dy) = w_C(\dot{Q}_D/S)y \qquad \text{(F4)}$$

Integrating:

$$-kA\int_{T_o}^{T_R} dT = w_C(\dot{Q}_D/S)\int_{D}^{L/2} y\ dy \qquad (F5)$$

where $w_C$ is the collector width, and $L$ is the collector length. The cross-sectional area is $A = w_C\tau_C$, where $\tau_C$ is collector thickness, so equation (F5) becomes:

$$T_o - T_R = \left[(\dot{Q}_D/S)L^2\right]/(8K\tau_C) \qquad (F6)$$

where $T_o$ is the peak temperature (at the middle of the collector length), and $T_R$ is the temperature of the collector support structure (at each end of the collector). Temperature difference $T_o - T_R$ is shown in Figure F3 for various thicknesses of aluminum collectors, and for a range of collector lengths. From this simplified analysis it can be concluded that a nearly uniform temperature profile can be maintained in aluminum collectors of a few mil thickness with lengths of about one foot.

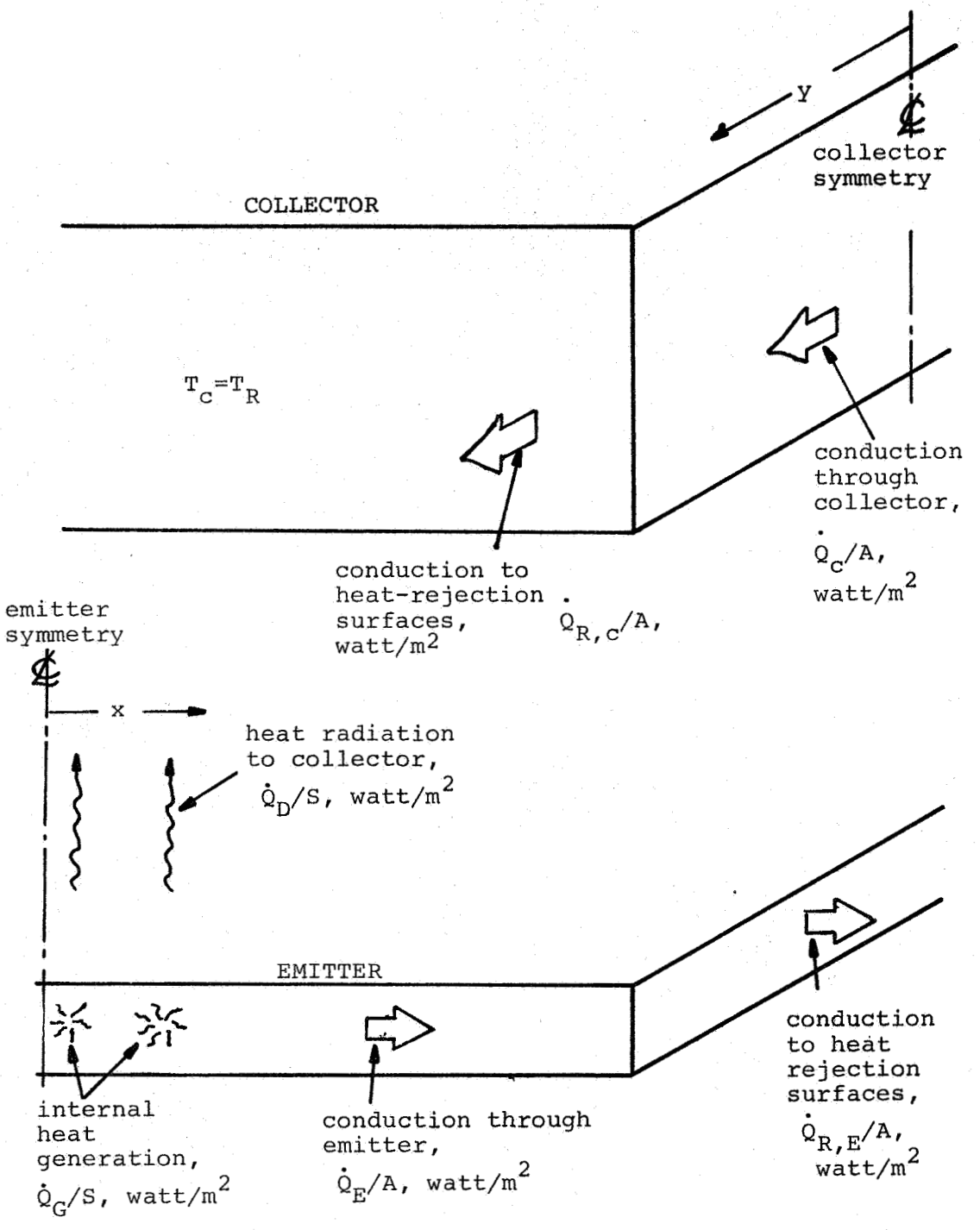


FIG. F1 - Heat generation and heat flow in vacuum dielectric electrogenerator.

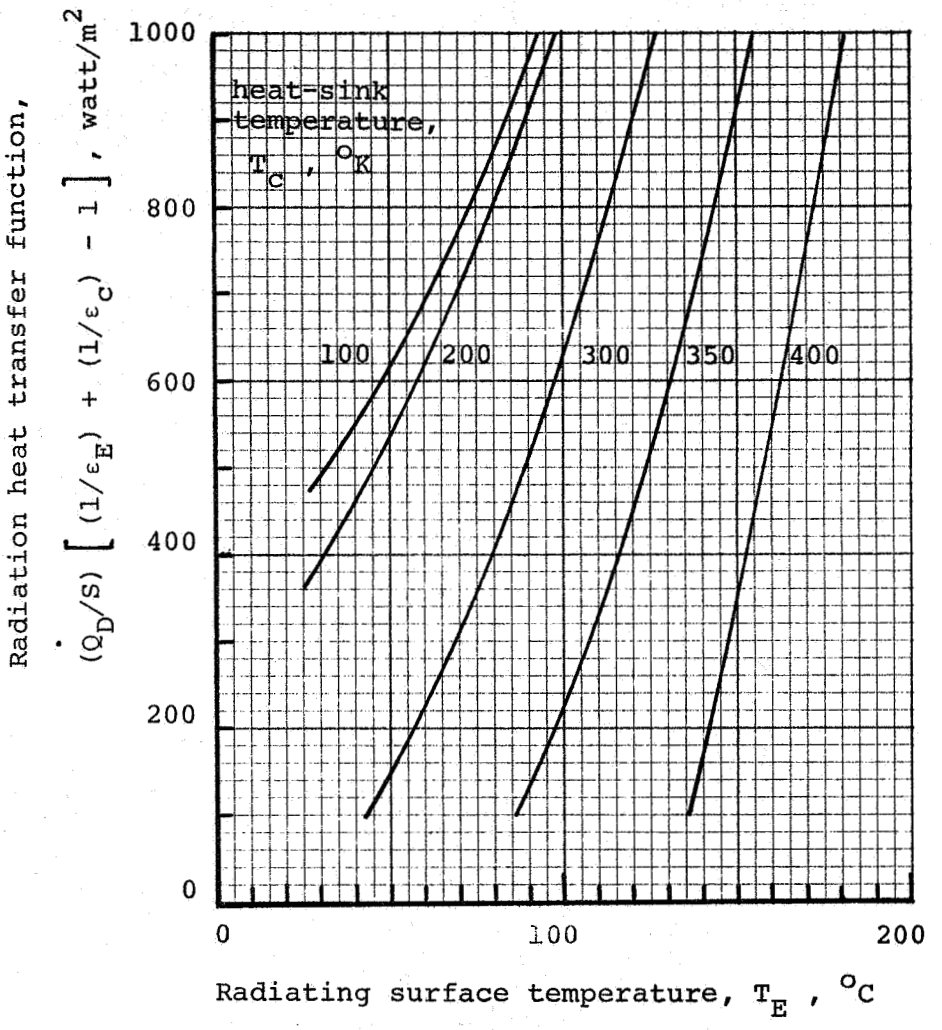


FIG. F2 - Radiation heat transfer between plane parallel surfaces.

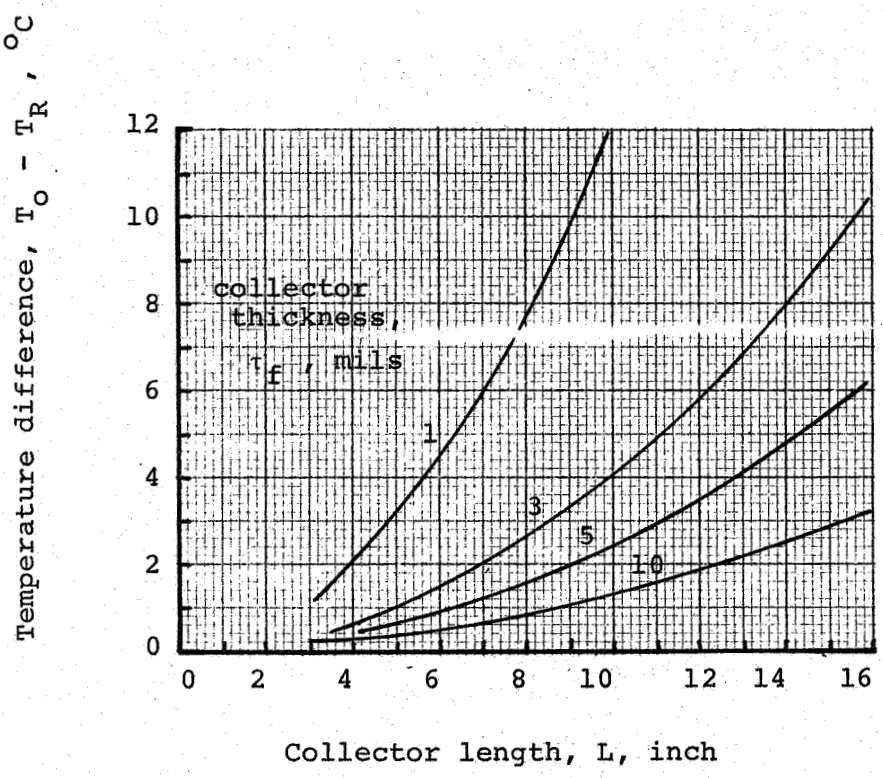


FIG. F3 - Temperature difference along collector length, $T_o$ = peak temperature, $T_R$ = temperature at end. Collector material, aluminum. Heat input to collector, $\dot{Q}_D/S$ = 90 watt/$m^2$ .

## APPENDIX G 1

### FUEL-ELEMENT FABRICATION METHODS

A number of methods of fabrication of the electrogenerator fuel elements have been studied by Pacific Northwest Laboratories, and the results of that study are reported in the following pages.

Another fabrication method has been described* as follows. A 5- or 10-mil aluminum or nickel disc of 1.5-inch diameter or larger, can be recessed to a 2- or 3-mil depth on one side (or probably both faces). A small peripheral land would remain. The recess would be filled with promethium-147-oxide powder and sintered in place. A 50- or 100-microinch nickel foil could be permanently fastened to the peripheral land, to seal the fuel layer if desired.

From the information described in this appendix, it can be concluded that fabrication of fuel elements to the ACCENT system is within the present state-of-the-art.

---

* Andelin, R. W. : private communication from D. W. Douglas Laboratories. (20 November 1967).

# ACCENT ELECTROGENERATOR FABRICATION FEASIBILITY STUDY

to

THE DANE COMPANY
BOX 668
FORT COLLINS, COLORADO

December 9, 1967

PACIFIC NORTHWEST LABORATORIES

a division of

BATTELLE MEMORIAL INSTITUTE

3000 Stevens Drive
Richland, Washington 99352

## ABSTRACT

A study was made to determine the fabrication feasibility of advanced thin plate radioisotopic fuels for the ACCENT electrogenerator. Two basic fuel form concepts were investigated: a high volume percent ceramic phase cermet and a radioisotopic ceramic coated light metal foil.

Pertinent fabrication techniques were reviewed and promising methods were investigated experimentally using stand-in materials for the radioisotopic ceramics. Fabricability was established for both concepts, and processes were outlined utilizing available technology.

The most promising sequence for the cermet plate configuration appears to be:

- Preparation of dense radioisotopic oxide particles in the 7 to 75 micron size range.
- Provision of a 10 to 20 vol% metal coating on the ceramic particles by chemical vapor deposition.
- Consolidation of the coated particles by hot pressing to form a 0.006 inch thick plate having $\geq$ 97% of theoretical density.

The most promising process for the laminated material appears to be vacuum vapor deposition of the radioisotopic compound onto a light metal foil substrate. Adherent coatings having excellent thickness uniformity were obtained by electron beam evaporation of the stand-in material. RF diode sputtering should produce higher deposition rates and better control of thick film integrity.

# ACCENT ELECTROGENERATOR FABRICATION FEASIBILITY STUDY

to

THE DANE COMPANY
BOX 668
FORT COLLINS, COLORADO

December 9, 1967

## INTRODUCTION

Advanced direct energy conversion system concepts have created a need for new composite materials formed of radioisotopic ceramics and light metals. System design requirements dictate a thin plate geometry for these materials. Candidate radioisotopes are promethium-147 and strontium-yttrium-90.

There are two forms of composite materials which appear to be congruent with the electrogenerator design requirements:

- A laminated composite consisting of a 0.002 inch thick coating of promethium oxide on each side of a 0.002 inch thick light metal foil.
- A promethium oxide-light metal cermet containing on the order of 80 vol% of the radioisotopic ceramic, and having a thickness of 0.006 inch.

Although both approaches appear to be technically feasibile using currently available technology and minimal development work, applicable fabrication techniques differ for the two systems. A difference is also seen in the number of processing steps required to obtain the end product in each case. For these reasons, the discussion section of this report is divided into two main sections.

- The first section will deal with the cermet plate approach, and will outline potential processes, experimental results and a recommended process sequence.
- The second part of the discussion section will deal with the laminated composite. Potential fabrication techniques, experimental results, and a recommended process will be discussed.

Since the ultimate choice of a material type for development lies with the electrogenerator system designers, no absolute comparison between the desirability of the two materials has been attempted. The cermet and laminated composites are compared in the conclusions section of the report solely on the basis of:

- Relative process development difficulty.
- Probable dimensional control using available technology.
- Maximum plate size potential without development of joining processes.

A preferred material form is indicated in the conclusions section. Preference is based on the fabrication considerations listed above and on currently available experimental data.

## SCOPE

The purpose of this study has been to assess the fabrication feasibility of radioisotope fuel-layer design concepts for the ACCENT electrogenerator.

Two basic design concepts have been considered:

- A cermet containing approximately 80 vol% radioisotopic ceramic as a discontinuous phase within a continuous light metal matrix.
- A laminated composite consisting of 0.002 inch thick coatings of radioisotopic ceramic on both sides of a 0.002 inch thick light metal substrate.

Although two candidate radioisotopes were considered, namely $^{147}$promethium and $^{90}$strontium-yttrium, primary consideration was given to $^{147}$promethium because of less stringent shielding requirements.

Conclusions are presented, affirming the fabrication feasibility of both radioisotope fuel-layer design concepts.

Investigation has been limited to the feasibility of material fabrication. System design factors such as shielding, vibration, re-entry and impact packaging were not considered in this study.

## DISCUSSION

A number of potentially useful processes were considered as candidate processes for fabrication of plate geometry fuels for the electrogenerator. These included:

- Cermet fabrication processes
- Vacuum vapor deposition
- Flame spraying
- Electrophoretic coating

The first four of these fabrication approaches were considered to be most promising within the context of currently available technology.

The following discussion is limited to actual experimental data obtained at Battelle-Northwest. The discussion is divided into two sections, the first of which deals with cermet fabrication and the second with coated foil techniques.

### CERMET FABRICATION

Experiments were conducted with high density $Sm_2O_3$ particles as a stand-in for $Pm_2O_3$. Cermets were prepared using conventional powder metallurgy techniques (i.e., constituent blending followed by consolidation).

#### Cold Pressing

Figure 1 shows 66 vol% $Sm_2O_3$-34 vol% Al plates formed by cold pressing blended powders at 60,000 psi. Four, 2.4 inch diameter

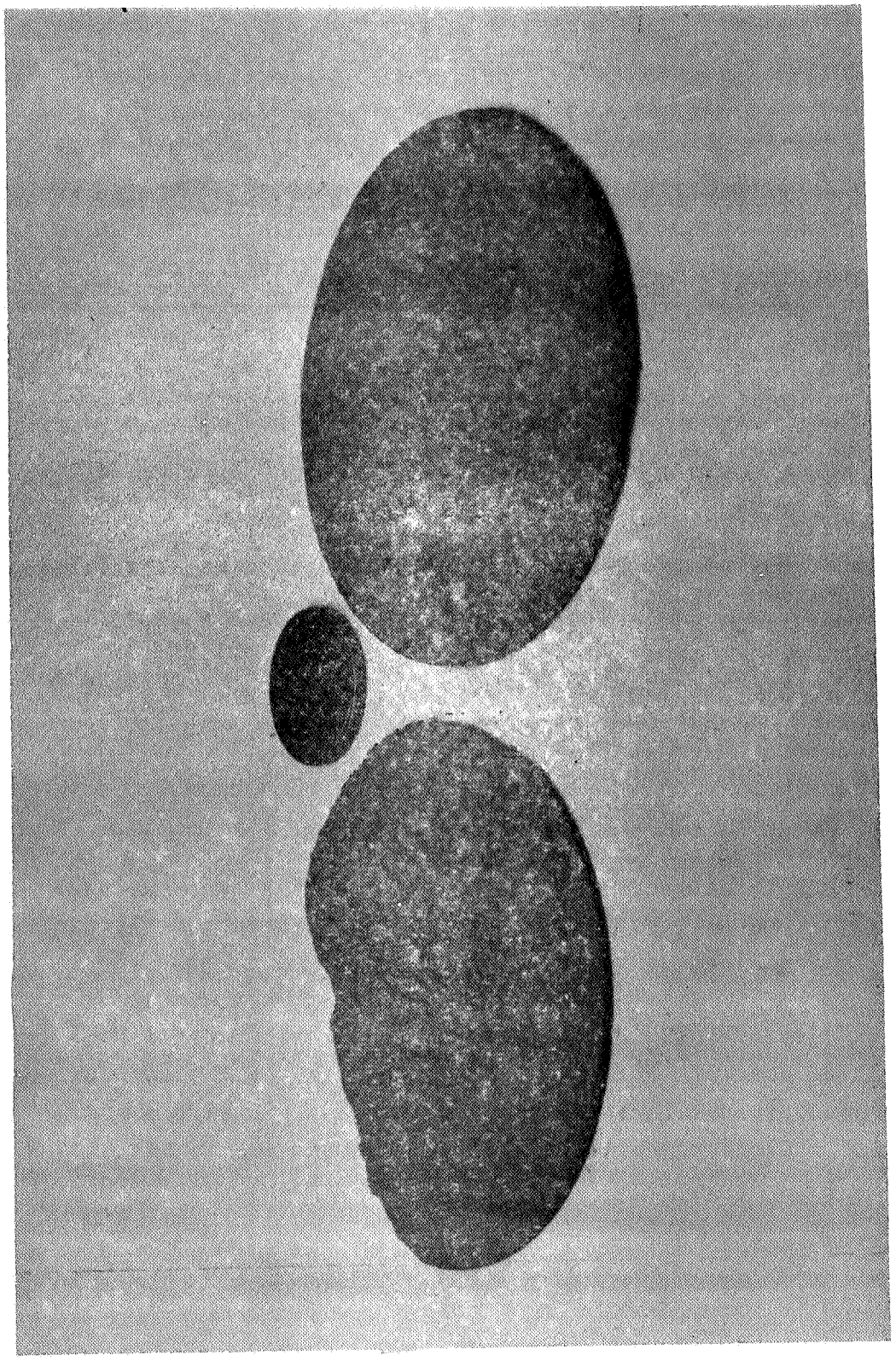

FIGURE 1. Cold Pressed 66 vol% $Sm_2O_3$-Al Cermets

plates were produced by this method. Properties of the plates are given in Table I.

TABLE I

PROPERTIES OF COLD PRESSED 66 VOL% $Sm_2O_3$ PLATES

| Plate | Thickness (inches) | Density ($9/Cm^3$) | % Theoretical Density |
|---|---|---|---|
| 1 | 0.008 | 3.8 | 66 |
| 2 | 0.013 | 3.6 | 63 |
| 3 | 0.018 | 3.4 | 59 |
| 4 | 0.035 | 3.9 | 67 |

The cold pressed $Sm_2O_3$-Al plates held together sufficiently well for handling. A density gradient was observed from the center to the edge of the sample. This effect could be alleviated by proper surfacing of the pressing die faces.

A dense cermet can be produced by repeated cold pressing and heat treatment stress relief. The process, called coining, is a standard powder metallurgy technique.

## Pneumatic Impaction

Figure 2 illustrates the microstructure of a dense 66 vol% $Sm_2O_3$-Al cermet produced by pneumatic impaction of blended $Sm_2O_3$ and aluminum powders.

High density $Sm_2O_3$ was prepared by pneumatic impaction of low density powder. The consolidated samaria was crushed and screened to obtain angular particles in a -70 +150 μ size range. Further processing was as follows:

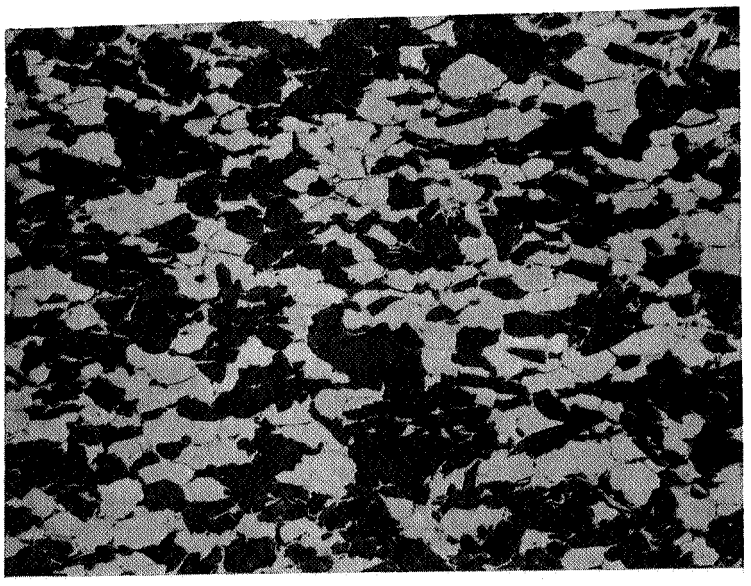

FIGURE 2. Pneumatically Impacted 66 vol% $Sm_2O_3$-Al Cermet

- Samaria powders were coated with a carbowax binder and agglomerated metallic coatings were produced by rolling in 1 to 2 μ diameter aluminum powder.
- Aluminum coated $Sm_2O_3$ particles were then mixed with ∿ 33 vol% -325 aluminum powder.
- The blended constituents were consolidated by pneumatic impaction at 590 °C and 225,000 psi.

As shown in Figure 2, distribution of $Sm_2O_3$ particles within the cermet is fairly uniform. Improvements could be made by closer control of particle size and blending processes. The slight amount of porosity seen in the sample may be traceable to the wax binder or may be the result of impaction parameters. Refinement of the process could yield:

- Decreased porosity
- An improved ceramic phase distribution
- A more continuous metallic phase
- A higher percentage of the ceramic phase

The thinnest plate produced by pneumatic impaction was 0.010 inch thick. Extension of current technology to plates having thicknesses of ∿ 0.006 inch is therefore quite reasonable.

## Cermet Fabrication Recommendations

One significant difficulty encountered with cermet fabrication, especially with the required thin plate geometry and high (80 to 90 vol%) ceramic phase content, is formation of a continuous metal phase. A microstructure consisting of a discontinuous ceramic phase, uniformly dispersed within a continuous, low vol% light metal phase must be achieved if maximum strength is to be obtained.

Fabrication of material having such a microstructure is dependent on achieving an optimum packing (> 80% TD) of ceramic particles, surrounded by metal, prior to densification.

Vibratory compaction of metal-coated ceramics in mixtures of two or three particle size ranges has been used at Battelle-Northwest to achieve such loading.

Dense promethia microspheres have been produced by plasma spheroidization and coated with refractory metal by chemical vapor deposition[1]. Well established chemical vapor deposition techniques are available for producing light metal coatings (e.g., aluminum[2]), and alternate ceramic powder densification and particle size control methods have been established for angular $Pm_2O_3$ particles.

Alternate processes for producing uniform, high density microspheres in size ranges of interest include the sol gel process. This process is applicable to $Pm_2O_3$, and economical use of the oxide could be expected.

## Recommended Process Sequence

A recommended processing sequence for producing a 0.006 inch thick cermet of 80 to 90 vol% $Pm_2O_3$ is as follows:

- Produce dense, particulate promethia in suitable particle size ranges and geometry for optimum high density loading.
- Coat the particles by chemical vapor deposition with the desired volume percent light metal (e.g., 10 to 20 vol%).
- Load the coated particles by vibrational compaction into a pressing mold, producing a close packed configuration of > 80% of theoretical density.
- Consolidate the high density cermet preform by pneumatic impaction or hot pressing to > 95% of theoretical density.

The microstructure of the resultant material should consist of uniformly dispersed $Pm_2O_3$ particles as a discontinuous phase within a continuous, uniform lattice of light metal.

## LAMINATED COMPOSITE FABRICATION

Three experimental approaches were used to investigate the fabricability of a 0.006 inch thick plate consisting of a 0.006 inch thick coating of $Pm_2O_3$ on a 0.002 inch thick light metal foil:

- Electrophoretic plating
- Flame spraying
- Vacuum vapor deposition

Samaria was used where possible as a stand-in material for promethia. Alumina was used for flame spraying experiments.

### Electrophoretic Plating

A 0.0005 inch thick coating of micronized $Sm_2O_3$ was applied to both sides of a sheet of 0.003 inch thick aluminum foil by electrophoretic plating. A slurry of nitromethane, isopropyl and micronized $Sm_2O_3$ was used, with a power level of 16 ma at 150V DC.

The coating appeared to be uniform, but did not adhere well to the aluminum. Foil surface treatments, parametric adjustments and postplating heat treatments might be tried to improve adherance. The process does not appear to be usable without further developmental work.

### Flame Spraying

Flame spraying was investigated using conventional oxyacetylene equipment and commercially available alumina flame spray powder.

Coatings were produced on 0.001 and 0.0035 inch thick aluminum foil. Although coating adherance was good, uniformity was not good on the micro scale.

Figure 3 is a photomicrograph of a sectioned, flame-sprayed coating of alumina on aluminum foil. Foil thickness is 0.0035. Poor coating uniformity is seen, and voids are also observed in the alumina.

Process results could probably be improved by changes in the feed material geometry (e.g., a finer particle size or a rod spraying approach) and parametrix refinement. No directly applicable experimental data is available on the response of $Pm_2O_3$ or $Sm_2O_3$ to such processing.

## Vacuum Vapor Deposition of $Sm_2O_3$

Physical vapor deposition of samarium was achieved by electron beam evaporation in vacuum. Deposition rates were high, with a maximum of approximately 1.8 microns per minute at a distance of 14 inches. Coatings from 0.0005 to 0.0015 inches in thickness were applied to glass and to aluminum foil substrates. Samaria coatings on aluminum foil are shown in the photomicrographs in Figure 4. Sectioned coatings show excellent uniformity.

Although crazing was observed in 0.0005 inch thick $Sm_2O_3$ films on glass, coating adherance appears to be excellent. Part of the crazing seen in Figure 5 is believed due to hydration of the samaria following a one week exposure to atmospheric conditions. The interference fringes in Figure 6, a photomicrograph of samaria on glass, indicate the degree of unbonding following hydration of the $Sm_2O_3$ after two weeks in air. Each interference fringe represents $\sim$ 0.25 $\mu$. Conoscopic examination of samaria on glass shows that an epitaxial layer has been produced.

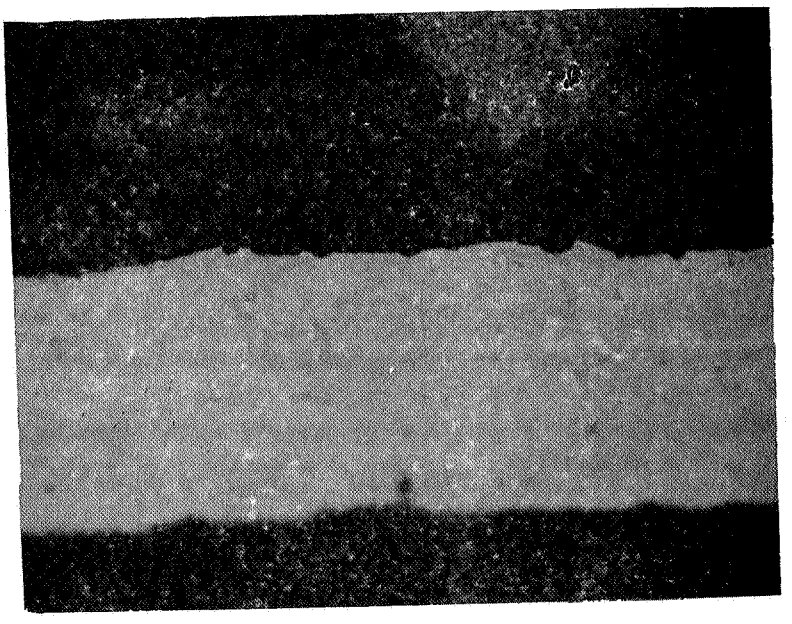

FIGURE 3. Flame Sprayed $Al_2O_3$ Coating on 0.0035 Inch Thick Aluminum Foil

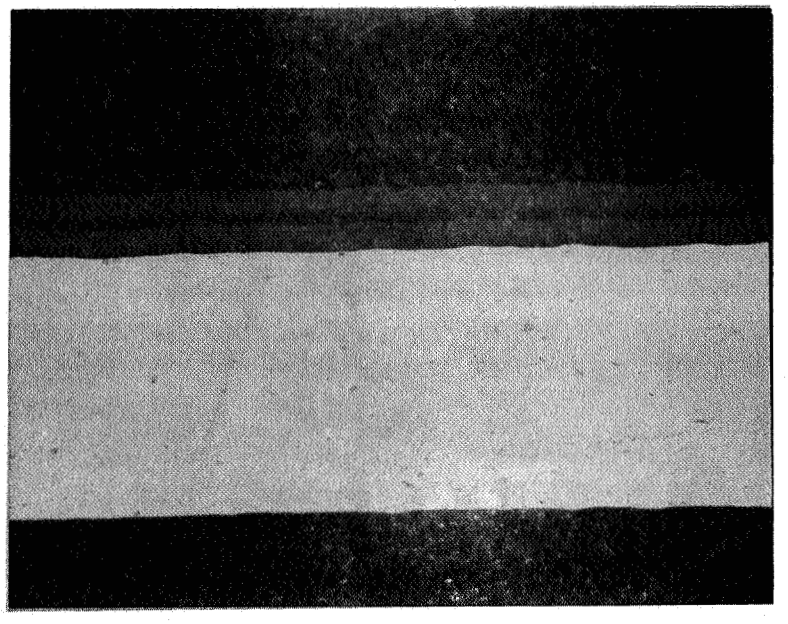

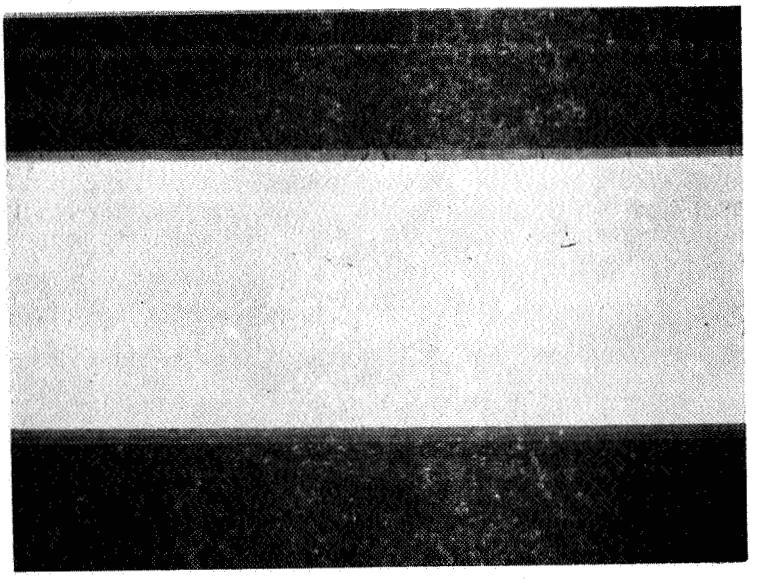

$\sim$ 0.0005 inch thick $Sm_2O_3$

FIGURE 4. Vacuum Vapor Deposited $Sm_2O_3$ on Aluminum Foil

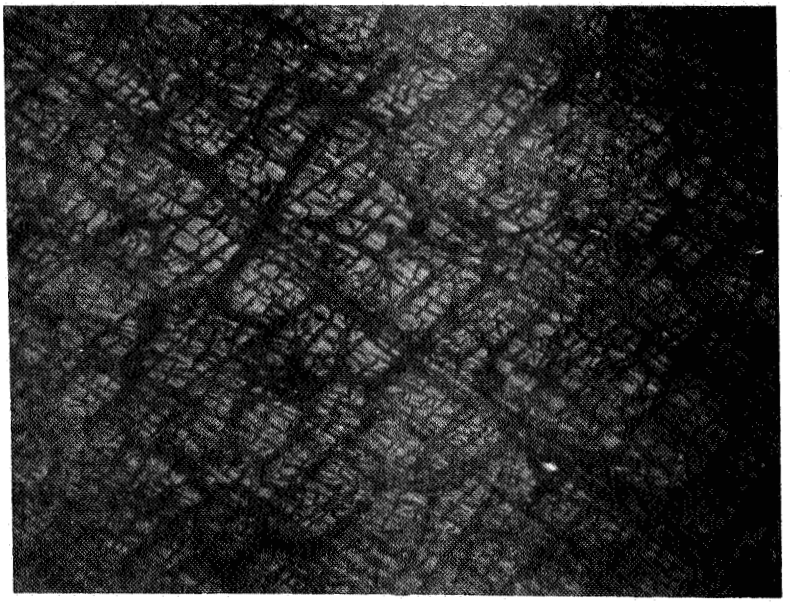

> 0.001 inch thick $Sm_2O_3$

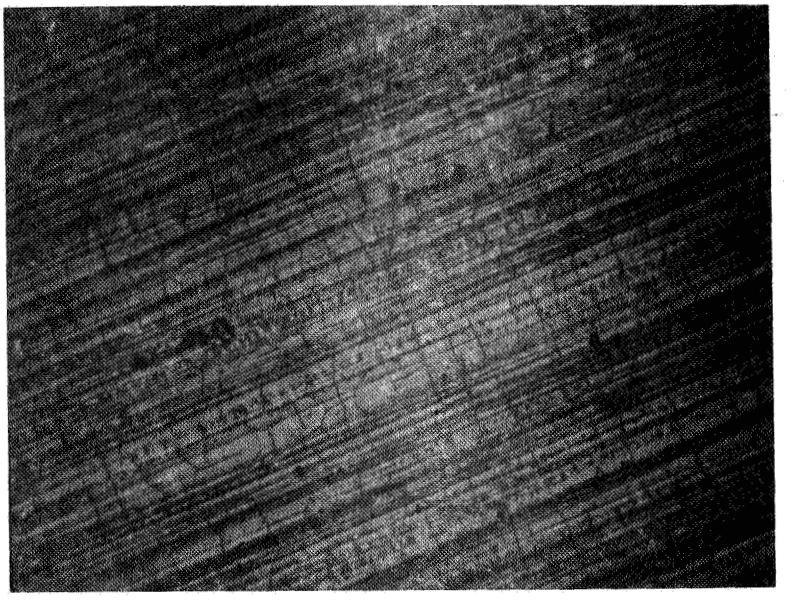

~ 0.0005 inch thick $Sm_2O_3$

FIGURE 5. Surface of Vacuum Deposited $Sm_2O_3$ Film on Aluminum

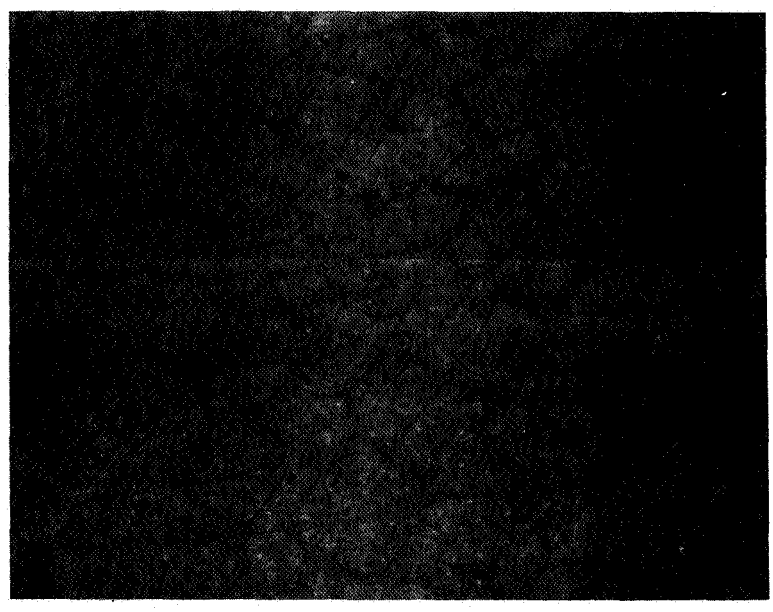

FIGURE 6. Interface of a 0.0005 Inch Thick $Sm_2O_3$ Coating and a Glass Substrate Following Two Weeks in Air

Use of RF diode sputtering rather than electron beam evaporation should permit production of a 0.002 inch thick coating of $Pm_2O_3$ with high deposition rates and elimination of crazing. Film uniformity by RF sputtering should not vary by more than 0.5% over a six inch diameter. Uniformity can be further refined by incorporating a rotary motion to average out variations in the deposition rate due to source distance and preferred evaporating direction.

## CONCLUSIONS AND RECOMMENDATIONS

Sufficient data has been obtained to draw conclusions regarding the fabricability of fuel plates for the ACCENT electrogenerator. These conclusions are based on experimental data and firm data on existing process capabilities.

Since stand-in materials were used in the experimentation described above, the application of these processes to radioactive materials will present additional process requirements. Stand-in materials have been used in the past and have provided results with excellent correlation. No unusual problems are foreseen in transferring the technology from stand-in to radioactive materials.

## FABRICATION FEASIBILITY

Either of the fuel form configurations for the electrogenerator are feasible from a fabricability standpoint, using currently available technology.

## PROCESS RECOMMENDATIONS

The physical vapor deposition process, specifically RF sputtering, appears to be the most attractive approach to fabrication. This approach appears to be advantageous in the following respects:

- Lower developmental costs and shorter program duration.
- Dimensional control refinement inherent in the process
- Greater plate size potential for more flexible system design
- Minimal processing required to obtain end product
- Potential for continuous, automated process providing a high level of quality assurance

In addition, the process can be used to add protective coatings to the radioisotope layer (e.g., a 4,000 to 10,000 angstrom aluminum coating).

The following qualifications are added for consideration by the system designers.

- The cost differential between the development of a cermet fuel form and a laminated fuel form would not be very great.
- Non-planar configurations could be produced readily by cermet fabrication.

The choice of material concepts is thus primarily a system design choice, and should be based on the importance of a variety of factors. The anticipated material requirements for a second generation system should also be considered.

## REFERENCES

1. Industrial Research, November 1967, P28.

2. Vapor Deposition, Edited by C. F. Powell, J. H. Oxley and J. M. Blocher, Jr., November 1966, P280.

## DISTRIBUTION LIST - FINAL REPORT CONTRACT NAS5-10366

| COPY NO. | ADDRESSEE |
|---|---|
| 1-9 | Mr. James Lazar, Chief<br>Electric Thruster Systems, Code RNT<br>NASA Headquarters, Building FOB-10B<br>Washington, D. C. 20546 |
| 10 | Dr. George W. Pfannebecker<br>Electric Thruster Systems, Code RNT<br>NASA Headquarters, Building FOB-10B |
| 11 | Dr. Fred Schulman, Chief<br>Nuclear Power Systems, Code RNP<br>Attn: Bernard I. Leefer<br>NASA Headquarters, Building FOB-10B<br>Washington, D. C. 20546 |
| 12 | Captain C. E. Franklin<br>Advanced Engines Branch<br>Space Nuclear Propulsion Office<br>U. S. Atomic Energy Commission<br>Washington, D. C. 20545 |
| 13 | Mr. Werner K. Kern<br>Isotopes and Materials Branch<br>Space Nuclear Systems Division<br>Mail Station F309<br>U. S. Atomic Energy Commission<br>Washington, D. C. 20545 |
| 14 | Mr. Robert Johnson<br>AFAPL/APIE<br>Area B<br>Wright Patterson Air Force Base<br>Dayton, Ohio 45433 |
| 15 | Mr. J. M. Turner<br>AFAPL/APIE<br>Area B<br>Wright Patterson Air Force Base<br>Dayton, Ohio 45433 |
| 16 | Office of the Director<br>NASA/Lewis Research Center<br>21000 Brookpark Road<br>Attn: Edward A. Richley<br>Cleveland, Ohio 44135 |

| COPY NO. | ADDRESSEE |
|---|---|
| 17 | Office of the Director<br>NASA/Lewis Research Center<br>21000 Brookpark Road<br>Attn: Bernard Lubarsky<br>Cleveland, Ohio 44135 |
| 18 | Office of the Director<br>NASA/Lewis Research Center<br>21000 Brookpark Road<br>Attn: W. E. Moeckel<br>Cleveland, Ohio 44135 |
| 19 | Office of the Director<br>NASA/Langley Research Center<br>Attn: M. C. Ellis, Jr.<br>Langley Station<br>Hampton, Virginia 23365 |
| 20 | Office of the Director<br>Jet Propulsion Laboratory<br>Attn: J. W. Stearns, Jr.<br>4800 Oak Grove Drive<br>Pasadena, California 91103 |
| 21 | Office of the Director<br>Jet Propulsion Laboratory<br>Attn: R. F. Rose<br>4800 Oak Grove Drive<br>Pasadena, California 91103 |
| 22 | Office of the Director<br>NASA/George C. Marshall Space Flight Center<br>Attn: Dr. Ernst Stuhlinger<br>Huntsville, Alabama 35812 |
| 23 | Office of the Director<br>NASA/George C. Marshall Space Flight Center<br>Attn: Nuclear Power Systems Office<br>Huntsville, Alabama 35812 |
| 24 | Office of the Director<br>NASA/Ames Research Center<br>Moffett Field, California 94035 |

| COPY NO. | ADDRESSEE |
|---|---|
| 25 | Office of the Director<br>NASA/Electronic Research Center<br>575 Technology Square<br>Cambridge, Massachusetts 01239 |
| 26 | Office of the Director<br>NASA/Manned Spacecraft Center<br>Houston, Texas 77058 |
| 27, 28 | NASA/Goddard Space Flight Center<br>Technical Information Division<br>Library Branch<br>Greenbelt, Maryland 20771 |
| 29 | NASA/Goddard Space Flight Center<br>Spacecraft Technology Division<br>Space Power Technology Branch<br>Attn: W. R. Cherry<br>Greenbelt, Maryland 20771 |
| 30 | NASA/Goddard Space Flight Center<br>Spacecraft Technology Division<br>Space Power Technology Branch<br>Attn: Joseph Epstein<br>Greenbelt, Maryland 20771 |
| 31 | NASA/Goddard Space Flight Center<br>Technology Directorate<br>Advanced Projects Staff<br>Attn: William S. West<br>Greenbelt, Maryland 20771 |
| 32 | NASA/Goddard Space Flight Center<br>Technology Directorate<br>Systems Division<br>Auxiliary Propulsion Branch<br>Attn: Dr. R. E. Hunter<br>Greenbelt, Maryland 20771 |